

SYNTHESIS OF NEW PBP PINCER IRIDIUM AND RHODIUM COMPLEXES AND
APPLICATION IN C–H ACTIVATION OF PYRIDINE BY UNIQUE METAL–
BORON COOPERATION

A Dissertation

by

WEI-CHUN SHIH

Submitted to the Office of Graduate and Professional Studies of
Texas A&M University
in partial fulfillment of the requirements for the degree of

DOCTOR OF PHILOSOPHY

Chair of Committee,	Oleg V. Ozerov
Committee Members,	Marcetta Y. Darensbourg
	François P. Gabbaï
	Katy C. Kao
Head of Department,	Simon W. North

December 2017

Major Subject: Chemistry

Copyright 2017 Wei-Chun Shih

ABSTRACT

Since first pincer ligand synthesized by Shaw, the chemistry of pincer ligands has been vastly expanded and applied in organic transformation and catalysis. Herein, we have developed new PBP-type pincer complexes that containing Lewis acidic boryl to achieve new reactivity.

In Chapter II, the facile insertion of Rh and Ir into the B–Ph bond (reversible for Rh) of PB^{Ph}P ligand was achieved, resulting in the formation of diarylboryl PBP pincer complexes. This type of PBP has a low-lying empty orbital at boron with a high degree of Lewis acidity, allowing the central boron to interconvert between boryl, borane, and borate in the reaction with dihydrogen.

In Chapter III, a series of PBP Rh complexes with potentially bidentate oxygenous ligands have been synthesized and characterized. These complexes displayed a variety of binding modes including Z-type borane, X-type boryl, η^2 -B,C binding, and bridging carboxylate.

In Chapter IV, new PBP iridium complexes that can serve as pre-catalysts for alkane transfer dehydrogenation have been reported. The turnover numbers achieved were relatively modest, but the structural and spectroscopic characterization of these PBP complexes enabled analysis of non-classical BH/Ir interactions.

In Chapter V, we have developed new PBP pincer Ir complexes that allowed pyridine to bind to the Lewis acidic boron and led to the activation of *ortho* C–H bond of pyridine selectively. The formation of four-membered products was achieved with several

pyridine derivatives. This discovery represents the first example of C–H activation directed by a Lewis acidic ligand backbone.

In Chapter VI, the synthesis of PCP/PNP-type pincer ligands and nickel complexes was achieved. By utilization of chlorophosphine as a phosphine source and magnesium or nickel powder as a reductant, this synthetic strategy permits one-pot synthesis of PCP/PNP ligands and nickel complexes from inexpensive and non-pyrophoric materials.

In Chapter VII, the synthesis of POCS bis-pincer Pd and Ni complexes has been developed. The hydroxo-bridged nickel complex demonstrated catalytic activity for nitrile hydration, but the binuclear cooperation was not verified because the monomeric complex displayed higher activity under the same condition. This result was further optimized by introducing base and up to a TON of 3050 was achieved.

DEDICATION

To my Wife, Son, and Parents

ACKNOWLEDGEMENTS

I would like to thank my committee chair and research advisor Prof. Oleg Ozerov for his guidance during my Ph.D. study at Texas A&M University. I appreciate his helpful suggestions and effort on my research. I would also like to thank my committee members, Prof. Marcetta Darensbourg, Prof. François Gabbai and Prof. Katy Kao.

I want to thank Dr. Morgan MacInnis for introducing me into the PBP chemistry before my preliminary exam and helping me to find my passion in boron and pincer chemistry. I want to thank Dr. Weixing Gu and Dr. Samuel Timpa to establish the synthetic methods for PBP Rh complexes. I would like to acknowledge my coworkers Dr. Chun-I Lee, Dr. Christopher Pell, Alex Kosanovich, Dr. Loren Press, Dr. Nattamai Bhuvanesh, Dr. Jia Zhou, and Yihan Cao for their knowledge and contributions to my graduate research. I would also like to thank the Ozerov group members that I have a good time to work with: Dr. Rafael Huacuja, Dr. Rodrigo Ramirez, Billy McCulloch, Dr. Jillian Davidson, Dr. Jessica DeMott, Dr. Chandra Palit, Chelsea Mandell, Soomin Park, Qingheng Lai, Bryan Foley, Andy Yu, Ming-Uei Hung, Olivia Gunther, and Yanwu Shao.

I would like to extend my gratitude to all of my friends at Texas A&M University and my softball teammates to enrich my graduate experience. Above all, I would like to thank my wife Chia-Hsiu Chen for all she has done for me and my Son for the good luck he has brought to me. I want to thank my Mom, Dad and family for their encouragement and support.

NOMENCLATURE

acac	Acetylacetonate
<i>ams</i>	<i>accessible molecular surface</i>
Ar	Aryl
^t Bu	<i>tert</i> -Butyl
bzac	benzoylacetate
COA	Cyclooctane
COD	1,5-Cyclooctadiene
COE	Cyclooctene
DAST	Diethylaminosulfur Trifluoride
DFT	Density Functional Theory
Et	Ethyl
ⁱ Pr	isopropyl
L	Ligand
Mes	Mesityl
Me	Methyl
nbd	2,5-norbornadiene
NBE	norbornene
NCS	<i>N</i> -Chlorosuccinimide
NMR	Nuclear Magnetic Resonance
OA	Oxidative Addition

OAc	Acetate
OPiv	Pivalate
OTf	Triflate
Ph	Phenyl
py	pyridine
RE	Reductive Elimination
RT	Room Temperature
TBA	<i>Tert</i> -Butylethane
TBE	<i>Tert</i> -Butylethylene
TFA	Trifluoroacetic Acid
THF	Tetrahydrofuran
TOF	Turnover Frequency
TON	Turnover Number
TMP	2,2,6,6-tetramethylpiperidide

TABLE OF CONTENTS

	Page
ABSTRACT	ii
DEDICATION	iv
ACKNOWLEDGEMENTS	v
NOMENCLATURE	vi
TABLE OF CONTENTS	viii
LIST OF SCHEMES	xii
LIST OF FIGURES	xvii
LIST OF TABLES	xxiv
CHAPTER I INTRODUCTION AND LITERATURE REVIEW	1
1.1 Pincer Ligands and Complexes	1
1.2 Electron-donating Ability of Central Donors on PXP-type Pincer Complexes	2
1.3 Reactivity of PXP-type Pincer Metal Complexes of Rh and Ir	6
1.3.1 Oxidative addition to PXP-type pincer complexes of Rh and Ir	6
1.3.2 Electronic effect on the thermodynamics of oxidative addition to (PXP)Ir(I)	12
1.4 Transfer Dehydrogenation of Alkanes Catalyzed by PXP-type Ir Complexes	15
1.4.1 Early examples of catalytic dehydrogenation of alkanes	15
1.4.2 Pincer Ir complexes mediated catalytic dehydrogenation of alkanes	20
1.5 Pincer Complexes Bearing a Central Boryl Ligand	24
1.5.1 Diaminoboryl-based pincer complexes	25
1.5.2 Carborane-based pincer complexes	29
1.5.3 Diarylboryl-based pincer complexes	34
1.6 Versatile Binding Modes of Boron on the PB ^{Ph} P Ligands	37
1.6.1. Group 9 metals	38
1.6.2 Group 10 metals	41
1.6.3 Group 11 metals	44

CHAPTER II FACILE INSERTION OF RHODIUM AND IRIDIUM INTO BORON-PHENYL BOND, LEADING TO BORYL/BIS(PHOSPHINE) PBP PINCER COMPLEXES	46
2.1 Introduction	46
2.2 Result and Discussion	49
2.2.1 Synthesis of PBP-type pincer Ir and Rh complexes via B–Ph oxidative addition	49
2.2.2 Reactivity of the new PBP pincer complexes	57
2.3 Conclusions	68
2.4 Experimental Section	68
2.4.1 General considerations	68
2.4.2 Physical methods	69
2.4.3 Synthesis and characterization of rhodium and iridium complexes	69
2.4.4 X-ray structural determination details	81
2.4.5 Computational details	86
CHAPTER III BORYL/BORANE INTERCONVERSION AND DIVERSITY OF BINDING MODES OF OXYGENOUS LIGANDS IN PBP PINCER COMPLEXES OF RHODIUM	87
3.1 Introduction	87
3.2 Results and Discussion	89
3.2.1 Synthesis and characterization of 301	89
3.2.2 Synthesis and characterization of carboxylate derivatives	92
3.2.3 Synthesis and characterization of 310, 311, and 312	101
3.2.4 Simulation of coupling patterns of 304, 305, 306, and 310	105
3.3 Conclusions	110
3.4 Experimental Section	110
3.4.1 General considerations	110
3.4.2 Physical methods	111
3.4.3 Synthesis and characterization of rhodium complexes	111
3.4.4 X-ray structural determination details	118
3.4.5 Van't Hoff plot	122
CHAPTER IV SYNTHESIS AND CHARACTERIZATION OF PBP PINCER IRIDIUM COMPLEXES AND THEIR APPLICATION IN ALKANE TRANSFER DEHYDROGENATION	124
4.1 Introduction	124
4.2 Results and Discussion	126
4.2.1 Synthesis and characterization of PBP-type pincer iridium complexes	126
4.2.2 Transfer dehydrogenation of COA to COE catalyzed by (PBP)Ir(H) ₄ (401) and (PBP)Ir(Ph)(H) (402)	136

4.3 Conclusions	137
4.4 Experimental Section	138
4.4.1 General considerations	138
4.4.2 Physical methods	138
4.4.3 Synthesis and characterization of iridium complexes	139
4.4.4 Catalytic transfer dehydrogenation of COA into COE	143
4.4.5 X-ray structural determination details	144
CHAPTER V SELECTIVE <i>ORTHO</i> C–H ACTIVATION OF PYRIDINE DIRECTED BY LEWIS ACIDIC BORON OF PBP Pincer Iridium COMPLEXES	146
5.1 Introduction	146
5.2 Results and Discussion	149
5.2.1 C–H activation of pyridine directed by (PBP)Ir(CO) ₂	149
5.2.2 C–H activation of pyridine directed by (PB ^{Ph} P)Ir(H)(CO)	155
5.2.3 Mechanistic study	161
5.2.3 Arylation of pyridine	170
5.3 Conclusions	171
5.4 Experimental Section	172
5.4.1 General considerations	172
5.4.2 Physical methods	172
5.4.3 Reactivity of complex 404 or 502 toward C–H activation of pyridine	173
5.4.4 Reactivity of complex 404 with pyridine under Ar or CO ₂	175
5.4.5 Thermolysis of complex 502 at 100 °C in benzene	176
5.4.6 Thermolysis of complex 502 with 2,6-lutidine at 100 °C in C ₆ D ₆	176
5.4.7 Exchange reaction of 501c to 501a in the presence of DMAP at 100 °C in C ₆ D ₆	177
5.4.8 Synthesis and characterization of iridium complexes	180
5.4.9 X-Ray structural determination details	193
CHAPTER VI ONE-POT SYNTHESIS OF 1,3- BIS(PHOSPHINOMETHYL)ARENE PCP/PNP Pincer Ligands and Their Nickel Complexes	196
6.1 Introduction	196
6.2 Results and Discussion	198
6.2.1 Synthesis of benzylphosphonium salts (606-X ₂) and benzylphosphines (606)	198
6.2.2 Synthesis of PCP and PNP ligands (610)	203
6.2.3 Synthesis of PCP and PNP nickel complexes (611/612 and 614)	205
6.3 Conclusions	208
6.4 Experimental Section	209
6.4.1 General considerations	209

6.4.2 Physical methods	209
6.4.3 Synthesis and characterization	210
6.4.4 General procedure for screening and optimization of synthesis of Phosphonium Salts (606a-X ₂)	219
6.4.5 Synthesis of ^t Bu(PCP)H by different methods	220
6.4.6 C–P bond cleavage observation in ^{Ph} (PCP)H and ⁱ Pr(PNP) synthesis	222
6.4.7 Control reactions related to the synthesis of ⁱ Pr(PCP)NiX (611/612)	225
CHAPTER VII SYNTHESIS OF BIS-PINCER PALLADIUM/NICKEL COMPLEXES AND APPLICATION IN CATALYTIC NITRILE HYDRATION	227
7.1 Introduction	227
7.2 Results and Discussion	230
7.2.1 Synthesis of PCS and POCS bis-pincer ligands	230
7.2.2 Synthesis and reactivity of binuclear palladium and nickel complexes	232
7.2.3 Nitrile hydration catalyzed by binuclear complexes	240
7.2.4 Nitrile hydration catalyzed via monomeric nickel complexes	245
7.3 Conclusions	253
7.4 Experimental Section	253
7.4.1 General considerations	253
7.4.2 Physical methods	254
7.4.3 Synthesis and characterization of palladium and nickel complexes	255
7.4.4 Catalytic nitrile hydration	259
7.4.5 X-ray structural determination details	261
CHAPTER VIII SUMMARY	263
REFERENCES	266
APPENDIX	288

LIST OF SCHEMES

	Page
Scheme I-1. General Equation of Oxidative Addition and Reductive Elimination	6
Scheme I-2. Transient Formation of (PCP)Ir(I) Intermediate ²⁷⁻²⁹	8
Scheme I-3. Kinetic C–H OA and Thermodynamic C–Cl OA on the (PNP)Ir(I) ³⁰	9
Scheme I-4. Synthesis of (POCOP)Ir(I) by Dehydrochlorination of 35 ³¹	9
Scheme I-5. Reductive Elimination of C–C Bond and Oxidative Addition of C–X Bond ³²	10
Scheme I-6. Synthesis of (PBP)Rh(I) and the Reactivity toward OA ^{33,34}	11
Scheme I-7. Synthesis of Ethylene-coordinated Boryl Complex ³⁷	13
Scheme I-8. Thermodynamic Stability of Amido Hydride Complexes vs. Ammonia Complexes ^{25,26,38}	14
Scheme I-9. Proposed Mechanism of Alkane Dehydrogenation Catalyzed by 66 ⁵⁸	18
Scheme I-10. Proposed Mechanism of Transfer Dehydrogenation of Alkane Catalyzed by 68 ⁶¹	20
Scheme I-11. Synthesis of Diaminoboryl-based Pincer Ligands ³⁷	25
Scheme I-12. Synthesis of the Long-tethered P–B–P Ligands ^{73,74}	26
Scheme I-13. Synthesis of (PBP)M(H)(Cl) (M = Ir or Rh) ^{33,37}	28
Scheme I-14. Synthesis of PBP Pincer Complexes of Cobalt ^{85,86}	29
Scheme I-15. Synthesis of Carborane-based SBS and SeBSe Pincer Ligands ⁹⁵	30
Scheme I-16. Synthesis of (EBE)PdCl Complexes (E = S, Se) ⁹⁵	31
Scheme I-17. Synthesis of Chiral Carborane-based NBN Pincer Ligands ⁹⁶	31
Scheme I-18. Synthesis of NBN-pincer Chiral Complexes of Rh, Pd, and Ni ⁹⁶	32
Scheme I-19. Synthesis of Carborane-based POBOP Ligand ^{97,100}	33

Scheme I-20. Synthesis of (POBOP)RhL _n Complexes ⁹⁷	34
Scheme I-21. Oxidative Addition of PhI to 129 and Reductive Elimination of Ph– B from 130 in the Presence of CH ₃ CN ⁹⁷	34
Scheme I-22. Synthesis of PB ^{Ph} P Ligand ^{103–106}	35
Scheme I-23. Synthesis of Diarylboryl-based (PBP)PdI and the Proposed Mechanism ²¹	36
Scheme I-24. Non-stabilized Boron on the Diarylboryl PBP with Lewis Acidic Property	37
Scheme I-25. Reactivity of PBP Complex 137 with Lewis Base and Nucleophile ²¹	37
Scheme I-26. Synthesis of PB ^{Ph} P Complexes of Rh Featuring the Z-type Borane Binding ¹⁰⁵	39
Scheme I-27. Synthesis of PB ^{Ph} P Complexes of Rh and Ir ¹⁰⁹	40
Scheme I-28. Synthesis and Reactivity of PB ^{Ph} P Complexes of Co ¹¹⁰	41
Scheme I-29. Synthesis of PB ^{Ph} P Complexes of Pd and Pt ¹¹²	42
Scheme I-30. Synthesis and Reactivity of PB ^{Ph} P Complexes of Pd ¹¹³	43
Scheme I-31. Synthesis of PB ^{Mes} P Complexes of Ni ¹¹⁴	43
Scheme I-32. Activation of H ₂ by Oxidative Addition across Ni–B Bond ¹¹⁴	44
Scheme I-33. Synthesis of PB ^{Ph} P Complexes of Au ¹⁰⁶	44
Scheme I-34. Synthesis of PB ^{Ph} P Complexes of Cu ¹¹⁵	45
Scheme II-1. Bourissou's Synthesis of Rh Complex 142	49
Scheme II-2. Synthesis of 201 via B–C Bond Oxidative Addition	49
Scheme II-3. Thermolysis of PBP Complexes with Dihydrogen	58
Scheme II-4. Mechanistic Study of the Conversion of 201 to 206	61
Scheme II-5. Synthesis of (PBP)MCl ₂	67

Scheme III-1. Insertion of Ir or Rh into B–Ph of 201 Leads to the Pincer Complexes. The Mixture of 142/202/203 was Observed in Equilibrium for Rh.....	89
Scheme III-2. The Reactions of the 142/202/203 Mixture with Sodium Acetylacetonate.....	90
Scheme III-3. Reactivity of 142/202/203 with Alkali Metal Carboxylates.....	93
Scheme III-4. Thermolysis of 304 and 305.....	97
Scheme III-5. The Reaction of the 142/202/203 Mixture with Me ₃ SiOTf.....	102
Scheme III-6. The Reactions of the 142/202/203 Mixture with Na(bzac).....	106
Scheme IV-1. Synthesis of PBP Complex by Insertion of Metal into a B–Ph Bond or by C–C Bond Cross Coupling.....	126
Scheme IV-2. Conversion of 201 to 206 from Intermediacy of 209.....	126
Scheme IV-3. Synthesis of PBP Ir Polyhydrides (401) and Conversion of 401 back to 206.....	127
Scheme IV-4. Reactivity of PBP Complexes of Iridium.....	131
Scheme IV-5. Comproportionation of 401 and 404 into 405.....	135
Scheme V-1. Strategies for C–H Activation of Pyridine.....	147
Scheme V-2. Lewis Acid Directed C–H Activation of Pyridine.....	148
Scheme V-3. Lewis-base-stabilized Boryl Complexes.....	149
Scheme V-4. Coordination of DMAP to 404 and Selective C–H Activation of DMAP after Thermolysis.....	150
Scheme V-5. Selective C–H Activation of Pyridine.....	151
Scheme V-6. Decrease of Reaction Rate by Treatment with CO.....	154
Scheme V-7. Selective C–H Activation of 2-Chloropyridine.....	155
Scheme V-8. Synthesis of Complex 502 by Comproportionation of 402 with 403.....	156
Scheme V-9. Thermolysis of Complex 502 at 100 °C in Benzene.....	163

Scheme V-10. Thermolysis of Complex 502 at 100 °C in C ₆ D ₁₂ and Subsequently Addition of Pyridine.....	165
Scheme V-11. Proposed Mechanism of Pyridine C–H Activation by 404 or 502.....	168
Scheme V-12. Thermolysis of Complex 502 with 2,6-Lutidine at 100 °C in C ₆ D ₆	169
Scheme V-13. Competition Reaction between Pyridine and 2,6-Lutidine	170
Scheme V-14. C–H Arylation of Pyridine from Complex 501c	171
Scheme VI-1. Traditional Synthesis of PCP or PNP Ligands.....	197
Scheme VI-2. New Method of Synthesis of PCP or PNP Ligands by Using ClPR ₂	198
Scheme VI-3. Synthesis of Phosphonium Salts (606-X ₂) from 604	201
Scheme VI-4. Synthesis of Benzylalkylphosphines (606) from 606-X ₂	202
Scheme VI-5. Proposed Mechanism of (P ^O C ^O P)NiCl Formation in the Study by Zargarian et al. ²³⁸	206
Scheme VI-6. Proposed Mechanism of (PCP)NiX Formation	206
Scheme VI-7. Synthesis of ⁱ Pr(PCP)NiX (611/612) and [ⁱ Pr(PNP)NiBr][Br] (614).....	208
Scheme VI-8. Synthesis of ^t Bu(PCP)H by using ClP ^t Bu ₂	220
Scheme VI-9. Synthesis of ^t Bu(PCP)H by using ClP ^t Bu ₂ and NaI	222
Scheme VII-1. Synthesis of PCS Bis-pincer Ligand.....	230
Scheme VII-2. Synthesis of POCS Bis-pincer Ligands	232
Scheme VII-3. Synthesis of POCS Bis-pincer Complexes of Pd and Ni (706).....	233
Scheme VII-4. Synthesis of Chloro-bridged Complex of Ni (707-Ni).....	233
Scheme VII-5. Synthesis of Bis-pincer Complex of Ni with Non-equivalent Metal Centers	234
Scheme VII-6. Synthesis of Hydroxo-bridged Complex of Ni (709-Ni).....	235
Scheme VII-7. Synthesis of Hydroxo-bridged Complexes of Pd and Ni (709).....	238
Scheme VII-8. Proposed Mechanism of Nitrile Hydration by Complex 709-Ni.....	241

Scheme VII-9. Nitrile Hydration Catalyzed by 709-Ni	242
Scheme VII-10. Dehydrogenation of Isopropanol by 709-Pd.....	244
Scheme VII-11. Possible Decomposition Pathway of Complex 709-Pd in Ethanol.....	245
Scheme VII-12. Nitrile Hydration Catalyzed by Monomeric Pincer Complex Pair.....	246
Scheme VII-13. Hydration of Benzonitrile using 713 and Exchange Reaction with Water in the Study by Piers et. al. ²⁷⁶	250
Scheme VII-14. Proposed Mechanism of Nitrile Hydration Catalyzed by Monomeric Pincer Complex 712	251

LIST OF FIGURES

	Page
Figure I-1. Early examples of pincer complexes reported by Shaw. ^{9,10}	1
Figure I-2. PXP-type pincer complexes with various central anionic donors.....	2
Figure I-3. Efficiencies of various pincer complexes for catalytic transfer dehydrogenation of COA to COA with TBE as hydrogen acceptor.	21
Figure I-4. Sterically controlled catalytic activity for alkane dehydrogenation.....	23
Figure I-5. Pincer metal complexes with a central boryl X-type donor.	24
Figure I-6. Possible coordination modes in complex 106.....	28
Figure I-7. Versatile binding modes of boron on PB ^{Ph} P complexes.	38
Figure II-1. Complexes featuring various boron-based ligands.....	47
Figure II-2. Donating ability of central ligand predicted by DFT calculation.	48
Figure II-3. Lewis acidic boron on Ozerov PBP and comparison with Yamashita PBP and Ozerov PNP.	48
Figure II-4. ¹ H NMR spectrum of 201 featuring restricted rotation of the Ir–Ph bond. C ₆ H ₅ gives rise to five separate ¹ H resonances (labeled as *), and one of the four CH ₃ signals of the P ⁱ Pr ₂ groups shifted upfield by ring current effect (labeled as •).	51
Figure II-5. POV-Ray rendition of the ORTEP drawing (50% thermal ellipsoids) of 201 showing selected atom labeling. The molecule of toluene present in the unit cell is not shown. Selected bond distances (Å) and angles (°): Ir1–B1, 1.988(3); Ir1–C11, 2.4096(11); Ir1–C1, 2.029(3); Ir1–P1, 2.3245(9); Ir1–P2, 2.3333(10); B1–Ir1–C1, 98.09(12); B1– Ir1–C11, 114.26(10); P1–Ir1–P2, 162.54(3).	52
Figure II-6. ³¹ P{ ¹ H} NMR spectra of 142, 202, and 203 in CDCl ₃ with different concentrations.....	54
Figure II-7. ³¹ P{ ¹ H} NMR spectra of 204 and 205 in CDCl ₃ with different concentrations.....	55
Figure II-8. 2D ³¹ P EXSY spectrum of 142, 202, and 203 in CDCl ₃ at room temperature with a mixing time of 0.15 seconds and d ₁ delay of 5	

seconds. The orange cross-peaks indicated dynamic exchange between 142 and 203 on the NMR time-scale.....	57
Figure II-9. POV-Ray rendition of the ORTEP drawing (50% thermal ellipsoids; left) and CYLView drawing (right) of 206 showing selected atom labeling. Only one of two independent structures in the unit cell is shown. Hydrogen atoms except Ir-H were omitted for clarity. Selected bond distances (Å) and angles (°): Ir1–B1, 2.003(4); Ir1–C11, 2.3815(9); Ir1–H1, 1.55(5); Ir1–P1, 2.2832(9); Ir1–P2, 2.2945(9); B1–Ir1–H1, 69.8(18); B1–Ir1–C11, 139.27(11); P1–Ir1–P2, 167.24(3).	59
Figure II-10. POV-Ray rendition of the ORTEP drawing (50% thermal ellipsoids; left) and CYLView drawing (right) of 207 showing selected atom labeling. Only one of two independent structures in the unit cell is shown. Hydrogen atoms except Rh-H were omitted for clarity. Selected bond distances (Å) and angles (°): Rh1–B1, 2.010(3); Rh1–C11, 2.3703(13); Rh1–H1, 1.51(3); Rh1–P1, 2.2951(13); Rh1–P2, 2.3158(14); B1–Rh1–H1, 51.1(11); B1–Rh1–C11, 143.97(8); P1–Rh1–P2, 167.48(2).	60
Figure II-11. Low temperature ¹ H NMR experiments of 209 in d ₈ -toluene.	62
Figure II-12. (a) ¹ H spectrum of 209 in d ₈ -toluene at –50 °C. (b) ¹ H{ ³¹ P} spectrum of 209 in d ₈ -toluene at –50 °C. (c~e) Homodecoupled ¹ H NMR spectrum of 209 in d ₈ -toluene at –50 °C ((c) for H _a decoupling, (d) for H _b decoupling, and (e) for H _c decoupling).	63
Figure II-13. POV-Ray rendition of the ORTEP drawing (50% thermal ellipsoids; left) and CYLView drawing (right) of 209 showing selected atom labeling. Only one of two independent structures in the unit cell is shown. Hydrogen atoms were omitted for clarity. Selected bond distances (Å) and angles (°): Ir1–B1, 2.137(4); Ir1–C11, 2.4180(13); Ir1–P1, 2.3032(13); Ir1–P2, 2.3030(12); B1–Ir1–P1, 84.72(11); B1–Ir1–C11, 138.94(11); P1–Ir1–P2, 169.55(3).	65
Figure II-14. ORTEP drawing (50% probability ellipsoids) of 206, 209 showing selected atom labeling. Only one of two independent structures in the unit cell is shown for all structures. Hydrogen atoms are omitted for clarity.....	66
Figure II-15. ORTEP drawing (50% probability ellipsoids) of 211, and 210, showing selected atom labeling. Only one of two independent structures in the unit cell is shown for all structures. Hydrogen atoms are omitted for clarity. Selected bond distances (Å) and	

angles (°) for 211: Rh1–B1, 1.969(5); Rh1–C11, 2.3322(10); Rh1–Cl2, 2.3275(10); Rh1–P1, 2.3413(11); Rh1–P2, 2.3544(11); B1–Rh1–C11, 98.26(14); C11–Rh1–Cl2, 164.39(4); P1–Rh1–P2, 163.73(4). Selected bond distances (Å) and angles (°) for 210: Ir1–B1, 1.995(8); Ir1–C11, 2.3324(17); Ir1–Cl2, 2.3359(17); Ir1–P1, 2.3445(18); Ir1–P2, 2.3504(18); B1–Ir1–C11, 97.2(2); C11–Ir1–Cl2, 164.43(6); P1–Ir1–P2, 164.31(6).....	67
Figure II-16. ³¹ P{ ¹ H} NMR spectra of 201 under hydrogen in C ₆ D ₁₂	79
Figure II-17. ¹ H NMR evidence of phenyl shift and benzene formation in C ₆ D ₁₂	79
Figure III-1. Pincer metal complexes with a central boryl donor in literature.	88
Figure III-2. POV-Ray rendition of the ORTEP drawing (50% thermal ellipsoids) of 301 showing selected atom labeling. Hydrogen atoms are omitted for clarity. Selected bond distances (Å) and angles (deg): Rh1–B1, 2.271(2); Rh1–P1, 2.2394(6); Rh1–P2, 2.2535(6); Rh1–O1, 2.067(1); Rh1–O2, 2.075(1); B1–C1, 1.597(3); O1–Rh1–O2, 87.83(5); P1–Rh1–P2, 98.73(2); O1–Rh1–P1, 176.51(4); O2–Rh1–P2, 172.14(4); P1–Rh1–B1, 83.74(5); P2–Rh1–B1, 80.06(5); O1–Rh1–B1, 96.49(6); O2–Rh1–B1, 103.37(6); C1–B1–Rh1, 101.0(1).	90
Figure III-3. Rh–B bond distance (in Å) of (PBP)Rh complexes in literature.	91
Figure III-4. POV-Ray rendition of the ORTEP drawing (50% thermal ellipsoids) of 305 showing selected atom labeling. Hydrogen atoms are omitted for clarity. Selected bond distances (Å) and angles (deg) for 305: Rh1–B1, 2.282(3); Rh1–O1, 2.1765(19); Rh1–O2, 2.1566(19); Rh1–P1, 2.2225(10); Rh1–P2, 2.2131(9); Rh1–C31, 2.504(3); O1–C31, 1.273(3); O2–C31, 1.268(3); O2–Rh1–O1, 60.90(7); P1–Rh1–P2, 99.86(3); O1–Rh1–P2, 101.62(6); O2–Rh1–P1, 97.51(6); O1–Rh1–B1, 107.38(10); P1–Rh1–B1, 81.94(9); O1–C31–O2, 119.6(3).....	94
Figure III-5. POV-Ray rendition of the ORTEP drawing (50% thermal ellipsoids) of 308 showing selected atom labeling. Hydrogen atoms and the disordered moiety are omitted for clarity. Selected bond distances (Å) and angles (deg) for 308: Rh1–B1, 2.141(4); Rh1–O2, 2.191(2); Rh1–P1, 2.3162(11); Rh1–P2, 2.3233(11); Rh1–C30, 2.011(3); B1–O1, 1.549(4); O1–C25, 1.296(4); O2–C25, 1.241(4); O2–Rh1–C30, 178.03(12); P1–Rh1–P2, 166.16(3); C30–Rh1–P1, 88.50(10); O2–Rh1–P1, 91.22(7); O1–B1–Rh1, 103.4(2); O2–Rh1–B1, 78.78(13); O1–C25–O2, 122.1(3).	98

Figure III-6. Two possible resonance structures of bridging acetate in 307.	101
Figure III-7. POV-Ray rendition of the ORTEP drawing (50% thermal ellipsoids) of 310 showing selected atom labeling. Hydrogen atoms are omitted for clarity. Selected bond distances (Å) and angles (deg) for 310: Rh1–B1, 2.3103(17); Rh1–P1, 2.1928(5); Rh1–P2, 2.2302(5); Rh1–O1, 2.2516(12); Rh1–O2, 2.3282(12); B1–C2, 1.605(2); B1–Rh1–O1, 81.81(4); B1–Rh1–O2, 108.30(5); B1–Rh1–P1, 81.81(4); B1–Rh1–P2, 80.28(4); P1–Rh1–P2, 100.02(2); O1–Rh1–P1, 96.37(3); O2–Rh1–P2, 100.58(3); O1–Rh1–O2, 62.49(4) ; C2–B1–Rh1, 103.22(10).	103
Figure III-8. POV-Ray rendition of the ORTEP drawing (50% thermal ellipsoids) of 312 showing selected atom labeling. Hydrogen atoms are omitted for clarity. Selected bond distances (Å) and angles (deg) for 312: Rh1–B1, 2.231(5); Rh1–P1, 2.2015(13); Rh1–P2, 2.2093(12); Rh1–O1, 2.244(3); Rh1–C1, 2.391(4); B1–C1, 1.569(6); B1–C8, 1.611(7); B1–C14, 1.599(6); B1–Rh1–C1, 39.50(16); B1–Rh1–O1, 131.45(14); B1–Rh1–P1, 87.01(14); B1–Rh1–P2, 80.97(13); P1–Rh1–P2, 99.54(4); O1–Rh1–P1, 101.58(9); O1–Rh1–P2, 141.75(8).	104
Figure III-9. Simulation of coupling pattern for methyl group on the <i>iso</i> -propyl group.	108
Figure III-10. Simulation of coupling pattern for methyl group on the <i>iso</i> -propyl group.	109
Figure III-11. Van't Hoff plot for the isomerization between 304 and 307.	123
Figure IV-1. Previously reported pincer complexes with a central boryl donor.	125
Figure IV-2. POV-Ray rendition of the ORTEP drawing (50% thermal ellipsoids) of 401 showing selected atom labeling. Hydrogen atoms are omitted, except for the hydrogens on Ir, for clarity. Selected bond distances (Å) and angles (deg): Ir1–B1, 2.159(3); Ir1–H1, 1.64(3); Ir1–H2, 1.71(3); Ir1–H7, 1.57(3); Ir1–H8, 1.50(3); B1–H1, 1.48(3); B1–H2, 1.34(3); Ir1–P1, 2.2840(7); Ir1–P2, 2.2804(7); B1–Ir1–H1, 43.3(10); B1–Ir1–H2, 38.3(10); B1–Ir1–H7, 138.6(11); B1–Ir1–H8, 139.9(10); H1–Ir1–H8, 176.0(14); H2–Ir1–H7, 176.0(13); H1–B1–H2, 101.5(17); H7–Ir1–H8, 81.5(15).	128
Figure IV-3. Different structural types for interaction of R ₂ BH ₂ with a transition metal, as presented by Radius and Braunschweig (A–C), and Yamashita's assignment of the intermediate structure D.	129

Figure IV-4. POV-Ray rendition of the ORTEP drawing (50% thermal ellipsoids) of 404 showing selected atom labeling. Hydrogen atoms are omitted for clarity. Selected bond distances (Å) and angles (deg): Ir1–B1, 2.137(3); Ir1–C1, 1.935(3); Ir1–C2, 1.890(3); C1–O1, 1.144(4); C2–O2, 1.142(4); Ir1–P1, 2.3082(14); Ir1–P2, 2.2985(13); B1–Ir1–C1, 159.32(13); B1–Ir1–C2, 88.42(13); C1–Ir1–C2, 112.26(14); P1–Ir1–P2, 139.45(3); C2–Ir1–P1, 109.97(11); C2–Ir1–P2, 104.32(12).....	133
Figure V-1. 2D ¹ H– ¹ H COSY NMR spectrum of 501b in C ₆ D ₆ at room temperature, showing the correlation between H3-H4, H4-H5, and H5-H6 through bonds.....	152
Figure V-2. POV-Ray rendition of the ORTEP drawing (50% thermal ellipsoids) of 501b showing selected atom labeling. Hydrogen atoms are omitted for clarity with the exception of the hydrogen bound to iridium. Selected bond distances (Å) and angles (°): Ir1–B1, 2.285(2); Ir1–C1, 1.920(2); Ir1–C2, 2.078(2); Ir1–P1, 2.2797(6); Ir1–P2, 2.2849(6); C1–O1, 1.145(3); N1–C2, 1.360(3); N1–B1, 1.613(3); Ir1–H1, 1.50(3); B1–Ir1–C1, 168.22(8); B1–Ir1–C2, 64.71(8); C1–Ir1–C2, 103.51(8); C2–Ir1–P1, 96.56(5); C2–Ir1–P2, 95.06(5); P1–Ir1–P2, 152.371(18); N1–B1–Ir1, 87.72(11); N1–C2–Ir1, 103.93(13).....	153
Figure V-3. POV-Ray rendition of the ORTEP drawing (50% thermal ellipsoids) of 502 showing selected atom labeling. Hydrogen atoms are omitted for clarity with the exception of the hydrogen bound to iridium. Selected bond distances (Å) and angles (°): Ir1–B1, 2.621(3); Ir1–C1, 1.824(3); Ir1–H1, 1.64(3); Ir1–P1, 2.2929(6); Ir1–P2, 2.2801(6); C1–O1, 1.151(3); B1–C2, 1.630(4); B1–H1, 1.33(3); C1–Ir1–H1, 164.4(10); B1–Ir1–H1, 24.8(10); Ir1–B1–H1, 31.2(13); P1–Ir1–P2, 161.10(2); C2–B1–C9, 111.4(2); C2–B1–C14, 110.3(2); C9–B1–C14, 116.0(2).....	157
Figure V-4. POV-Ray rendition of the ORTEP drawing (50% thermal ellipsoids) of 501g showing selected atom labeling. Hydrogen atoms are omitted for clarity with the exception of the hydrogen bound to iridium. Selected bond distances (Å) and angles (°): Ir1–B1, 2.280(2); Ir1–C1, 1.921(2); Ir1–C2, 2.061(2); Ir1–P1, 2.2969(5); Ir1–P2, 2.2861(6); C1–O1, 1.148(3); N1–C2, 1.344(2); N1–B1, 1.635(3); Ir1–H1, 1.46(3); B1–Ir1–C1, 166.13(9); B1–Ir1–C2, 64.17(7); C1–Ir1–C2, 102.09(9); C2–Ir1–P1, 93.96(5); C2–Ir1–P2, 97.02(5); P1–Ir1–P2, 154.193(17); N1–B1–Ir1, 87.47(10); N1–C2–Ir1, 105.98(12).....	161

Figure V-5. $^{31}\text{P}\{^1\text{H}\}$ NMR spectrum of thermolysis of complex 502 in benzene for 2 h.	164
Figure V-6. $^{11}\text{B}\{^1\text{H}\}$ NMR spectrum of thermolysis of complex 502 in benzene for 2 h.	164
Figure V-7. $^{31}\text{P}\{^1\text{H}\}$ NMR spectrum after thermolysis of complex 502 for 1 h at 100 °C in C_6D_{12} followed by addition of pyridine.	166
Figure V-8. Hydride region of ^1H NMR spectrum after thermolysis of complex 502 for 1 h at 100 °C in C_6D_{12} followed by addition of pyridine.	166
Figure V-9. Kinetic plots of (a) [501c] vs. time; (b) $\ln[501c]$ vs. time.	179
Figure VI-1. ^1H NMR and $^{31}\text{P}\{^1\text{H}\}$ NMR spectra of 610a in C_6D_6 at RT measured on a 500 MHz Varian NMR spectrometer.	221
Figure VI-2. ^1H NMR and $^{31}\text{P}\{^1\text{H}\}$ NMR spectra of 610a in C_6D_6 at RT measured on a 500 MHz Varian NMR spectrometer.	222
Figure VI-3. ^1H NMR spectrum of 610d and 610d' in C_6D_6 at RT measured on a 500 MHz Varian NMR spectrometer.	223
Figure VI-4. ^1H NMR spectrum of 610e and 610e' in C_6D_6 at RT measured on a 500 MHz Varian NMR spectrometer.	224
Figure VI-5. ^1H NMR spectrum of the mixture resulting after treatment of 607, with Ni powder in CD_3CN at 100 °C for 15 h. The spectrum was measured at ambient temperature on a 500 MHz Varian NMR spectrometer. Signals corresponding to 607 (72% unreacted) and to tentatively assigned products highlighted.	226
Figure VII-1. (a) Active site of urease. (b) Active site of [NiFe]-hydrogenase. (c) Active site of the FeMo cofactor from nitrogenase.	228
Figure VII-2. Hydrolysis of urea mediated by hydroxide-bridged binuclear nickel complex. ²⁶⁵	228
Figure VII-3. Strategy of making binuclear bis-pincer complex with two non-equivalent metal centers.	229
Figure VII-4. ^{31}P NMR spectrum of complex 708-Ni and 707-Ni in an 85:15 ratio.	234
Figure VII-5. 2D ^1H - ^1H gCOSY spectrum of 709-Ni showing ^1H - ^1H correlations through bonds.	236

Figure VII-6. 2D ^1H - ^1H NOESY spectrum of 709-Ni showing ^1H - ^1H correlations through space.	237
Figure VII-7. POV-Ray rendition of the ORTEP drawing (50% thermal ellipsoids) of 709-Ni showing selected atom labeling. Hydrogen atoms and $\text{B}(\text{C}_6\text{F}_5)_4^-$ anion are omitted for clarity. Selected bond distances (Å) and angles (deg): Ni1-O3, 1.9270(18); Ni2-O3, 1.9300(19); Ni1-P1, 2.1647(10); Ni2-P2, 2.1683(12); Ni1-S1, 2.2223(12); Ni2-S2, 2.2238(13); Ni1-O3-Ni2, 131.19(10); P1-Ni1-S1, 166.05(3); P2-Ni2-S2, 164.99(3); O3-Ni1-S1, 89.85(6); O3-Ni2-S2, 93.08(5); O3-Ni1-P1, 101.86(7); O3-Ni2-P2, 99.07(6).	239
Figure VII-8. POV-Ray rendition of the ORTEP drawing (50% thermal ellipsoids) of 709-Pd showing selected atom labeling. Hydrogen atoms and $\text{B}(\text{C}_6\text{F}_5)_4^-$ anion are omitted for clarity. Selected bond distances (Å) and angles (deg): Pd1-O3, 2.097(2); Pd2-O3, 2.089(2); Pd1-P1, 2.2255(11); Pd2-P2, 2.2261(10); Pd1-S1, 2.3593(11); Pd2-S2, 2.3491(11); Pd2-O3-Pd1, 120.98(11); P1-Pd1-S1, 163.54(3); P2-Pd2-S2, 165.27(4); O3-Pd1-S1, 97.30(7); O3-Pd2-S2, 90.67(7); O3-Pd1-P1, 97.91(7); O3-Pd2-P2, 103.45(7).	240
Figure VII-9. Catalytic activity with various amounts of HBF_4	247
Figure VII-10. Catalytic activity with various amounts of KOH	249
Figure VII-11. Comparison of efficiencies for hydration of acetonitrile catalyzed by various metal complexes.	252

LIST OF TABLES

	Page
Table I-1. Various Types of 2c-2e Metal-Ligand Interaction	2
Table I-2. CO Stretching Frequencies Predicted by DFT Calculation ¹²	3
Table I-3. Structural Analysis of σ -Donating Abilities of Central Donors on PXP Pincer Complexes via Metric Data.....	5
Table I-4. Pt–Cl Distances Predicted by DFT Calculations of $[\text{XPtCl}(\text{PMe}_3)_2]^{23}$	6
Table I-5. Efficiency of Catalysts for Transfer Dehydrogenation of Cyclooctane	17
Table II-1. Ratios of 142, 202, 203 in CDCl_3 with Various Concentrations of Rh.....	53
Table II-2. Ratios of 204 and 205 in CDCl_3 with Various Concentrations of Rh.....	55
Table II-3. ^{11}B NMR and ^{31}P NMR Chemical Shifts of Ir and Rh Complexes (in ppm) and $^2J_{\text{Rh-P}}$ Values	56
Table II-4. Selected Bond Distances (\AA) and Angles ($^\circ$) of X-ray Crystal Structure and DFT Calculation of 206.....	59
Table II-5. Selected Bond Distances (\AA) and Angles ($^\circ$) of X-ray Crystal Structure and DFT Calculation of 207.....	60
Table II-6. Selected Bond Distances (\AA) and Angles ($^\circ$) of X-ray Crystal Structure and DFT Calculation of 209.....	65
Table III-1. $^{11}\text{B}\{^1\text{H}\}$ NMR, $^{31}\text{P}\{^1\text{H}\}$ NMR, ^{19}F NMR, and the Feature of $^{13}\text{C}\{^1\text{H}\}$ NMR Chemical Shifts of Rh Complexes (in ppm) and J values (in Hz)	96
Table IV-1. Chemical Shifts in $^{11}\text{B}\{^1\text{H}\}$ NMR and $^{31}\text{P}\{^1\text{H}\}$ NMR Spectra of Ir Complexes (in ppm)	130
Table IV-2. TONs for Dehydrogenation of COA to COE Catalyzed by (PBP)Ir(H) ₄ (401) and (PBP)Ir(Ph)(H) (402) ^a	137
Table V-1. Selective C–H Activation of Pyridines ^a	158
Table V-2. Reaction of Complex 404 with Pyridine under Ar or CO ^a	162
Table V-3. Selective C–H Activation of Pyridines by complex 404 or 502 ^a	173

Table V-4. Exchange Reaction of 501c to 501a ^a	178
Table V-5. ¹¹ B{ ¹ H} NMR, ³¹ P{ ¹ H} NMR, ¹ H NMR of Ir–H, and ¹³ C{ ¹ H} NMR of CO Chemical Shifts of Ir Complexes (in ppm), <i>J</i> Values (in Hz), and CO Stretching Frequencies (in cm ⁻¹)	180
Table V-6. ¹ H NMR Chemical Shifts of C3– <i>H</i> , C4– <i>H</i> , C5– <i>H</i> , and C6– <i>H</i> in Ir Complexes (in ppm) and <i>J</i> Values (in Hz)	181
Table VI-1. Screening and Optimization of the Reaction of Benzyl Halide with Halodi- <i>tert</i> -butylphosphine ^a	200
Table VI-2. Synthesis of Various PCP and PNP Ligands ^a	204
Table VII-1. Nitrile Hydration Catalyzed by Bis-pincer Complexes ^a	243
Table VII-2. Catalytic Activity with Various Amounts of HBF ₄ ^a	247
Table VII-3. Catalytic Activity with Various Amounts of KOH ^a	248
Table VII-4. Solvent Test for Nitrile Hydration Catalyzed by 709-Ni ^a	260

CHAPTER I

INTRODUCTION AND LITERATURE REVIEW

1.1 Pincer Ligands and Complexes

Pincer-ligated transition metal complexes have been designed and synthesized for the study of reactivity at the metal center, as well as applications in bond activation, organic transformation, and catalysis.¹⁻⁸ Pincer ligands are tridentate ligands that typically bind to a metal in a meridional configuration. Early examples can be tracked back to the 1970s when Shaw reported PCP-type pincer ligands containing two flanking neutral phosphine donors with an aryl-based (**1A**) or alkyl-based (**1B**) carbanionic central donor (Figure I-1).^{9,10}

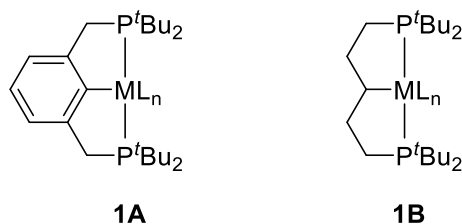


Figure I-1. Early examples of pincer complexes reported by Shaw.^{9,10}

Based on the classification of ligand type, the three donors of a pincer ligand can be either neutral (L-type) or anionic (X-type) (Table I-1).¹¹ A third-type of ligand, the Z-type, which accepts two electrons from the metal center, will be discussed in section 1.6. Considering the different binding modes with a wide range of donors that are available to coordinate with transition metals allows organometallic chemists to design and create

numerous pincer ligands with an extensive diversity. Among these, PXP-type pincer ligands have been broadly studied because the electronic properties and the reactivity of complexes are tunable by changing to different central X-type donors, including amido (**1C**), phosphide (**1D**), alkyl (**1E**), silyl (**1F**), or boryl (**1G**). (Figure I-2).

Table I-1. Various Types of 2c-2e Metal-Ligand Interaction

Type of ligand	Illustration	Donor type	Representative examples
L-type (neutral)	$M \leftarrow \text{O} \leftarrow :L$	2e donor	phosphine, CO, <i>N</i> -heterocarbene
X-type (anionic)	$M \leftarrow \text{O} \cdot X$	1e donor	amido, aryl, alkyl, hydrido
Z-type	$M : \rightarrow \text{O} Z$	2e acceptor	borane, aluminum, gallium

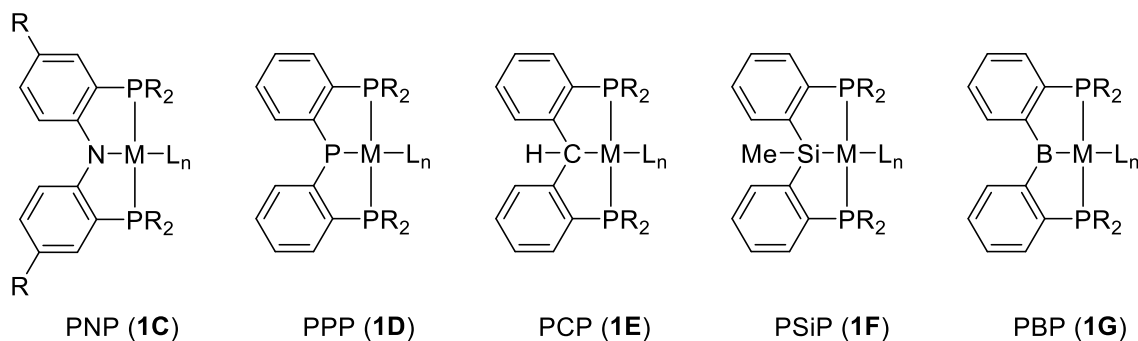


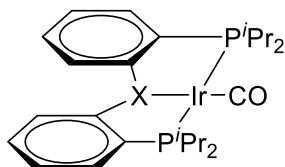
Figure I-2. PXP-type pincer complexes with various central anionic donors.

1.2 Electron-donating Ability of Central Donors on PXP-type Pincer Complexes

Electronic donor and acceptor ability regarding ligand-transition metal interactions can generally be divided into two types, which are σ - and π -contributions. For example, amido is a poor σ -donor but a good π -donor, whereas boryl is a strong σ -donor and a potential π -acceptor. The electron-donating ability of ligands can be measured or predicted

by an experimental analysis or DFT calculation of the stretching frequencies of CO on a PXP-type pincer iridium complex.¹² The more electron density the central ligand donates to the metal, the more π -back donation occurs to the antibonding orbital of carbonyl ligand (CO π^*), leading to a lower ν_{CO} IR stretching frequency. This comparison is particularly reliable for PXP-type iridium carbonyl complexes owing to all complexes adopting square-planar geometry with the CO trans to the central donor. The magnitude of this specific phenomenon is determined by the level of electron richness at the transition metal center, as dictated, usually, by the nature of the central donor in various PXP-type pincers. In Table I-2, it is clear that the donating abilities of central donors follows the decreasing order of B > Si(Me) > CH > P > N > P(=O) > P(=NPh) > P(=S).

Table I-2. CO Stretching Frequencies Predicted by DFT Calculation¹²



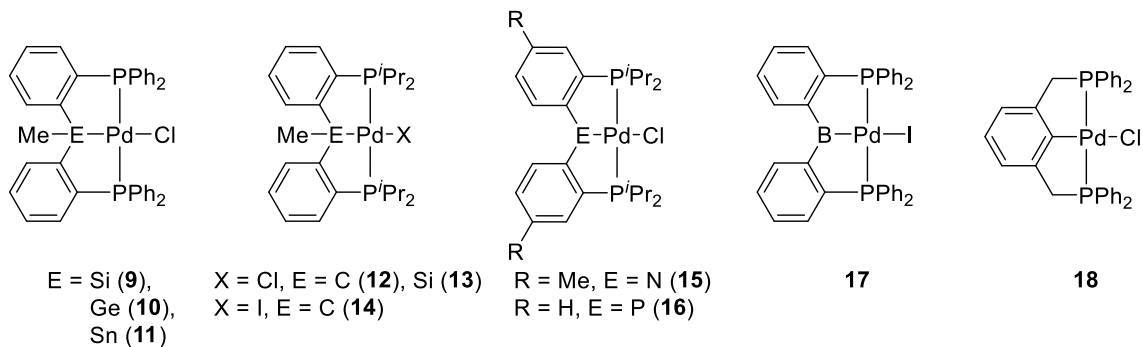
Entry	X	(PXP)Ir(CO)	ν_{CO} (cm ⁻¹)
1	B	1	2020.6
2	Si(Me)	2	2022.5
3	CH	3	2023.2
4	P	4	2026.5
5	N	5	2030.3
6	P(=O)	6	2039.3
7	P(=NPh)	7	2043.8
8	P(=S)	8	2044.3

Another method, which allows for measuring the σ -donating ability of the central donors, and therefore the extent of their trans influence, is to analyze complexes structurally in X-ray diffraction studies.¹³ Strong σ -donating ability of a central donor may significantly lengthen the bond distance between the metal and the trans ligand compared to those with a weaker σ -donor character.^{14,15} In Table I-3, all palladium complexes adopted square-planar geometry with a Cl trans to the central donors, allowing a systematic analysis for trans influence of the central donors.

For the group 14 elements, the PSiP pincer complex **9** exhibits a longer Pd–Cl bond distance (2.4414(17) Å) than those of the analogous PGeP and PSnP pincer complexes **10** and **11** (2.4219(11) Å and 2.4270(8) Å),¹⁶ demonstrating the stronger trans influence of the silyl central donor. The PCP pincer complex **12** displays a shorter Pd–Cl bond distance (2.407(1) Å)¹⁷ than the one in complex **13** (2.4572(6) Å),¹⁸ probably owing to the higher electronegativity of central carbon atom that preferably keeps the electron density on itself. The structural similarity is also presented by the group 15 elements that the Pd–Cl bond distance is shorter in the PNP pincer complex **15** bearing a central amido¹⁹ than in the PPP pincer complex **16** bearing a central phosphido²⁰ by ca. 0.10 Å. Based on this concept, the element from group 13 might be a better σ -donor than the one from group 14 and 15 due to a lower electronegativity if they are incorporated in a similar connectivity of ligand set. In 2016, Tauchert reported the synthesis of ^{Ph}(PBP)PdI (**17**)²¹ and demonstrated a stronger trans influencing boron center compared to ^{iPr}(PCP)PdI (**14**).¹⁷ The PCP complex **18** containing central phenyl donor²² displayed a weaker donating ability than the one in **12** bearing the aliphatic backbone.

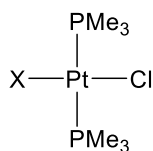
Table I-3. Structural Analysis of σ -Donating Abilities of Central Donors on PXP

Pincer Complexes via Metric Data



Entry	Central Donor	trans-halide	PXP pincer	Pd-X (Å)	Ref.
1	Si	Cl	9	2.4414(17)	16
2	Ge	Cl	10	2.4219(11)	16
3	Sn	Cl	11	2.4270(8)	16
4	C	Cl	12	2.407(1)	17
5	Si	Cl	13	2.4572(6)	18
6	C	I	14	2.6857(3)	17
7	N	Cl	15	2.3157(7)	19
8	P	Cl	16	2.4123(9)	20
9	B	I	17	2.7173(5)	21
10	C	Cl	18	2.313(5)	22

The trans influence of ligands have also been investigated theoretically by DFT calculations on a series of square-planar platinum complexes. By comparison of calculated Pt-Cl bond distances in a *trans*-[XPtCl(PMe₃)₂], the relative donating ability of X ligands can be analyzed.²³ In Table I-4, it revealed the following order of trans influence as BMe₂ > SiMe₃ > Bpin > Bcat > H > Me > Ph. By combination of DFT calculations and structural measurements, we can conclude the trans influence and electron-donating ability of ligands follow the order of boryl > silyl > hydrido > alkyl \approx phosphide > aryl > amido.

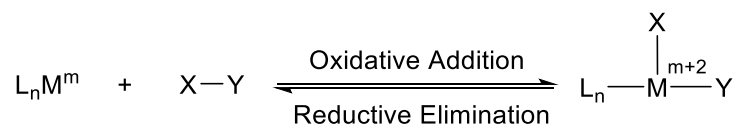
Table I-4. Pt–Cl Distances Predicted by DFT Calculations of [XPtCl(PMe₃)₂]²³

Entry	X	trans-[XPtCl(PMe ₃) ₂]	Pt–Cl (Å)
1	BMe ₂	19	2.608
2	Bpin	20	2.563
3	Bcat	21	2.542
4	SiMe ₃	22	2.594
5	Me	23	2.501
6	Ph	24	2.496
7	H	25	2.504

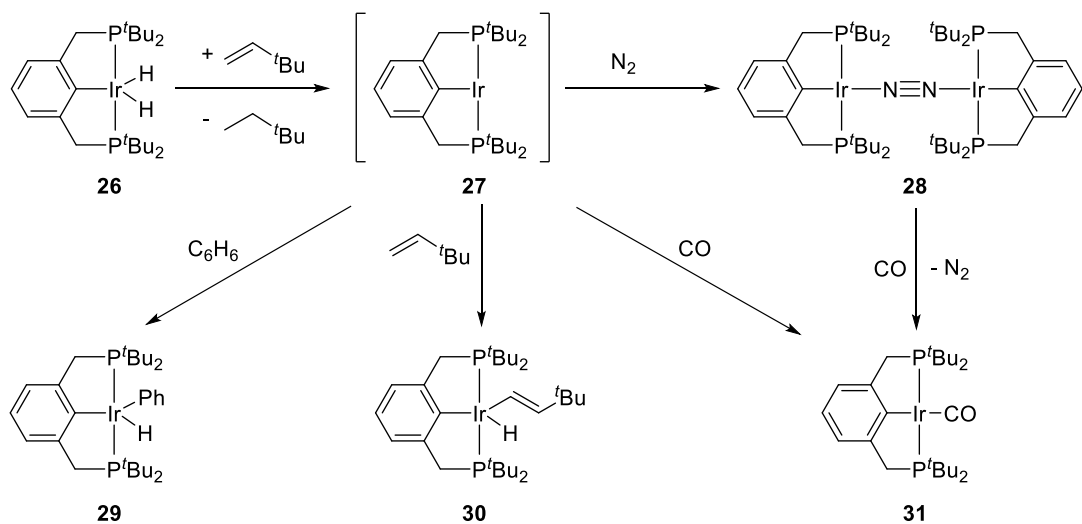
1.3 Reactivity of PXP-type Pincer Metal Complexes of Rh and Ir

1.3.1 Oxidative addition to PXP-type pincer complexes of Rh and Ir

Oxidative addition (OA) involves cleavage of a covalent X–Y bond across a metal center, with concomitant formation of corresponding M–X and M–Y bonds. This process results in an oxidation state increase of +2 at the metal. The reverse reaction is called reductive elimination (RE), which forms a covalent X–Y bond with an oxidation state decrease of 2 at the metal (Scheme I-1).

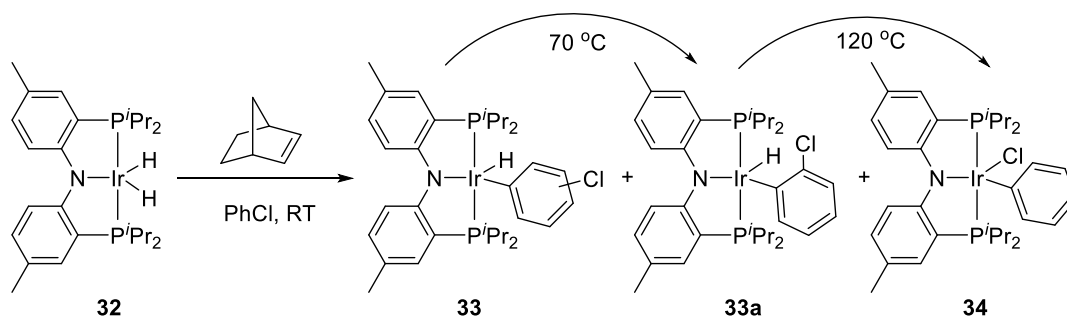
**Scheme I-1. General Equation of Oxidative Addition and Reductive Elimination**

Recently, the oxidative addition of X–H bond (X = C or a heteroatom) on the PXP-type pincer complexes of Rh and Ir has gained great attention because it is one of the steps toward various organic transformation and catalysis including cross-couplings, C–H functionalizations, and dehydrogenations. From the mechanistic view, a 14-electron, T-shaped Rh(I) or Ir(I) center is a plausible intermediate for the cleavage of X–H bond on the empty coordination site trans to the central X ligand of the pincer.^{24–26} Although the 14-electron species is difficult to isolate due to its high reactivity, it can be trapped by addition of π -accepting ligands to form a square-planar, 16-electron complex or addition of substrates to directly undergo oxidative addition. Early examples have been illustrated that dehydrogenation of (PCP)Ir(H)₂ (**26**) by the hydrogen acceptor *tert*-butylethylene (TBE) resulted in the formation of (PCP)Ir(I) intermediate **27**, which can bind with N₂ or CO to form the μ -dinitrogen complex **28** or carbonyl complex **31** (Scheme I-2).^{27,28} In the benzene solution, the reaction of **26** with TBE resulted in the formation of phenyl hydride complex **29** via oxidative addition of C–H bond of benzene. In the absence of benzene, the reaction of **26** with neat TBE afforded the vinyl hydride complex **30** via oxidative addition of trans C–H bond of TBE (Scheme I-2).²⁹



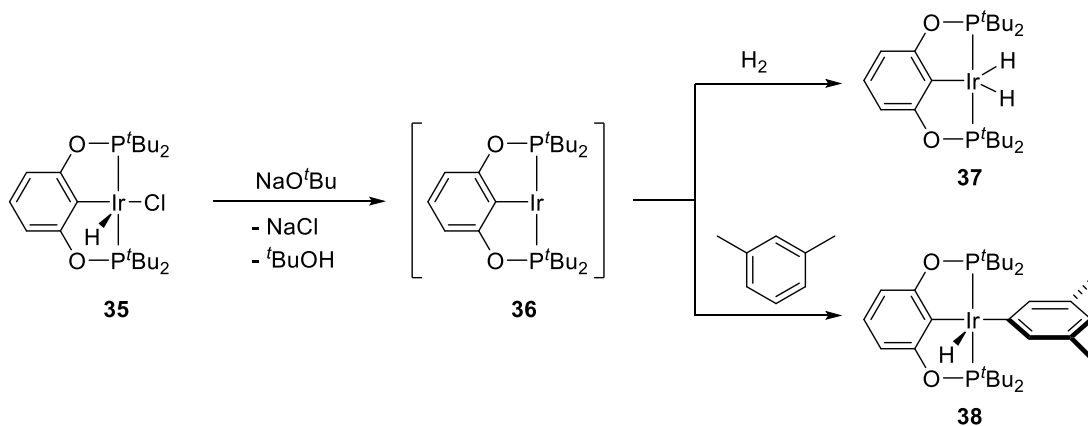
Scheme I-2. Transient Formation of (PCP)Ir(I) Intermediate^{27–29}

Oxidative addition of phenyl chloride to a (PNP)Ir(I) intermediate has been reported by the Ozerov group (Scheme I-3).³⁰ The reaction of **32** with norbornen (NBE) as a hydrogen acceptor in the presence of PhCl at room temperature resulted in a mixture of *ortho*, *meta*, *para*-selective C–H activation products **33** as the kinetic products. Among this mixture, the *ortho*-selective C–H activation product **33a** had the lowest energy. Thermolysis of the C–H OA mixture at 120 °C gave rise to the C–Cl OA product **34** as the thermodynamic product.



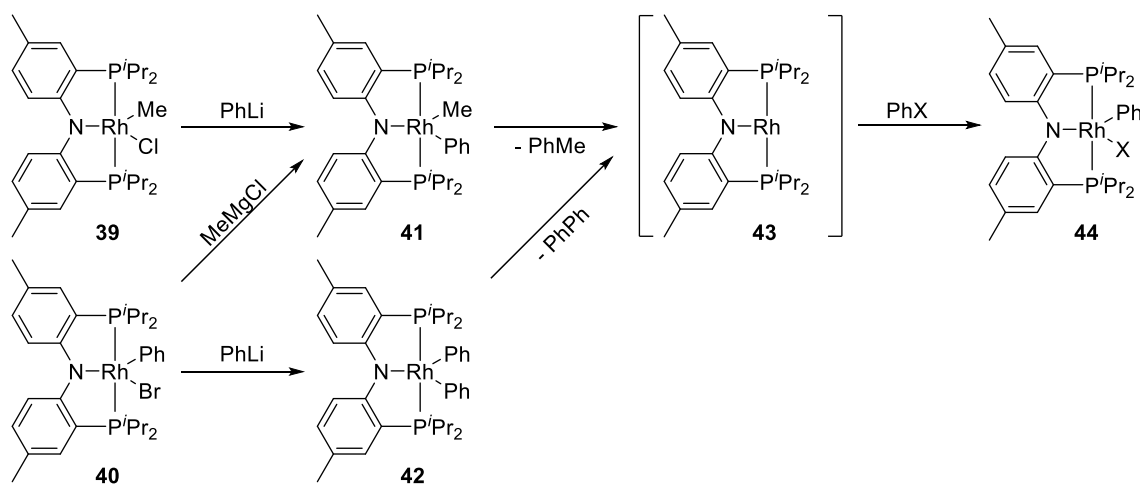
Scheme I-3. Kinetic C–H OA and Thermodynamic C–Cl OA on the (PNP)Ir(I)³⁰

The transient, three-coordinate, 14-electron intermediate (PXP)M (M= Rh, Ir) can conveniently be generated by dehydrochlorination of (PXP)M(H)(Cl) *via* addition of a strong base. Thus, the reaction of (POCOP)Ir(H)(Cl) (**35**) with NaO^tBu in the presence of hydrogen or *m*-xylene gave rise to (POCOP)Ir(H)₂ (**37**) or (POCOP)Ir(H)(*m*-xylyl) (**38**), suggesting the reactions were achieved through intermediate **36** (Scheme I-4).³¹



Scheme I-4. Synthesis of (POCOP)Ir(I) by Dehydrochlorination of 35³¹

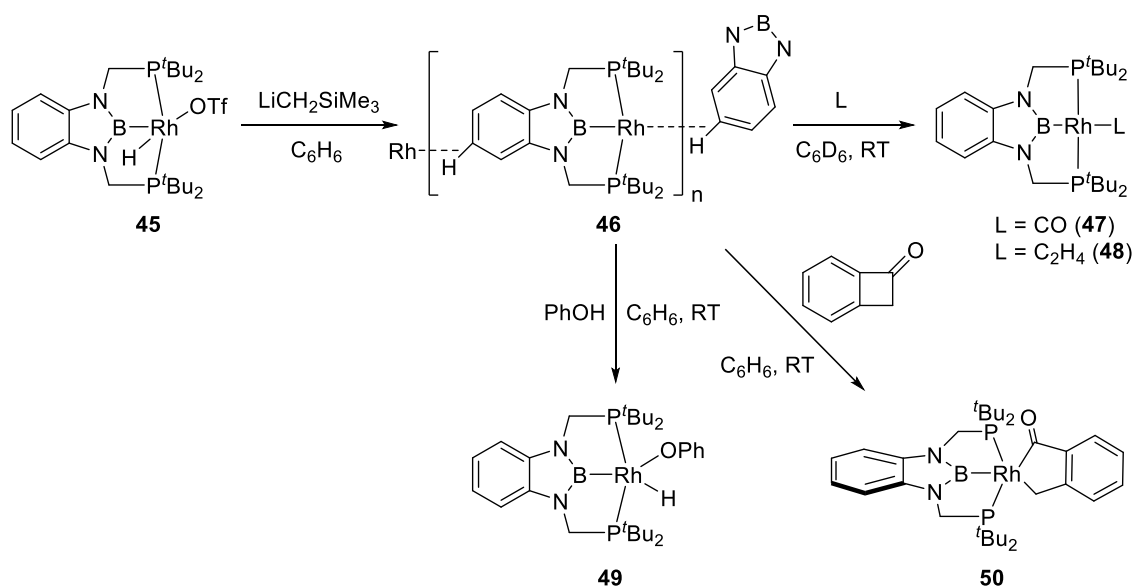
Another, orthogonal method to generate the three-coordinate intermediate is *via* reductive elimination of R–R' (R,R' = alkyl, aryl) from an *in situ* generated complex of the general formula (PXP)M(R)(R') (M = Rh, Ir). The Ozerov group has reported access to (PNP)Rh(I) *via* reductive elimination and concurrent C–C bond formation from (PNP)Rh(I) **39** *via* reductive elimination and concurrent C–C bond formation from (PNP)Rh(Ph)(Me) (**41**) or (PNP)Rh(Ph)(Ph) (**42**).³² Addition of PhLi to **39** or **40** produced **41** or **42**, from which the reductive elimination of toluene or biphenyl was observed for the formation of (PNP)Rh(I) **43**. In the presence of phenyl halide in the reaction, the C–X oxidative addition to **43** was occurred and gave rise to **44** as the final product (Scheme I-5).



Scheme I-5. Reductive Elimination of C–C Bond and Oxidative Addition of C–X Bond³²

In most cases, the 14-electron pincer iridium and rhodium complexes were only transient intermediates proposed on the basis of their reactivity. The stabilization of such

reactive key intermediate was closely approached by incorporation of a strong trans influencing boryl ligand on the PBP pincer to enforce the formation of low-coordinated, T-shaped structure.³³ The reaction of **45** with $\text{LiCH}_2\text{SiMe}_3$ in C_6H_6 induced the dehydrotriflation and led to the formation of (PBP)Rh(I) complex **46** (Scheme I-6). The X-ray diffraction study of **46** revealed the fourth ligand was the C–H bond from PBP ligand backbond as a weak σ -donor. However, in the C_6D_6 , d_{14} -methylcyclohexane, and d_8 -toluene, this intermolecular interaction may not exist or rapidly exchanged with solvent C–H bonds because the C_{2v} symmetry of **46** was exhibited even at -90°C in the NMR time scale. The (PBP)Rh(I) unit displayed the ability to bind a π -acceptor such as carbonyl and ethylene to form **47** and **48**, or undergo oxidative addition with phenol and benzocyclobutanone at room temperature to give the corresponding **49** and **50** via oxidative addition of the polar O–H or the strained C–C bond.^{33,34}



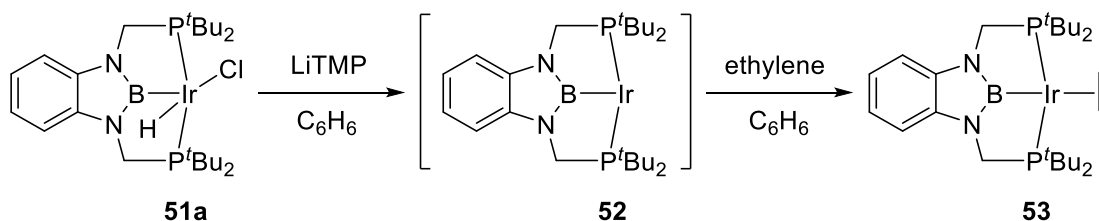
Scheme I-6. Synthesis of (PBP)Rh(I) and the Reactivity toward OA^{33,34}

1.3.2 Electronic effect on the thermodynamics of oxidative addition to (PXP)Ir(I)

In general, oxidative addition is favored by installing the strongly donating ligands on the metal center in order to stabilize the oxidizing form of metal complex. However, it is not entirely true for the case of oxidative addition of X–H bond (X = C or a heteroatom) to a 14-electron, T-shaped PXP-type pincer complex, which is an assumed intermediate for the bond activation reaction. In the early computational study, the methane C–H activation by trans-Ir(PH₃)₂(X) complexes (X = H, Cl) revealed the reaction was thermodynamically favored with a weaker central σ -donor (X = Cl) than a stronger central σ -donor (X = H).³⁵ Recently, a more systematic study by the Goldman group also demonstrated oxidative addition of C–H bond of methane to trans-(PH₃)₂IrX strongly disfavored thermodynamically by more σ -donating ligand X.³⁶ The explanation can be simply rationalized based on the orbital interactions. Oxidative addition of C–H bond to metal center required electron density transfer from non-bonding metal d-orbitals to two reduced fragments (for C–H OA of methane, methyl and hydrido are two reduced ligands). One of the incoming ligands shared the same orbital with the central X-type ligand to form a 3c-2e bond, which was disfavored by the stronger σ -donation of central ligand.

This calculation is supported by the previously reported experimental observation that the oxidative addition of vinyl or aryl C–H bond was more accessible by the PCP or PNP pincer complex of iridium with a weaker central aryl or amido σ -donor than the PBP pincer complex of iridium with a stronger central boryl σ -donor. The sp² C–H activations of benzene and TBE were successfully achieved by the reaction of (PCP)Ir(H)₂ (**26**) with hydrogen acceptor in the benzene or neat TBE solution (Scheme I-2).²⁹ In comparison,

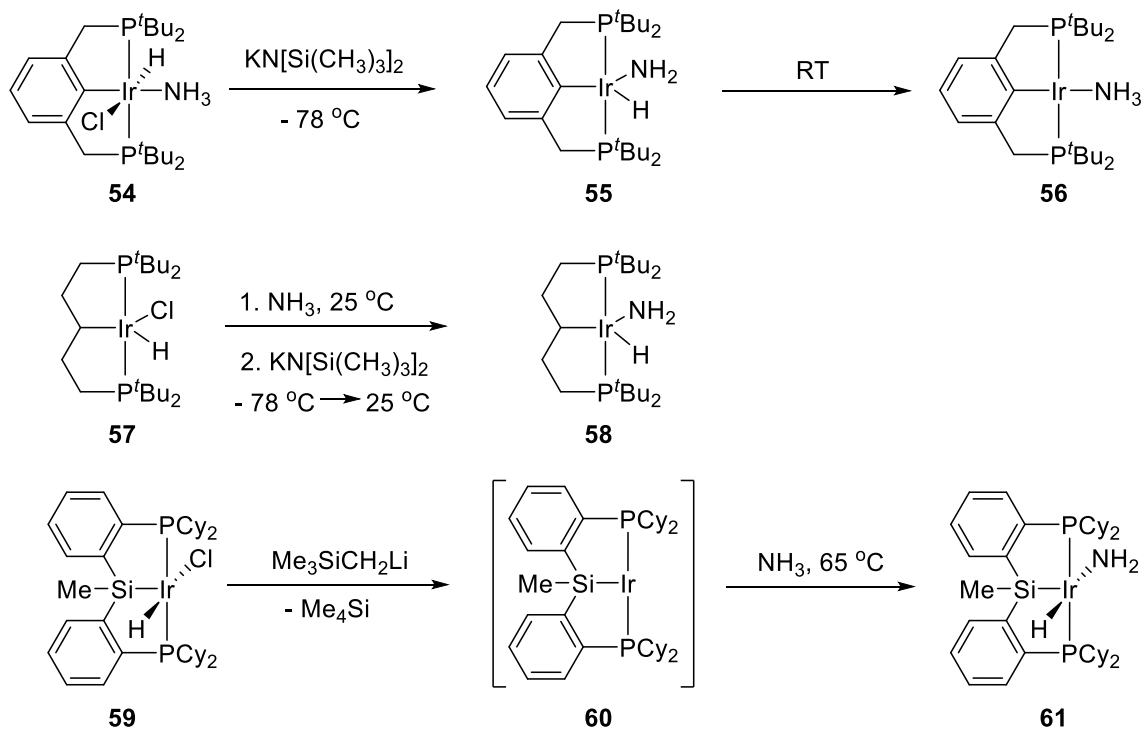
only the ethylene-coordinated boryl complex **53** was afforded by the reaction of (PBP)Ir(H)(Cl) (**51a**) with LiTMP in benzene under an ethylene atmosphere (Scheme I-7).³⁷ The C–H activation of ethylene or benzene by the (PBP)Ir(I) intermediate **52** was not observed.



Scheme I-7. Synthesis of Ethylene-coordinated Boryl Complex³⁷

Unlike oxidative addition of C–H bonds to form alkyl and aryl hydride complexes, oxidative addition of N–H bond of ammonia to a 14-electron Ir(I) center leading to a stable amido hydride complex was more thermodynamically favorable by a stronger σ -donating central ligand. The dehydrochlorination of **54** by KN[Si(CH₃)₂] at –78 °C led to the formation of N–H activation product **55**, which was stable below –10 °C but instantly generated ammonia complex **56** at room temperature by reductive elimination of N–H bond from amido hydride complex **55** (Scheme I-8, top).²⁵ Thus, the ammonia complex **56** had a greater thermodynamic stability than the corresponding amido hydride complex **55** with an aryl-based PCP pincer ligand. In comparison, by incorporation of a aliphatic-based PCP pincer ligand with a stronger central alkyl donor, the N–H activation was achieved by the reaction of **57** with KN[Si(CH₃)₂] in the presence of ammonia to form the

amido hydride complex **58** even after warming up to room temperature (Scheme I-8, middle).²⁶ The thermodynamically stable amido hydrido complex **61** with a strongly σ -donating silyl ligand was reported by Turculet (Scheme I-8, bottom).³⁸



Scheme I-8. Thermodynamic Stability of Amido Hydride Complexes vs. Ammonia Complexes^{25,26,38}

On the basis of DFT calculations by Goldman,³⁶ the oxidative addition of N–H bond of ammonia to form an amido hydride complex of iridium was more unfavorable thermodynamically with a stronger central σ -donor of PXP pincer ligand. This trend is consistent with the oxidative addition of methane C–H bond to a PXP pincer iridium complex. However, the formation of an ammonia complex even more disfavored

thermodynamically than the formation of an N–H addition product with a stronger central σ -donor, and this energy compensation allowed the N–H addition product favored while increasing σ -donation of central ligand.

1.4 Transfer Dehydrogenation of Alkanes Catalyzed by PXP-type Ir Complexes

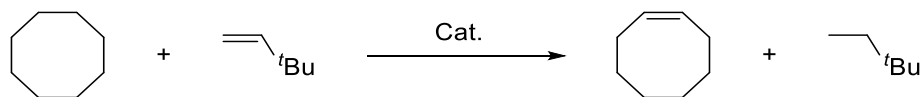
Dehydrogenation of alkanes into alkenes is of great interest because alkenes are very important feedstocks in industrial reactions including transition-metal-catalyzed olefin polymerization,^{39–44} hydroformylation,^{45–47} and oligomerization.^{48–50} The large scale synthesis of alkenes via dehydrogenation of alkanes is mainly catalyzed by heterogeneous catalysts at high temperatures (ca. 450–900 °C), and the methodologies are only suitable for the simple molecules (eg. propane to propylene, butane to butadiene, and ethylbenzene to styrene) owing to the poor selectivity.^{51,52} In comparison, homogeneous catalysis of alkane dehydrogenation typically requires relatively lower temperature (<220 °C) with higher selectivity. The following literature review is mainly focused on the transfer dehydrogenation of alkanes catalyzed by PXP-type iridium complexes, with the comparison of catalytic effectiveness by various central X ligands.

1.4.1 Early examples of catalytic dehydrogenation of alkanes

One of the homogeneous catalytic systems, so-called transfer dehydrogenation of alkane, were pioneered and established independently by the Felkin^{53–55} and Crabtree^{56–58} groups, using cycloalkane (eg. cyclooctane) as a model substrate and *tert*-butylethylene (TBE) as a hydrogen acceptor to screen the effectiveness of catalysts. Crabtree noted the

presence of TBE was essential to make the process thermodynamically favorable, and the absence of allylic hydrogen on TBE avoided the formation of stable allyl complex via allylic C–H activation. The bulkiness of TBE also prevented the deactivation of catalysis from strong binding to the metal.^{59,60}

Efficiency of early catalysts prior to pincer complexes for transfer dehydrogenation of COA in the presence of TBE was summarized in Table I-5. The first successful catalysis reported by the Felkin group demonstrated the reaction can be catalyzed by $[(p\text{-FC}_6\text{H}_4)_3\text{P}]_2\text{ReH}_7$ (**62**) with a turnover number of 1.6 at 30 °C and up to a turnover number of 9 at 80 °C (entry 1).⁵³ The follow-up study reported by the same group showed iridium and ruthenium hydrides (**63** and **64**) were active catalysts for transfer alkane dehydrogenation (entry 2 and 3) and **63** was the most effective complex with a turnover number of 70 at 150 °C for 5 days.⁴³ From the independent research, Crabtree reported the transfer alkane dehydrogenation catalyzed by $(\text{PR}_3)_2\text{Ir}(\text{CF}_3\text{CO}_2)\text{H}_2$ (R = *p*- FC_6H_4 (**66**) and cyclohexyl (**67**)) both thermally and photochemically with relatively lower turnover numbers (entry 5~8).⁵⁷ Interestingly, the photochemical dehydrogenation of alkane was achieved even without hydrogen acceptor.

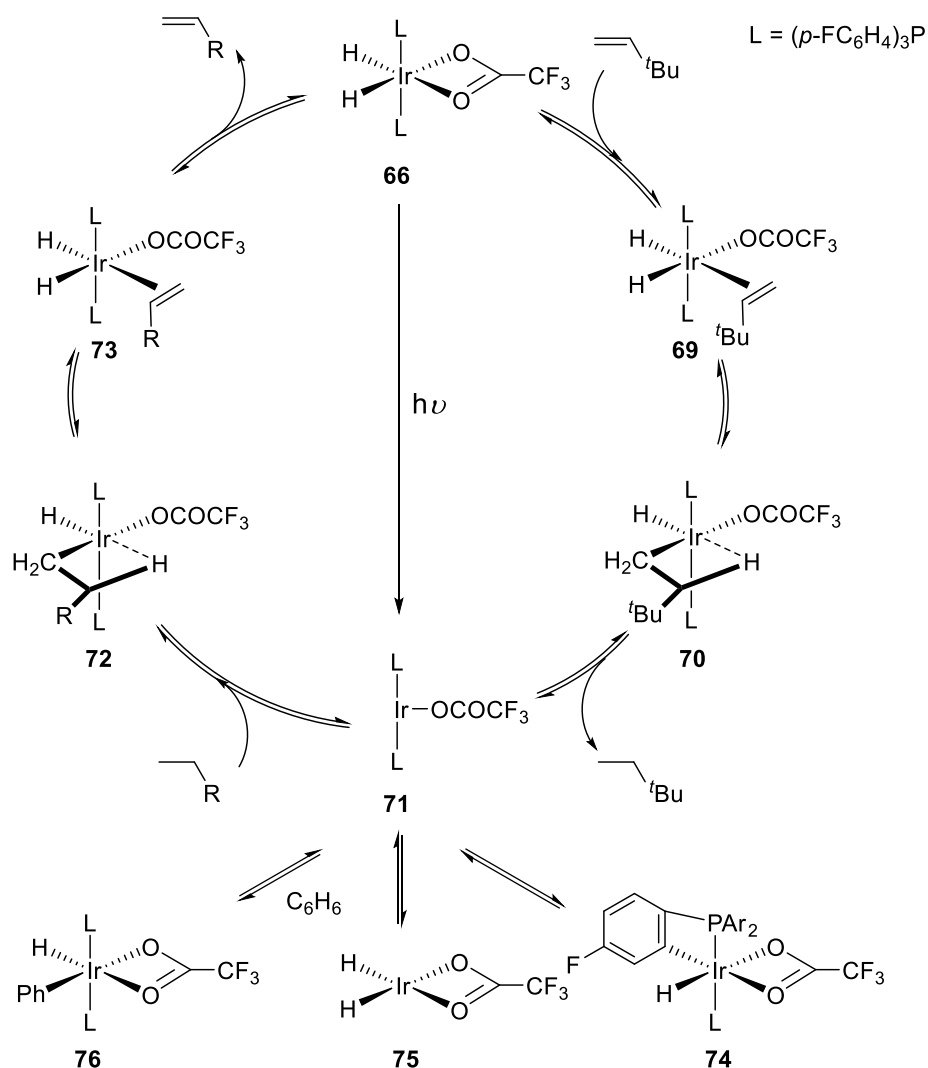
Table I-5. Efficiency of Catalysts for Transfer Dehydrogenation of Cyclooctane

Entry	Catalyst		Condition	TONs	Ref.
1	[(<i>p</i> -FC ₆ H ₄) ₃ P] ₂ ReH ₇	62	80 °C, 10 min	9	53
2	(<i>i</i> Pr ₃ P) ₂ IrH ₅	63	150 °C, 5 d	70	54
3	[(<i>p</i> -FC ₆ H ₄) ₃ P] ₃ RuH ₄	64	150 °C, 10 d	45-55	54
4	[(<i>p</i> -FC ₆ H ₄) ₃ P] ₂ IrH ₅	65	150 °C, 5 d	30-35	54
5	[(<i>p</i> -FC ₆ H ₄) ₃ P] ₂ Ir(CF ₃ CO ₂)H ₂	66	150 °C, 2 d	16	57
6	(Cy ₃ P) ₂ Ir(CF ₃ CO ₂)H ₂	67	150 °C, 2 d	2	57
7	(Cy ₃ P) ₂ Ir(CF ₃ CO ₂)H ₂	67	<i>hν</i> , 7 d	28	57
8 ^a	(Cy ₃ P) ₂ Ir(CF ₃ CO ₂)H ₂	67	<i>hν</i> , 7 d	7	57
9	(<i>i</i> Pr ₃ P) ₂ Ir(Cl)H ₂	68	150 °C, 2 d	4	61

a. Without hydrogen acceptor.

The detailed mechanistic study of transfer dehydrogenation of alkane catalyzed by **66** are shown in Scheme I-9.⁵⁸ In the first step, the conversion of κ^2 -OCOCF₃ complex **66** to κ^1 -OCOCF₃ complex and subsequently association of TBE gave rise to TBE adduct **69**. The equilibrium of TBE adduct **69** and **66** at -80 °C was observed with $K_{eq} = 0.58$, which is much lower than the COE adduct ($K_{eq} = 5500$), reflecting the steric bulk of *tert*-butyl group of TBE. Dehydrogenation of **69** took place at 25 °C by insertion of TBE into Ir–H bond followed by reductive elimination of TBA (2,2-dimethylbutane), resulting in the proposed 14-electron intermediate **71**. The intermediate **71** was capable of activating aromatic C–H bond of the phosphine ligand or benzene to form **74** and **76**, respectively. Therefore, the oxidative addition of aliphatic C–H bond to iridium center was achieved in the presence of cycloalkane as solvent at required temperature. Finally, the corresponding alkyl hydride complex **72** underwent β -hydride elimination and subsequently dissociation

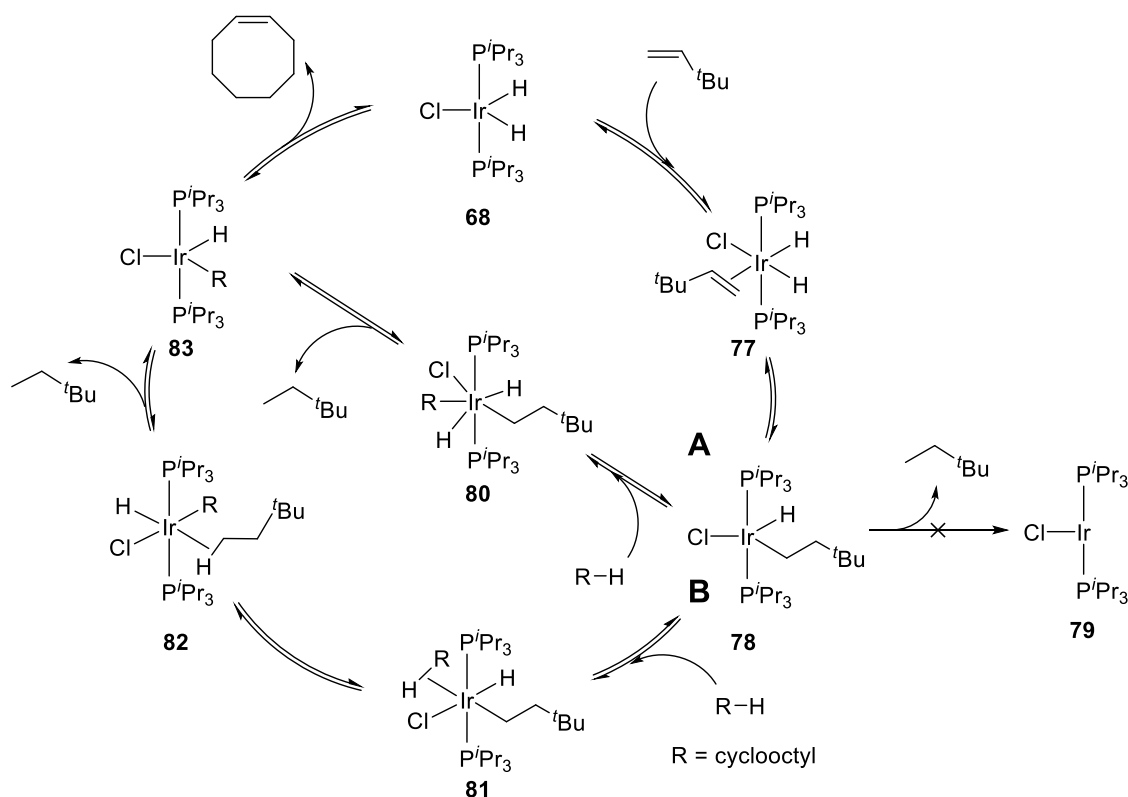
of alkene from **73** to regenerate the catalyst. For the photochemical catalysis, the mechanism was proposed as similar as the thermal catalysis except that the dehydrogenation of **66** was induced by light irradiation to form the 14-electron intermediate **71**. This proposal was evidenced by the reaction was achievable by photo irradiation without addition of hydrogen acceptor.



Scheme I-9. Proposed Mechanism of Alkane Dehydrogenation Catalyzed by **66⁵⁸**

It is accepted the transfer dehydrogenation catalyzed by $(\text{Cy}_3\text{P})_2\text{Ir}(\text{CF}_3\text{CO}_2)\text{H}_2$ (**67**) and $(i\text{Pr}_3\text{P})_2\text{IrH}_5$ (**63**) go through the same mechanism as **66** via the oxidative addition of alkane C–H bond to the 14-electron $(\text{PR}_2)\text{IrX}$ fragment with different X donor (H^- vs. CF_3CO_2^-). However, comparing the catalytic activity of **67** with **63**, the former was obviously less reactive, possibly owing to the bulkiness of Cy_3P and the potential $\kappa^2\text{-CF}_3\text{CO}_2^-$ donor to form a stable intermediate.

As mentioned in Section 1.3.2, oxidative addition of C–H bonds to a 14-electron $(\text{PR}_2)\text{IrX}$ is more thermodynamically favorable with a weakly donating X central ligand. In order to favor the oxidative addition process, Jensen reported the transfer alkane dehydrogenation catalyzed by $(i\text{Pr}_3\text{P})_2\text{IrClH}_2$ (**68**),⁶¹ which was assumed to form a very reactive $(P^i\text{Pr}_3)_2\text{IrCl}$ fragment toward C–H bond activation compared to the analogous complex **63**.³⁵ However, only a turnover number of 4 of cyclooctane to cyclooctene occurred at 150 °C for 2 days (Table I-5, entry 9). In a more detailed study, **68** catalyzed the dehydrogenation of alkanes through different mechanisms (Scheme I-10). Unlike **63**, the reaction of **68** with neat TBE gave rise to alkyl hydride complex **78**, which was incapable of reductive elimination of TBA to form 14-electron species **79** at 150 °C. In comparison, the addition of alkane (cyclooctane, cyclohexane, and *n*-nonane) as solvent induced the reductive elimination of TBA catalytically during heating. Therefore, Jensen proposed two possible pathways: (A) oxidative addition of cyclooctane to **78** gave rise to the Ir(V) intermediate **80**, or (B) association of cyclooctane induced reductive elimination of TBA. Both pathways led to the formation of cyclooctyl hydride complex **83**, and subsequently β -hydride eliminated COE to regenerate catalyst.



Scheme I-10. Proposed Mechanism of Transfer Dehydrogenation of Alkane Catalyzed by **68**⁶¹

1.4.2 Pincer Ir complexes mediated catalytic dehydrogenation of alkanes

Efficiencies of various pincer complexes for catalytic transfer dehydrogenation of cyclooctane in the presence of TBE as hydrogen acceptor were summarized in Figure I-3. In 1996, Kaska and Jensen first introduced PCP-type pincer complex of iridium **26** as an efficient catalyst for the transfer alkane dehydrogenation of COA to COE.⁶² Up to a turnover number of 1000 was achieved at the rate of 12 turnovers min⁻¹. The successful result compared to the early work (Section 1.4.1) was attributed to the thermal stability of pincer complex, which displayed no sign of complex decomposition at 200 °C for one

week. The thermostable pincer complexes allow to accelerate the reaction rates by activation of the less reactive alkane C–H bonds and elimination of hydrogenated alkane product at high temperature.

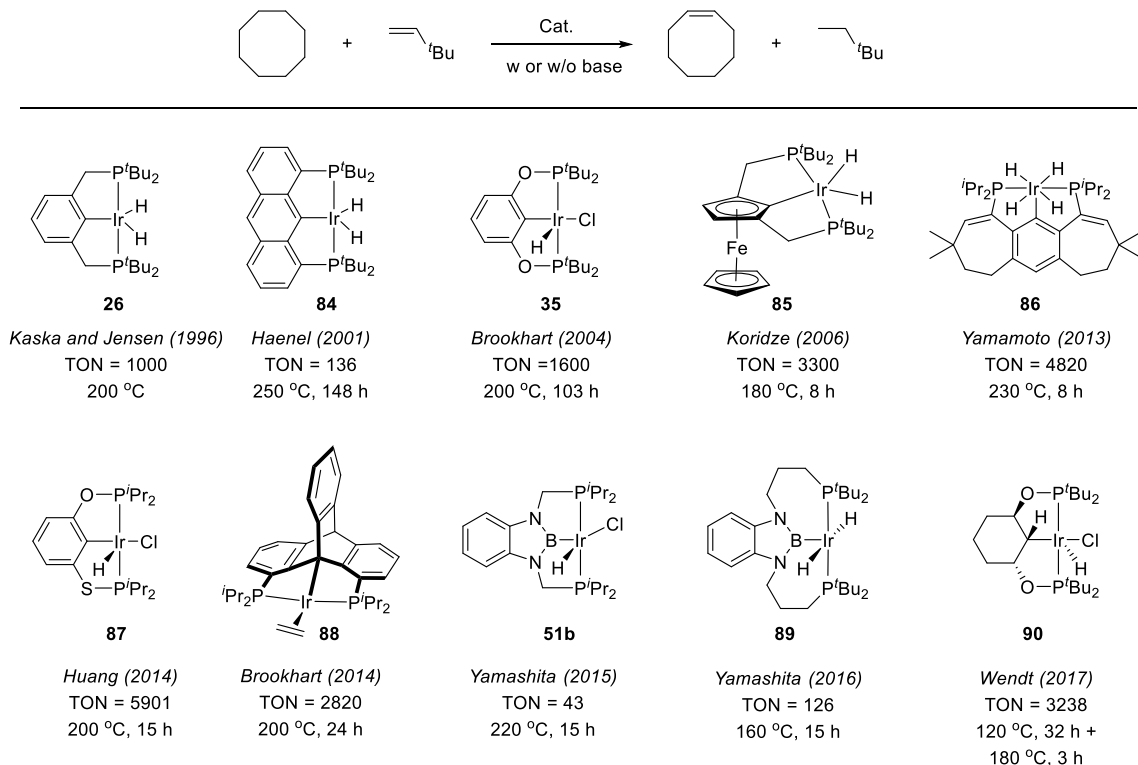


Figure I-3. Efficiencies of various pincer complexes for catalytic transfer dehydrogenation of COA to COA with TBE as hydrogen acceptor.

Although **26** displayed the excellent thermal stability compared to most of organometallic compounds, the decomposition was still observable at 250 °C over time.⁶³ In order to test the reactivity with more thermostable pincer complex, Haenel synthesized the anthracene-based PCP complex **84** and demonstrated **84** catalyzed transfer

dehydrogenation at 250 °C for 148 h without decomposition of catalyst, albeit with only a turnover number of 136.⁶⁴ The relatively lower activity of catalysis by **84** compared to **26** were simply rationalized by *accessible molecular surface (ams)*. The calculated size of *ams* at Ir center is 5.6 Å (1258 conformers) for **26**, but only 3.5 Å (50 conformers) for **84**. Interestingly, the efficiencies of alkane dehydrogenation catalyzed by PCP-type pincer complexes were greatly controlled sterically by *ams*. For example, the POCOP pincer complex **35** reported by Brookhart⁶⁵ and ferrocene-based PCP pincer complex **85** reported by Koridze⁶⁶ both displayed higher catalytic activities (TONs of 1600 for **35** and 3300 for **85**) than PCP pincer complex **26** in the benchmark COA/TBE transfer alkane dehydrogenation. DFT calculations demonstrated the iridium center of **26** was more sterically hindered than that of **35**, leading to a lower catalytic activity.⁵ In the X-ray diffraction studies of (PCP)Ir(CO) (**31**), (POCOP)Ir(CO) (**91**), and ferrocene-based (PCP)Ir(CO) **92**, the P–Ir–P angle in **91** (157.55(3)°) and **92** (157.91(3)°) are smaller than the one in **31** (164.510(8)°), likely resulting from the short P–O bonds in POCOP ligand and ring strain of cyclopentadienyl group in ferrocene-based PCP ligand.⁶⁶ The smaller P–Ir–P angle caused the Ir center more open and sterically accessible for substrates, resulting in higher catalytic activities for **35** and **85** than **26** (Figure I-4).

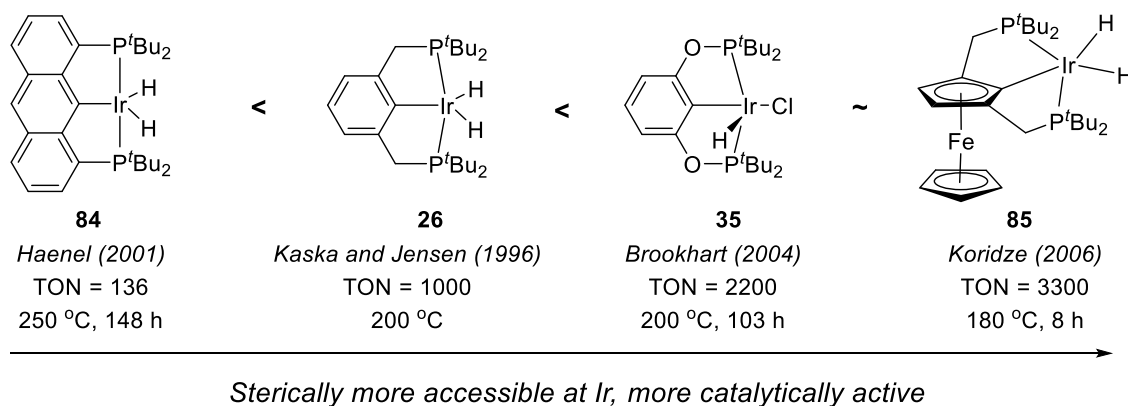


Figure I-4. Sterically controlled catalytic activity for alkane dehydrogenation.

Other types of PCP pincer complexes of iridium such as 7-6-7 ring-based pincer complex **86**⁶⁷ and PSCOP pincer complex **87**⁶⁸ were used as efficient catalysts for transfer dehydrogenation of COA to COE with very high turnover numbers (Figure I-3). Among these catalysts, **87** was the most active catalyst with up to a turnover number of 5901.⁶⁸ Pincer complexes of iridium with a stronger trans influence and σ -donating central ligand were also employed for such reaction. On the basis of mechanistic study by Goldman, the rate-determining step in alkane transfer dehydrogenation catalyzed by **26** is the reductive elimination of hydrogenated alkane product TBA.⁶⁹ Hence, incorporation of a strong central σ -donor such as alkyl or boryl on pincer complexes may facilitate the C–H elimination process³⁶ and improve the catalytic activity. Brookhart⁷⁰ and Wendt⁷¹ independently reported transfer dehydrogenation catalyzed by PC(sp³)P pincer iridium complex **88** and **90** with turnover numbers of 2820 and 3238. Yamashita reported the synthesis of PBP and long-tethered P–B–P iridium complexes **51b** and **89**, which applied in transfer dehydrogenation of alkane with moderate activities.^{72,73}

1.5 Pincer Complexes Bearing a Central Boryl Ligand

Since first pincer ligand designed and synthesized by Shaw in 1976,⁹ the chemistry of pincer ligands with the various central anionic donors (${}^{-}\text{CX}_3$, ${}^{-}\text{NX}_2$, ${}^{-}\text{PX}_2$ etc.) have been vastly expanded and applied in organic transformation and catalysis. Among these, the central boryl donor (${}^{-}\text{BX}_2$) is the latest element to incorporate into such a structure and possibly the strongest σ -donor and the strongest trans influence ligand. Before 2016, the boron-containing pincer complexes were mainly subdivided into two classes, diaminoboryl pincer complexes (**1H**) and carborane-derived pincer complexes (**1I**) according to their structures. In 2016, the Ozerov group reported the third-type boron-containing pincer complexes (**1J**) featuring bis(phosphine)/diarylboryl structure (Figure I-5). The synthesis and chemistry of these three types of pincer metal complexes with a central boryl ligand will be discussed in the sequence.

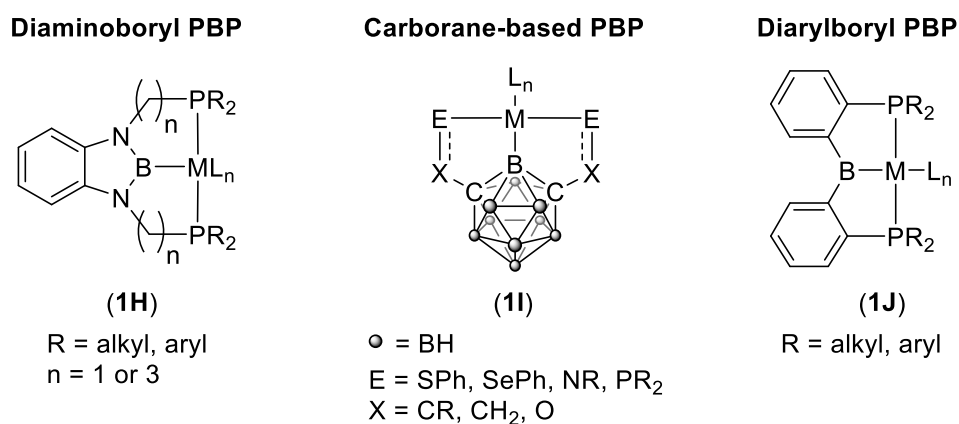
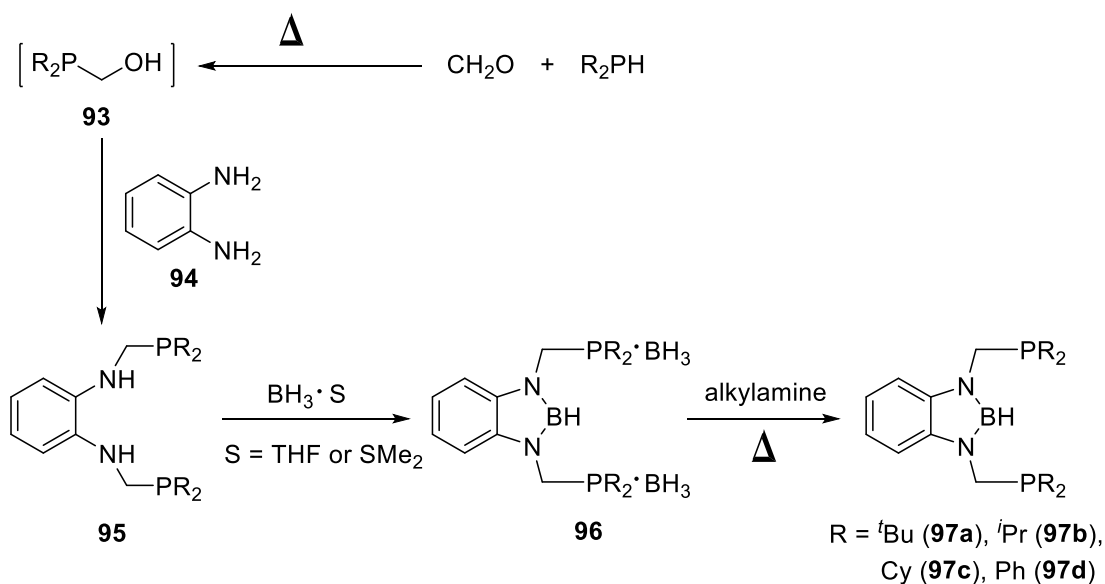


Figure I-5. Pincer metal complexes with a central boryl X-type donor.

1.5.1 Diaminoboryl-based pincer complexes

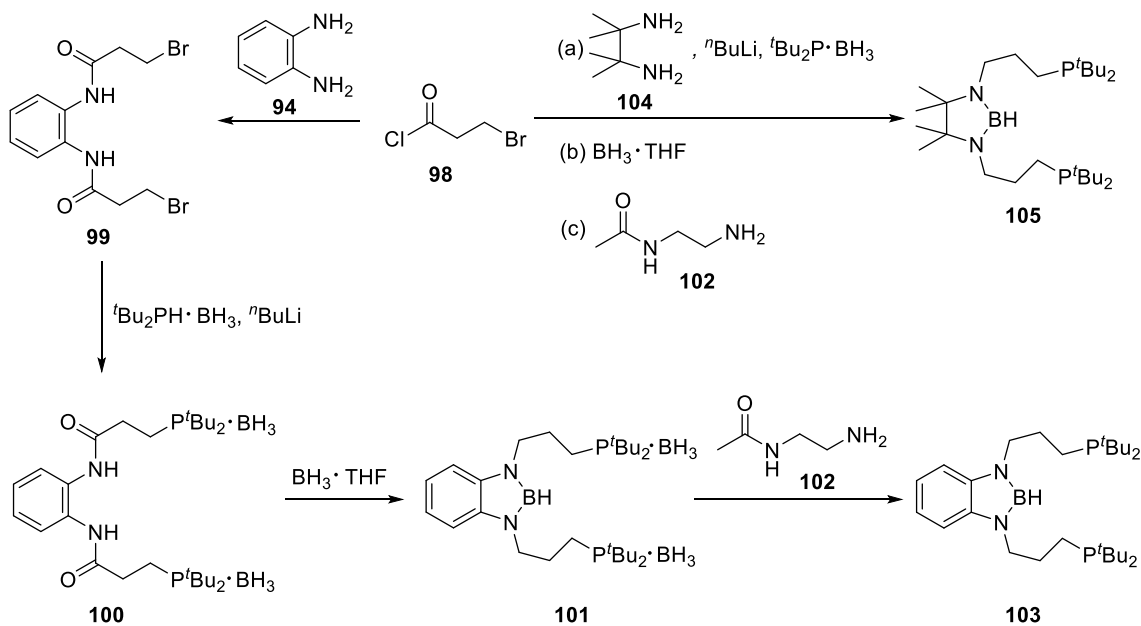
The diaminoboryl PBP pincer ligand was designed and synthesized by Yamashita and Nozaki in 2009 (Scheme I-11).³⁷ The reaction of formaldehyde with secondary phosphine gave rise to phosphinomethanol (**93**) *in situ*, which was condensed with *ortho*-phenylenediamine (**94**) to form 1,2-bis(phosphinomethylamino)benzene derivatives **95**. Treatment of $\text{BH}_3 \cdot \text{THF}$ or $\text{BH}_3 \cdot \text{SMe}_2$ to **95** resulted in the formation of five-membered diaminoborane **96** with coordination of BH_3 to phosphine. Removal of BH_3 by addition of alkylamine afforded the desired PBP ligands **97a~97d**.



Scheme I-11. Synthesis of Diaminoboryl-based Pincer Ligands³⁷

In 2016, the long-tethered P–B–P pincer ligand was also synthesized by Yamashita (Scheme I-12).^{73,74} The reaction of 3-bromopropionyl chloride (**98**) with *ortho*-phenylenediamine (**94**) gave rise to *N,N'*-(1,2-phenylene)bis(3-bromopropanamide) (**99**),

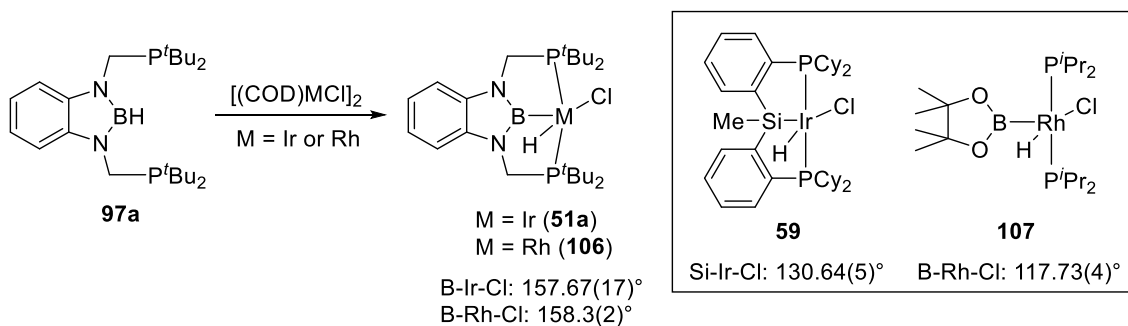
which reacted with di-*tert*-butylphosphinoborane and *n*-BuLi and subsequently introduced BH₃·THF to afford five-membered diaminoborane **101** with the phosphine protected by BH₃ and tethered by propylene group on the nitrogen. Removal of BH₃ by *N*-acetyethylenediamine (**102**) resulted in the formation of desired P–B–P pincer ligand **103**. The similar P–B–P pincer ligand **105** with an aliphatic tetramethylethylene backbone was synthesized via the similar procedure with **98** and 2,3-dimethylbutane-2,3-diamine (**104**) as the starting materials.



Scheme I-12. Synthesis of the Long-tethered P–B–P Ligands^{73,74}

The synthesis of PBP pincer complexes of iridium^{37,72,74,75} and rhodium^{33,76} was reported by Yamashita and Nozaki. The reaction of the diaminoboryl PBP ligand **97a** with [(COD)MCl]₂ (M = Ir or Rh) gave rise to (PBP)Ir(H)(Cl) (**51a**)³⁷ or (PBP)Rh(H)(Cl)

(**106**)³³ via oxidative addition of B–H to metal (Scheme I-13). In the X-ray diffraction studies of complex **51a** and **106**, the hydrides were located by Fourier difference map and were shown leaning toward boron atom with a bent B–M–Cl angle (157.67(17)° for **51a** and 158.3(2)° for **106**). This type of structures is similar with the complex **59** with a bent Si–Ir–Cl angle of 130.64(5)° and the complex **107** with a bent B–Rh–Cl angle of 117.73(4)° reported independently by Turculet⁷⁷ and Marder.⁷⁸ The Si–H distance (2.24(5) Å) of **59** is shorter than the sum of the van Der Waals radii (3.3 Å), but longer than the typical σ -silane complexes of ruthenium (ca. 1.7~2.0 Å).⁷⁹ In those iridium complexes, the small $^2J_{\text{Si-H}} (< 10 \text{ Hz})$ of complex **59** and no observable B–H coupling of complex **51a** in solution NMR spectra suggested there is no or little Si–H and B–H interaction. In comparison, a modest residual B \cdots H interaction was found in those rhodium complexes **106** and **107**. In complex **106**, a doublet of triplets hydride resonance was broaden in ^1H NMR spectrum but sharpen in $^1\text{H}\{^{11}\text{B}\}$ NMR spectrum, indicating the hydride was coupled to ^{11}B with a residual B \cdots H interaction. In the single crystal X-ray and neutron diffraction studies, a short B–H distance (2.013(5) Å) in complex **107** was confirmed by accurately locating the hydride position,⁸⁰ but still longer than the distances in the typical σ -borane complexes (ca. 1.2~1.5 Å),^{81–84} indicating the formulation is close to boryl hydride complex with a modest B \cdots H interaction as type B (Figure I-6).



Scheme I-13. Synthesis of (PBP)M(H)(Cl) (M = Ir or Rh)^{33,37}

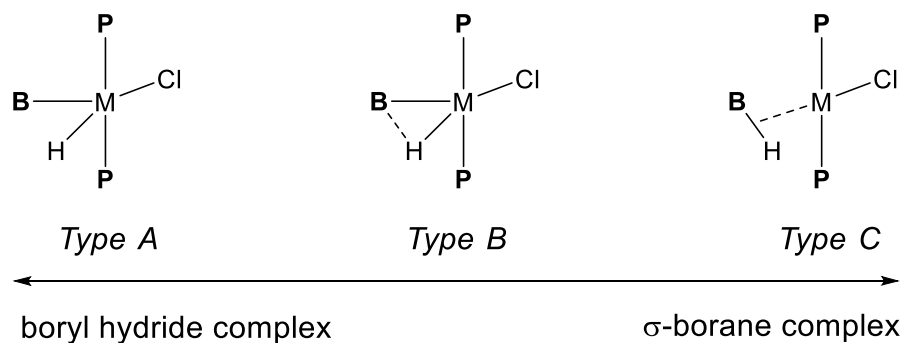
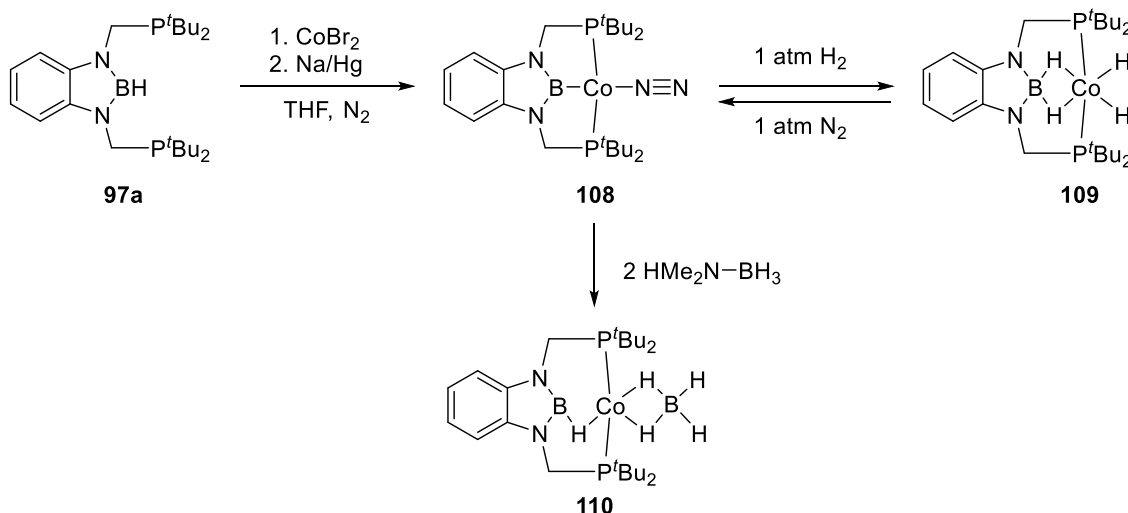


Figure I-6. Possible coordination modes in complex **106**.

The synthesis and characterization of diamino-boryl PBP pincer complexes of cobalt and the applications in catalytic hydrogenation and dehydrogenation was reported by Peters (Scheme I-14).^{85,86} The reaction of diamino-boryl PBP ligand **97a** with CoBr_2 and sodium amalgam under N_2 atmosphere resulted in the formation of (PBP)Co(N_2)**108** with a terminal N_2 ligand. Treatment of **108** under H_2 atmosphere afforded (PBP)Co($\mu^2\text{-H}_2$)(H)**109**, which reversibly lost hydrides from cobalt upon exposure to 1 atm of N_2 . The ability of reversible activation of dihydrogen allows complex **108** to apply to the catalytic hydrogenation of 1-octene and styrene with up to 1000/h turnover frequency.

Reaction of complex **108** with 2 equivalent of amine–borane gave rise to a hydridoborane cobalt tetrahydridoborate complex **110**. Complexes **108** and **110** were able to act as catalysts in the dehydrogenation of amine–borane without hydrogen acceptor.



Scheme I-14. Synthesis of PBP Pincer Complexes of Cobalt^{85,86}

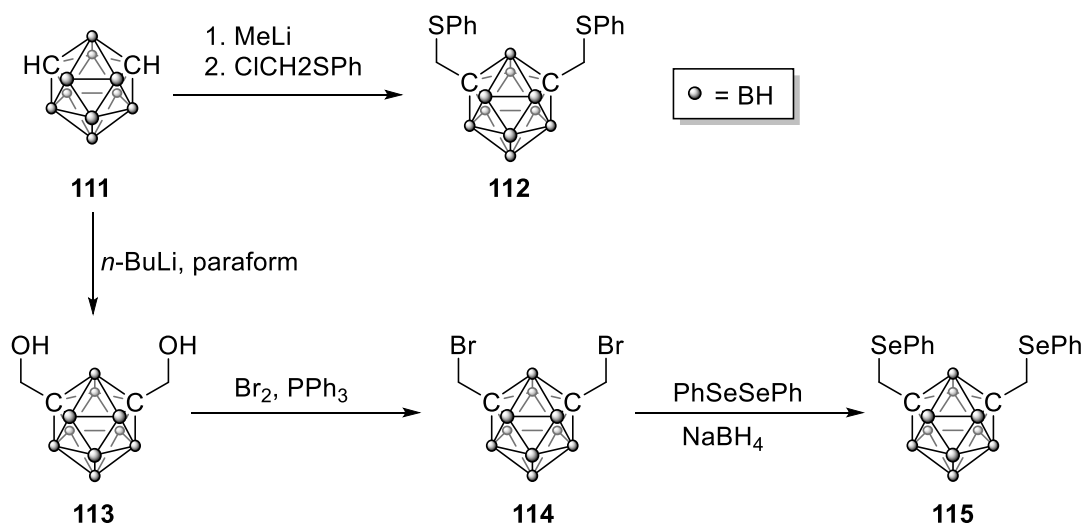
Other than group 9 metal, the diaminoboryl PBP pincer ligands have been complexed with various metal including Os,⁸⁷ Ru,^{88–91} Pt,^{92,93} and Ni.^{86,94} However, there is no literature report for complexation of diaminoboryl PBP pincer ligand with early transition metal.

1.5.2 Carborane-based pincer complexes

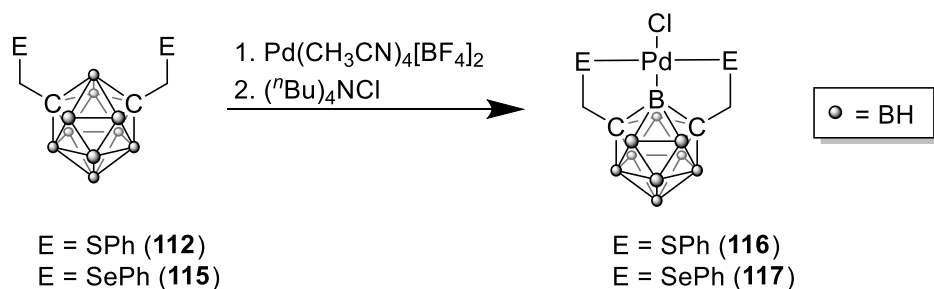
The first carborane-based pincer ligands and metal complexes were successfully synthesized by Spokoyny and Mirkin (Scheme I-15).⁹⁵ The SBS pincer ligand **112** was

synthesized in one step by deprotonation of *m*-carborane (**111**) by MeLi and subsequently quench with chloromethylphenylsulfide, whereas the synthesis of SeBSe pincer ligand **115** required three steps. Deprotonation of *m*-carborane (**111**) by *n*-BuLi and treatment with paraform gave rise to bis(hydroxymethyl)-*m*-carborane **113**, which was converted into bis(bromomethyl)-*m*-carborane **114** by addition of bromine and triphenylphosphine. The reaction of **114** with diphenylselenide followed by quench with NaBH₄ resulted in the desired SeBSe pincer ligand **115**.

Metalation of pincer ligands **112** and **115** was achieved by reacting with Pd(CH₃CN)₄[BF₄]₂ followed by adding two equivalents of (*n*-Bu)₄NCl to afford complexes **116** and **117** (Scheme I-16).⁹⁵ In the solid-state structure, the Pd–Cl bond length (2.44 Å) in **117** was slightly longer than the one in PCP pincer complex **18** (2.313(5) Å), indicating a stronger trans influence of the boryl on carborane than the phenyl.

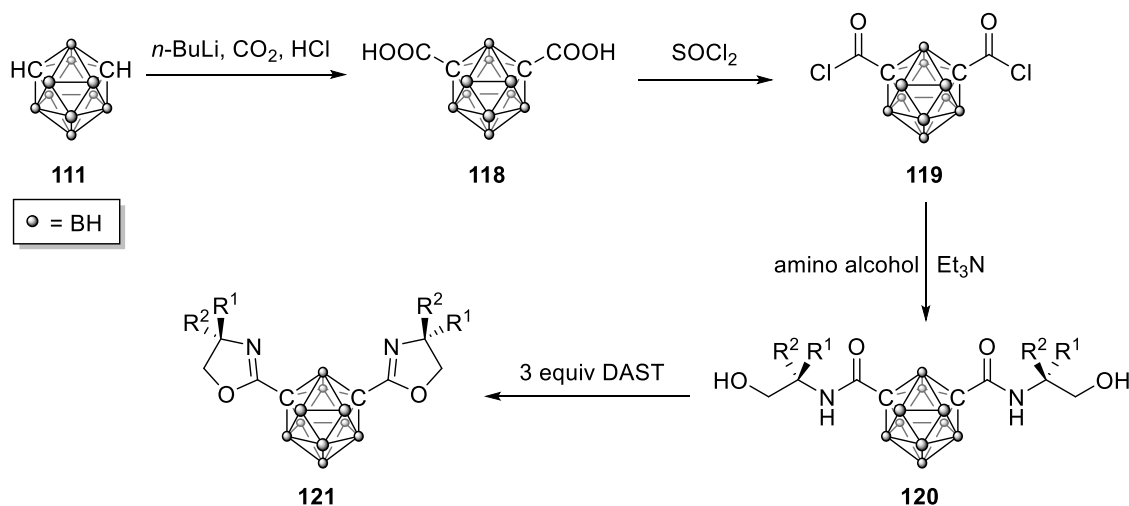


Scheme I-15. Synthesis of Carborane-based SBS and SeBSe Pincer Ligands⁹⁵



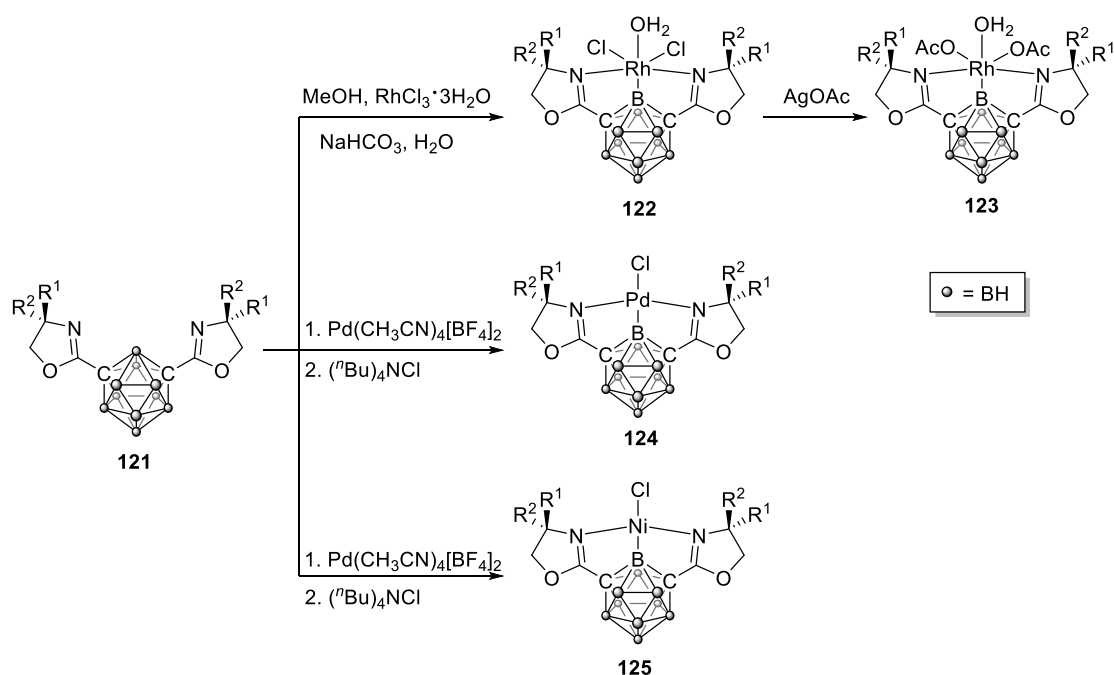
Scheme I-16. Synthesis of (EBE)PdCl Complexes (E = S, Se)⁹⁵

In 2011, Nakamura reported the synthesis of chiral carborane-based NBN pincer ligands and complexes.⁹⁶ Carboxylation of *m*-carborane (**111**) followed by treatment with SOCl_2 gave rise to **119**, which was then condensed with chiral amino alcohols to form the corresponding bis(hydroxyamide)-*m*-carboranes **120**. The cyclization of **120** was achieved by addition of three equivalents of diethylaminosulfur trifluoride (DAST), resulting in the formation of NBN pincer ligands **121** (Scheme I-17).



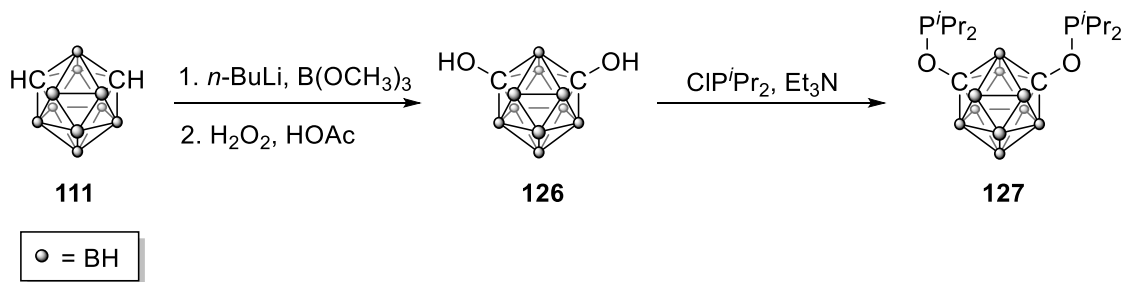
Scheme I-17. Synthesis of Chiral Carborane-based NBN Pincer Ligands⁹⁶

The metalation of pincer ligands **121** was obtained by introducing Rh, Pd, and Ni precursors (Scheme I-18).⁹⁶ The reaction of NBN pincer ligands with $\text{RhCl}_3 \cdot 3\text{H}_2\text{O}$ and NaHCO_3 in a MeOH/water cosolvent gave rise to the rhodium complexes **122**, which can convert into acetate complexes **123** in quantitative yields by adding silver acetate. The NBN pincer palladium complexes **124** were made by reacting **121** with $\text{Pd}(\text{CH}_3\text{CN})_4[\text{BF}_4]_2$ followed by adding two equivalents of $(n\text{-Bu})_4\text{NCl}$. The similar protocol was employed in the synthesis of nickel complexes **125** with $[\text{Ni}(\text{COD})]_2$ as nickel precursor. The chiral nature of NBN pincer ligands allowed their corresponding rhodium complexes **123** to catalyze asymmetric reduction of α,β -unsaturated esters and asymmetric reductive aldol reaction of *tert*-butyl acrylate and benzaldehyde.



Scheme I-18. Synthesis of NBN-pincer Chiral Complexes of Rh, Pd, and Ni⁹⁶

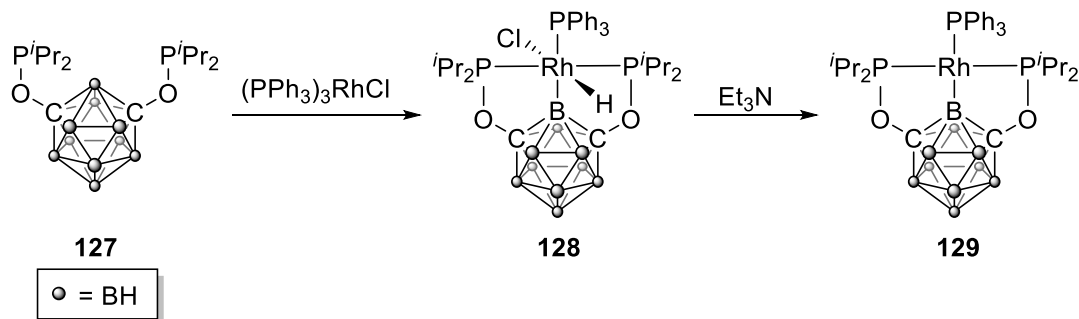
Recently, Peryshkov reported the synthesis of *m*-carborane-based POBOP pincer ligand and its complexes of rhodium,⁹⁷ ruthenium,⁹⁸ and nickel.⁹⁹ The *m*-carborane-based POBOP ligand **127** was synthesized from dihydroxy-*m*-carborane (**126**), which was prepared by lithiation of *m*-carborane (**111**) and subsequently addition of trimethyl borate to afford carboranyl boron esters *in situ*. An excess amount of H₂O₂ and acetic acid was added followed by quench with NaOH gave rise to **126**.¹⁰⁰ The reaction of **126** with ClP^{*i*}Pr₂ in the presence of Et₃N resulted in the formation of carborane-based POBOP pincer ligand **127** (Scheme I-19).



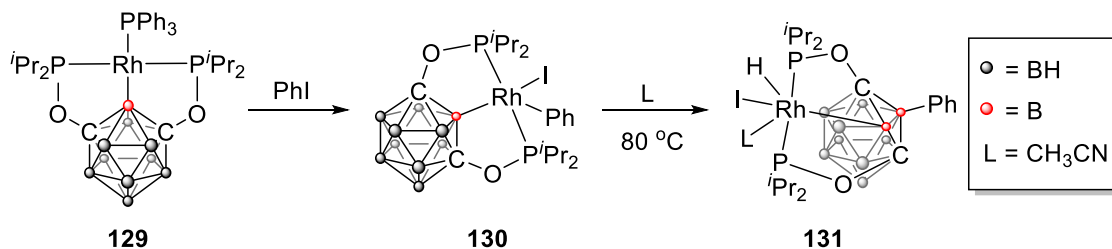
Scheme I-19. Synthesis of Carborane-based POBOP Ligand^{97,100}

The reaction of **127** with (PPh₃)₃RhCl afforded the (POBOP)Rh(H)(Cl)(PPh₃) (**128**) via the insertion of Rh to B–H bond (Scheme I-20).⁹⁷ Dehydrochlorination of **128** by addition of Et₃N resulted in the formation of (POBOP)Rh(PPh₃) (**129**) (Scheme I-20). The reaction of **129** with iodobenzene gave rise to the 16-electron complex (POBOP)Rh(Ph)(I) (**130**), presumably via dissociation of PPh₃ from **129** to form a 14-electron intermediate followed by oxidative addition of iodobenzene to Rh center (Scheme I-21). The reductive elimination of Ph–B bond from **130**, similar to the metal-mediated

B–C coupling reactions,¹⁰¹ was achieved by heating at 80 °C in the presence of acetonitrile as an L-type ligand. The corresponding reductive elimination product was further converted into complex **131** through activation of *ortho*-B–H bond.



Scheme I-20. Synthesis of (POBOP)RhL_n Complexes⁹⁷



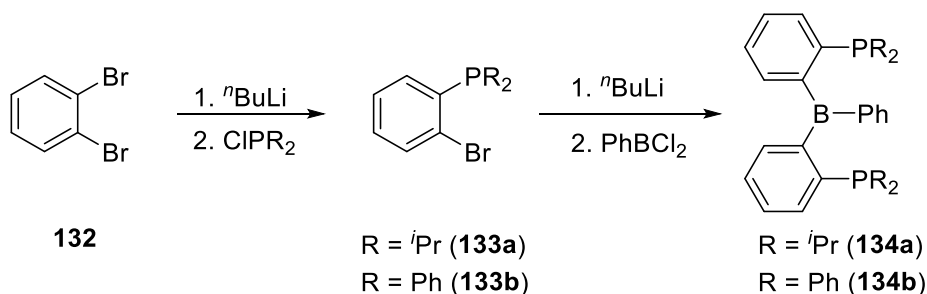
Scheme I-21. Oxidative Addition of PhI to 129 and Reductive Elimination of Ph–B from 130 in the Presence of CH₃CN⁹⁷

1.5.3 Diarylboryl-based pincer complexes

In 2016, the Ozerov group reported the first example of diarylboryl-based PBP complexes of iridium and rhodium by insertion of Rh and Ir to the B–Ph bond of PB^{Ph}P

ligand **134a**.¹⁰² The chemistry of diarylboryl-based PBP pincer complexes of Rh and Ir will be discussed in Chapter 2~5.

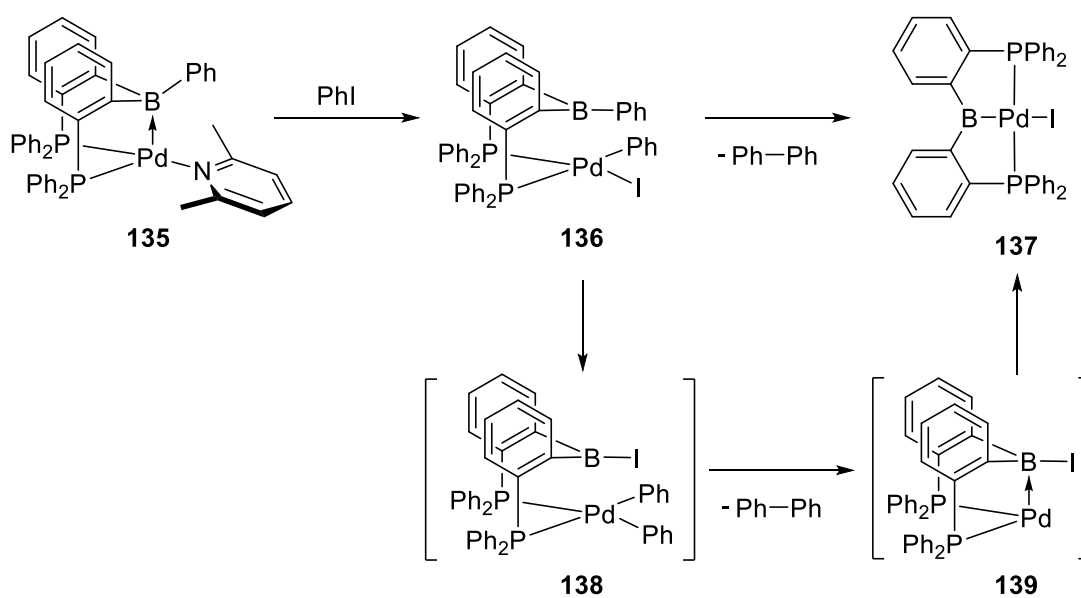
The PB^{Ph}P ligands bearing isopropyl (**134a**) or phenyl groups (**135a**) on the phosphines were synthesized in two steps. The selective mono-lithiation of 1,2-dibromobenzene (**132**) at -110 °C followed by treatment with ClPR₂ (R = *i*Pr or Ph) afforded mono-phosphination products **133a** and **133b**.^{103,104} Lithiation of **133a** and **133b** and subsequently introduction of half equivalent of PhBCl₂ gave rise to the PB^{Ph}P ligands **134a** and **134b** (Scheme I-22).^{105,106}



Scheme I-22. Synthesis of PB^{Ph}P Ligand^{103–106}

The synthesis of diarylboryl-based (PBP)PdI (**137**) was reported by Tauchert (Scheme I-23).²¹ The reaction of Z-type palladium complex **135** with iodobenzene gave the oxidative addition product **136**, which was further converted to (PBP)PdI **137** with the concurrent formation of biphenyl. The possible mechanism for generation of **137** was similar to the C–C cross coupling in Suzuki reaction.¹⁰⁷ First, the oxidative addition of iodobenzene to Pd resulted in the formation of **136**. Then exchange of the iodide on the Pd with the phenyl on the boron gave rise to palladium diphenyl complex **138**, similar to

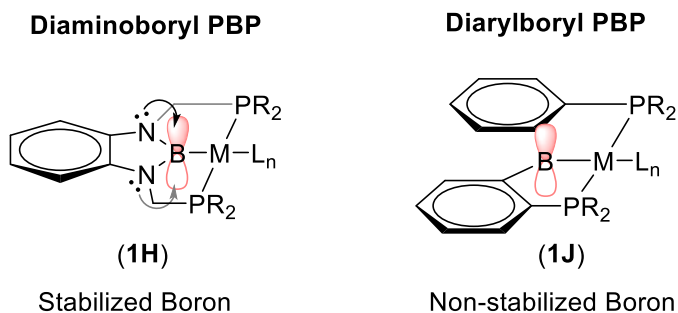
the transmetalation process in Suzuki reaction. This type of transmetalation from palladium iodide species was rare (typically from oxygenous ligands such as OAc^- and OH^-), and therefore the formation of Pd–I–B bridge may be the key intermediate to facilitate this exchange process.¹⁰⁸ The reductive elimination of biphenyl from **138** gave the Pd(0) complex **139**, which was converted to **137** via oxidative addition of B–I to Pd.



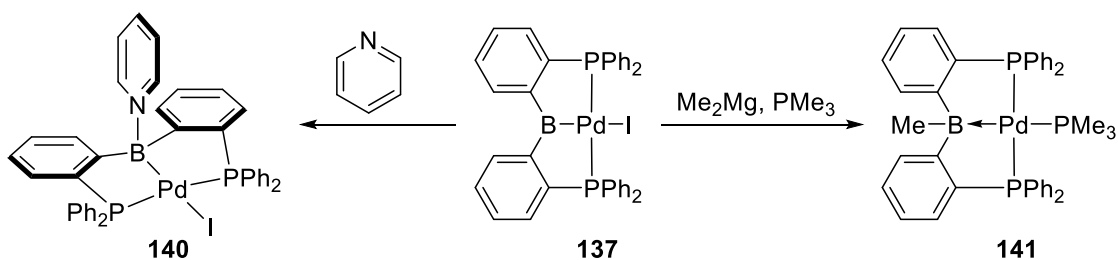
Scheme I-23. Synthesis of Diarylboryl-based (PBP)PdI and the Proposed Mechanism²¹

The borons on the diaminoboryl PBP and carborane PBP pincer complexes (**1H** and **1I**) might be stabilized by adjacent nitrogen lone pairs or the electrons in the carborane cage, whereas the boron on the diarylboryl PBP pincer complexes (**1J**) has a lower-lying empty orbital, which can be expected to behave as a non-innocent ligand with Lewis acidic properties (Scheme I-24). Hence, the coordination of a Lewis base to the boron of complex

137 was observed by introducing pyridine derivatives (Scheme I-25). The nucleophilic attack on the boron center of **137** by Grignard reagent followed by addition with trimethylphosphine afforded the Z-type PBP palladium complex **141**.



Scheme I-24. Non-stabilized Boron on the Diarylboryl PBP with Lewis Acidic Property



Scheme I-25. Reactivity of PBP Complex 137 with Lewis Base and Nucleophile²¹

1.6 Versatile Binding Modes of Boron on the PB^{Ph}P Ligands

In transition metal coordination chemistry, ligands were usually divided into two classes, L-type ligands or X-type ligands, to describe a ligand donating either two electrons (L-type) or one electron (X-type) into a metal to form the 2c-2e metal-ligand

interaction (Table I-1). In contrast, the Lewis acidic borane on the PB^{Ph}P ligands can accept two electrons from metal to form a metal–boron bond, and this type of ligands called Z-type ligand. Besides Z-type binding mode (**1K**), the boron on the PB^{Ph}P metal complexes has been shown the ability to form compounds with B–H–M linkage (**1L**), zwitterionic interaction (**1M**), and η^2 -B,C binding (**1N**), and η^7 -B,Ph binding (**1O**) (Figure I-7). This section will be mainly focused on the synthesis and reactivity of PB^{Ph}P metal complexes (group 9~11 metals) with versatile boron coordinations and their applications in catalysis.

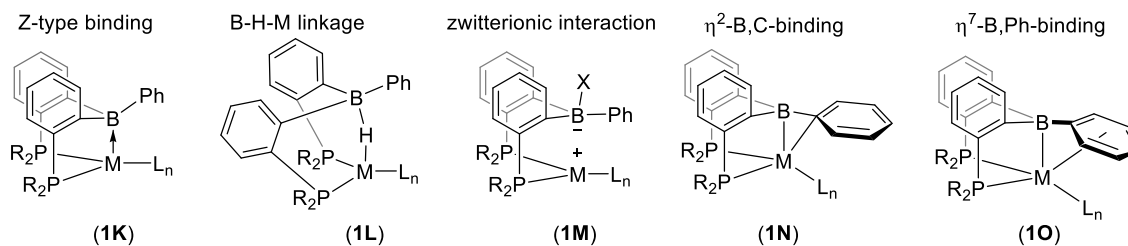
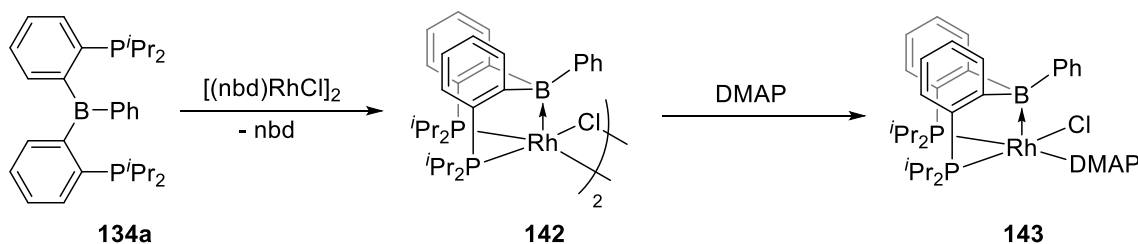


Figure I-7. Versatile binding modes of boron on PB^{Ph}P complexes.

1.6.1. Group 9 metals

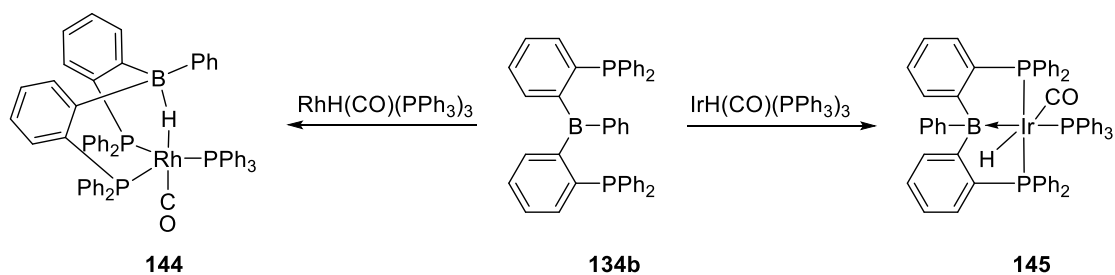
In 2006, Bourissou first introduced PB^{Ph}P ligand **134a** as a ridge skeleton for the complexation with rhodium in order to study M→B interaction (Scheme I-26).¹⁰⁵ The reaction of **134a** with [(nbd)RhCl]₂ afforded the chloro-bridged dimeric complex **142** featuring the Z-type borane binding. Treatment of DMAP to **142** resulted in the formation of complex **143** via cleavage of one of the chloro-bridge and coordination of DMAP onto Rh, which revealed the coordination of DMAP on boron was inhibited by the Rh→B

interaction. DFT calculations suggested this type of interaction is a 2c-2e interaction between the occupied d_{z^2} orbital of rhodium to the vacant p orbital of boron.



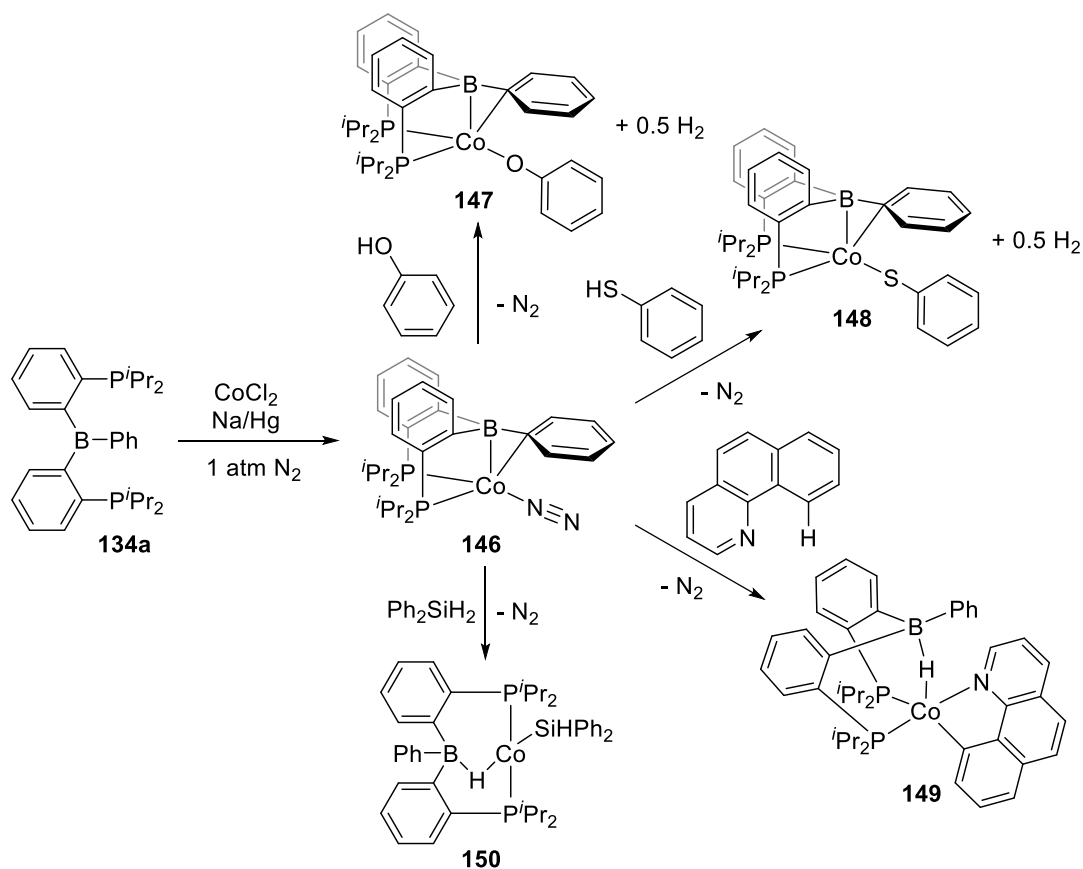
Scheme I-26. Synthesis of PB^{hP} Complexes of Rh Featuring the Z-type Borane Binding¹⁰⁵

Later, Nakazawa reported the similar reaction by using **134b** and $\text{HRh}(\text{CO})(\text{PPh}_3)_3$ as the Rh(I) precursor (Scheme I-27).¹⁰⁹ Interestingly, instead of formation of Z-type borane complex, the reaction resulted in the formation of **144** featuring B–H–Rh linkage. In contrast, the reaction of **134b** with $\text{HIr}(\text{CO})(\text{PPh}_3)_3$ afforded the complex **145** featuring terminal hydride and $\text{Ir} \rightarrow \text{B}$ interaction. DFT calculations suggested a significant electron donation from rhodium to boron caused this 3c-2e interaction in **144**. The complex **144** displayed catalytic activity in the transfer hydrogenation of ethyl phenyl ketone with isopropanol.



Scheme I-27. Synthesis of PB^{Ph}P Complexes of Rh and Ir¹⁰⁹

The synthesis and reactivity of PB^{Ph}P complexes of cobalt were reported by Peters (Scheme I-28).¹¹⁰ The reaction of **134a** with CoCl₂ and sodium amalgam under 1 atm of N₂ gave the complex **146** featuring the η²-B,C binding.¹¹¹ Treatment of phenol or thiophenol in **146** resulted in the formation of (PB^{Ph}P)Co(OPh) (**147**) and (PB^{Ph}P)Co(SPh) (**148**) with release of 0.5 equivalent of H₂. In contrast, the reactions of **146** with benzo[*h*]quinolone and diphenylsilane afforded the C–H activation and Si–H activation products **149** and **150** featuring B–H–Co linkage. Complex **150** exhibited high catalytic activity in hydrosilylation of ketones and aldehydes.

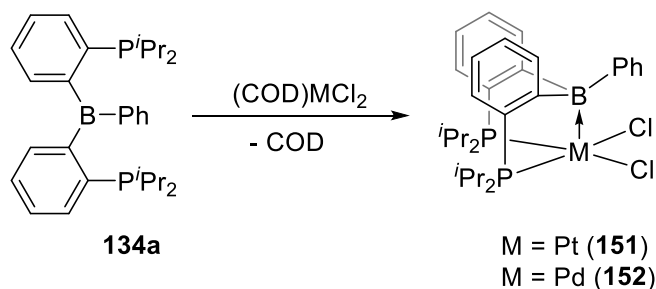


Scheme I-28. Synthesis and Reactivity of PB^{PhP} Complexes of Co^{110}

1.6.2 Group 10 metals

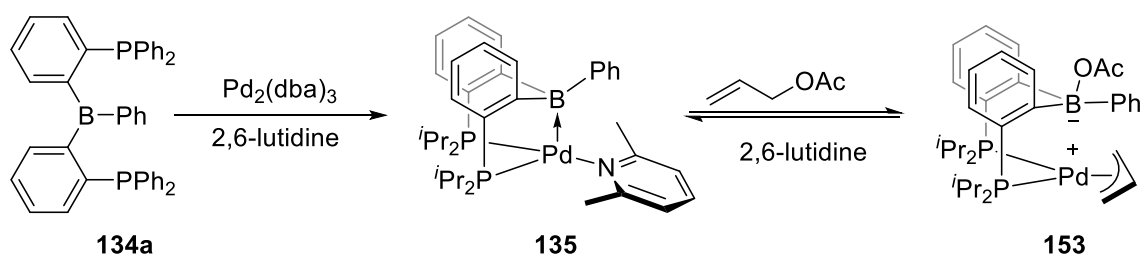
The synthesis of Z-type borane complexes of palladium **151** and platinum **152** by treatment of **134a** with $[(\text{COD})\text{MCl}_2]$ ($\text{M} = \text{Pd}, \text{Pt}$) as a $\text{M}(\text{II})$ precursor was reported by Bourissou (Scheme I-29).¹¹² Similar to PB^{PhP} rhodium complexes **142** and **143**, Complexes **151** and **152** adopt square-pyramidal geometry with the boron on the apical position. The $\text{M} \rightarrow \text{B}$ interactions in **151** and **152** were significantly weaker than the one in analogous rhodium complex **142** evidenced by longer $\text{M}-\text{B}$ distances ($2.650(3) \text{ \AA}$ for **151**,

2.429(3) Å for **152**, and 2.306(3) Å for **142**) and lower degree of pyramidalization of boron ($\Sigma B_{\alpha} = 354.9^{\circ}$ for **151**, 346.6° for **152**, and 338.8° for **142**).



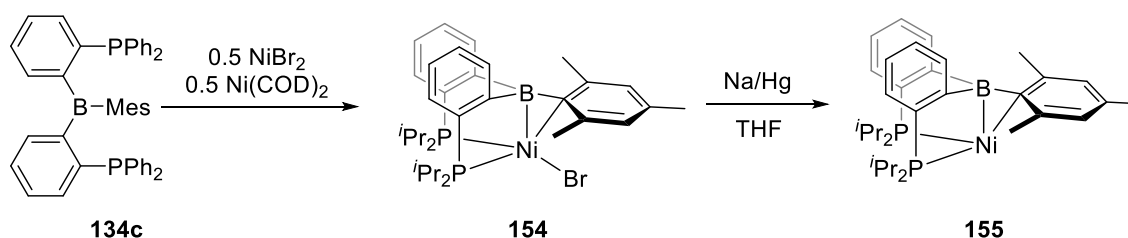
Scheme I-29. Synthesis of $PB^{Ph}P$ Complexes of Pd and Pt¹¹²

The synthesis of palladium complex **135** was also achieved by using $Pd_2(dba)_3$ as a Pd(0) precursor (Scheme I-30).¹¹³ Complex **135** featured a very strong Pd→B interaction with a short Pd–B distance (2.194(3) Å) and a highly pyramidalized boron ($\Sigma B_{\alpha} = 346^{\circ}$). The distance between the *ipso* carbon of phenyl group and Pd was found to be short (Pd– $C_{ipso} = 2.463(3)$ Å), suggesting a certain degree of η^2 -B,C interaction. Treatment of **135** with allyl acetate resulted in the formation of zwitterionic compound **153** via transfer the acetate group to boron. The reaction can be reversed by addition of 2,6-lutidine. This unique reversible reactivity mediated by metal–boron cooperation allowed the complex **135** and **153** to apply in the catalytic allylic substitution reaction of allyl acetate with diethylamine.

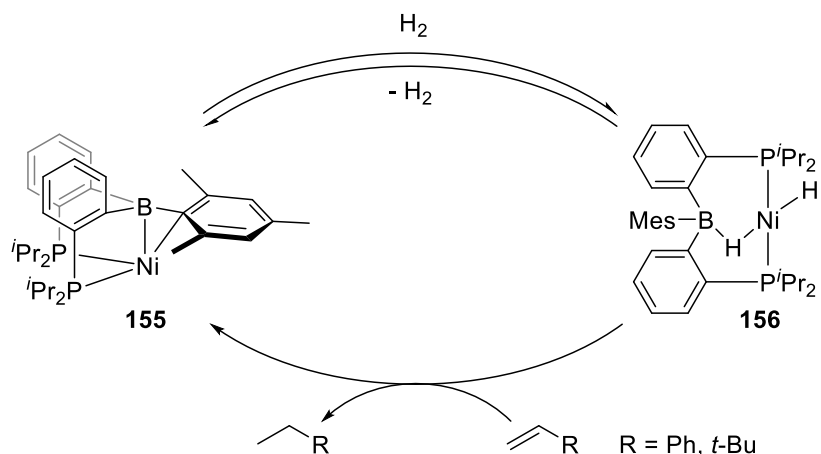


Scheme I-30. Synthesis and Reactivity of PB^{Ph}P Complexes of Pd¹¹³

The PB^{Mes}P nickel complexes were synthesized and reported by Peters (Scheme I-31).¹¹⁴ Comproportionation of NiBr₂ and Ni(COD)₂ in the presence of PB^{Mes}P ligand **134c** gave rise to Nickel(I) complex **154**, which was reduced by Na/Hg to afford a pseudo-three-coordinate Ni(0) species **155**. Similar to the PB^{Ph}P cobalt chemistry, complexes **154** and **155** contained the η²-B,C coordination. Facile activation of dihydrogen across the Ni–B bond of **155** resulted in the formation of borohydrido-hydride complex **156** featuring the B–H–Ni bridge (Scheme I-32). This process was reversible by freeze-pump-thaw to regenerate **155**. On the basis of this reactivity, catalytic hydrogenation of TBE or styrene was achieved by using **155** or **156** as catalysts.



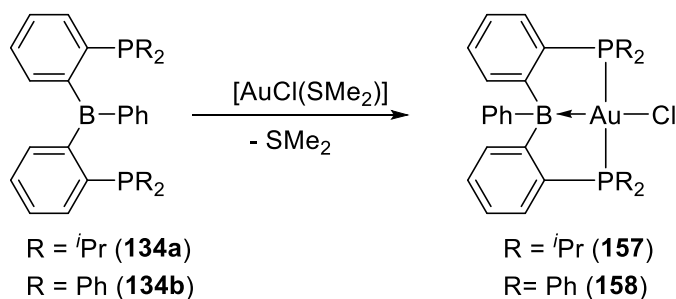
Scheme I-31. Synthesis of PB^{Mes}P Complexes of Ni¹¹⁴



Scheme I-32. Activation of H₂ by Oxidative Addition across Ni–B Bond¹¹⁴

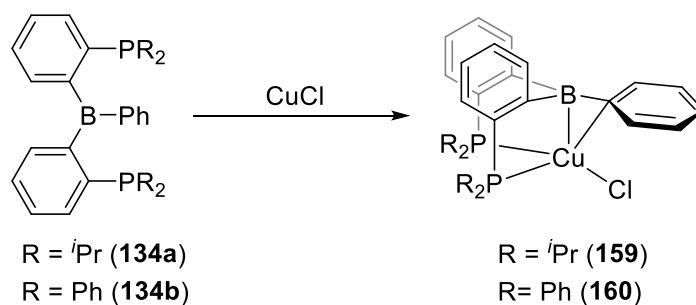
1.6.3 Group 11 metals

The PB^{Ph}P Gold complexes **157** and **158** were accessed by replacement of SMe₂ ligand in [AuCl(SMe₂)] with PB^{Ph}P ligands **134a** and **134b** (Scheme I-33).¹⁰⁶ The complex **157** adopted square-planar geometry with a short Au–B distance (2.309(8) Å) and a highly pyramidalized boron ($\Sigma\text{B}\alpha = 341.2^\circ$), featuring a strong Au→B interaction. Substitution of *i*Pr groups by less electron-donating Ph groups on the phosphines of PB^{Ph}P slightly weaken the Au→B interaction evidenced by a longer Au–B distance (2.335(5) Å).



Scheme I-33. Synthesis of PB^{Ph}P Complexes of Au¹⁰⁶

Unlike PB^{PhP} gold complexes, the PB^{PhP} copper complexes **159** and **160** adopted $\eta^2\text{-B,C}$ coordination (Scheme I-34).¹¹⁵ The NBO analysis of complex **159** suggested this interaction was contributed by electron donation from $\sigma\text{-B,C}_{\text{ipso}}$ and $\pi\text{-C}_{\text{ipso,Cortho}}$ to Cu and back donation from Cu to boron.



Scheme I-34. Synthesis of PB^{PhP} Complexes of Cu¹¹⁵

Other than the transition metal complexes mentioned above, the PB^{PhP} ligands have been complexed with Ru^{116,117} and Fe.^{110,118,119} However, there is no literature report for complexation of PB^{PhP} ligands with Ag, Os, and early transition metal.

CHAPTER II

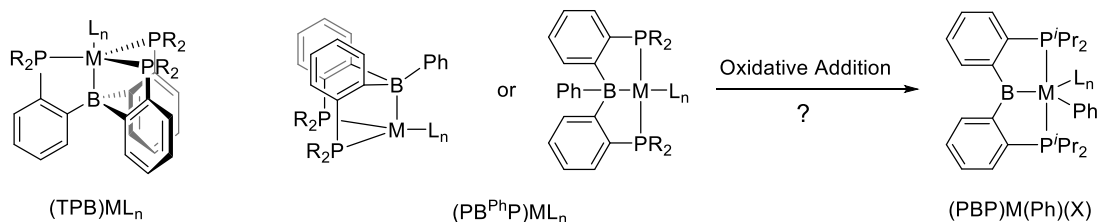
FACILE INSERTION OF RHODIUM AND IRIDIUM INTO BORON-PHENYL BOND, LEADING TO BORYL/BIS(PHOSPHINE) PBP PINCER COMPLEXES*

2.1 Introduction

Polydentate ligands combining a central boron-based moiety with two or three flanking neutral donors have emerged over the last decade as some of the most versatile frameworks for studies of transition metal reactivity. A great deal of attention has been devoted to complexes with a central borane unit as a Z-type ligand such as TPB^{121–126} and PB^{PhP}^{106,109,113,119,127–129} (Figure II-1a). These molecules raised important fundamental questions about the nature and nomenclature of metal-ligand bonding and have already been harnessed in catalysis.^{109,113,125,128,130} Borane-containing ligands have been treated as robust supporting ligands, but we wondered if they might be vulnerable to insertion of a metal into the boron–aryl bond. In particular, insertion into the B–Ph bond in the PB^{PhP} ligand^{106,109,113,119,127–129} (Figure II-1a) seemed most plausible, as the B–Ph bond is unbuttressed by a phosphine. Such an insertion would result in a boryl/bis(phosphine) pincer complex. It can be viewed as B–C oxidative addition, which has not been previously observed for classical B–C bonds.¹³¹

* Reproduced in part from “Facile Insertion of Rh and Ir into Boron–Phenyl Bond, Leading to Boryl/Bis(phosphine) PBP Pincer Complexes” by Shih, W.-C.; Gu, W.; MacInnis, M. C.; Timpa, S. D.; Bhuvanesh, N.; Zhou, J.; Ozerov, O. V. *J. Am. Chem. Soc.* **2016**, *138*, 2086. Copyright [2016] by The American Chemical Society. Part of rhodium chemistry has been developed by our former group members Dr. Weixing Gu,¹²⁰ Dr. Morgan MacInnis, and Dr. Samuel Timpa.

(a) Z-type borane complexes and possible boryl pincer formation



(b) Known pincer metal complexes with a central boryl X-type donor

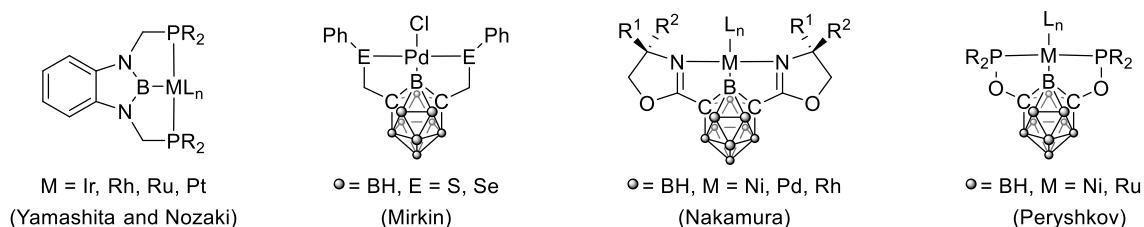


Figure II-1. Complexes featuring various boron-based ligands.

Tridentate pincer-type ligands with a central boryl X-type (Figure II-1b) donor were only recently introduced, first by Yamashita and Nozaki.^{33,37,75,87,132,133} Spokoyny and Mirkin⁹⁵ ingeniously constructed a boryl-centered pincer based on the meta-dicarborane core, and similar design was employed by Nakamura⁹⁶ and Peryshkov.^{99,134} As discussed by Yamashita and Nozaki, boryl is the strongest trans influence ligand to be incorporated in pincer ligands and thus complements the more common N- and C-based donors. Bourissou also suggested the boryl on a (PXP)Ir(CO) complex (X = N, P, CH, Si(Me), or B) is the strongest donating central donor among others based on the prediction of the stretching frequencies of CO by DFT calculation (Figure II-2).¹² The diarylboryl/bis(phosphine) PBP pincer (Figure II-3) should possess a boryl donor with a more accessible empty orbital compared to the Yamashita/Nozaki ligand (stabilized by π -

donation from the amino groups) or the Spokoyny-Mirkin ligand, where the boron orbitals are tied up in the carborane cage. The diarylboryl/bis(phosphine) PBP pincer would have analogous connectivity to the variety of other PXP pincer ligands built on the “bis(ortho-phosphinoaryl)X” core, with X = C,¹³⁵ N,¹³⁶ O,¹³⁷ P,^{138,139} Sb,¹⁴⁰ and Si.^{141–145} The analogy with amido-PNP seemed especially intriguing, as the simple "swap" of N with B replaces an electronegative atom carrying a lone pair of electrons with an electropositive atom carrying an empty orbital, while preserving the geometry and charge (Figure II-3).

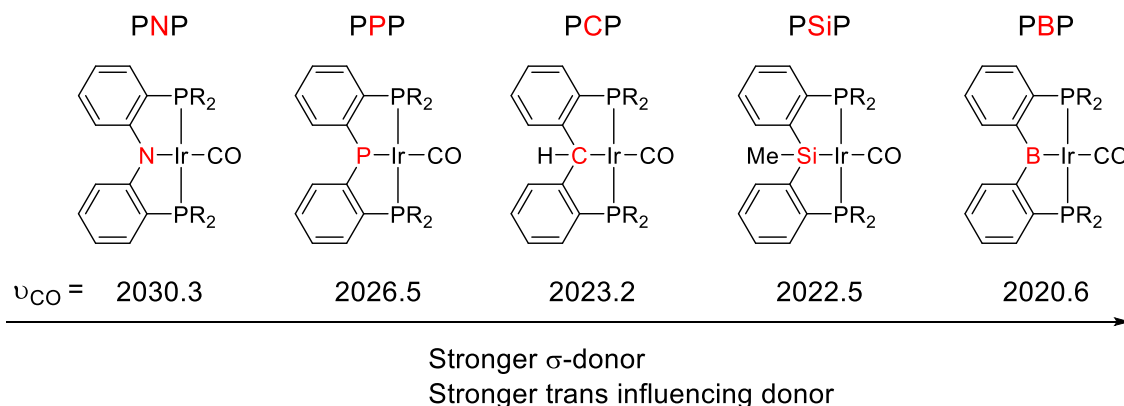


Figure II-2. Donating ability of central ligand predicted by DFT calculation.

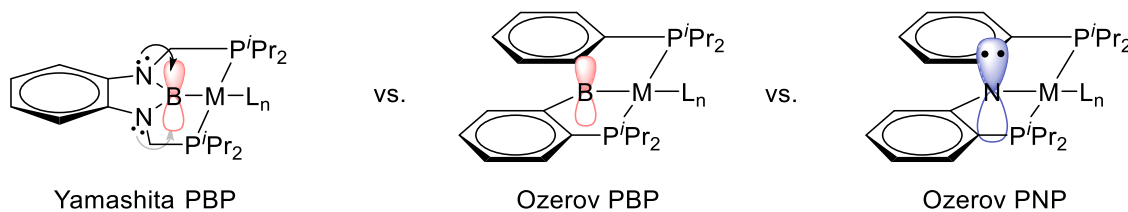
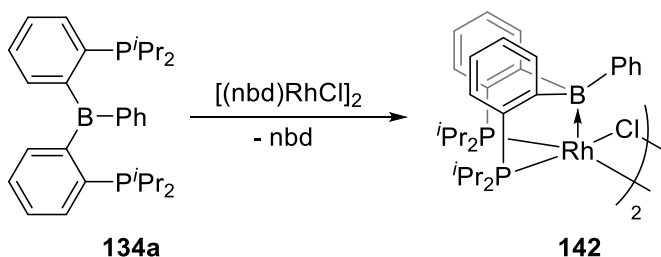


Figure II-3. Lewis acidic boron on Ozerov PBP and comparison with Yamashita PBP and Ozerov PNP.

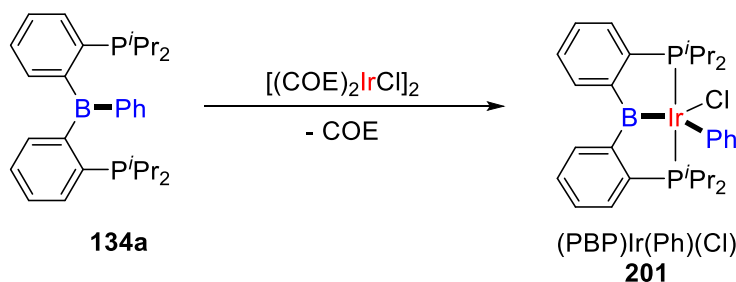
2.2 Result and Discussion

2.2.1 Synthesis of PBP-type pincer Ir and Rh complexes via B–Ph oxidative addition

We turned our attention to the report by Bourissou et al. on the isolation of **142** (Scheme II-1) from the reaction of borane/bis(phosphine) ligand **134a** with $[(\text{nbd})\text{RhCl}]_2$ as a source of monovalent Rh (nbd = 2,5-norbornadiene).¹²⁷ Keeping in mind the generally greater thermodynamic propensity of 5d versus 4d metals for oxidative addition, we pursued an Ir analogue of the Bourissou synthesis of **142**. To our delight, thermolysis of **134a** with $[\text{Ir}(\text{COE})_2\text{Cl}]_2$ at 100 °C for 5 h (COE = cyclooctene) led to the single product (PBP)Ir(Ph)(Cl) (**201**), a result of the desired insertion of Ir into the B–Ph bond (Scheme II-2).



Scheme II-1. Bourissou's Synthesis of Rh Complex 142



Scheme II-2. Synthesis of 201 via B–C Bond Oxidative Addition

The downfield ^{11}B NMR chemical shift (δ 75.9 for **201**) appears to be diagnostic for the presence of a diarylboryl ligand.^{146,147} Chemical shifts around ca. 80–90 ppm are common for triorganoboranes with an sp^2 -hybridized boron. Diphenylboryl complexes $(\text{C}_5\text{Me}_5)\text{Ir}(\text{PMe}_3)(\text{H})(\text{BPh}_2)$ and $\text{CpFe}(\text{CO})_2\text{BPh}_2$ were reported at 93 and 121 ppm, respectively.^{148,149} Triarylborane adducts with transition metals typically resonate in the 14–30 ppm region^{121–128,106,109,113,129,119} (δ 20.8 ppm for **142**). **201** displays features in the ^1H NMR spectrum associated with the restricted rotation of the phenyl group bound cis to the central pincer donor and sandwiched between the two P^iPr_2 flanking donors: C_6H_5 gives rise to five separate ^1H resonances, and one of the four CH_3 signals of the P^iPr_2 groups is shifted by ~ 0.5 – 1.0 ppm upfield from the rest (Figure II-4).

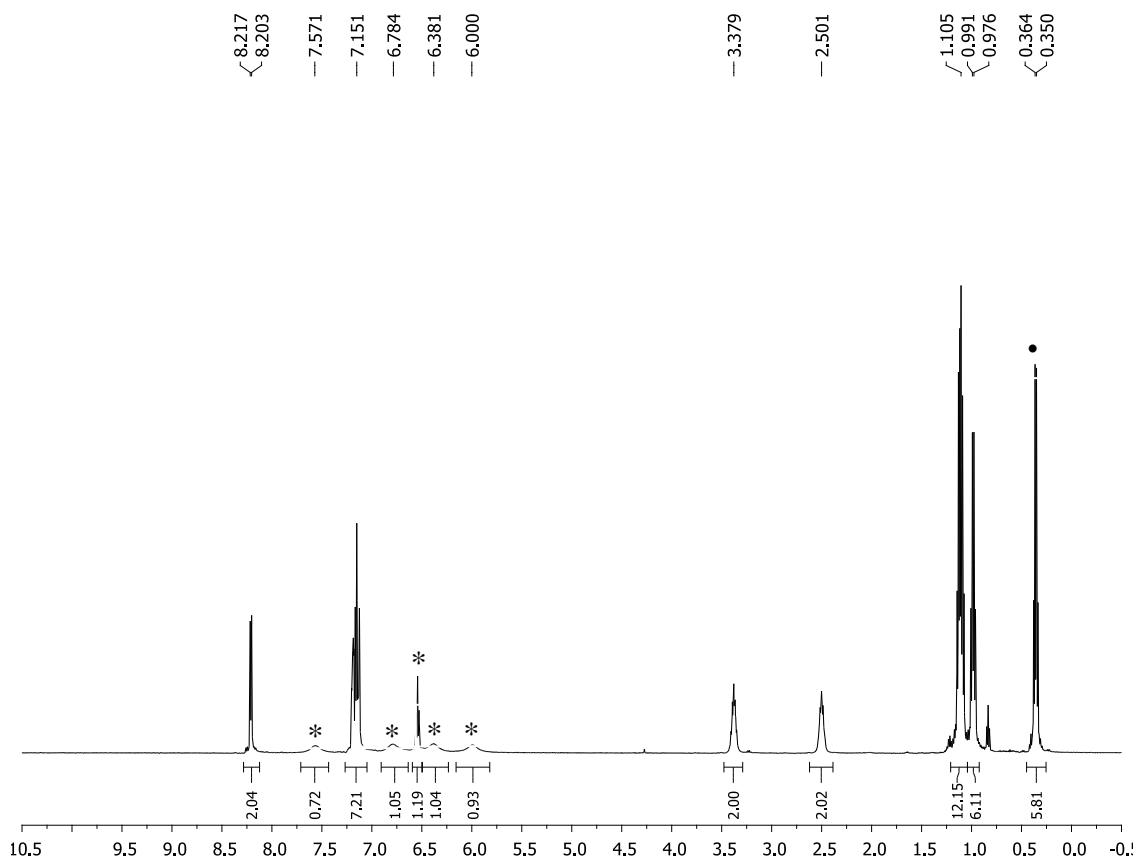


Figure II-4. ^1H NMR spectrum of **201** featuring restricted rotation of the Ir–Ph bond. C_6H_5 gives rise to five separate ^1H resonances (labeled as *), and one of the four CH_3 signals of the P^iPr_2 groups shifted upfield by ring current effect (labeled as •).

An X-ray diffraction study on a single crystal of **201** confirmed the proposed structure. The Ir1–B1 bond length (1.988(3) Å) was comparable to the Ir–B_{boryl} distances (ca. 1.97–1.98 Å) in the Nozaki–Yamashita pincer complexes.^{37,75} The geometry about boron is strictly planar, and the coordination environment of Ir is a distorted square pyramid with boryl trans to the empty site, as would be expected for the strongest trans influencing ligand (Figure II-5).

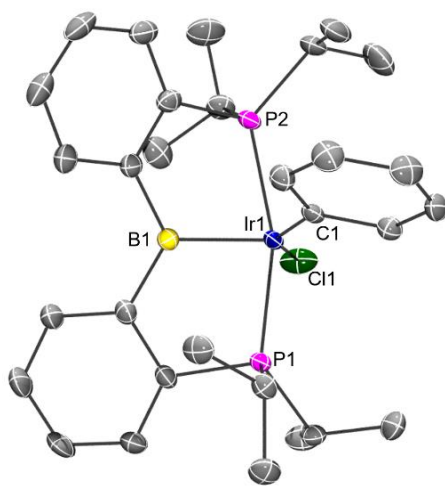


Figure II-5. POV-Ray rendition of the ORTEP drawing (50% thermal ellipsoids) of **201** showing selected atom labeling. The molecule of toluene present in the unit cell is not shown. Selected bond distances (Å) and angles (°): Ir1–B1, 1.988(3); Ir1–Cl1, 2.4096(11); Ir1–C1, 2.029(3); Ir1–P1, 2.3245(9); Ir1–P2, 2.3333(10); B1–Ir1–C1, 98.09(12); B1–Ir1–Cl1, 114.26(10); P1–Ir1–P2, 162.54(3).

Bourissou et al. reported three ^{31}P NMR resonances at ambient temperature, resulting from the reaction of **134a** with 0.5 equiv of $[(\text{nbd})\text{RhCl}]_2$ in CDCl_3 , and tentatively proposed that they may belong to different conformers of **142**.¹²⁷ We observed the same three signals in a reaction of **134a** with 0.5 equiv of $[\text{Rh}(\text{COD})\text{Cl}]_2$ in CDCl_3 or $\text{C}_6\text{D}_5\text{Br}$ (COD = 1,5-cyclooctadiene); however, we have arrived at a new interpretation of these observations.

The ratio of the observed three resonances was not affected by thermolysis (in $\text{C}_6\text{D}_5\text{Br}$) at 100 °C for 18 h. On the other hand, lowering the total concentration of Rh

resulted in a decrease of the relative intensity of the broad ^{31}P NMR resonance assigned to **142**, while the other two resonances remained in the same ratio to each other (Table II-1 & Figure II-6). This suggested that, in addition to the dimeric **142**, the mixture contained two monomeric isomers. The NMR spectra of this mixture contained features similar to those observed for **201**: an upfield-shifted Me resonance from the P^iPr_2 groups in the ^1H NMR spectrum and a downfield resonance at 94.3 ppm in the ^{11}B NMR spectrum. These corresponded to the ^{31}P NMR resonance at 50.4 ppm ($J_{\text{Rh-P}} = 126$ Hz).

Table II-1. Ratios of 142, 202, 203 in CDCl_3 with Various Concentrations of Rh.

Entry	Concentration (M)	142 : 202 : 203
1	0.050	1.1 : 1.6 : 1.0
2	0.033	0.8 : 1.6 : 1.0
3	0.025	0.7 : 1.7 : 1.0
4	0.010	0.6 : 1.5 : 1.0

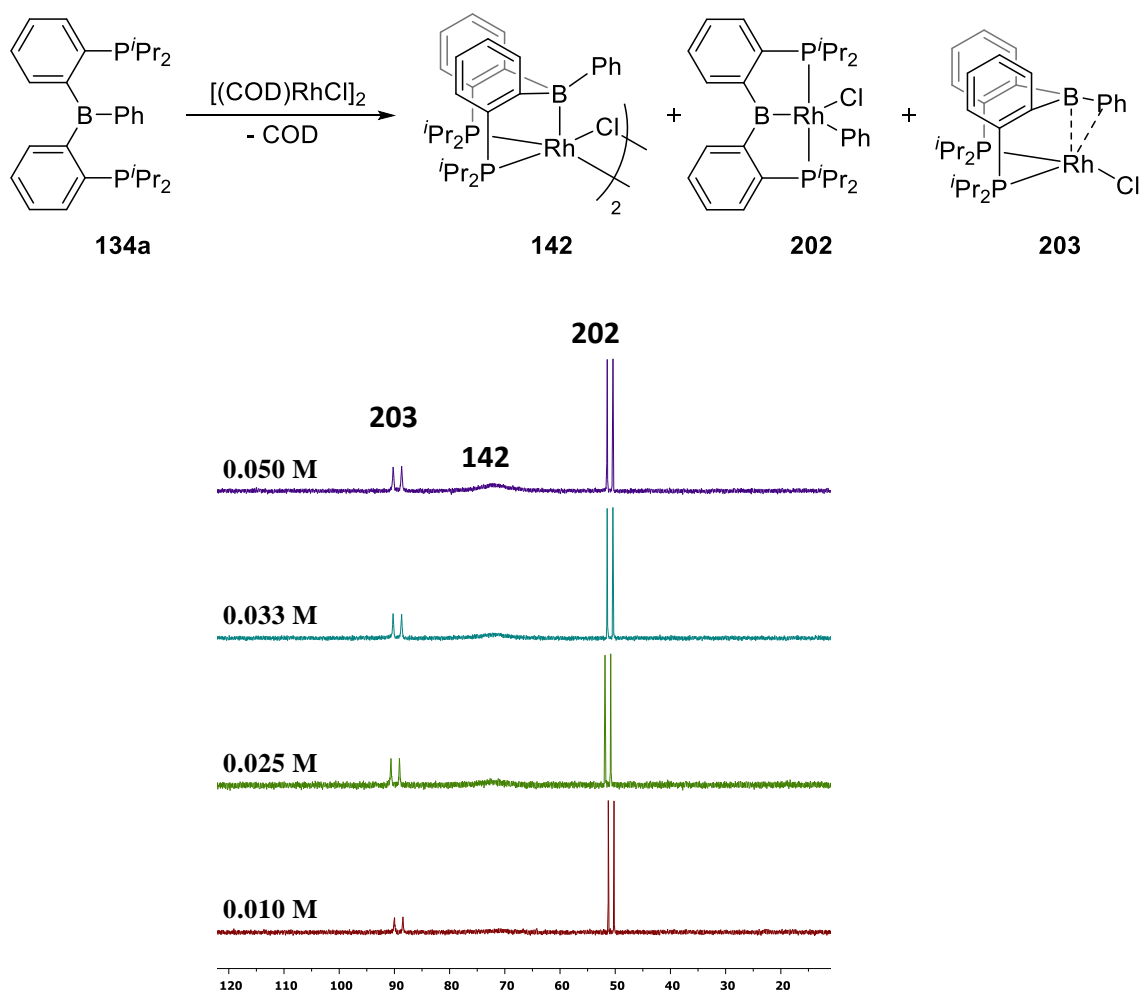


Figure II-6. $^{31}\text{P}\{^1\text{H}\}$ NMR spectra of **142**, **202**, and **203** in CDCl_3 with different concentrations.

Utilization of $[\text{Rh}(\text{COD})\text{I}]_2$ in the reaction with **134a** led to a mixture with only two components, with NMR observations closely corresponding to the two monomeric components of the “RhCl” mixture and the ratio unchanged by the variation of total $[\text{Rh}]$ (Table II-2 & Figure II-7).

Table II-2. Ratios of 204 and 205 in CDCl₃ with Various Concentrations of Rh.

Entry	Concentration (M)	204 : 205
1	0.050	1.6 : 1.0
2	0.033	1.6 : 1.0
3	0.025	1.6 : 1.0
4	0.010	1.7 : 1.0

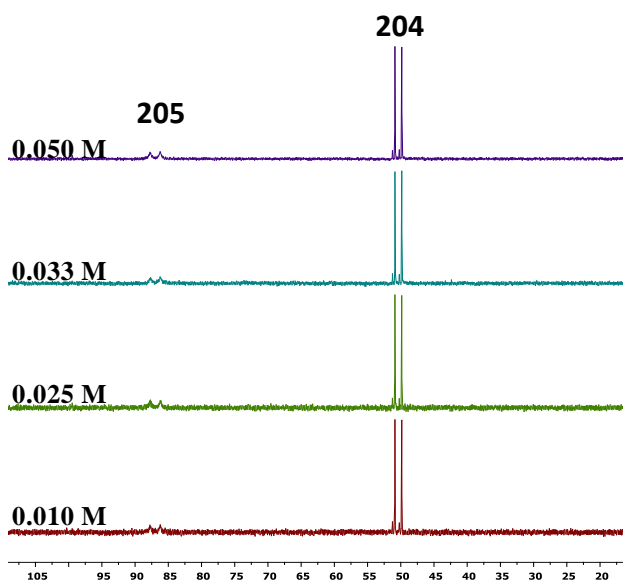
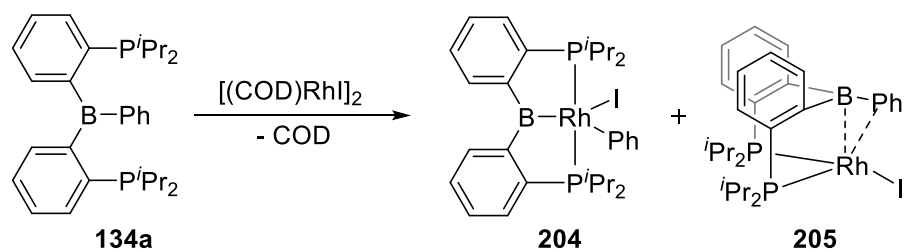


Figure II-7. $^{31}\text{P}\{^1\text{H}\}$ NMR spectra of 204 and 205 in CDCl₃ with different concentrations.

These observations led us to conclude that the RhCl mixture contained **142**, **202**, and a third isomer **203** (Figure II-6), while the RhI mixture is composed of **204** and **205** (Figure II-7). Selected NMR data for all Rh and Ir complexes are collected in Table II-3. The exact nature of **203/205** remains undetermined, but the unusually large Rh–P coupling constant (>190 Hz) finds analogy in π -arene complexes of a $(R_3P)_2Rh^I$ fragment, such as $(R_3P)_2Rh(\eta^6\text{-PhBPh}_3)$. We tentatively propose a structure for **203/205**, where the BPh unit is bound to Rh in a η^x -fashion ($x > 1$) as a “borabenzyl” π -system. Similar binding modes of B–Ph to transition metals have been reported.^{115,116,118,129,150} EXSY NMR experiments detected exchange between **142** and **203** (Figure II-8).

Table II-3. ^{11}B NMR and ^{31}P NMR Chemical Shifts of Ir and Rh Complexes (in ppm) and $^2J_{Rh-P}$ Values

Compound	201	142	202	203	204	205
^{11}B NMR	75.9	20.8	94.3	20.8	95.3	22.5
^{31}P NMR	44.9	65.0~80.0	50.4 (d, J_{Rh-P} = 126 Hz)	88.8 (d, J_{Rh-P} = 194 Hz)	50.4 (d, J_{Rh-P} = 125 Hz)	87.1 (d, J_{Rh-P} = 191 Hz)

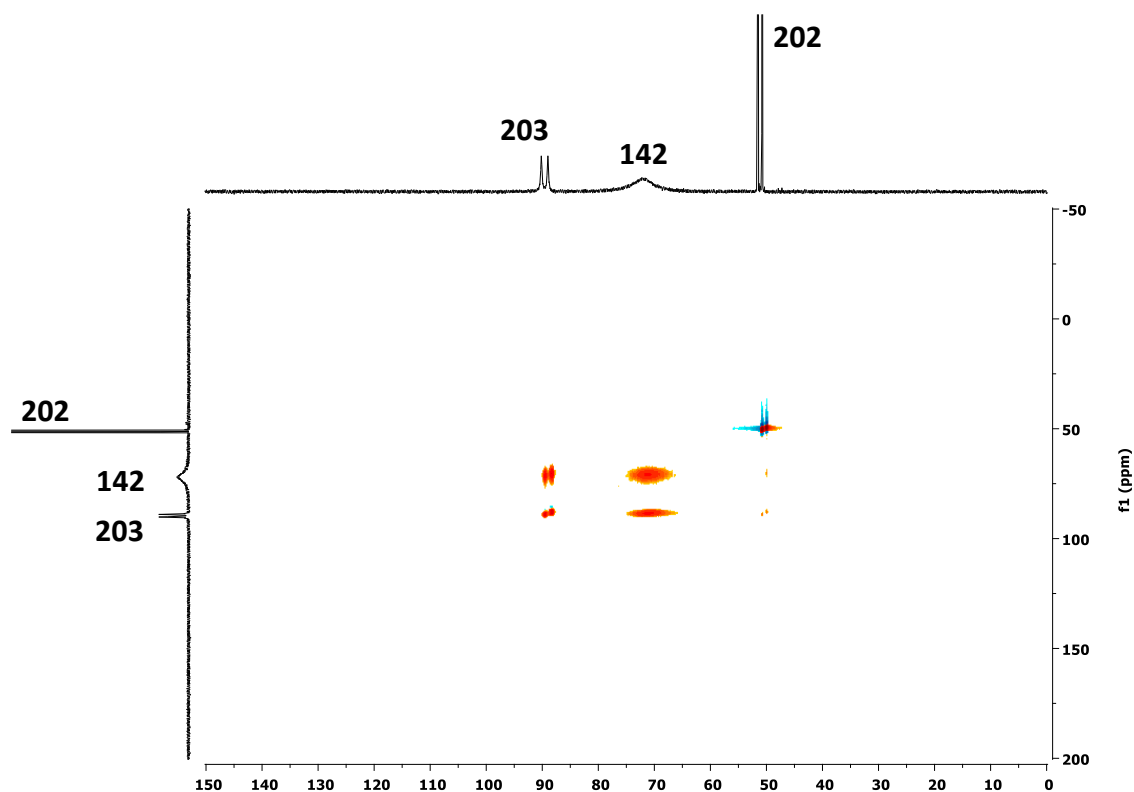
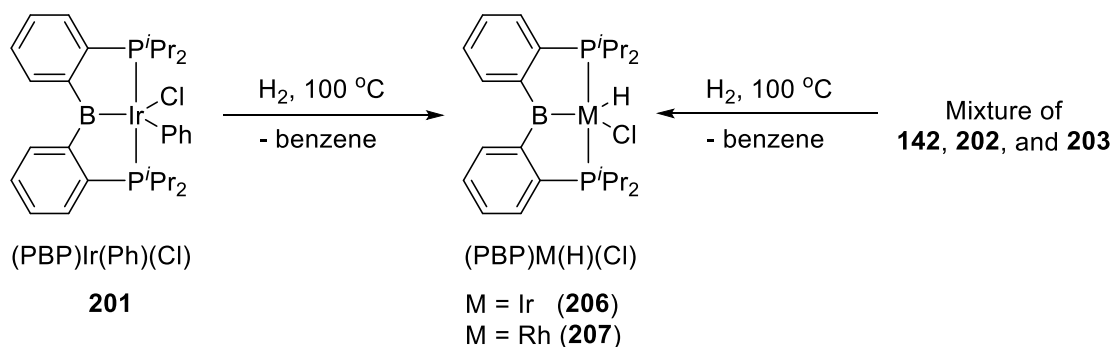


Figure II-8. 2D ³¹P EXSY spectrum of **142**, **202**, and **203** in CDCl₃ at room temperature with a mixing time of 0.15 seconds and d₁ delay of 5 seconds. The orange cross-peaks indicated dynamic exchange between **142** and **203** on the NMR time-scale.

2.2.2 Reactivity of the new PBP pincer complexes

Next, we explored reactions of the new PBP pincer complexes with dihydrogen. Thermolysis of either **201** or the mixture of **142**, **202**, and **203** under an atmosphere of H₂ at 100 °C led to the isolation, upon workup, of the corresponding **206** and **207** with 77% and 89% isolated yields, respectively (Scheme II-3). Both **206** and **207** displayed well-resolved multiplets for their hydride resonances [-22.17 ppm (t, $J_{\text{H-P}} = 11.5$ Hz, Ir-H) and -18.95 ppm (dt, $J_{\text{H-Rh}} = 41.0$ Hz, $J_{\text{H-P}} = 9.9$ Hz, Rh-H)] with no evidence of

broadening from coupling to boron. The ^{11}B NMR chemical shifts (**206**, 72.6 ppm; **207**, 80.1 ppm) were consistent with a boryl moiety, and the value of $^1J_{\text{Rh-P}} = 126$ Hz in **207** matched that of **202** and **204**. Thus, the spectroscopic data indicate that **206/207** is a classical boryl/hydride complex of trivalent Rh/Ir.



Scheme II-3. Thermolysis of PBP Complexes with Dihydrogen

In the solid-state structures determined by XRD (Figure II-9 & Figure II-10), the strictly planar environment on boron atoms and the short M–B distances (1.99–2.01 Å)^{37,75} are consistent with the metal–boryl formulation. From the Fourier difference maps, **206** and **207** showed the hydrogens on the metal leaning toward the boron atom, similar to the results found by Yamashita^{33,37} and Marder.⁷⁸ The XRD-derived and the DFT-calculated values for the B···H distance (2.07(4) and 1.82 Å for **206**; 1.59(3) and 1.48 Å for **207**) may indicate a residual B–H interaction for Rh, but spectroscopic evidence suggests such interaction to be weak (Table II-4 & Table II-5).

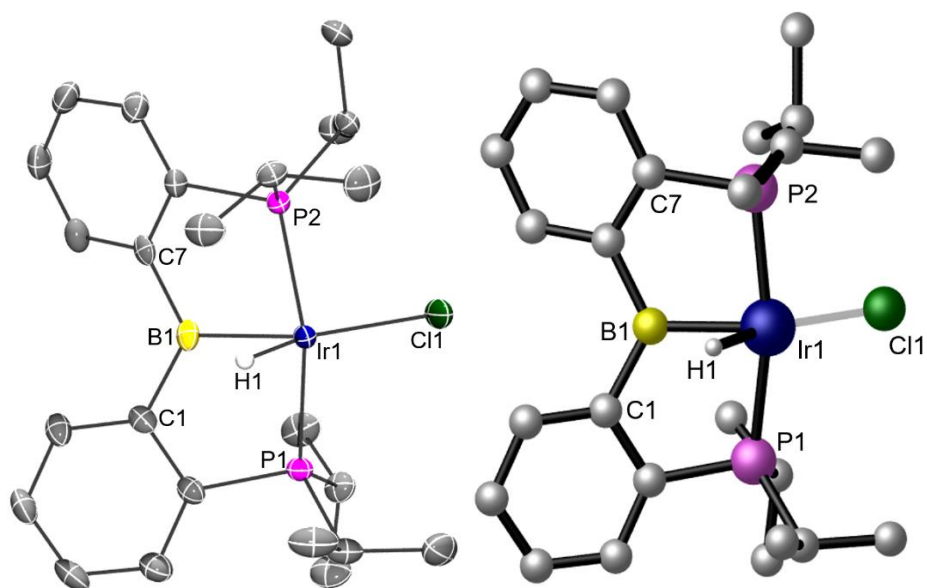


Figure II-9. POV-Ray rendition of the ORTEP drawing (50% thermal ellipsoids; left) and CYLView drawing (right) of **206** showing selected atom labeling. Only one of two independent structures in the unit cell is shown. Hydrogen atoms except Ir-H were omitted for clarity. Selected bond distances (Å) and angles (°): Ir1–B1, 2.003(4); Ir1–Cl1, 2.3815(9); Ir1–H1, 1.55(5); Ir1–P1, 2.2832(9); Ir1–P2, 2.2945(9); B1–Ir1–H1, 69.8(18); B1–Ir1–Cl1, 139.27(11); P1–Ir1–P2, 167.24(3).

Table II-4. Selected Bond Distances (Å) and Angles (°) of X-ray Crystal Structure and DFT Calculation of 206.

	Ir1-B1	Ir1-Cl1	Ir1-H1	B1---H1	B1-Ir1-H1	B1-Ir1-Cl1
XRD	2.003(4)	2.3815(9)	1.55(5)	2.07(4)	69.8(18)	139.27(11)
DFT	2.02	2.43	1.61	1.82	58.7	143.0

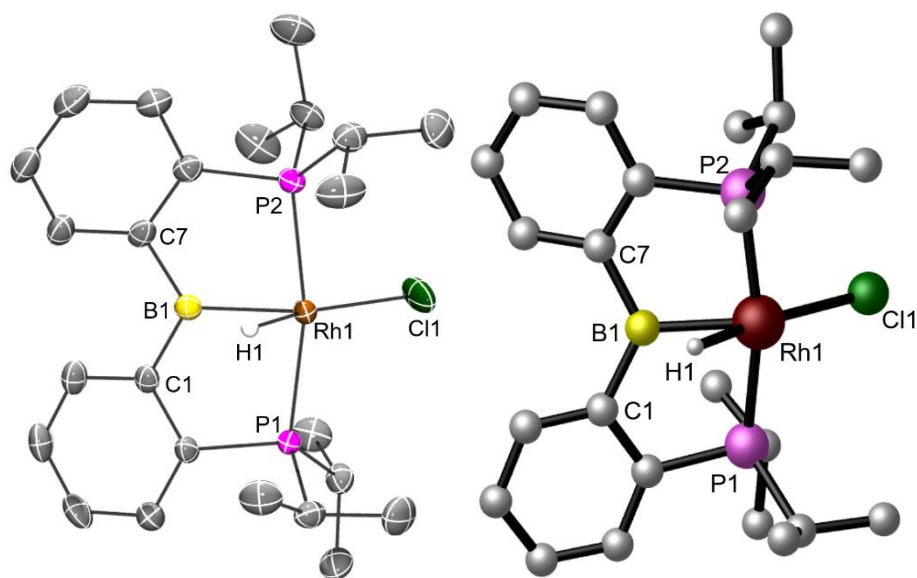
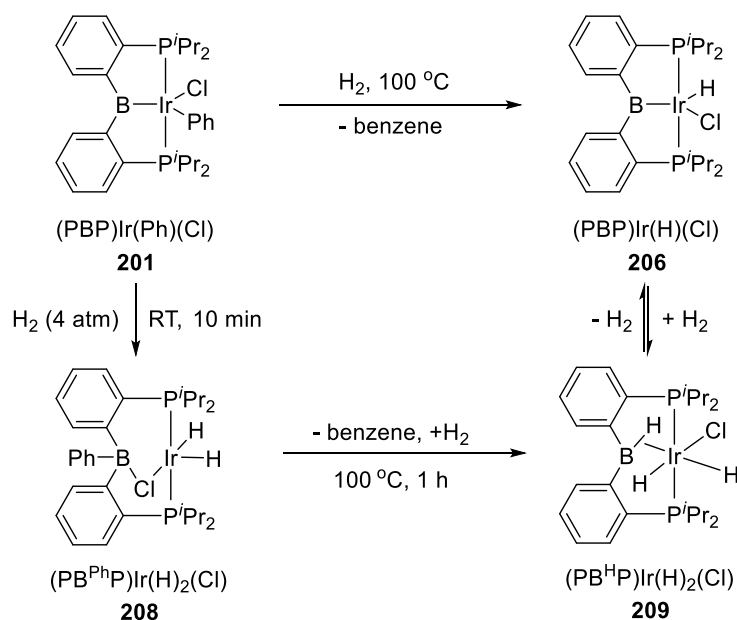


Figure II-10. POV-Ray rendition of the ORTEP drawing (50% thermal ellipsoids; left) and CYLView drawing (right) of **207** showing selected atom labeling. Only one of two independent structures in the unit cell is shown. Hydrogen atoms except Rh-H were omitted for clarity. Selected bond distances (Å) and angles (°): Rh1–B1, 2.010(3); Rh1–Cl1, 2.3703(13); Rh1–H1, 1.51(3); Rh1–P1, 2.2951(13); Rh1–P2, 2.3158(14); B1–Rh1–H1, 51.1(11); B1–Rh1–Cl1, 143.97(8); P1–Rh1–P2, 167.48(2).

Table II-5. Selected Bond Distances (Å) and Angles (°) of X-ray Crystal Structure and DFT Calculation of 207.

	Rh1-B1	Rh1-Cl1	Rh1-H1	B1---H1	B1-Rh1-H1	B1-Rh1-Cl1
XRD	2.010(3)	2.3703(13)	1.51(3)	1.59(3)	51.1(11)	143.97(8)
DFT	2.05	2.38	1.64	1.48	45.5	147.5

Intermediate **208**, resulting from addition of 1 equiv of H₂, was observed in situ in NMR spectra in the reaction of (PBP)Ir(Ph)(Cl) (**201**) with 4 atm of H₂ at room temperature after a few minutes. The loss of boryl metal character is apparent from the upfield ¹¹B NMR resonance at 11.7 ppm, most consistent with a borate. The ¹H NMR phenyl group resonances in **208** were no longer split into five, giving instead the more normal 2:2:1 distribution, suggesting a phenyl shift from Ir to B. The two hydrides gave rise to two doublets of triplets from coupling to each other and two ³¹P nuclei, definitively placing them on Ir. A single ³¹P resonance and virtual coupling evident in the ¹H NMR spectrum suggest trans disposition of the phosphines. The structure we favor for **208** (Scheme II-4) appears to match the NMR observations best, although we cannot exclude additional weak interaction with the B–Ph group. **208** may be viewed as the product of H₂-induced B–C reductive elimination from **201**.



Scheme II-4. Mechanistic Study of the Conversion of 201 to 206

Thermolysis of **208** under H₂ atmosphere (100 °C, 1 h) results in a mixture of **209** and **206**, in equilibrium with free H₂. The two Ir-bound hydrides in **209** gave rise to broad resonances in the ¹H NMR spectrum at room temperature, but cooling of the solution to -50 °C revealed two sharp signals with clear coupling patterns (Figure II-11 & Figure II-12a). The ¹H NMR resonance ascribed to B-H was not part of the exchange process between the two Ir-H sites.

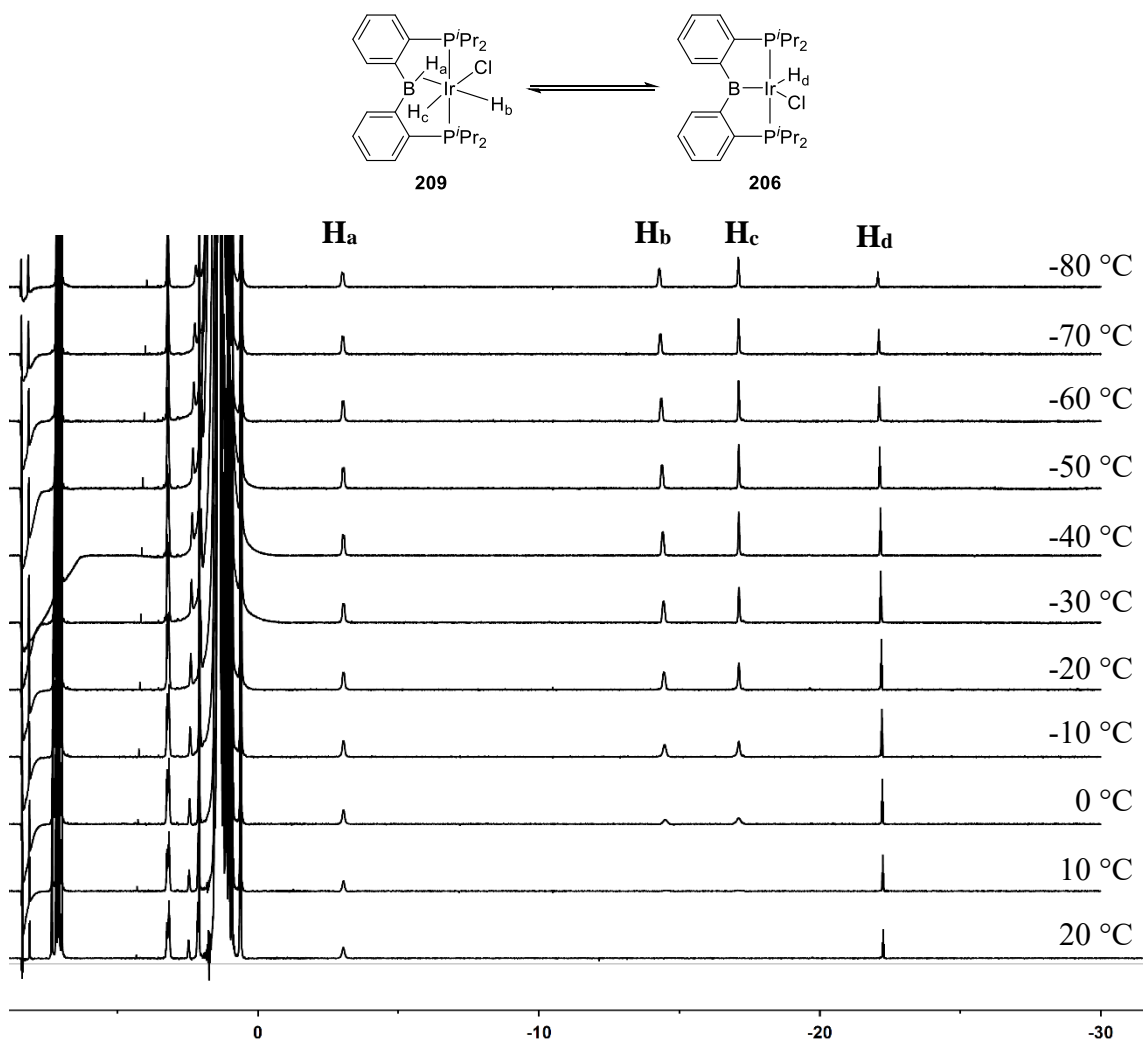


Figure II-11. Low temperature ¹H NMR experiments of **209** in d₈-toluene.

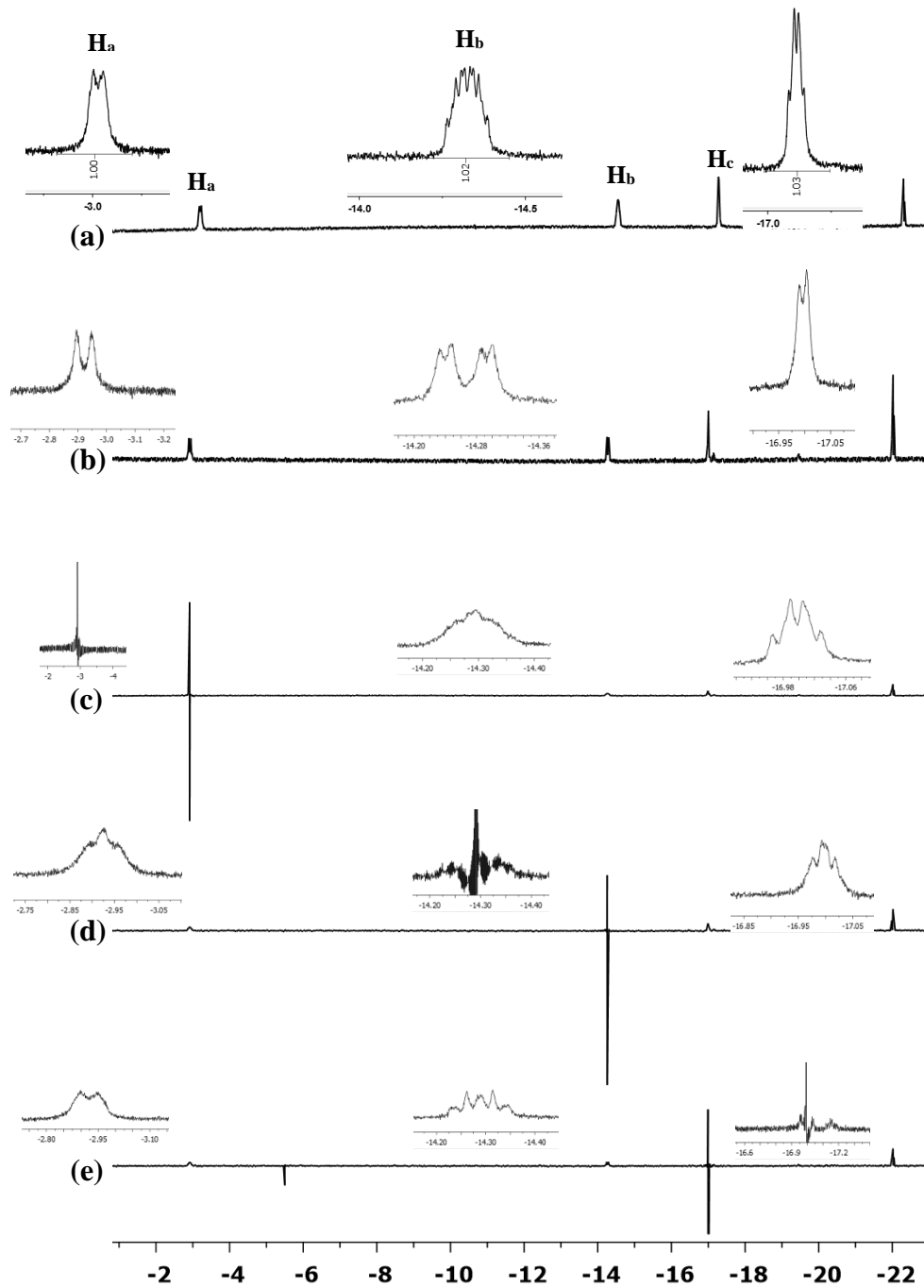


Figure II-12. (a) ^1H spectrum of **209** in d_8 -toluene at $-50\text{ }^\circ\text{C}$. (b) $^1\text{H}\{^{31}\text{P}\}$ spectrum of **209** in d_8 -toluene at $-50\text{ }^\circ\text{C}$. (c~e) Homodecoupled ^1H NMR spectrum of **209** in d_8 -toluene at $-50\text{ }^\circ\text{C}$ ((c) for H_a decoupling, (d) for H_b decoupling, and (e) for H_c decoupling).

In order to simplify the observed multiplicity, a $^1\text{H}\{^{31}\text{P}\}$ spectrum was acquired at $-50\text{ }^\circ\text{C}$ (Figure II-12b). The doublet of doublets signal from H_b indicated coupling of H_b to H_a ($J_{\text{H}_a,\text{H}_b} = 21.6\text{ Hz}$) and H_c ($J_{\text{H}_b,\text{H}_c} = 6\text{ Hz}$), but no observable coupling of H_a to H_c . This observation was also confirmed by homodecoupling experiments at $-50\text{ }^\circ\text{C}$. When H_a was decoupled, H_b showed a broad multiplet, which mainly coupled with H_c and two P; H_c showed a broad quartet, which mainly coupled with H_b and two P (Figure II-12c). When H_b was decoupled, H_a showed a broad triplet, which mainly coupled with two P; H_c showed a broad triplet, which mainly coupled with two P (Figure II-12d). When H_c was decoupled, H_a showed a broad doublet, which mainly coupled with H_b ; H_b showed a broad doublet of triplets, which mainly coupled with H_a and two P (Figure II-12e). Therefore, the connectivity of the three hydrides of **209** proposed in Scheme II-4 greatly matches the homodecoupling experiments.

We were not able to prepare pure bulk samples of **209** because of facile H_2 loss, but we succeeded in obtaining a single crystal for an X-ray diffraction study (Figure II-13). The X-ray structures of **206** and **209** contain the same non-hydrogen atoms attached to Ir with similar attendant angles, and the B–H or Ir–H hydrogen atoms of **209** were not located. However, the Ir–B distance in **209** (2.137(4) and 2.135(4) Å for two independent molecules) is considerably longer than that in **206** (2.003(4) and 1.995(4) Å). In addition, the sum of angles from non-hydrogen substituents on boron in **209** is ca. 357.5 versus 360° for **206**. These metrics of the structure of **209** are closely reproduced in the DFT-optimized geometry of this molecule, which also gave a short (1.33 Å) distance for the coordinated B–H (Figure II-13 & Table II-6).

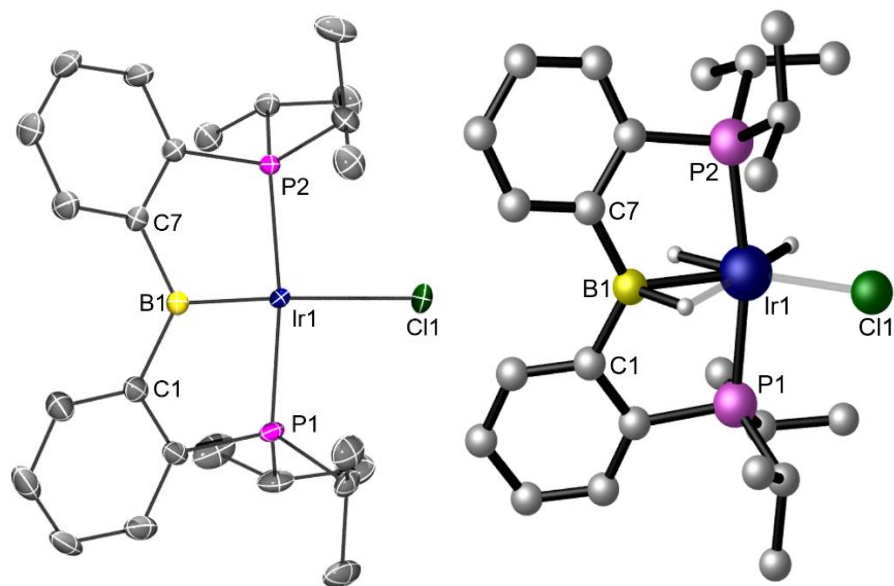


Figure II-13. POV-Ray rendition of the ORTEP drawing (50% thermal ellipsoids; left) and CYLView drawing (right) of **209** showing selected atom labeling. Only one of two independent structures in the unit cell is shown. Hydrogen atoms were omitted for clarity. Selected bond distances (Å) and angles (°): Ir1–B1, 2.137(4); Ir1–Cl1, 2.4180(13); Ir1–P1, 2.3032(13); Ir1–P2, 2.3030(12); B1–Ir1–P1, 84.72(11); B1–Ir1–Cl1, 138.94(11); P1–Ir1–P2, 169.55(3).

Table II-6. Selected Bond Distances (Å) and Angles (°) of X-ray Crystal Structure and DFT Calculation of 209.

	Ir1-B1	Ir1-Cl1	Ir1-P1	B1-Ir1-Cl1	B1-Ir1-P1
XRD	2.137(4)	2.4180(13)	2.3032(13)	138.94(11)	84.72(11)
DFT	2.15	2.47	2.34	136.8	84.3

The views of **206** and **209** shown in Figure II-14 (down the B–Ir view axis) emphasize that the aryl groups on B adopt different conformations in **206** and **209**. The structural data and the ^{11}B NMR chemical shift of **209** (53.7 ppm) are consistent with the proposed σ -borane/dihydride formulation.

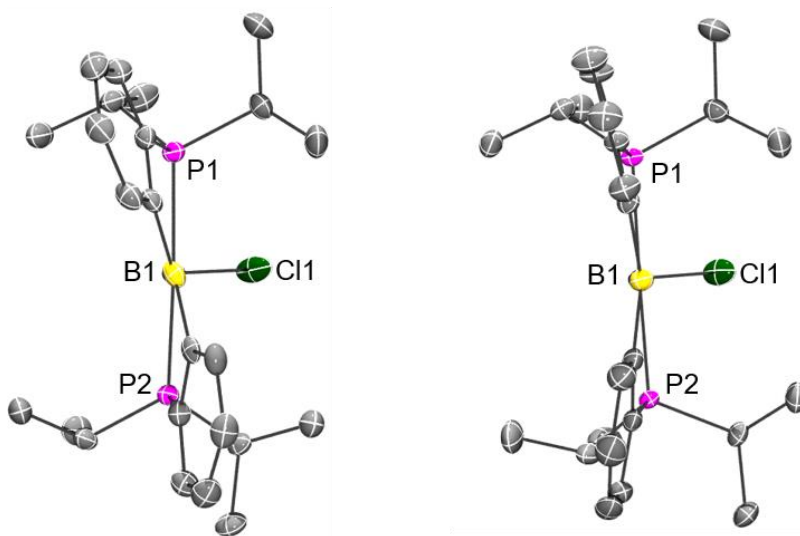
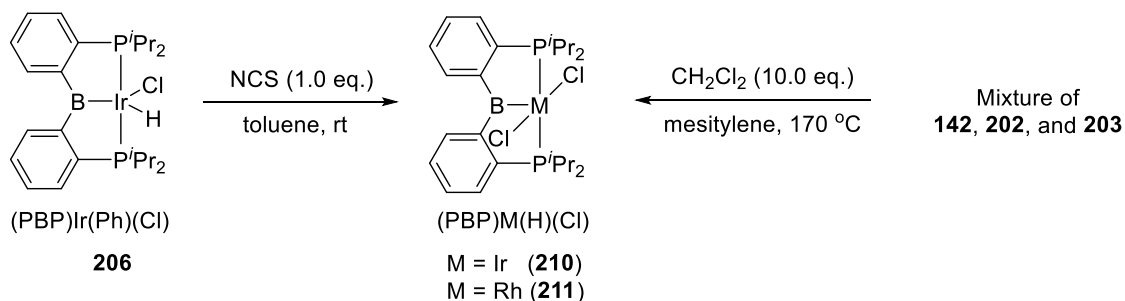


Figure II-14. ORTEP drawing (50% probability ellipsoids) of **206**, **209** showing selected atom labeling. Only one of two independent structures in the unit cell is shown for all structures. Hydrogen atoms are omitted for clarity.

206 reacted cleanly with 1 equiv of *N*-chlorosuccinimide in toluene to give (PBP)IrCl₂ (**210**) in 81% yield after workup. The Rh analogue (**211**) was synthesized via thermolysis of the mixture of **142**, **202**, and **203** in mesitylene in the presence of CH₂Cl₂ at 170 °C for 18 h (Scheme II-5). The presence of a boryl ligand was corroborated by ^{11}B

NMR spectroscopy (**210**, 73.0 ppm; **211**, 91.3 ppm) and by single-crystal X-ray diffraction studies (Figure II-15).



Scheme II-5. Synthesis of (PBP)MCl₂

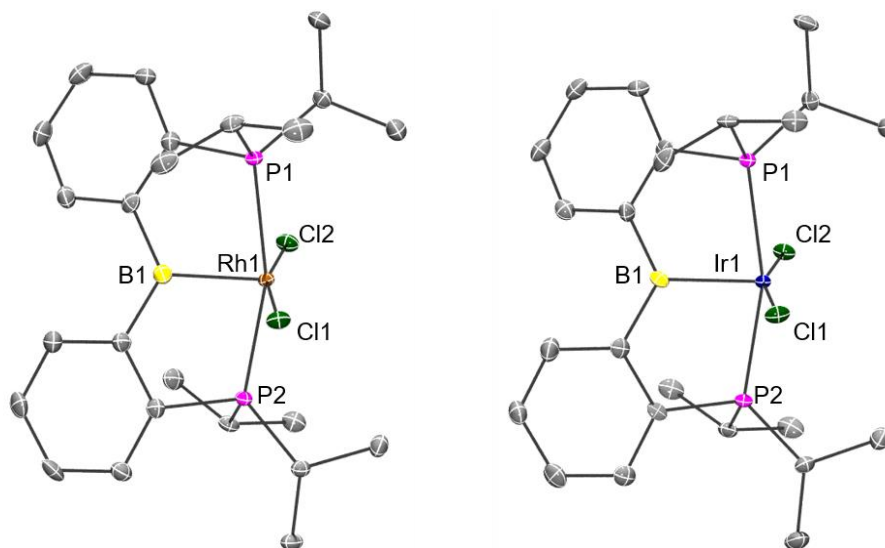


Figure II-15. ORTEP drawing (50% probability ellipsoids) of **211**, and **210**, showing selected atom labeling. Only one of two independent structures in the unit cell is shown for all structures. Hydrogen atoms are omitted for clarity. Selected bond distances (Å) and angles (°) for **211**: Rh1–B1, 1.969(5); Rh1–Cl1, 2.3322(10); Rh1–Cl2, 2.3275(10); Rh1–P1, 2.3413(11); Rh1–P2, 2.3544(11); B1–Rh1–Cl1, 98.26(14); Cl1–Rh1–Cl2, 164.39(4);

P1–Rh1–P2, 163.73(4). Selected bond distances (Å) and angles (°) for **210**: Ir1–B1, 1.995(8); Ir1–C11, 2.3324(17); Ir1–C12, 2.3359(17); Ir1–P1, 2.3445(18); Ir1–P2, 2.3504(18); B1–Ir1–C11, 97.2(2); C11–Ir1–C12, 164.43(6); P1–Ir1–P2, 164.31(6).

2.3 Conclusions

We have shown that boryl/bis(phosphine) PBP pincer complexes can be accessed by facile insertion of Rh and Ir into the B–Ph bond of a borane/bis(phosphine) ligand. This formal B–C oxidative addition can be viewed as an inverse of the B–C reductive elimination postulated in transition-metal-catalyzed C–H borylation catalysis.¹⁵¹ The PBP ligand displays a diversity of structural forms, with boryl, borane, and borate variants possible.

2.4 Experimental Section

2.4.1 General considerations

Unless specified otherwise, all manipulations were performed under an Ar atmosphere using standard Schlenk line or glovebox techniques. Toluene, diethyl ether, pentane, and isooctane were dried and deoxygenated (by purging) using a solvent purification system (Innovative Technology Pure Solv MD-5 Solvent Purification System) and stored over molecular sieves in an Ar-filled glove box. C₆D₆ was dried over NaK/Ph₂CO/18-crown-6, distilled or vacuum transferred and stored over molecular sieves in an Ar-filled glovebox. CH₂Cl₂, CDCl₃, cyclohexane, and C₆D₁₂ were dried over CaH₂, distilled or vacuum transferred and stored over molecular sieves in an Ar-filled glove box.

$[\text{Rh}(\text{COD})\text{Cl}]_2$,¹⁵² $[\text{Rh}(\text{COD})\text{I}]_2$,¹⁵³ $[\text{Ir}(\text{COE})_2\text{Cl}]_2$,¹⁵⁴ Diisopropyl(2-bromophenyl) phosphine (**133a**),¹⁰⁴ and $\text{PB}^{\text{Ph}}\text{P}$ ligand **134a**¹²⁷ were prepared via literature procedures. All other chemicals were used as received from commercial vendors.

2.4.2 Physical methods

NMR spectra were recorded on a Varian Inova 400 (^1H NMR, 399.535 MHz; ^{13}C NMR, 100.467 MHz; ^{11}B NMR, 128.185 MHz; ^{31}P NMR, 161.734 MHz) and Varian Inova 500 (^1H NMR, 499.703 MHz; ^{13}C NMR, 125.697 MHz; ^{31}P NMR, 202.265 MHz) spectrometer. Chemical shifts are reported in δ (ppm). For ^1H and ^{13}C NMR spectra, the residual solvent peak was used as an internal reference (^1H NMR: δ 7.16 for C_6D_6 , 7.26 for CDCl_3 , and 1.38 for C_6D_{12} ; ^{13}C NMR: δ 128.06 for C_6D_6 , 77.16 for CDCl_3 , and 26.43 for C_6D_{12}). ^{11}B NMR spectra were referenced externally with BF_3 etherate at δ 0. ^{31}P NMR spectra were referenced externally with 85% phosphoric acid at δ 0. ^{31}P EXSY spectrum was measured on a Bruker 400 NMR spectrometer. Elemental analyses were performed by CALI Labs, Inc. (Parsippany, NJ).

2.4.3 Synthesis and characterization of rhodium and iridium complexes

Mixture of $(\text{PBP})\text{Rh}(\text{Ph})(\text{Cl})$ (142, 202, and 203). To a cold solution of **134a** (1.54 g, 3.24 mmol) in CH_2Cl_2 (6 mL) was added $[\text{Rh}(\text{COD})\text{Cl}]_2$ (800 mg, 1.62 mmol). The resulting orange solution was stirred at room temperature for 3 h, and yellow solids slowly precipitated from the solution over time. The yellow powder was collected on an “M” frit, washed with CH_2Cl_2 and dried under vacuum for 3 h, yielding a yellow solid

(1.90 g, 95%). Three isomers **142**, **202**, and **203** were observed in $^{31}\text{P}\{^1\text{H}\}$ NMR spectrum with a ratio of 31:43:26 (65.0~80.0 ppm (br), 50.4 ppm (d), 88.8 ppm (d)) in CDCl_3 (0.050 M) at ambient temperature. **142**: $^{31}\text{P}\{^1\text{H}\}$ NMR (202 MHz, CDCl_3): δ 65.0~80.0 (br). ^{11}B NMR (128 MHz, CDCl_3): δ 20.8 (br). The featured peaks in $^{13}\text{C}\{^1\text{H}\}$ NMR (101 MHz, CDCl_3): δ 168.8 (br, $C_{\text{Ar-B}}$), 156.2 (br, $C_{\text{Ph-B}}$), 139.3 (d, $J_{\text{P-C}} = 47$ Hz, $C_{\text{Ar-P}}$). The full assignment of **202** was reported in $^{13}\text{C}\{^1\text{H}\}$ NMR spectrum at low temperature (213 K) in previous literature.¹²⁷ **202**: $^{31}\text{P}\{^1\text{H}\}$ NMR (202 MHz, CDCl_3): δ 50.4 (d, $J_{\text{Rh-P}} = 126$ Hz). $^{11}\text{B}\{^1\text{H}\}$ NMR (128 MHz, CDCl_3): δ 94.3 (br). ^1H NMR (500 MHz, CDCl_3): δ 8.07 (m, 2H, Ar-H), 7.92 (br s, 1H, Ph-H), 7.59 (m, 2H, Ar-H), 7.52 (m, 4H, Ar-H), 6.69 (br s, 1H, Ph-H), 3.10 (m, 2H, CHMe_2), 2.40 (m, 2H, CHMe_2), 1.31 (dvt, $J_{\text{H-H}} = 6.7$ Hz, $J_{\text{H-P}} = 6.7$ Hz, 6H, CHMe_2), 1.11 (dvt, $J_{\text{H-H}} = 7.6$ Hz, $J_{\text{H-P}} = 7.6$ Hz, 6H, CHMe_2), 0.90 (dvt, $J_{\text{H-H}} = 7.6$ Hz, $J_{\text{H-P}} = 7.6$ Hz, 6H, CHMe_2), 0.33 (dvt, $J_{\text{H-H}} = 7.1$ Hz, $J_{\text{H-P}} = 7.1$ Hz, 6H, CHMe_2). Resonances for three phenyl protons were obscured by overlap with peaks from other isomers. The featured peaks in $^{13}\text{C}\{^1\text{H}\}$ NMR (101 MHz, CDCl_3): δ 155.4 (br, $C_{\text{Ar-B}}$), 148.9 (dt, $J_{\text{Rh-C}} = 35$ Hz, $J_{\text{P-C}} = 8.8$ Hz, $C_{\text{Ph-Rh}}$), 144.0 (vt, $J_{\text{P-C}} = 19$ Hz, $C_{\text{Ar-P}}$). **203**: $^{31}\text{P}\{^1\text{H}\}$ NMR (202 MHz, CDCl_3): δ 88.8 (d, $J_{\text{Rh-P}} = 194$ Hz). $^{11}\text{B}\{^1\text{H}\}$ NMR (128 MHz, CDCl_3): δ 20.8 (br). The featured peaks in $^{13}\text{C}\{^1\text{H}\}$ NMR (101 MHz, CDCl_3): δ 164.9 (br, $C_{\text{Ar-B}}$). The unidentifiable resonances in $^{13}\text{C}\{^1\text{H}\}$ NMR (101 MHz, CDCl_3): δ 137.6 (s), 134.6 (s), 131.8 (m), 131.1 (s), 130.2 (s), 129.5 (s), 128.9 (s), 128.1 (s), 127.4 (s), 126.4 (s), 126.2 (s), 124.9 (s), 123.6 (s), 122.0 (s), 28.7 (br, CHMe_2), 27.7 (br, CHMe_2), 27.0 (m, CHMe_2), 23.6 (m, CHMe_2), 22.2 (br, CHMe_2), 21.6 (s, CHMe_2), 21.4 (s, CHMe_2), 19.9 (s, CHMe_2), 18.1 (s, CHMe_2), 17.6 (s, CHMe_2).

Mixture of (PBP)Rh(Ph)(I) (204 and 205). To a solution of **134a** (95 mg, 0.20 mmol) in CH₂Cl₂ (3 mL) was added [Rh(COD)I]₂ (82 mg, 0.12 mmol). The resulting brown solution was stirred at room temperature for 2 h, and the volatiles were removed under vacuum. The residues were redissolved in pentane and filtered through a pad of Celite. Pentane solvent was removed under vacuum, yielding an orange solid (115 mg, 82%). Two isomers (**204** and **205**) were observed in ³¹P{¹H} NMR spectrum with a ratio of 1.6:1 (50.4 ppm (d) and 87.1 ppm (d)) in CDCl₃ (0.050 M). **204**: ³¹P{¹H} NMR (202 MHz, CDCl₃) δ 50.4 (d, *J*_{Rh-P} = 125 Hz). ¹¹B{¹H} NMR (128 MHz, CDCl₃): δ 95.3 (br). ¹H NMR (400 MHz, CDCl₃) δ 8.11 (m, 2H, Ar-*H*), 7.61 (m, 2H, Ar-*H*), 7.53 (m, 4H, Ar-*H*), 6.60 (br s, 2H, Ph-*H*), 6.54 (t, *J*_{H-H} = 6.6 Hz, 1H, Ph-*H*), 3.42 (m, 2H, CHMe₂), 2.57 (m, 2H, CHMe₂), 1.27 (m, 12H, CHMe₂), 0.75 (dvt, *J*_{H-H} = 7.5 Hz, *J*_{H-P} = 7.5 Hz, 6H, CHMe₂), 0.23 (dvt, *J*_{H-H} = 7.2 Hz, *J*_{H-P} = 7.2 Hz, 6H, CHMe₂). Resonances for two phenyl protons were obscured by overlap with peaks from other isomers. The featured peaks in ¹³C{¹H} NMR (126 MHz, CDCl₃): δ 154.9 (br vt, *J*_{P-C} = 22 Hz, C_{Ar-B}), 147.9 (dt, *J*_{Rh-C} = 36 Hz, *J*_{P-C} = 8.5 Hz, C_{Ph-Rh}), 143.9 (dvt, *J*_{P-C} = 20 Hz, *J*_{Rh-C} = 2.5 Hz, C_{Ar-P}), 131.9 (vt, *J*_{P-C} = 9.6 Hz, C_{Ar}), 26.8 (vt, *J*_{P-C} = 12 Hz, CHMe₂), 24.2 (vt, *J*_{P-C} = 10.9 Hz, CHMe₂), 20.0 (s, CHMe₂), 18.4 (s, CHMe₂), 18.3 (s, CHMe₂), 17.4 (s, CHMe₂). **205**: ³¹P{¹H} NMR (202 MHz, CDCl₃) δ 87.1 (d, *J*_{Rh-P} = 191 Hz). ¹¹B{¹H} NMR (128 MHz, CDCl₃): δ 22.5 (br). ¹H NMR (400 MHz, CDCl₃) δ 8.06 (d, *J*_{H-H} = 7.4 Hz, 2H), 7.45 (t, *J*_{H-H} = 7.3 Hz, 2H), 7.36 (t, *J*_{H-H} = 7.1 Hz, 3H), 7.20 (m, 2H), 7.14 (t, *J*_{H-H} = 7.4 Hz, 2H), 6.31 (d, *J*_{H-H} = 7.3 Hz, 2H), 2.30 (m, 2H, CHMe₂), 2.08 (m, 2H, CHMe₂), 1.48 (dd, *J*_{H-P} = 15.6, *J*_{H-H} = 7.0 Hz, 12H, CHMe₂), 1.20 (m, 6H, CHMe₂), 0.86 (m, 6H, CHMe₂). The featured peaks in

$^{13}\text{C}\{^1\text{H}\}$ NMR (126 MHz, CDCl_3): δ 162.7 (br, $C_{\text{Ar-B}}$), 137.8 (br, $C_{\text{Ph-B}}$), 137.2 (d, $J_{\text{P-C}} = 48$ Hz, $C_{\text{Ar-P}}$), 131.6 (d, $J_{\text{P-C}} = 22$ Hz, C_{Ar}), 130.4 (d, $J_{\text{P-C}} = 4.1$ Hz, C_{Ar}), 125.2 (d, $J_{\text{P-C}} = 7.2$ Hz), 28.7 (d, $J_{\text{P-C}} = 26$ Hz, CHMe_2), 27.9 (d, $J_{\text{P-C}} = 22$ Hz, CHMe_2), 21.2 (s, CHMe_2), 19.3 (s, CHMe_2), 19.0 (s, CHMe_2), 18.8 (s, CHMe_2). The unidentifiable resonances in $^{13}\text{C}\{^1\text{H}\}$ NMR (126 MHz, CDCl_3): δ 133.5 (s), 131.0 (s), 129.6 (m), 128.4 (s), 127.5 (s), 122.3 (s).

(PBP)Ir(Ph)(Cl) (201). In a 10 mL Teflon screw-capped round-bottomed flask, $[(\text{COE})_2\text{IrCl}]_2$ (896 mg, 1.00 mmol) was added to a toluene solution (4 mL) of **134a** (949 mg, 2.00 mmol), and the mixture was stirred at 100 °C for 5 h. After being cooled down to room temperature, the solution was layered with isooctane, and the flask was placed in a -35 °C freezer overnight. The solid was collected, washed with isooctane, and dried under vacuum, yielding an orange solid (1.24 g, 88%). Single crystals were obtained from a pentane solution of **201** in a -35 °C freezer overnight. $^{31}\text{P}\{^1\text{H}\}$ NMR (202 MHz, C_6D_6): δ 44.9. $^{11}\text{B}\{^1\text{H}\}$ NMR (128 MHz, C_6D_6): δ 75.9 (br). ^1H NMR (500 MHz, C_6D_6): δ 8.21 (d, $J_{\text{H-H}} = 7.0$ Hz, 2H, Ar-H), 7.57 (br, 1H, Ph-H), 7.15 (m, 6H, Ar-H), 6.78 (br, 1H, Ph-H), 6.54 (t, $J_{\text{H-H}} = 7.0$ Hz, 1H, Ph-H), 6.38 (br, 1H, Ph-H), 6.00 (br, 1H, Ph-H), 3.38 (m, 2H, CHMe_2), 2.50 (m, 2H, CHMe_2), 1.11 (m, 12H, CHMe_2), 0.98 (dvt, $J_{\text{H-H}} \approx J_{\text{H-P}} = 7.5$ Hz, 6H, CHMe_2), 0.36 (q, $J_{\text{H-H}} \approx J_{\text{H-P}} = 7.5$ Hz, 6H, CHMe_2). $^{13}\text{C}\{^1\text{H}\}$ NMR (126 MHz, C_6D_6): δ 158.6 (vt, $J_{\text{P-C}} = 19.2$ Hz), 143.1 (vt, $J_{\text{P-C}} = 23.9$ Hz), 137.9 (br), 131.5, 130.9 (vt, $J_{\text{P-C}} = 8.7$ Hz), 130.3 (vt, $J_{\text{P-C}} = 7.2$ Hz), 129.6, 128.4 (vt, $J_{\text{P-C}} = 3.5$ Hz), 125.6 (br), 121.8, 23.1 (vt, $J_{\text{P-C}} = 13.0$ Hz, CHMe_2), 22.5 (vt, $J_{\text{P-C}} = 14.2$ Hz, CHMe_2), 19.6 (CHMe_2), 17.9

(vt, $J_{P-C} = 2.2$ Hz, $CHMe_2$), 17.8 ($CHMe_2$), 17.8 ($CHMe_2$). Elem. Anal. Calcd for $C_{30}H_{41}BClIrP_2$: C, 51.32; H, 5.89. Found: C, 51.41; H, 5.77.

(PBP)Ir(H)(Cl) (206). In a 25 mL Teflon screw-capped round-bottomed flask, **(PBP)Ir(Ph)(Cl) (201)** (362 mg, 0.52 mmol) was dissolved in cyclohexane (5 mL), and the solution was degassed via freeze-pump-thaw. The flask was refilled with H_2 (1 atm) and stirred at 100 °C for 1 h. The products were **206** and **209** in this step. In order to remove hydrogen from **209**, the reaction was degassed via freeze-pump-thaw and stirred at 100 °C for another 1 h. Repeating the degassing-heating cycle twice more was necessary in order to achieve >99% conversion to **206**. The volatiles were removed under vacuum, and the product was washed with isooctane and dried under vacuum, yielding a yellow solid (250 mg, 77%). Single crystals were obtained from a pentane solution of **206** in a -35 °C freezer overnight. $^{31}P\{^1H\}$ NMR (202 MHz, C_6D_6): δ 61.9. $^{11}B\{^1H\}$ NMR (128 MHz, C_6D_6): δ 72.6 (br). 1H NMR (500 MHz, C_6D_6) δ 8.22 (d, $J_{H-H} = 7.3$ Hz, 2H, Ar-*H*), 7.35 (m, 2H, Ar-*H*), 7.21 (t, $J_{H-H} = 7.3$ Hz, 2H, Ar-*H*), 7.16 (m, 2H, Ar-*H*), 3.31 (m, 2H, $CHMe_2$), 2.48 (m, 2H, $CHMe_2$), 1.25 (dvt, $J_{H-H} \approx J_{H-P} = 7.6$ Hz, 6H, $CHMe_2$), 1.19 (m, 12H, $CHMe_2$), 0.96 (dvt, $J_{H-H} \approx J_{H-P} = 7.6$ Hz, 6H, $CHMe_2$), -22.17 (t, $J_{H-P} = 11.5$ Hz, 1H, Ir-*H*). $^{13}C\{^1H\}$ NMR (126 MHz, C_6D_6): δ 160.1 (br), 146.3 (vt, $J_{P-C} = 23.4$ Hz), 130.7 (vt, $J_{P-C} = 1.6$ Hz), 130.5 (vt, $J_{P-C} = 8.5$ Hz), 129.7 (s), 128.3 (vt, $J_{P-C} = 3.4$ Hz), 24.4 (vt, $J_{P-C} = 14.3$ Hz, $CHMe_2$), 22.9 (vt, $J_{P-C} = 13.8$ Hz, $CHMe_2$), 19.9 ($CHMe_2$), 18.9 ($CHMe_2$), 18.6 ($CHMe_2$), 17.3 ($CHMe_2$). Elem. Anal. Calcd for $C_{24}H_{37}BClIrP_2$: C, 46.05; H, 5.96. Found: C, 46.22; H, 6.08.

(PBP)Rh(H)(Cl) (207). In a 25 mL Teflon screw-capped round-bottomed flask, a suspension of a mixture of **142**, **202**, and **203** (368 mg, 0.60 mmol) in cyclohexane (9 mL) was degassed via freeze-pump-thaw, and then the flask was refilled with H₂ (1 atm). The reaction was stirred at 100 °C for 12 h. During the heating, the solid completely dissolved in cyclohexane and the solution turned dark-orange. After cooling down to room temperature, the volatiles were removed under vacuum, and the product was washed with isooctane, yielding an orange solid (288 mg, 89%). Single crystals were obtained from a pentane solution of **207** in a -35 °C freezer overnight. ³¹P{¹H} NMR (162 MHz, C₆D₆): δ 63.3 (d, J_{P-Rh} = 126). ¹¹B{¹H} NMR (128 MHz, C₆D₆): δ 80.1 (br). ¹H NMR (400 MHz, C₆D₆) δ 8.16 (m, 2H, Ar-H), 7.37 (m, 2H, Ar-H), 7.19 (m, 4H, Ar-H), 3.12 (m, 2H, CHMe₂), 2.25 (m, 2H, CHMe₂), 1.34 (dvt, J_{H-H} = 7.4 Hz, J_{H-P} = 7.4 Hz, 6H, CHMe₂), 1.18 (m, 12H, CHMe₂), 0.99 (dvt, J_{H-H} = 7.5 Hz, J_{H-P} = 7.5 Hz, 6H, CHMe₂), -18.95 (dvt, J_{H-Rh} = 41.0 Hz, J_{H-P} = 9.9 Hz, 1H, Rh-H). ¹³C{¹H} NMR (126 MHz, C₆D₆) δ 157.7 (br), 145.7 (vtd, J_{P-C} = 18.6, J_{C-Rh} = 2.6 Hz), 131.4 (vt, J_{P-C} = 9.2 Hz), 130.8, 129.8, 129.2 (vt, J_{P-C} = 2.9 Hz), 24.6 (vt, J_{P-C} = 11.1 Hz, CHMe₂), 23.4 (vt, J_{P-C} = 11.2 Hz, CHMe₂), 20.0 (vt, J_{P-C} = 2.5 Hz, CHMe₂), 19.3 (vt, J_{P-C} = 2.1 Hz, CHMe₂), 18.9 (vt, J_{P-C} = 3.5 Hz, CHMe₂), 17.1 (CHMe₂). Elem. Anal. Calcd for C₂₄H₃₇BCIP₂Rh: C, 53.71; H, 6.95. Found: C, 53.79; H, 7.23.

In-situ observation of (PB^{Ph}P)Ir(H)₂Cl (208). In a J. Young tube, (PBP)Ir(Ph)(Cl) (**201**) (14 mg, 0.02 mmol) was dissolved in C₆D₆ (0.5 mL). The entire tube was cooled in a liquid nitrogen cooling bath under vacuum, refilled with H₂ (1 atm) and allowed to warm up to ambient temperature. [*Caution! This procedure results in pressures of several*

atmospheres inside the Y. Young NMR tube. Although we have performed this without incident on multiple occasions using proper personal protective equipment (goggles or face mask, flame-resistant laboratory coat, and a blast shield), potential for tube failure and explosion exists. Readers are encouraged to evaluate the potential hazards of this procedure within their own laboratory context before attempting to reproduce the experiment] Within 10 minutes, about 80% conversion was detected by ^1H , $^{31}\text{P}\{^1\text{H}\}$, and $^{11}\text{B}\{^1\text{H}\}$ NMR spectra. $^{31}\text{P}\{^1\text{H}\}$ NMR (202 MHz, C_6D_6): δ 37.9. $^{11}\text{B}\{^1\text{H}\}$ NMR (128 MHz, C_6D_6): δ 11.7 (br). ^1H NMR (500 MHz, C_6D_6) δ 8.27 (d, $J_{\text{H-H}} = 7.6$ Hz, 2H, Ar-H), 7.66 (d, $J_{\text{H-H}} = 7.5$ Hz, 2H, Ph-H), 7.48 (t, $J_{\text{H-H}} = 7.1$ Hz, 1H, Ph-H), 7.36 (m, 2H, Ar-H), 7.25 (t, $J_{\text{H-H}} = 7.3$ Hz, 2H, Ar-H), 7.09 (t, $J_{\text{H-H}} = 7.3$ Hz, 2H, Ar-H), 6.88 (t, $J_{\text{H-H}} = 7.6$ Hz, 2H, Ph-H), 2.84 (m, 2H, CHMe_2), 2.14 (m, 2H, CHMe_2), 1.44 (m, 12H, CHMe_2), 1.04 (dvt, $J_{\text{H-H}} \approx J_{\text{H-P}} = 8.3$ Hz, 6H, CHMe_2), 0.66 (dvt, $J_{\text{H-H}} \approx J_{\text{H-P}} = 6.7$ Hz, 6H, CHMe_2), -16.46 (td, $J_{\text{H-P}} = 11.2$, $J_{\text{H-H}} = 5.2$ Hz, 1H, Ir-H), -20.50 (td, $J_{\text{H-P}} = 13.8$, $J_{\text{H-H}} = 5.2$ Hz, 1H, Ir-H). $^{13}\text{C}\{^1\text{H}\}$ NMR (126 MHz, C_6D_6) δ 159.5 (br m), 142.8 (vt, $J_{\text{P-C}} = 22.5$ Hz), 142.0, 133.8, 132.5 (vt, $J_{\text{P-C}} = 7.9$ Hz), 130.7, 129.8, 125.7 (vt, $J_{\text{P-C}} = 3.6$ Hz), 117.6 (br s), 30.1 (vt, $J_{\text{P-C}} = 11.8$ Hz, CHMe_2), 28.5 (vt, $J_{\text{P-C}} = 17.2$ Hz, CHMe_2), 21.0 (CHMe_2), 20.2 (CHMe_2), 19.8 (CHMe_2), 19.5 (CHMe_2). One ^{13}C NMR signal from aromatic region was missing due to overlap with the signals from **201** and **209**. Satisfactory elemental analysis data cannot be obtained due to the facile transformation of **208** to **209** in C_6D_6 at room temperature under hydrogen atmosphere. After 1 h, about 2% conversion was observed. After 40 h, 78% conversion was detected.

In-situ observation of (PB^HP)Ir(H)₂(Cl) (209). In a J. Young tube, (PBP)Ir(Ph)(Cl) (201) (14 mg, 0.02 mmol) was dissolved in C₆D₆ (0.5 mL). The entire tube was cooled in a liquid nitrogen cooling bath under vacuum, and then refilled with H₂ (1 atm), followed by slow warming to ambient temperature and then thermolysis at 100 °C for 1 h. [*Caution! This procedure results in pressures of several atmospheres inside the Y. Young NMR tube. Although we have performed this without incident on multiple occasions using proper personal protective equipment (goggles or face mask, flame-resistant laboratory coat, and a blast shield), potential for tube failure and explosion exists. Readers are encouraged to evaluate the potential hazards of this procedure within their own laboratory context before attempting to reproduce the experiment*] After cooling down to room temperature, about 90% conversion was detected by ¹H, ³¹P{¹H}, and ¹¹B{¹H} NMR spectra. ³¹P{¹H} NMR (162 MHz, C₆D₆): δ 53.7. ¹¹B{¹H} NMR (128 MHz, C₆D₆): δ 53.5 (br). ¹H NMR (399 MHz, C₆D₆) δ 8.48 (d, J_{H-H} = 7.6 Hz, 2H, Ar-H), 7.35 (m, 2H, Ar-H), 7.22 (t, J_{H-H} = 7.4 Hz, 2H, Ar-H), 7.09 (t, J_{H-H} = 7.3 Hz, 2H, Ar-H), 3.28 (m, 2H, CHMe₂), 2.15 (m, 2H, CHMe₂), 1.36 (dvt, J_{H-H} ≈ J_{H-P} = 7.9 Hz, 6H, CHMe₂), 1.13 (m, 12H, CHMe₂), 0.67 (dvt, J_{H-H} ≈ J_{H-P} = 7.7 Hz, 6H, CHMe₂), -2.84 (br, 1H, B-H), -14.70 (br, 1H, Ir-H), -16.89 (br, 1H, Ir-H). ¹³C{¹H} NMR (126 MHz, C₆D₆): δ 160.4 (br), 146.3 (vt, J_{P-C} = 23.1 Hz), 131.9 (vt, J_{P-C} = 7.9 Hz), 130.8 (vt, J_{P-C} = 2.0 Hz), 130.2 (s), 127.6 (vt, J_{P-C} = 3.6 Hz), 23.4 (vt, J_{P-C} = 16.5 Hz, CHMe₂), 21.4 (vt, J_{P-C} = 14.0 Hz, CHMe₂), 19.0 (CHMe₂), 19.0 (CHMe₂), 18.7 (CHMe₂), 16.0 (CHMe₂). Satisfactory elemental analysis data cannot be obtained due to the facile transformation of 209 to 206

in C₆D₆ at room temperature under argon atmosphere, which reached a ratio of 1:1 after 30 minutes.

Single crystals of (PB^HP)Ir(H)₂Cl (209) were obtained by following procedure. In a 10 mL Teflon screw-capped round-bottomed flask, (PBP)Ir(Ph)(Cl) (**201**) (35 mg, 0.05 mmol) was dissolved in cyclohexane (1 mL). The entire flask was cooled in a liquid nitrogen cooling bath under vacuum, and then refilled with H₂ (1 atm). The reaction was stirred at 100 °C for 1 h. During the heating, the solid completely dissolved in cyclohexane. After cooling down to room temperature, pale yellow crystals gradually formed. [*Caution! This procedure results in pressures of several atmospheres inside the flask. Although we have performed this without incident using proper personal protective equipment (goggles or face mask, flame-resistant laboratory coat, and a blast shield), potential for flask failure and explosion exists. Readers are encouraged to evaluate the potential hazards of this procedure within their own laboratory context before attempting to reproduce the experiment*]

In Situ Observation and Characterization of 208 and 209 in C₆D₁₂. In a J. Young tube, (PBP)Ir(Ph)(Cl) (**201**) (14 mg, 0.02 mmol) was dissolved in C₆D₁₂ (0.5 mL). The entire tube was cooled in a liquid nitrogen cooling bath under vacuum, then refilled with H₂ (1 atm) and allowed to warm up to ambient temperature. [*Caution! This procedure results in pressures of several atmospheres inside the Y. Young NMR tube. Although we have performed this without incident on multiple occasions using proper personal protective equipment (goggles or face mask, flame-resistant laboratory coat, and a blast shield), potential for tube failure and explosion exists. Readers are encouraged to evaluate the potential hazards of this procedure within their own laboratory context before attempting to reproduce the experiment*] After 10 minute at room temperature, 22% of **201**, 76% of **208**, and 2% of **209** were detected in ³¹P{¹H} NMR spectrum (Figure II-16b). The tube was subsequently heated at 100 °C for 1 hour and analyzed by ³¹P{¹H} NMR and ¹H NMR spectroscopy, which showed 6% of **208**, 84% of **209**, and 10% of **206** in ³¹P{¹H} NMR spectrum (Figure II-16c). After heating at 100 °C for 1 h, the peaks of phenyl on **208** was disappeared in ¹H NMR spectrum, yielding **209** and benzene (Figure II-17c).

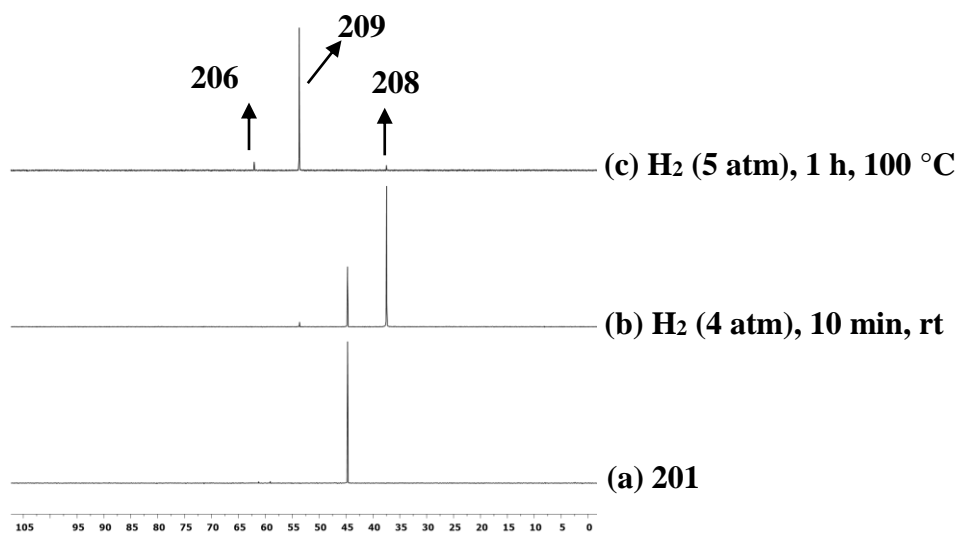


Figure II-16. $^{31}\text{P}\{^1\text{H}\}$ NMR spectra of **201** under hydrogen in C_6D_{12} .

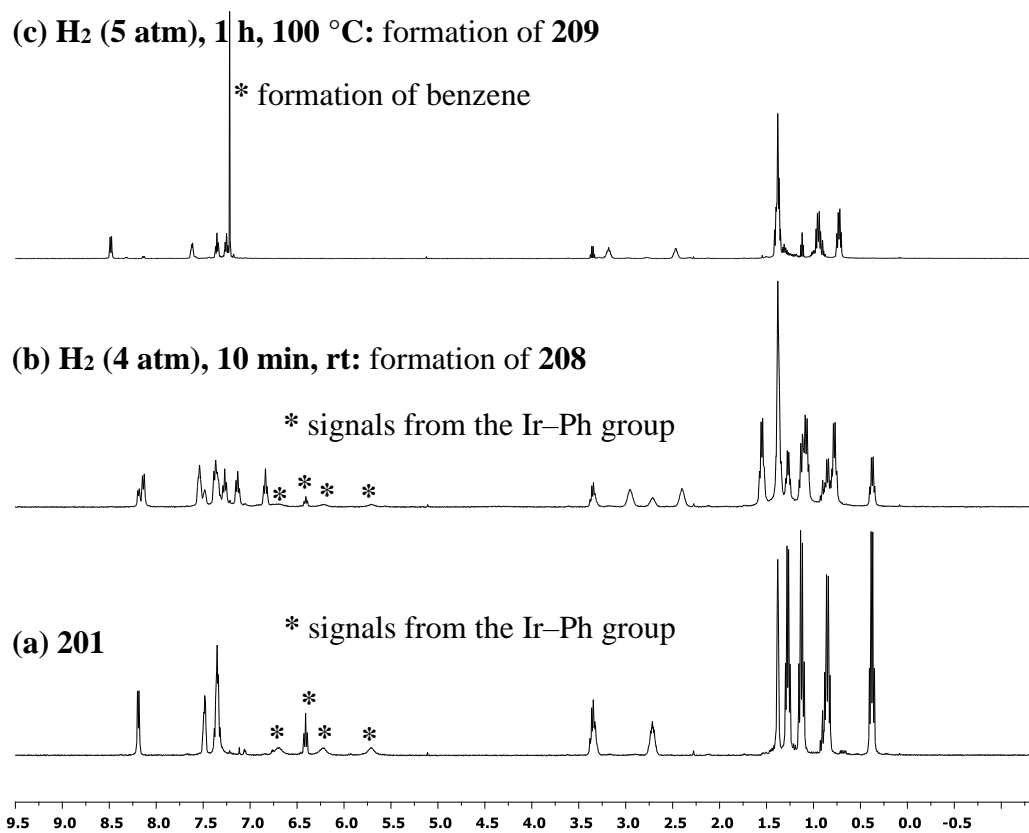


Figure II-17. ^1H NMR evidence of phenyl shift and benzene formation in C_6D_{12} .

(PBP)IrCl₂ (210). In a 50 mL round-bottomed flask, *N*-chlorosuccinimide (33 mg, 0.25 mmol) was added to a toluene solution (4 mL) of (PBP)Ir(H)(Cl) (**206**) (125 mg, 0.20 mmol), and the mixture was stirred at room temperature for 1 h. The solution was filtered through silica gel, and the volatiles were removed under vacuum. The resulting solid was washed with Et₂O, yielding a yellow solid (134 mg, 81%). Single crystals were obtained from a CH₂Cl₂ solution of **210** in a -35 °C freezer overnight. ³¹P{¹H} NMR (202 MHz, CDCl₃): δ 35.6. ¹¹B{¹H} NMR (128 MHz, CDCl₃): δ 73.0 (br). ¹H NMR (500 MHz, CDCl₃): δ 7.92 (d, J_{H-H} = 7.2 Hz, 2H, Ar-*H*), 7.74 (m, 2H, Ar-*H*), 7.50 (t, J_{H-H} = 7.2 Hz, 2H, Ar-*H*), 7.41 (t, J_{H-H} = 7.2 Hz, 2H, Ar-*H*), 3.13 (m, 4H, CHMe₂), 1.40 (dvt, J_{H-H} = 6.9 Hz, J_{H-P} = 6.9 Hz, 12H, CHMe₂), 1.26 (dvt, J_{H-H} = 7.3 Hz, J_{H-P} = 7.3 Hz, 12H, CHMe₂). ¹³C{¹H} NMR (100 MHz, C₆D₆): δ 157.0 (m), 145.2 (vt, J_{P-C} = 23.3 Hz), 131.2 (vt, J_{P-C} = 1.6 Hz), 129.5 (vt, J_{P-C} = 8.4 Hz), 129.2 (vt, J_{P-C} = 3.5 Hz), 129.1, 23.1 (vt, J_{P-C} = 13.5 Hz, CHMe₂), 19.90 (CHMe₂), 19.22 (CHMe₂). Elem. Anal. Calcd for C₂₄H₃₆BCl₂P₂Ir: C, 43.65; H, 5.49. Found: C, 43.71; H, 5.60.

(PBP)RhCl₂ (211). In a 10 mL Teflon screw-capped round-bottomed flask, dichloromethane (200 μL, 3.12 mmol) was added to a mesitylene solution (2 mL) of a mixture of **142**, **202**, and **203** (192 mg, 0.31 mmol), and the resultant mixture was stirred at 170 °C for 18 h. After the solution was cooled to room temperature, the volatiles were removed under vacuum, and the residues were washed with Et₂O, yielding a yellow solid (107 mg, 60%). Single crystals were obtained from a CH₂Cl₂ solution of **211** in a -35 °C freezer overnight. ³¹P{¹H} NMR (202 MHz, CDCl₃): δ 45.6 (d, J_{Rh-P} = 106 Hz). ¹¹B{¹H} NMR (128 MHz, CDCl₃): δ 91.3 (br). ¹H NMR (500 MHz, CDCl₃): δ 7.89 (d, J_{H-H} = 7.2

Hz, 2H, Ar-H), 7.78 (m, 2H, Ar-H), 7.54 (t, $J_{\text{H-H}} = 7.2$ Hz, 2H, Ar-H), 7.48 (t, $J_{\text{H-H}} = 7.2$ Hz, 2H, Ar-H), 2.89 (m, 4H, CHMe₂), 1.38 (dvt, $J_{\text{H-H}} = 7.3$ Hz, $J_{\text{H-P}} = 7.3$ Hz, 12H, CHMe₂), 1.30 (dvt, $J_{\text{H-H}} = 7.3$ Hz, $J_{\text{H-P}} = 7.3$ Hz, 12H, CHMe₂). ¹³C{¹H} NMR (126 MHz, CDCl₃): δ 154.0 (m), 145.5 (t, $J_{\text{P-C}} = 19.3$ Hz), 130.6, 130.4 (t, $J_{\text{P-C}} = 9.0$ Hz), 130.2 (t, $J_{\text{P-C}} = 3.2$ Hz), 129.2, 24.0 (t, $J_{\text{P-C}} = 10.9$ Hz, CHMe₂), 19.9 (CHMe₂), 19.4 (CHMe₂). Elem. Anal. Calcd for C₂₄H₃₆BCl₂P₂Rh: C, 50.47; H, 6.35. Found: C, 50.29; H, 6.26.

2.4.4 X-ray structural determination details

The X-ray crystal data (cifs) could be obtained by the follow link:

<http://pubsdc3.acs.org/doi/suppl/10.1021/jacs.5b11706>

X-Ray data collection, solution, and refinement for (PBP)Ir(Ph)(Cl) (201). A yellow, multi-faceted block of suitable size (0.22 x 0.15 x 0.10 mm) and quality was selected from a representative sample of crystals of the same habit using an optical microscope, mounted onto a nylon loop and placed in a cold stream of nitrogen. Low temperature (150 K) X-ray data were obtained on a Bruker APEXII CCD based diffractometer (Mo sealed X-ray tube, $K_{\alpha} = 0.71073$ Å). All diffractometer manipulations, including data collection, integration and scaling were carried out using the Bruker APEXII software.¹⁵⁵ An absorption correction was applied using SADABS.¹⁵⁶ The space group was determined on the basis of systematic absences and intensity statistics and the structure was solved by direct methods and refined by full-matrix least squares on F^2 . The structure was solved in the monoclinic P 2₁/c space group using XS¹⁵⁷ (incorporated in

SHELXLE). All non-hydrogen atoms were refined with anisotropic thermal parameters. All hydrogen atoms were placed in idealized positions and refined using riding model. The structure was refined (weighted least squares refinement on F^2) to convergence. No additional symmetry was found using ADDSYM incorporated in PLATON program.¹⁵⁸

X-Ray data collection, solution, and refinement for (PBP)Ir(H)(Cl) (206). A yellow, multi-faceted block of suitable size (0.55 x 0.45 x 0.30 mm) and quality was selected from a representative sample of crystals of the same habit using an optical microscope, mounted onto a nylon loop and placed in a cold stream of nitrogen. Low temperature (110 K) X-ray data were obtained on a Bruker APEXII CCD based diffractometer (Mo sealed X-ray tube, $K_{\alpha} = 0.71073 \text{ \AA}$). All diffractometer manipulations, including data collection, integration and scaling were carried out using the Bruker APEXII software.¹⁵⁵ An absorption correction was applied using SADABS.¹⁵⁶ The space group was determined on the basis of systematic absences and intensity statistics and the structure was solved by direct methods and refined by full-matrix least squares on F^2 . The structure was solved in the monoclinic $P 2_1/c$ space group using XS¹⁵⁷ (incorporated in SHELXLE). All non-hydrogen atoms were refined with anisotropic thermal parameters. All hydrogen atoms were placed in idealized positions and refined using riding model with the exception of the hydrogen bound to iridium which was located from the difference map. The structure was refined (weighted least squares refinement on F^2) to convergence. No additional symmetry was found using ADDSYM incorporated in PLATON program.¹⁵⁸

X-Ray data collection, solution, and refinement for (PBP)Rh(H)(Cl) (207). An orange, multi-faceted plate of suitable size (0.40 x 0.33 x 0.09 mm) and quality was selected from a representative sample of crystals of the same habit using an optical microscope, mounted onto a nylon loop and placed in a cold stream of nitrogen. Low temperature (150 K) X-ray data were obtained on a Bruker APEXII CCD based diffractometer (Mo sealed X-ray tube, $K_{\alpha} = 0.71073 \text{ \AA}$). All diffractometer manipulations, including data collection, integration and scaling were carried out using the Bruker APEXII software.¹⁵⁵ An absorption correction was applied using SADABS.¹⁵⁶ The space group was determined on the basis of systematic absences and intensity statistics and the structure was solved by direct methods and refined by full-matrix least squares on F^2 . The structure was solved in the monoclinic $P 2_1/c$ space group using XS¹⁵⁷ (incorporated in SHELXLE). All non-hydrogen atoms were refined with anisotropic thermal parameters. All hydrogen atoms were placed in idealized positions and refined using riding model with the exception of the hydrogen bound to rhodium which was located from the difference map. The structure was refined (weighted least squares refinement on F^2) to convergence. No additional symmetry was found using ADDSYM incorporated in PLATON program.¹⁵⁸

X-Ray data collection, solution, and refinement for (PB^HP)Ir(H)₂(Cl) (209). A colorless, multi-faceted block of suitable size (0.375 x 0.240 x 0.094 mm) and quality was selected from a representative sample of crystals of the same habit using an optical microscope, mounted onto a nylon loop and placed in a cold stream of nitrogen. Low temperature (110 K) X-ray data were obtained on a Bruker APEXII CCD based

diffractometer (Mo sealed X-ray tube, $K_{\alpha} = 0.71073 \text{ \AA}$). All diffractometer manipulations, including data collection, integration and scaling were carried out using the Bruker APEXII software.¹⁵⁵ An absorption correction was applied using SADABS.¹⁵⁶ The space group was determined on the basis of systematic absences and intensity statistics and the structure was solved by direct methods and refined by full-matrix least squares on F^2 . The structure was solved in the monoclinic $P 2_1/c$ space group using XS¹⁵⁷ (incorporated in SHELXLE). All non-hydrogen atoms were refined with anisotropic thermal parameters. All hydrogen atoms were placed in idealized positions and refined using riding model with the exception of the hydrogen bound to iridium and boron, which were omitted because they cannot locate from the difference map. The structure was refined (weighted least squares refinement on F^2) to convergence. No additional symmetry was found using ADDSYM incorporated in PLATON program.¹⁵⁸

X-Ray data collection, solution, and refinement for (PBP)IrCl₂ (210). An orange, multi-faceted block of suitable size (0.33 x 0.29 x 0.19 mm) and quality was selected from a representative sample of crystals of the same habit using an optical microscope, mounted onto a nylon loop and placed in a cold stream of nitrogen. Low temperature (110 K) X-ray data were obtained on a Bruker APEXII CCD based diffractometer (Mo sealed X-ray tube, $K_{\alpha} = 0.71073 \text{ \AA}$). All diffractometer manipulations, including data collection, integration and scaling were carried out using the Bruker APEXII software.¹⁵⁵ The absorption correction program TWINABS¹⁵⁶ was employed to correct the data for absorption effects as well as to generate TWIN4.hkl with reflections from only the major component, and TWIN5.hkl with all the reflections. While the former

was used for structure solution, the latter was used for final least squares refinement. The space group was determined on the basis of systematic absences and intensity statistics and the structure was solved by direct methods and refined by full-matrix least squares on F^2 . The structure was solved in the triclinic P-1 space group using XS¹⁵⁷ (incorporated in SHELXLE). All non-hydrogen atoms were refined with anisotropic thermal parameters. All hydrogen atoms were placed in idealized positions and refined using riding model. The structure was refined (weighted least squares refinement on F^2) to convergence. No additional symmetry was found using ADDSYM incorporated in PLATON program.¹⁵⁸

X-Ray data collection, solution, and refinement for (PBP)RhCl₂ (211). A yellow, multi-faceted block of suitable size (0.25 x 0.10 x 0.10 mm) and quality was selected from a representative sample of crystals of the same habit using an optical microscope, mounted onto a nylon loop and placed in a cold stream of nitrogen. Low temperature (110 K) X-ray data were obtained on a Bruker APEXII CCD based diffractometer (Mo sealed X-ray tube, $K_{\alpha} = 0.71073 \text{ \AA}$). All diffractometer manipulations, including data collection, integration and scaling were carried out using the Bruker APEXII software.¹⁵⁵ An absorption correction was applied using SADABS.¹⁵⁶ The space group was determined on the basis of systematic absences and intensity statistics and the structure was solved by direct methods and refined by full-matrix least squares on F^2 . The structure was solved in the monoclinic P-1 space group using XT/XS¹⁵⁷ (incorporated in SHELXLE). All non-hydrogen atoms were refined with anisotropic thermal parameters. All hydrogen atoms were placed in idealized positions and refined using riding model.

The structure was refined (weighted least squares refinement on F^2) to convergence. No additional symmetry was found using ADDSYM incorporated in PLATON program.¹⁵⁸

2.4.5 Computational details

All computations were carried out with the Gaussian09 program.¹⁵⁹ All of the geometries were fully optimized by M06¹⁶⁰ functional. The Stuttgart basis set and the associated effective core potential (ECP) was used for Rh and Ir atoms, and an all-electron 6-311++G(d,p) basis set was used for the other atoms. The 3D structures of molecules were generated using CYLView.¹⁶¹

CHAPTER III

BORYL/BORANE INTERCONVERSION AND DIVERSITY OF BINDING MODES OF OXYGENOUS LIGANDS IN PBP Pincer COMPLEXES OF RHODIUM[‡]

3.1 Introduction

Complexes of tridentate pincer-type ligands have become commonly studied for the purposes of exploration of catalysis and elementary reactivity at transition metal centers.^{1,2,4-6,162,163} A combination of flanking neutral donors, especially phosphines, and a central anionic donor harkens back to the earliest pincer history^{9,164} and remains possibly the most popular type of pincer design to this day. A boryl group as the central donor in a pincer is arguably the strongest σ donor and the strongest trans-influence ligand that can be incorporated into such a structure. This was realized for the first time by Yamashita and Nozaki in 2009 with the central diaminoboryl moiety (Figure III-1).^{37,72,86,87,165,166} Several reports in the intervening years reported on pincers derived from *m*-carborane (Figure III-1).^{95,98,167}

[‡] Reproduced in part from “Boryl/Borane Interconversion and Diversity of Binding Modes of Oxygenous Ligands in PBP Pincer Complexes of Rhodium” by Shih, W.-C.; Gu, W.; MacInnis, M. C.; Herbert, D. E.; Ozerov, O. V. *Organometallics* **2017**, *36*, 1718. Copyright [2017] by The American Chemical Society. Parts of chemistry has been developed by our former group members Dr. Weixing Gu¹²⁰ and Dr. Morgan MacInnis.

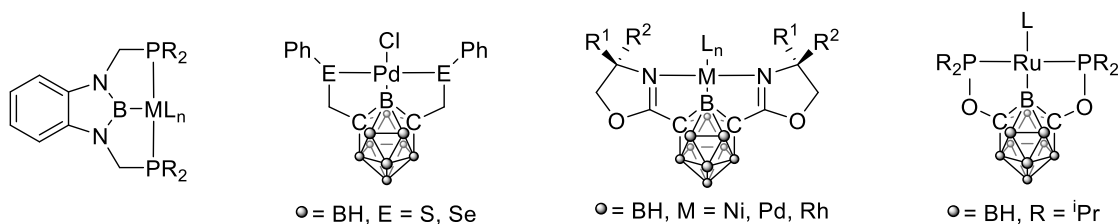
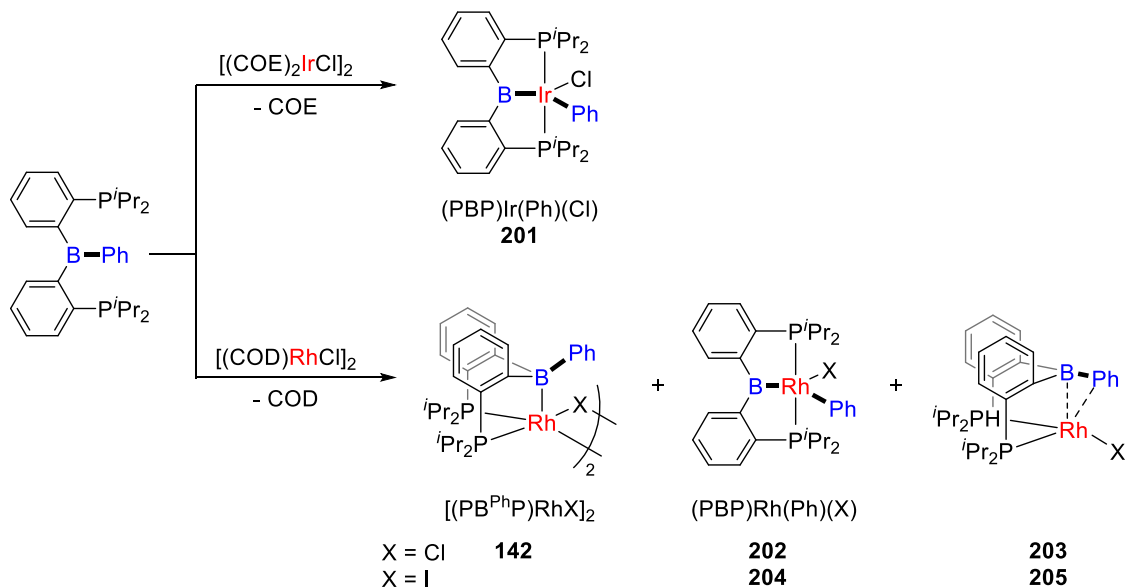


Figure III-1. Pincer metal complexes with a central boryl donor in literature.

Our group has been especially interested in a PBP pincer ligand combining a central diarylboryl donor with two flanking phosphines. In comparison to the carborane-derived boryls or the diaminoboryl in Figure III-1, it may be expected that a diarylboryl would possess a higher degree of Lewis acidity. In a recent publication,¹⁰² we described syntheses of Ir and Rh complexes of this PBP ligand, while Tauchert et al. reported on its Pd complexes.²¹ The synthetic introduction of the PBP ligand was accomplished via insertion of monovalent Ir or Rh into the B–Ph bond of **134a** (Scheme III-1). Whereas this reaction gave a single product with Ir, a mixture of **142**, **202**, and **203**, ostensibly in equilibrium on the time scale of handling, was observed for Rh. In the case of the iodide analogue, only the two isomers **204** and **205** were observed. We set out to explore substitution of the halide in these complexes with potentially bidentate oxygenous ligands, such as acetylacetonate, carboxylates, and triflate. We reasoned that substitution of the halide with a bidentate ligand would lead to saturation of the metal center to an 18-electron count for the pincer structure type, while only the 16-electron count would be maintained in structure type as **142**. We therefore surmised that bidentate ligands instead of halide might favor the “pincerized” isomer. This hypothesis has not turned out to be entirely correct, underscoring that such simplistic arguments have limited applicability. Moreover,

our efforts in this report show that several isomeric structures in this system are energetically similar and small changes in the nature of the X ligand in Scheme III-1 lead to different isomeric preferences.



Scheme III-1. Insertion of Ir or Rh into B–Ph of 201 Leads to the Pincer Complexes.

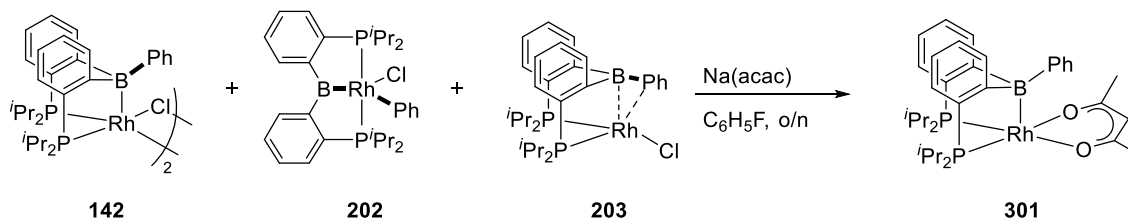
The Mixture of 142/202/203 was Observed in Equilibrium for Rh.

3.2 Results and Discussion

3.2.1 Synthesis and characterization of 301

The reaction of the mixture of **142**, **202**, and **203** with sodium acetylacetonate in $\text{C}_6\text{H}_5\text{F}$ at ambient temperature overnight resulted in the isolation of the single product **301** in 79% yield upon workup (Scheme III-2). The solid-state structure determined by single-crystal X-ray diffractometry (Figure III-2) established that the borane center in **301** is acting as a Z-type ligand.^{168,169} This is consistent with the solution

NMR data, featuring a broad resonance at 17.6 ppm in the $^{11}\text{B}\{^1\text{H}\}$ NMR spectrum indicative of an sp^3 -hybridized boron and the overall C_s symmetry in ^1H , $^{13}\text{C}\{^1\text{H}\}$, and $^{31}\text{P}\{^1\text{H}\}$ NMR spectra.



Scheme III-2. The Reactions of the 142/202/203 Mixture with Sodium Acetylacetonate

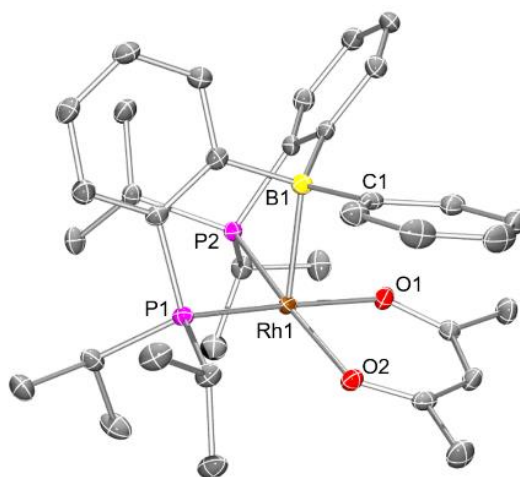


Figure III-2. POV-Ray rendition of the ORTEP drawing (50% thermal ellipsoids) of **301** showing selected atom labeling. Hydrogen atoms are omitted for clarity. Selected bond distances (\AA) and angles (deg): Rh1–B1, 2.271(2); Rh1–P1, 2.2394(6); Rh1–P2, 2.2535(6); Rh1–O1, 2.067 (1); Rh1–O2, 2.075 (1); B1–C1, 1.597 (3); O1–Rh1–O2, 87.83(5); P1–Rh1–P2, 98.73(2); O1–Rh1–P1, 176.51(4); O2–Rh1–P2, 172.14(4); P1–

Rh1–B1, 83.74(5); P2–Rh1–B1, 80.06(5); O1–Rh1–B1, 96.49(6); O2–Rh1–B1, 103.37(6); C1–B1–Rh1, 101.0(1).

The coordination environment about Rh in **301** is quite similar to that in **142** and also to a few other related complexes (**143**, **302**, and **303**; Figure III-3).^{127,128} In all of these cases, the (*Z*)-borane occupies an apical position in a square pyramid, with two *cis* phosphines and two other donors filling out the basal plane. These structures can be analyzed as arising from σ donation from a square-planar Rh(I) center to the triarylborane Lewis acid. The Rh center in the resultant structures can be viewed as trivalent,¹⁷⁰ and square-pyramidal geometry is quite common for trivalent Rh. The nature of Rh–B bonding in (*Z*)-borane complexes has been extensively studied in greater detail using computational methods.^{112,115} The Rh–B distance in **301** is quite similar to those in **142**, **143**, and **302**; **303** is an outlier, likely because of diminished Rh \rightarrow B donation under the influence of two strongly π accepting carbonyls.

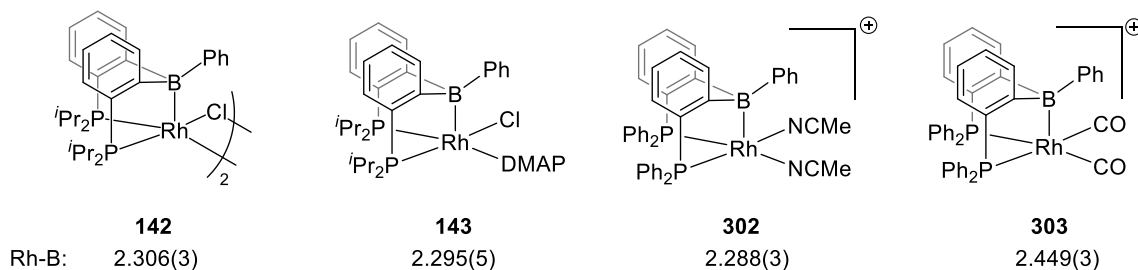
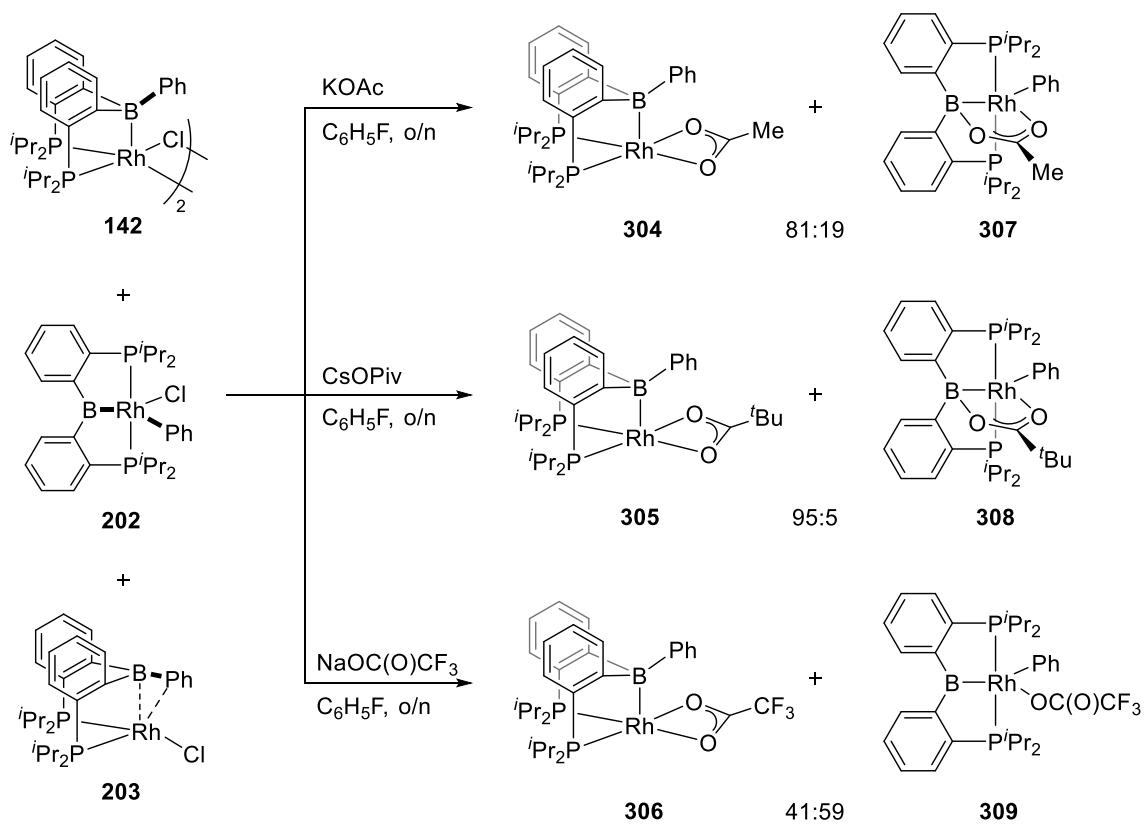


Figure III-3. Rh–B bond distance (in Å) of (PBP)Rh complexes in literature.

Thermolysis of **301** at 50 °C in CDCl₃ led only to a minor degree of decomposition (<10% after 3 days). There was no evidence for the formation of the putative boryl pincer complex via insertion of Rh into the B–Ph bond.

3.2.2 Synthesis and characterization of carboxylate derivatives

Reactions of the **142/202/203** mixture with alkali-metal carboxylates carried out in fluorobenzene overnight at ambient temperature resulted in the replacement of chloride with acetate, pivalate, or trifluoroacetate (Scheme III-3). Upon isolation, all three materials consisted of a mixture of two isomers. The isomer analogous to **301** featuring a Z-type borane and a κ^2 -carboxylate was found in all three mixtures (**304**, **305**, **306** in Scheme III-3; **307**, **308**, and **309** are discussed later in the text). This isomer was dominant for acetate (81%) and pivalate (95%) but constituted only 41% of the TFA-containing mixture.



Scheme III-3. Reactivity of 142/202/203 with Alkali Metal Carboxylates.

It was not possible to isolate a bulk sample of any of these compounds free of the other isomers; however, single crystals of **305** suitable for an X-ray diffraction study were obtained upon recrystallization (Figure III-4). The structure of **305** is closely analogous to that of **301**, with the Rh–B distances within ca. 0.01 Å of each other and similar pyramidalization of the boron center ($\sum B_\alpha = 342.4^\circ$ for both **301** and **305**).

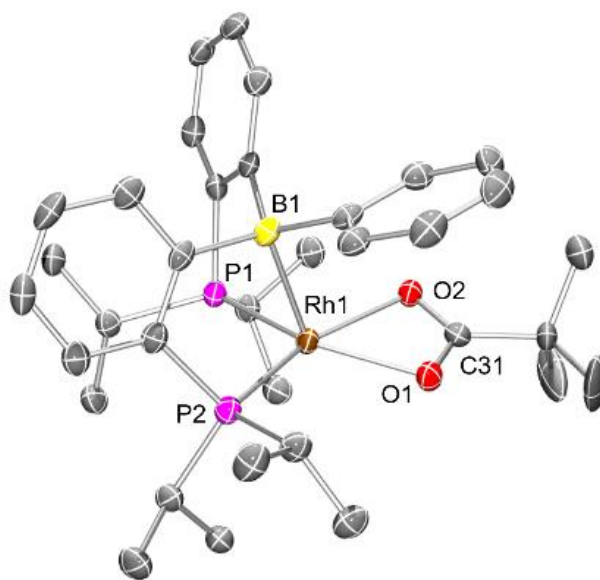


Figure III-4. POV-Ray rendition of the ORTEP drawing (50% thermal ellipsoids) of **305** showing selected atom labeling. Hydrogen atoms are omitted for clarity. Selected bond distances (Å) and angles (deg) for **305**: Rh1–B1, 2.282(3); Rh1–O1, 2.1765(19); Rh1–O2, 2.1566(19); Rh1–P1, 2.2225(10); Rh1–P2, 2.2131(9); Rh1–C31, 2.504(3); O1–C31, 1.273(3); O2–C31, 1.268(3); O2–Rh1–O1, 60.90(7); P1–Rh1–P2, 99.86(3); O1–Rh1–P2, 101.62(6); O2–Rh1–P1, 97.51(6); O1–Rh1–B1, 107.38(10); P1–Rh1–B1, 81.94(9); O1–C31–O2, 119.6(3).

Complex **301** also shares key spectroscopic features with **304**, **305**, and **306** (Table III-1). The $^{11}\text{B}\{^1\text{H}\}$ NMR chemical shifts are clustered around 20 ppm, as is common for Z-type triarylborane adducts.^{168,169} The $^{13}\text{C}\{^1\text{H}\}$ resonance for the ipso-C of the phenyl group is found in a narrow range of chemical shift (152–156 ppm), is broadened by the contact with the quadrupolar ^{11}B nucleus, and does not display discernible coupling to ^{31}P or ^{103}Rh that would be expected for a Rh–Ph connection. The values of $^1J_{\text{Rh-}}$

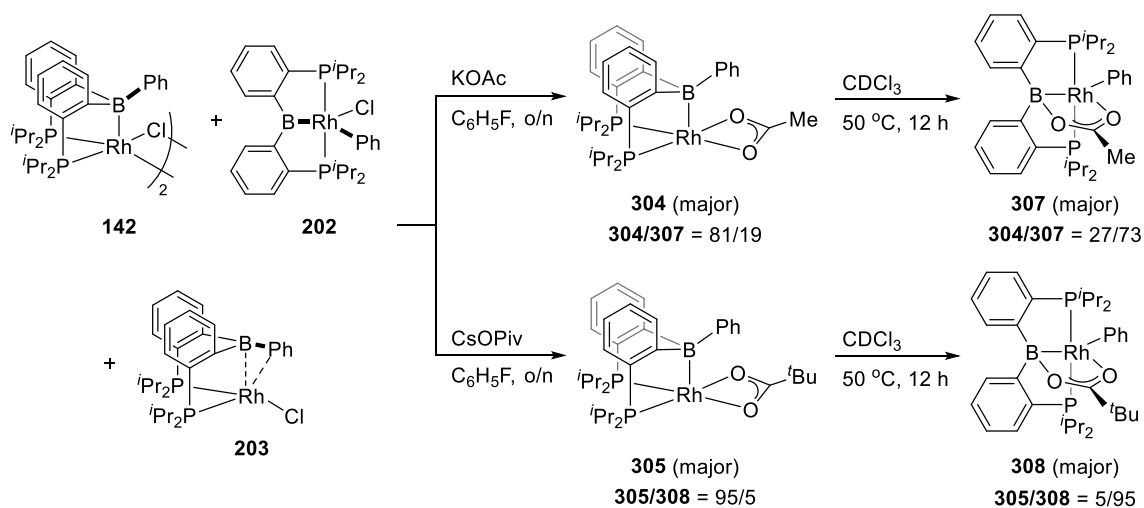
^1P coupling constants are similar, and the differences are easily rationalized. They are lowest for **301** (163 Hz), slightly higher for **304** and **305** (168 Hz), and highest for **306** (178 Hz). This is likely because of the weaker trans influence exerted by the oxygens of the carboxylates (especially trifluoroacetate) vs those of acac, leading to tighter Rh–P interaction in the carboxylate complexes. In support of this explanation, the Rh–P distances in **301** are about 0.02 Å longer than those in **305**.

**Table III-1. $^{11}\text{B}\{^1\text{H}\}$ NMR, $^{31}\text{P}\{^1\text{H}\}$ NMR, ^{19}F NMR, and the Feature of $^{13}\text{C}\{^1\text{H}\}$ NMR
Chemical Shifts of Rh Complexes (in ppm) and J values (in Hz)**

	^{11}B	^{31}P NMR ($^1J_{\text{Rh-P}}$)	^{19}F	^{13}C NMR for C_{ipso} of Ph ^a
142	20.8	65.0-80.0	--	156.2 (br)
301	17.6	68.9 (d, $J_{\text{Rh-P}} = 163$ Hz)	--	155.0 (br)
304	21.2	75.2 (d, $J_{\text{Rh-P}} = 168$ Hz)	--	155.1 (br)
305	20.5	76.0 (d, $J_{\text{Rh-P}} = 168$ Hz)	--	155.5 (br)
306	22.5	78.8 (d, $J_{\text{Rh-P}} = 178$ Hz)	-76.8	152.5 (br)
310	22.6	82.3 (d, $J_{\text{Rh-P}} = 193$ Hz)	-77.9	149.3 (br)
202	94.3	50.4 (d, $J_{\text{Rh-P}} = 126$ Hz)	--	148.9 (dt, $J_{\text{Rh-C}} = 35$ Hz, $J_{\text{P-C}} = 8.8$ Hz)
203	95.3	50.4 (d, $J_{\text{Rh-P}} = 125$ Hz)	--	147.9 (dt, $J_{\text{Rh-C}} = 36$ Hz, $J_{\text{P-C}} = 8.5$ Hz)
309	90.8	51.3 (d, $J_{\text{Rh-P}} = 133$ Hz)	-75.5	146.6 (dt, $J_{\text{Rh-C}} = 34$ Hz, $J_{\text{P-C}} = 9.6$ Hz)
311	95.6	51.3 (d, $J_{\text{Rh-P}} = 130$ Hz)	-77.1	141.0 (dt, $J_{\text{Rh-C}} = 39$ Hz, $J_{\text{P-C}} = 8.5$ Hz)
307	18.4	48.6 (d, $J_{\text{Rh-P}} = 140$ Hz)	--	151.7 (dt, $J_{\text{Rh-C}} = 34$ Hz, $J_{\text{P-C}} = 12$ Hz)
308	18.5	48.8 (d, $J_{\text{Rh-P}} = 142$ Hz)	--	152.6 (dt, $J_{\text{Rh-C}} = 34$ Hz, $J_{\text{P-C}} = 12$ Hz)
202	20.8	88.8 (d, $J_{\text{Rh-P}} = 194$ Hz)	--	not found due to overlap
204	22.5	87.1 (d, $J_{\text{Rh-P}} = 191$ Hz)	--	137.8 (br)

a. The ipso carbon of the C_6H_5 group attached to B, Rh, or both.

Thermolysis (50 °C, CDCl₃, 12 h) of the carboxylate-derived mixtures resulted in no significant change in the ratio of TFA-derived compounds. On the other hand, the acetate- and pivalate-containing mixtures were enriched in the isomers (**307**, **308**) that were minor in the ambient-temperature synthesis (Scheme III-4). Van't Hoff analysis of the mixture of **304** and **307** at different temperatures allowed determination of the values $\Delta H_{\text{rxn}} = 1.0(1)$ kcal/mol and $\Delta S_{\text{rxn}} = 5.3(2)$ cal/(mol K) (for the **304** → **307** direction; Section 3.4.5 Van't Hoff plot). In the case of pivalate, **308** accounted for 95% of the mixture after thermolysis and we were able to grow X-ray-quality crystals of **308** out of this mixture (Figure III-5).



Scheme III-4. Thermolysis of 304 and 305

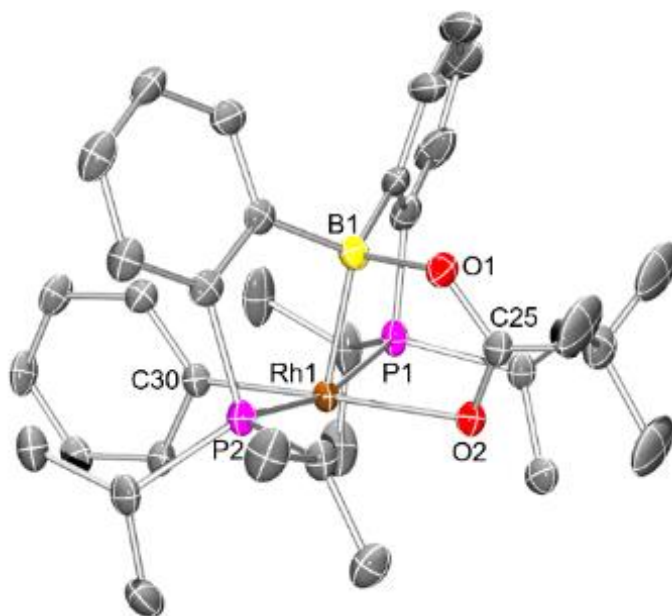


Figure III-5. POV-Ray rendition of the ORTEP drawing (50% thermal ellipsoids) of **308** showing selected atom labeling. Hydrogen atoms and the disordered moiety are omitted for clarity. Selected bond distances (Å) and angles (deg) for **308**: Rh1–B1, 2.141(4); Rh1–O2, 2.191(2); Rh1–P1, 2.3162(11); Rh1–P2, 2.3233(11); Rh1–C30, 2.011(3); B1–O1, 1.549(4); O1–C25, 1.296(4); O2–C25, 1.241(4); O2–Rh1–C30, 178.03(12); P1–Rh1–P2, 166.16(3); C30–Rh1–P1, 88.50(10); O2–Rh1–P1, 91.22(7); O1–B1–Rh1, 103.4(2); O2–Rh1–B1, 78.78(13); O1–C25–O2, 122.1(3).

The solid-state structure of **308** revealed that the Ph group migrated from B to Rh (vs **305**).¹⁷¹ However, unlike the case in the structures of **202**, **204**, or its Ir analogue (PBP)Ir(Ph)(Cl) (**201**), the boron center in **308** is not sp^2 -hybridized because the pivalate group is bridging B and Rh. The sum of angles associated with B–C and B–Rh bonds is ca. 331° . The solid-state structural features evident for **308** are consistent with the solution

NMR observations for **307** and **308**. The attachment of the Ph group to Rh is apparent from the strong coupling of the ipso-C of the Ph group to ^{103}Rh and also from coupling to the two ^{31}P nuclei, similarly to **202** and **204**. In addition, **307/308** displayed features arising from the restricted rotation about the Rh–C_{Ph} bond that are typical for a phenyl group position cis to the central donor of a pincer ligand with flanking PⁱPr₂ groups: five distinct ^1H NMR resonances for the phenyl group and an upfield shift of a pair of Me groups in the PⁱPr₂ arms that are most affected by the ring current of the Ph group. The $^1J_{\text{Rh-P}}$ values were also consistent with a significant change in the disposition of the phosphines in comparison to structures of the **201** type (Table III-1).

The other isomer formed with trifluoroacetate (**309**) also displayed the distinct solution NMR features associated with a Ph group attached to Rh cis to the boron. However, the ^{11}B NMR chemical shift for **309** (90.8 ppm) indicated an sp²-hybridized boryl donor as in **202** and **204**, while the ^{11}B NMR chemical shifts of 18.4–18.5 ppm supported sp³-hybridization of the boron center in **307** and **308**. We thus conclude that the trifluoroacetate in **309** is attached solely to Rh and not to B. Presumably, the weaker basicity of trifluoroacetate oxygens makes the formation of the B–O bond less favorable than for acetate or pivalate. The available data do not allow the determination of whether both oxygens of trifluoroacetate in **309** are bound to Rh.

The structure of **308** can be analyzed with two limiting localized-bonding descriptions (**A** and **B**, Figure III-6) in mind. Krossing et al. penned a thoughtful essay on the dangers of overuse of arrows, potentially resulting in favoring extreme notations and disregard of the more conventional assignments.¹⁷² **A** and **B** should both be considered

and can be regarded as resonance structures because of the assignment of electrons to different bonds in the O–C–O π system. The depictions in Figure III-6 use arrows and simple straight lines to emphasize what should be thought of as “dative” or “covalent” bonds in each depiction, but an arrow or a straight line each assigns a pair of electrons to a bond between two atoms. Carboxylates are well-known to bridge direct metal–metal bonds, including many complexes of the $\text{Rh}_2(\text{O}_2\text{CR})_4$ form that have gained special prominence in C–H activation studies.¹⁷³ The symmetrical bridging in $\text{Rh}_2(\text{O}_2\text{CR})_4$ results in equal C–O distances of ca. 1.25 Å¹⁷⁴ (cf. also 1.268(4) and 1.267(4) Å for the two C–O bonds in the pivalate in **305**). The bonding in a molecule of MeOAc can be considered maximally localized for a carboxylate, and MeOAc was determined to possess unequal C–O distances of ca. 1.20 and 1.34 Å in the solid state.^{175,176} In **308**, the two C–O distances in the bridging pivalate are 1.296(4) Å for C–O_B and 1.241(4) Å for C–O_{Rh}.¹⁷⁷ The disparity is much smaller than in MeOAc, and thus both **A** and **B** can be viewed as contributing meaningfully. In accord with this view, the Rh–B distance in **308** (2.141(4) Å) is intermediate between the Rh–B distances in complexes with Z-type triarylboranes (Figure III-3) and the Rh–B distances in complexes with a trigonal-planar boryl PBP ligand (ca. 2.0 Å).¹⁰² The B–O bond distance is 1.549(4) Å and is similar to the B–O bond distances in adducts of triarylboranes with anionic oxygen donors.¹⁷⁸

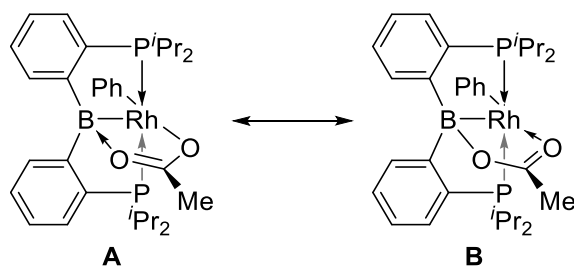
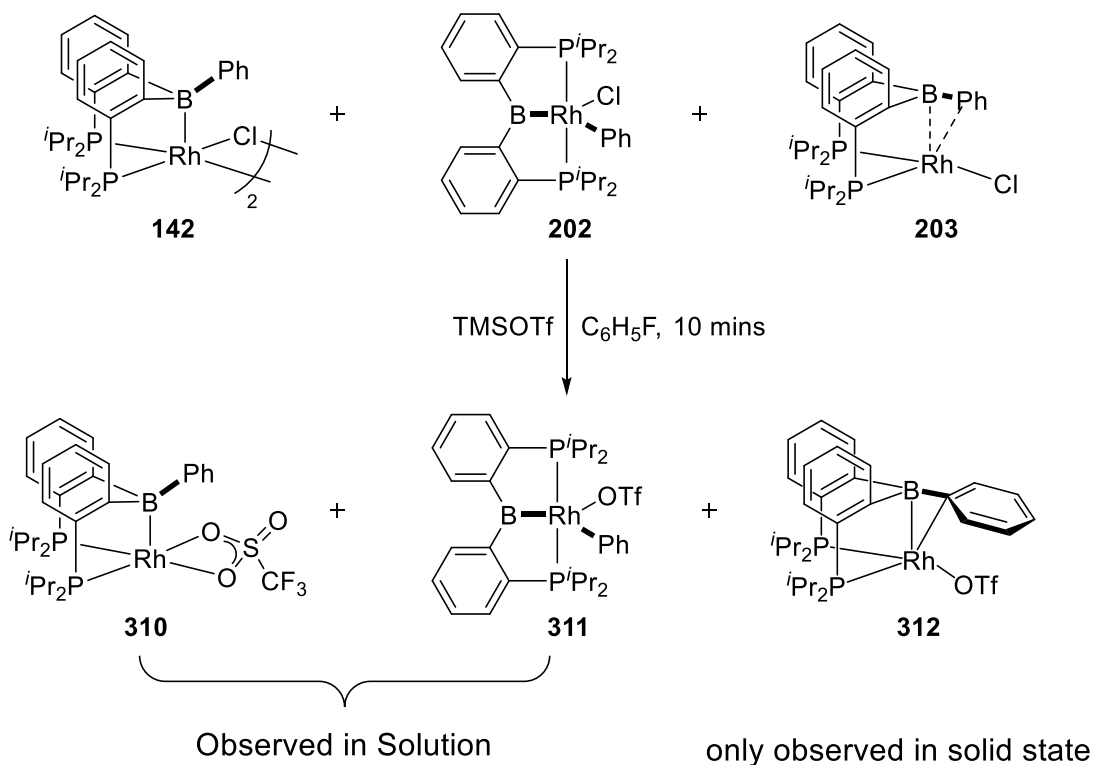


Figure III-6. Two possible resonance structures of bridging acetate in **307**.

3.2.3 Synthesis and characterization of **310**, **311**, and **312**

The addition of Me_3SiOTf to an Et_2O suspension of the mixture of **142**, **202**, and **203** generated a brown solution containing a mixture of **310** and **311**. Upon workup, a mixture of **310** and **311** was isolated, showing a ratio of 63:37 upon dissolution in CDCl_3 (Scheme III-5). Thermolysis of **310/311** at $50\text{ }^\circ\text{C}$ in CDCl_3 for 20 h did not change the observed ratio. Notably, the reaction of Me_3SiOTf with **304/307** mixtures present in different ratios (81:19 or 27:73) generated the same ratio (63:37) of **310** and **311** in CDCl_3 , indicating that **310/311** are in equilibrium that is rapid on the time scale of experimental handling. Remarkably, we were able to obtain two different types of single crystals from the solutions of **310/311**. Crystals grown from saturated ambient-temperature Et_2O solutions were green and needle-shaped in appearance, while crystals grown from Et_2O solutions at $-35\text{ }^\circ\text{C}$ afforded orange block-shaped crystals.



Scheme III-5. The Reaction of the 142/202/203 Mixture with Me₃SiOTf.

X-ray diffraction studies on these two types of crystals revealed that the orange block crystals represent complex **310** (Figure III-7), whereas the green needle crystals contain the new isomer **312** with η²-B,Ph binding to rhodium (Figure III-8). The solid-state structure of **310** is analogous to those of **305** and **301**. The triflate group is bound to rhodium via two oxygens, but the two corresponding Rh–O distances (2.2516(12) and 2.3282(12) Å) in **310** are much longer than those in **301** (2.067(1) and 2.075(1) Å) or **305** (2.174(2) and 2.155(2) Å), consistent with the much more weakly donating nature of triflate. The Rh–B distance in **310** (2.3103(17) Å) is comparable to the other examples of (Z)-borane structures (Figure III-3).

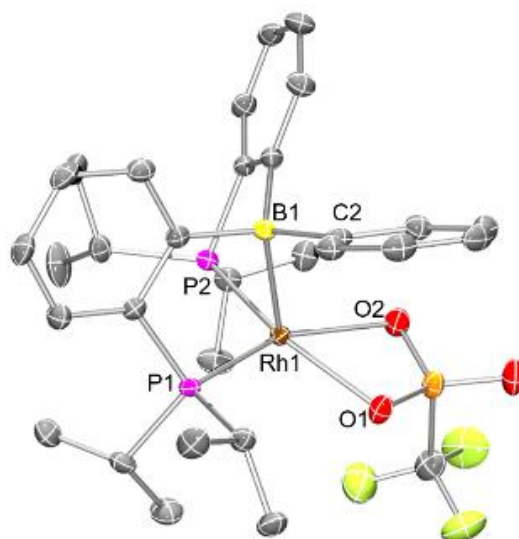


Figure III-7. POV-Ray rendition of the ORTEP drawing (50% thermal ellipsoids) of **310** showing selected atom labeling. Hydrogen atoms are omitted for clarity. Selected bond distances (Å) and angles (deg) for **310**: Rh1–B1, 2.3103(17); Rh1–P1, 2.1928(5); Rh1–P2, 2.2302(5); Rh1–O1, 2.2516(12); Rh1–O2, 2.3282(12); B1–C2, 1.605(2); B1–Rh1–O1, 81.81(4); B1–Rh1–O2, 108.30(5); B1–Rh1–P1, 81.81(4); B1–Rh1–P2, 80.28(4); P1–Rh1–P2, 100.02(2); O1–Rh1–P1, 96.37(3); O2–Rh1–P2, 100.58(3); O1–Rh1–O2, 62.49(4); C2–B1–Rh1, 103.22(10).

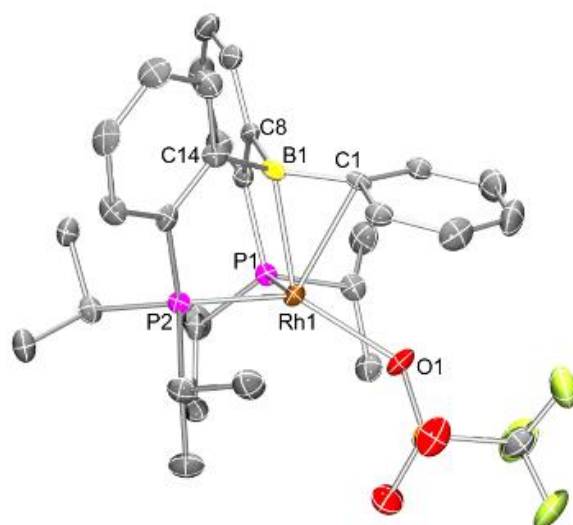


Figure III-8. POV-Ray rendition of the ORTEP drawing (50% thermal ellipsoids) of **312** showing selected atom labeling. Hydrogen atoms are omitted for clarity. Selected bond distances (Å) and angles (deg) for **312**: Rh1–B1, 2.231(5); Rh1–P1, 2.2015(13); Rh1–P2, 2.2093(12); Rh1–O1, 2.244(3); Rh1–C1, 2.391(4); B1–C1, 1.569(6); B1–C8, 1.611(7); B1–C14, 1.599(6); B1–Rh1–C1, 39.50(16); B1–Rh1–O1, 131.45(14); B1–Rh1–P1, 87.01(14); B1–Rh1–P2, 80.97(13); P1–Rh1–P2, 99.54(4); O1–Rh1–P1, 101.58(9); O1–Rh1–P2, 141.75(8).

On the other hand, the crystal structure of **312** adopts a distorted four-coordinate geometry with an η^2 -B,C-coordination mode. Similar binding modes of η^x -B,Ph ($x > 1$) from ligand **134a** to a number of transition metals have been reported by the Bourissou and Peters groups,^{115,118,129,150} and Emslie et al. reviewed such binding of arylboranes in general.¹¹¹ Interestingly, the Rh–B (2.231(5) Å) and the B–C_{Ph} (1.569(6) Å) bond distances in **312** are shorter than those in **310** (2.3103(17) and 1.611(7) Å, respectively).

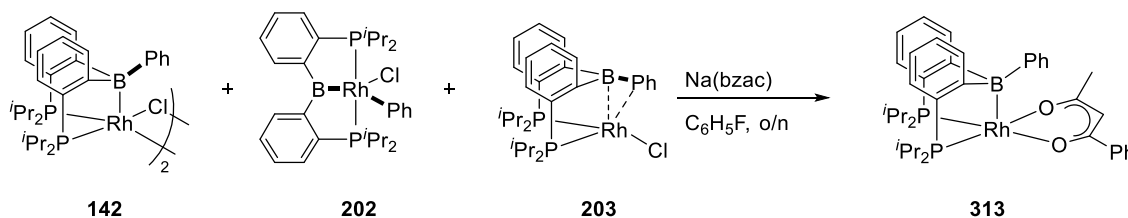
The shorter B–C bond may be partially a reflection of the boron environment in **312** being only slightly pyramidalized ($\sum B_\alpha = \text{ca. } 353^\circ$), implying a more sp^2 -like hybridization. The shortening of B–C bonds upon η^2 -B,C coordination has been observed before.^{115,118,129,150} The structure of **312** can also be viewed as an intermediate along the reaction pathway of the insertion of Rh into the B–Ph bond.

The fact that both structures can be crystallized out of the same solution and that these two compounds are distinct at least in the solid state is rather surprising, considering that they are only different in the modest change in the positioning of the phenyl ring and a slight change in the coordination of the already weakly bound triflate. However, Bourissou's (PB(Ph)P)CuCl complex¹¹⁵ contained multiple crystallographically independent molecules, even within a single unit cell. These molecules could all be described as containing a η^2 -B,Ph interaction, but they possessed meaningfully different Cu–B and Cu–C_{ipso} distances. We have no direct evidence of the presence of **312** in solution. However, it is possible that **310** and **312** are in rapid equilibrium on the NMR time scale at ambient temperature, especially if the equilibrium fraction of **312** is small. The temperatures for preferential crystallization of **310** vs **312** are different; thus, it is also possible that the equilibrium ratio of these two compounds is temperature-dependent.

3.2.4 Simulation of coupling patterns of 304, 305, 306, and 310

One interesting aspect for **304**, **305**, **306**, and **310** is that the methyl groups of *iso*-propyl groups on the phosphine arms display quartet peaks in ¹H NMR spectra, which is similar as virtual triplet of doublet peaks observed in PXP-type pincer complexes with

trans-bisphosphines structure. It is abnormal for the complexes that possess cis-bisphosphines especially the P–Rh–P angle is only 99.83(4)° and 100.02(2)° observed in **305** and **310** (Figure III-4 & Figure III-7). Virtual coupling requires two equivalent phosphines with a large P–P coupling constant, which is normally achieved only when the phosphines are approximately trans to each other. It was thus of interest to us to find out the P–P coupling constant in **304**, **306**, **305** and **310** to further understand the observed apparent virtual coupling. Obviously, we are not able to observe the P–P coupling in **304**, **305**, **306**, and **310**, since the two phosphine groups are equivalent to each other on the NMR time scale. Therefore, **313** (bzac = benzoylacetate) was synthesized by the reaction of the mixture of **142**, **202**, and **203** with Na(bzac) at room temperature overnight in 69% isolated yield (Scheme III-6). Two sets of doublet of doublets were observed at 71.1 ppm (dd, $J_{\text{Rh-P}} = 167$ Hz, $J_{\text{P-P}} = 41$ Hz) and 66.8 ppm (dd, $J_{\text{Rh-P}} = 161$ Hz, $J_{\text{P-P}} = 41$ Hz) in the $^{31}\text{P}\{^1\text{H}\}$ NMR spectrum. The fairly small P–P coupling constant of 41 Hz is rather unusual for the observation of virtual coupling.



Scheme III-6. The Reactions of the 142/202/203 Mixture with Na(bzac)

This unusual coupling pattern in cis-bisphosphines complex was simulated by spin simulation tool in MestReNova. In order to simplify the model, $A_3BXX'B'A_3'$ system was used and the spectroscopic information was set as the following: spectrometer frequency 500 MHz; A = A' (methyl proton), 1.2 ppm; B = B' (methine proton), 2.5 ppm; X (P1), 180.0 ppm; X' (P2), 180.0 ppm. Based on the experimental data of **313** in ^1H NMR spectrum, the coupling constants of $J_{A-B} = J_{A'-B'} = 7.0\sim 7.6$ Hz, $J_{A-X} = J_{A'-X'} = 12\sim 16$ Hz, and $J_{X-X'} = 41$ Hz, but the coupling constants of $J_{A-X'} = J_{A'-X}$, $J_{B-X'} = J_{B'-X}$, and $J_{B-X} = J_{B'-X'}$ are unknown. We assume $J_{B-X'} = J_{B'-X}$, and $J_{B-X} = J_{B'-X'}$ are small because the similar structure $\text{PhCH}_2\text{P}^i\text{Pr}_2$ shows the methine proton and phosphorus have a very small coupling constant as $^2J_{\text{H-P}} = 2.3$ Hz.¹⁷⁹ Therefore, the first simulation was set as $J_{A-B} = J_{A'-B'} = 7.0$ Hz, $J_{A-X} = J_{A'-X'} = 12$ Hz, $J_{X-X'} = 40$ Hz, and assumed $J_{B-X'} = J_{B'-X} = 0$ Hz, $J_{B-X} = J_{B'-X'} = 2$ Hz, then changed values of $J_{A-X'} = J_{A'-X}$ between 0 to 6 Hz (Figure III-9). It shows a quartet while the coupling constant of $J_{A-X'} = J_{A'-X} = 2\sim 4$ Hz.

In order to understand the effect of coupling of two phosphorus nuclei to this system, the second simulation was set as $J_{A-B} = J_{A'-B'} = 7.0$ Hz, $J_{A-X} = J_{A'-X'} = 12$ Hz, and assumed $J_{A-X'} = J_{A'-X} = 2$ Hz, $J_{B-X'} = J_{B'-X} = 0$ Hz, $J_{B-X} = J_{B'-X'} = 2$ Hz, then changed values of $J_{X-X'}$ between 20 to 80 Hz (Figure III-10). It displays a quartet while $J_{X-X'}$ is larger than 40 Hz. The above two simulations demonstrates that the virtual coupling can occur from cis-bisphosphine system at certain condition, including $^{31}\text{P}-^{31}\text{P}$ coupling constant only requires to be larger than 40 Hz. Hence, the traditional concept that virtual triplet was only occurred from trans-bisphosphine metal complexes was debatable.

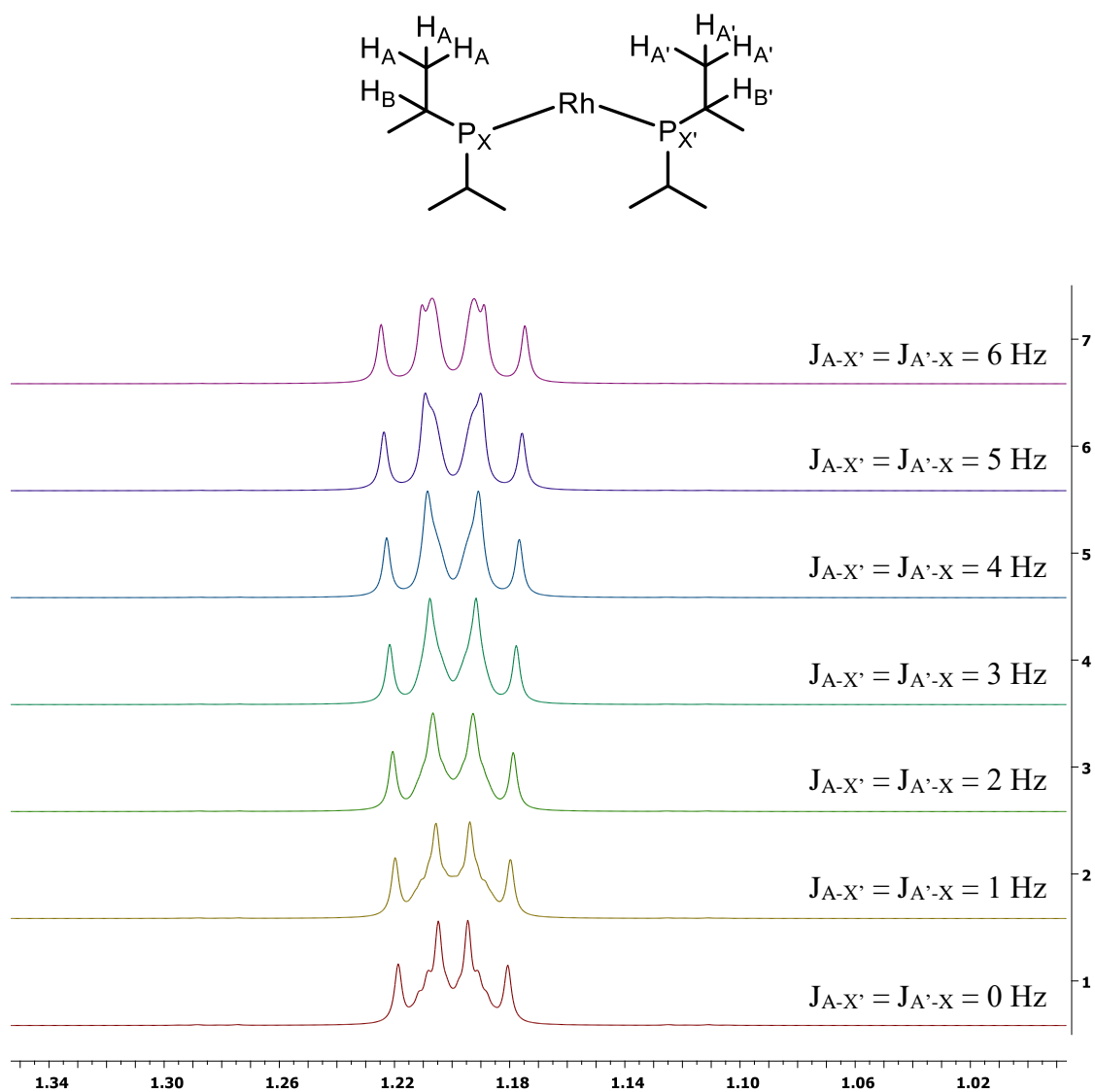


Figure III-9. Simulation of coupling pattern for methyl group on the *iso*-propyl group.

$A_3BXX'B'A_3'$ system was used and the spectroscopic information was set as the following: spectrometer frequency 500 MHz; $A = A'$ (methyl), 1.2 ppm; $B = B'$ (methine), 2.5 ppm; X (P1), 180.0 ppm; X' (P2), 180.0 ppm. The simulation was set as $J_{A-B} = J_{A'-B'} = 7.0$ Hz, $J_{A-X} = J_{A'-X'} = 12$ Hz, $J_{X-X'} = 40$ Hz, and assumed $J_{B-X} = J_{B'-X} = 0$ Hz, $J_{B-X} = J_{B'-X}$.

$X' = 2$ Hz, then changed values of $J_{A-X'} = J_{A'-X}$ between 0 to 6 Hz. While $J_{A-X'} = J_{A'-X} = 2 \sim 4$ Hz, it shows a quartet.

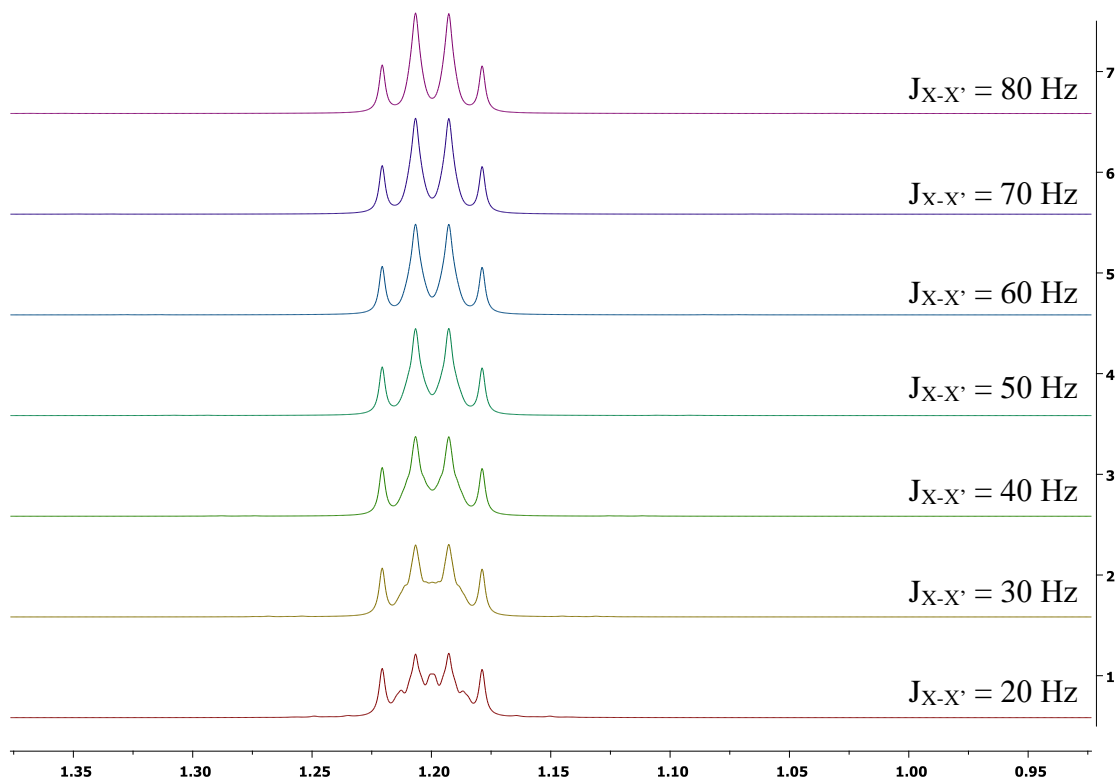


Figure III-10. Simulation of coupling pattern for methyl group on the *iso*-propyl group. $A_3BXX'B'A_3'$ system was used and the spectroscopic information was set as the following: spectrometer frequency 500 MHz; $A = A'$ (methyl), 1.2 ppm; $B = B'$ (methine), 2.5 ppm; X (P1), 180.0 ppm; X' (P2), 180.0 ppm. The coupling constants are set as $J_{A-B} = J_{A'-B'} = 7.0$ Hz, $J_{A-X} = J_{A'-X'} = 12$ Hz, and assumed $J_{A-X'} = J_{A'-X} = 2$ Hz, $J_{B-X'} = J_{B'-X} = 0$ Hz, $J_{B-X} = J_{B'-X'} = 2$ Hz, then changed values of $J_{X-X'}$ between 20 to 80 Hz. While $J_{X-X'}$ is larger than 40 Hz, it shows a quartet.

3.3 Conclusions

In summary, we have described a variety of structures that are accessible in PBP-supported Rh complexes with potentially bidentate oxygenous ligands. The different structures that we observed are related to each other by means of a few key differences. The oxygenous ligands exhibited monodentate, chelating bidentate, and B/Rh bridging modes. We also observed migration of the Ph group from B to Rh and vice versa, as well as different coordination modes of a triarylborane moiety. All of these transformations occur at ambient temperature or 50 °C and in many cases result in equilibrium mixtures with observable concentrations of more than one component. We find it rather extraordinary that this system gives rise to so many isomeric structures of ostensibly similar energies.

3.4 Experimental Section

3.4.1 General considerations

Unless specified otherwise, all manipulations were performed under an Ar atmosphere using standard Schlenk line or glovebox techniques. Pentane, diethyl ether, and isooctane were dried and deoxygenated (by purging) using a solvent purification system (Innovative Technology Pure Solv MD-5 Solvent Purification System) and stored over molecular sieves in an Ar-filled glove box. C₆D₆ was dried over NaK/Ph₂CO/18-crown-6, distilled or vacuum transferred and stored over molecular sieves in an Ar-filled glovebox. CH₂Cl₂, CDCl₃, fluorobenzene were dried over CaH₂, distilled or vacuum transferred and stored over molecular sieves in an Ar-filled glove box. The mixture of

142/202/203 and the mixture of **204/205** were prepared via literature procedure.¹⁰² All other chemicals were used as received from commercial vendors.

3.4.2 Physical methods

NMR spectra were recorded on a Varian Inova 400, or a Bruker Avance III 400 (¹H NMR, 399.535 MHz; ¹³C NMR, 100.467 MHz; ¹¹B NMR, 128.185 MHz; ³¹P NMR, 161.734 MHz), or a Varian Inova 500 (¹H NMR, 499.703 MHz; ¹³C NMR, 125.697 MHz; ³¹P NMR, 202.265 MHz) spectrometer. Chemical shifts are reported in δ (ppm). For ¹H and ¹³C NMR spectra, the residual solvent peak was used as an internal reference (¹H NMR: δ 7.16 for C₆D₆ and 7.26 for CDCl₃; ¹³C NMR: δ 128.06 for C₆D₆ and 77.16 for CDCl₃). ¹¹B NMR spectra were referenced externally with BF₃ etherate at δ 0. ³¹P NMR spectra were referenced externally with 85% phosphoric acid at δ 0. ¹⁹F NMR spectra were referenced externally with trifluoroacetic acid at δ -78.5. Elemental analyses were performed by CALI Labs, Inc. (Parsippany, NJ).

3.4.3 Synthesis and characterization of rhodium complexes

301: To a solution of a mixture of **142**, **202**, and **203** (60 mg, 0.098 mmol) in C₆H₅F (5 mL) was added sodium acetylacetonate (60 mg, 0.49 mmol). The resulting yellow suspension was stirred at room temperature overnight, and then the reaction mixture was filtered through a short plug of Celite. After removal of all volatiles, the resulting residue was washed with isooctane and dried under vacuum, yielding a yellow solid (53 mg, 79%). X-ray-quality crystals were obtained by slow diffusion of pentane

into a saturated fluorobenzene solution of **301**. $^{31}\text{P}\{^1\text{H}\}$ NMR (202 MHz, CDCl_3): δ 68.9 (d, $^1J_{\text{Rh-P}} = 163$ Hz). $^{11}\text{B}\{^1\text{H}\}$ NMR (120.4 MHz, CDCl_3): δ 17.6 (br). ^1H NMR (500 MHz, CDCl_3): δ 7.48 (m, 2H, Ar-H), 7.28 (d, $^3J_{\text{H-H}} = 7.4$ Hz, 2H, Ar-H), 7.12 (t, $^3J_{\text{H-H}} = 7.4$ Hz, 2H, Ar-H), 7.04 (t, $^3J_{\text{H-H}} = 7.5$ Hz, 2H, Ar-H), 6.95 (m, 3H, Ar-H), 6.90 (m, 2H, Ar-H), 5.15 (s, 1H, C-H (acac)), 2.78 (m, 2H, CHMe_2), 1.91 (m, 2H, CHMe_2), 1.50 (s, 6H, CMe (acac)), 1.43 (m, 18H, CHMe_2), 1.15 (dvt, $^3J_{\text{H-H}} \approx ^{3,5}J_{\text{H-P}} = 6.5$ Hz, 6H, CHMe_2). $^{13}\text{C}\{^1\text{H}\}$ NMR (126 MHz, CDCl_3): δ 184.1 (s, $\text{C}=\text{O}$ (acac)), 168.8 (br, $\text{C}_{\text{Ar-B}}$), 155.0 (br, $\text{C}_{\text{Ph-B}}$), 139.6 (d, $^1J_{\text{C-P}} = 48$ Hz, $\text{C}_{\text{Ar-P}}$), 135.6 (s), 131.7 (m, C_{Ar}), 129.0 (s), 128.1 (s), 126.1 (s), 124.4 (s, C_{Ph}), 123.5 (s), 100.2 (s, C-H (acac)), 27.6 (m, CHMe_2), 26.9 (vt, $^{4,4}J_{\text{C-P}} = 3.1$ Hz, CMe (acac)), 25.1 (m, CHMe_2), 22.7 (s, CHMe_2), 22.1 (s, CHMe_2), 21.1 (s, CHMe_2), 20.9 (s, CHMe_2). Anal. Calcd for $\text{C}_{35}\text{H}_{48}\text{BO}_2\text{P}_2\text{Rh}$: C, 62.15; H, 7.15. Found: C, 62.08; H, 7.09.

Mixture of 304 and 307. To a solution of a mixture of **142**, **202**, and **203** (50 mg, 0.082 mmol) in $\text{C}_6\text{H}_5\text{F}$ (4 mL) was added potassium acetate (40 mg, 0.41 mmol). The resulting yellow suspension was stirred at room temperature overnight, and then the reaction mixture was filtered through a short plug of Celite. After removal of all volatiles, the resulting residue was washed with isooctane and dried under vacuum, yielding a yellow solid (52 mg, 79%). Analysis of a freshly prepared C_6D_6 or CDCl_3 solution of this solid by $^{31}\text{P}\{^1\text{H}\}$ NMR spectroscopy revealed the presence of **304** and **307** in a 84:16 ratio in C_6D_6 or in a 81:19 ratio in CDCl_3 . The solid of **304** and **307** reached a 42:58 ratio after 15 h at room temperature in CDCl_3 . Thermolysis of a CDCl_3 solution of the same solid at 50 °C for 12 h resulted in an equilibrium mixture of **304** and **307** with a 27:73 ratio. Data

for **304** are as follows. $^{31}\text{P}\{^1\text{H}\}$ NMR (202 MHz, C_6D_6): δ 75.2 (d, $^1J_{\text{Rh-P}} = 168$ Hz). $^{11}\text{B}\{^1\text{H}\}$ NMR (128 MHz, C_6D_6): δ 21.2 (br). ^1H NMR (500 MHz, C_6D_6): δ 7.77 (m, 2H, Ar-H), 7.72 (d, $^3J_{\text{H-H}} = 7.3$ Hz, 2H, Ar-H), 7.22 (m, 2H, Ar-H), 7.13–7.18 (m, 5H, Ar-H), 6.99 (m, 2H, Ar-H), 2.49 (m, 2H, CHMe₂), 1.88 (m, 2H, CHMe₂), 1.53 (s, 3H, CMe (acetate)), 1.36 (m, 12H, CHMe₂), 1.18 (dvt, $^3J_{\text{H-H}} \approx ^{3,5}J_{\text{H-P}} = 7.4$ Hz, 6H, CHMe₂), 0.79 (dvt, $^3J_{\text{H-H}} \approx ^{3,5}J_{\text{H-P}} = 7.0$ Hz, 6H, CHMe₂). $^{13}\text{C}\{^1\text{H}\}$ NMR (126 MHz, CDCl_3): δ 190.5 (s, C=O (acetate)), 168.3 (br, C_{Ar-B}), 155.1 (br, C_{Ph-B}), 136.8 (s), 136.5 (s), 132.2 (vt, $J_{\text{P-C}} = 10$ Hz, C_{Ar}), 129.0 (s), 128.1 (s), 126.6 (s), 126.1 (s, C_{Ph}), 124.3 (vt, $J_{\text{P-C}} = 3.2$ Hz, C_{Ar}), 27.7 (m, CHMe₂), 27.3 (m, CHMe₂), 25.2 (s, CMe (acetate)), 22.5 (s, CHMe₂), 20.3 (s, CHMe₂), 20.1 (s, CHMe₂), 19.8 (s, CHMe₂). Data for **307** are as follows. $^{31}\text{P}\{^1\text{H}\}$ NMR (202 MHz, CDCl_3): δ 48.6 (d, $^1J_{\text{Rh-P}} = 140$ Hz). $^{11}\text{B}\{^1\text{H}\}$ NMR (128 MHz, C_6D_6): δ 18.4 (br). ^1H NMR (500 MHz, CDCl_3): δ 8.21 (d, $^3J_{\text{H-H}} = 7.6$ Hz, 2H, Ar-H), 7.65 (d, $^3J_{\text{H-H}} = 7$ Hz, 1H, Ph-H), 7.40 (t, $^3J_{\text{H-H}} = 7.5$ Hz, 2H, Ar-H), 7.30 (m, 2H, Ar-H), 7.22 (t, $^3J_{\text{H-H}} = 7.4$ Hz, 2H, Ar-H), 6.76 (t, $^3J_{\text{H-H}} = 7.5$ Hz, 1H, Ph-H), 6.45 (t, $^3J_{\text{H-H}} = 7.2$ Hz, 1H, Ph-H), 6.16 (t, $^3J_{\text{H-H}} = 7.6$ Hz, 1H, Ph-H), 5.91 (d, $^3J_{\text{H-H}} = 7.7$ Hz, 1H, Ph-H), 2.44 (m, 2H, CHMe₂), 1.91 (m, 2H, CHMe₂), 1.87 (s, 3H, CMe (acetate)), 1.29 (m, 12H, CHMe₂), 1.24 (dvt, $^3J_{\text{H-H}} \approx ^{3,5}J_{\text{H-P}} = 6.6$ Hz, 6H, CHMe₂), 0.07 (dvt, $^3J_{\text{H-H}} \approx ^{3,5}J_{\text{H-P}} = 6.8$ Hz, 6H, CHMe₂). $^{13}\text{C}\{^1\text{H}\}$ NMR (125.6 MHz, CDCl_3): δ 177.4 (s, C=O (acetate)), 161.5 (br, C_{Ar-B}), 151.7 (dt, $^1J_{\text{Rh-C}} = 34$ Hz, $^2J_{\text{P-C}} = 12$ Hz, C_{Ph-Rh}), 140.7 (s, Ph), 137.9 (dvt, $^2J_{\text{Rh-C}} = 3$ Hz, $^{1,3}J_{\text{P-C}} = 20$ Hz, C_{Ar-P}), 133.0 (s, C_{Ph}), 131.9 (t, $J_{\text{P-C}} = 10$ Hz, C_{Ar}), 130.9 (s, C_{Ar}), 128.4 (s, C_{Ar}), 125.6 (s, C_{Ph}), 125.4 (s, C_{Ar}), 124.2 (s, C_{Ph}), 120.3 (s, C_{Ph}), 27.4 (vt, $^{1,3}J_{\text{P-C}} = 9.1$ Hz, CHMe₂), 22.2 (vt, $^{1,3}J_{\text{P-C}} = 11$ Hz, CHMe₂), 21.6 (s, CMe (acetate)), 21.2

(vt, ${}^2,4J_{P-C} = 2.7$ Hz, $CHMe_2$), 19.3 (vt, ${}^2,4J_{P-C} = 3.2$ Hz, $CHMe_2$), 18.5 (s, $CHMe_2$), 17.9 (s, $CHMe_2$). Anal. Calcd for $C_{32}H_{44}BO_2P_2Rh$ (mixture of **304** and **307**): C, 60.38; H, 6.91. Found: C, 60.40; H, 6.97.

Mixture of 305 and 308. To a solution of a mixture of **142**, **202**, and **203** (93 mg, 0.15 mmol) in C_6H_5F (10 mL) was added cesium pivalate (176 mg, 0.75 mmol). The resulting yellow suspension was stirred at room temperature overnight, and then the reaction mixture was filtered through a short plug of Celite. After removal of all volatiles, the resulting residue was washed with isooctane and dried under vacuum, yielding a yellow solid (78 mg, 76%). X-ray-quality crystals of **305** were obtained by slow diffusion of pentane into a saturated fluorobenzene solution of this solid. Analysis of a freshly prepared $CDCl_3$ solution of this solid (40 mg, 0.07 mmol) by ${}^31P\{^1H\}$ NMR spectroscopy revealed the presence of **305** and **308** in a 95:5 ratio. Thermolysis of this solution at 50 °C for 12 h resulted in an equilibrium mixture of **305** and **308** with a 5:95 ratio. After removal of volatiles, the resulting yellow solid was dissolved in fluorobenzene with pentane layered on the top of this solution. X-ray-quality crystals of **308** were obtained by slow diffusion of pentane to this fluorobenzene solution. Data for **305** are as follows. ${}^31P\{^1H\}$ NMR (202 MHz, $CDCl_3$): δ 76.0 (d, ${}^1J_{Rh-P} = 168$ Hz). ${}^{11}B\{^1H\}$ NMR (128 MHz, $CDCl_3$): δ 20.5 (br). 1H NMR (500 MHz, $CDCl_3$): δ 7.49 (d, ${}^3J_{H-H} = 7.5$ Hz, 2H, Ar-*H*), 7.39 (m, 2H, Ar-*H*), 7.31 (d, ${}^3J_{H-H} = 8.0$ Hz, 2H, Ar-*H*), 7.23 (t, ${}^3J_{H-H} = 7.5$ Hz, 2H, Ar-*H*), 7.10 (m, 3H, Ar-*H*), 7.04 (m, 2H, Ar-*H*), 2.57 (m, 2H, $CHMe_2$), 2.07 (m, 2H, $CHMe_2$), 1.43 (dvt, ${}^3J_{H-H} \approx {}^{3,5}J_{H-P} = 7.3$ Hz, 12H, $CHMe_2$), 1.29 (dvt, ${}^3J_{H-H} \approx {}^{3,5}J_{H-P} = 7.2$ Hz, 6H, $CHMe_2$), 1.01 (dvt, ${}^3J_{H-H} \approx {}^{3,5}J_{H-P} = 7.0$ Hz, 6H, $CHMe_2$), 0.85 (s, 9H, CMe_3). ${}^{13}C\{^1H\}$

NMR (126 MHz, CDCl₃): δ 197.6 (s, C=O (pivalate)), 168.8 (br, C_{Ar}-B), 155.5 (br, C_{Ph}-B), 137.0 (s), 136.7 (s), 132.1 (vt, $J_{P-C} = 10$ Hz, C_{Ar}), 128.8 (s), 127.8 (s), 126.4 (s), 125.6 (s, C_{Ph}), 124.2 (vt, $J_{P-C} = 3.2$ Hz, C_{Ar}), 40.0 (s, CMe₃), 27.5 (m, CHMe₂), 27.2 (m, CHMe₂), 26.8 (s, CMe₃), 22.5 (s, CHMe₂), 20.1 (s, CHMe₂), 20.0 (s, CHMe₂), 19.5 (s, CHMe₂). Data for **308** are as follows. ³¹P{¹H} NMR (202 MHz, CDCl₃): δ 48.8 (d, $^1J_{Rh-P} = 142$ Hz). ¹¹B{¹H} NMR (128 MHz, CDCl₃): δ 18.5 (br). ¹H NMR (500 MHz, CDCl₃): δ 8.13 (d, $^3J_{H-H} = 7.5$ Hz, 2H, Ar-*H*), 7.66 (d, $^3J_{H-H} = 7.7$ Hz, 1H, Ph-*H*), 7.38 (m, 2H, Ar-*H*), 7.31 (m, 2H, Ar-*H*), 7.21 (m, 2H, Ar-*H*), 6.78 (t, $^3J_{H-H} = 7.4$ Hz, 1H, Ph-*H*), 6.48 (m, 1H, Ph-*H*), 6.20 (t, $^3J_{H-H} = 7.6$ Hz, 1H, Ph-*H*), 5.83 (d, $^3J_{H-H} = 7.5$ Hz, 1H, Ph-*H*), 2.33 (m, 2H, CHMe₂), 1.98 (m, 2H, CHMe₂), 1.42 (dvt, $^3J_{H-H} \approx ^{3,5}J_{H-P} = 7.5$ Hz, 6H, CHMe₂), 1.26 (dvt, $^3J_{H-H} \approx ^{3,5}J_{H-P} = 5.5$ Hz, 6H, CHMe₂), 1.16 (dvt, $^3J_{H-H} \approx ^{3,5}J_{H-P} = 7.3$ Hz, 6H, CHMe₂), 0.90 (s, 9H, CMe₃), 0.16 (dvt, $^3J_{H-H} \approx ^{3,5}J_{H-P} = 6.7$ Hz, CHMe₂). ¹³C{¹H} NMR (101 MHz, CDCl₃): δ 184.3 (s, C=O (pivalate)), 161.4 (br, C_{Ar}-B), 152.6 (dt, $^1J_{Rh-C} = 34$ Hz, $^2J_{P-C} = 12$ Hz, C_{Ph}-Rh), 140.5 (s, C_{Ph}), 138.0 (vt, $^{1,3}J_{P-C} = 20$ Hz, C_{Ar}-P), 132.9 (s, C_{Ph}), 131.9 (vt, $J_{P-C} = 10$ Hz, C_{Ar}), 130.7 (s, C_{Ar}), 128.2 (s, C_{Ar}), 125.6 (s, C_{Ph}), 125.1 (s, C_{Ar}), 124.2 (s, C_{Ph}), 120.3 (s, C_{Ph}), 38.2 (s, CMe₃), 27.0 (s, CMe₃), 26.4 (vt, $^{1,3}J_{P-C} = 8.3$ Hz, CHMe₂), 21.6 (vt, $^{1,3}J_{P-C} = 11$ Hz, CHMe₂), 21.4 (s, CHMe₂), 19.7 (br, CHMe₂), 18.7 (s, CHMe₂), 17.6 (s, CHMe₂). Anal. Calcd for C₃₅H₅₀BO₂P₂Rh (mixture of **305** and **308**): C, 61.73; H, 7.44. Found: C, 61.69; H, 7.43.

Mixture of 306 and 309. To a solution of a mixture of **142**, **202**, and **203** (107 mg, 0.18 mmol) in C₆H₅F (10 mL) was added sodium trifluoroacetate (119 mg, 0.88 mmol). The resulting yellow suspension was stirred at room temperature overnight, and then the

reaction mixture was filtered through a short plug of Celite. After removal of all volatiles, the residue was washed with isooctane and dried under vacuum, yielding a yellow solid (87 mg, 72%). The two isomers **306** and **309** were observed in a $^{31}\text{P}\{^1\text{H}\}$ NMR spectrum with a ratio of 41:59 in CDCl_3 . The purity of the isolated mixture of **306** and **309** was gauged to be >95% by NMR spectroscopy. Data for **306** are as follows. $^{31}\text{P}\{^1\text{H}\}$ NMR (202 MHz, CDCl_3): δ 78.8 (d, $^1J_{\text{Rh-P}} = 178$ Hz). $^{11}\text{B}\{^1\text{H}\}$ NMR (128 MHz, CDCl_3): δ 22.5 (br). ^{19}F NMR (470 MHz, CDCl_3): δ -76.8 (s). ^1H NMR (500 MHz, CDCl_3): δ 7.40 (m, 2H, Ar-H), 7.26 (m, 2H, Ar-H), 7.18 (t, $^3J_{\text{H-H}} = 7.3$ Hz, 1H, Ar-H), 7.12 (t, $^3J_{\text{H-H}} = 7.5$ Hz, 2H, Ar-H), 7.07 (t, $^3J_{\text{H-H}} = 7.5$ Hz, 1H, Ar-H), 2.56 (m, 2H, CHMe_2), 2.08 (m, 2H, CHMe_2), 1.43 (m, 12H, CHMe_2), 1.32 (dvt, $^3J_{\text{H-H}} \approx ^{3,5}J_{\text{H-P}} = 7.3$ Hz, 6H, CHMe_2), 1.01 (dvt, $^3J_{\text{H-H}} \approx ^{3,5}J_{\text{H-P}} = 7.0$ Hz, 6H, CHMe_2). Four aromatic protons are obscured due to overlap with the signals from isomer **309**. Selected resonances of **306** are as follows. ^{13}C NMR (101 MHz, CDCl_3): δ 170.2 (q, $^2J_{\text{C-F}} = 39$ Hz, $\text{C}(\text{O})\text{CF}_3$), 167.2 (br, $\text{C}_{\text{Ar-B}}$), 152.5 (br, $\text{C}_{\text{Ph-B}}$), 127.8 (d, $^1J_{\text{C-P}} = 25$ Hz, $\text{C}_{\text{Ar-P}}$), 115.2 (q, $^1J_{\text{C-F}} = 288$ Hz, $\text{C}(\text{O})\text{CF}_3$), 27.7 (m, CHMe_2 , 4C), 22.5 (s, CHMe_2), 20.3 (s, CHMe_2), 20.1 (s, CHMe_2), 19.6 (s, CHMe_2). Data for **309** are as follows. $^{31}\text{P}\{^1\text{H}\}$ NMR (202 MHz, CDCl_3): δ 51.3 (d, $^1J_{\text{Rh-P}} = 133$ Hz). $^{11}\text{B}\{^1\text{H}\}$ NMR (128 MHz, CDCl_3): δ 90.8 (br). ^{19}F NMR (470 MHz, CDCl_3): δ -75.5 (s). ^1H NMR (500 MHz, CDCl_3): δ 8.05 (s, 1H, Ph-H), 8.03 (d, $^3J_{\text{H-H}} = 7.0$ Hz, 2H, Ar-H), 7.56 (m, 2H, Ar-H), 6.87 (br, 1H, Ph-H), 6.60 (t, $^3J_{\text{H-H}} = 7.2$ Hz, 1H, Ph-H), 6.35 (br, 1H, Ph-H), 5.77 (br, 1H, Ph-H), 2.33 (m, 2H, CHMe_2), 2.17 (m, 2H, CHMe_2), 1.18 (dvt, $^3J_{\text{H-H}} \approx ^{3,5}J_{\text{H-P}} = 6.7$ Hz, 6H, CHMe_2), 0.93 (dvt, $^3J_{\text{H-H}} \approx ^{3,5}J_{\text{H-P}} = 7.4$ Hz, 6H, CHMe_2), 0.40 (dvt, $^3J_{\text{H-H}} \approx ^{3,5}J_{\text{H-P}} = 7.0$ Hz, 6H, CHMe_2). Four aromatic protons are

obscured due to overlap with the signals from isomer **306**. Selected resonances of **309** are as follows. ^{13}C NMR (101 MHz, CDCl_3): δ 162.5 (q, $^2J_{\text{C-F}} = 37$ Hz, $\text{C}(\text{O})\text{CF}_3$), 156.1 (br, $\text{C}_{\text{Ar-B}}$), 146.6 (dt, $^1J_{\text{Rh-C}} = 34$ Hz, $^2J_{\text{C-P}} = 9.6$ Hz, $\text{C}_{\text{Ph-B}}$), 142.8 (vt, $^{1,3}J_{\text{P-C}} = 20$ Hz, $\text{C}_{\text{Ar-P}}$), 131.5 (vt, $J_{\text{P-C}} = 9.5$ Hz, C_{Ar}), 131.5 (vt, $J_{\text{C-P}} = 9.5$ Hz, C_{Ar}), 115.7 (q, $^1J_{\text{C-F}} = 288$ Hz, $\text{C}(\text{O})\text{CF}_3$), 23.5 (vt, $^{1,3}J_{\text{P-C}} = 9.8$ Hz, CHMe_2), 23.0 (vt, $^{1,3}J_{\text{P-C}} = 11$ Hz, CHMe_2), 19.1 (s, CHMe_2), 18.5 (s, CHMe_2), 18.1 (s, CHMe_2), 17.6 (s, CHMe_2).

Mixture of 310 and 311. To a solution of a mixture of **142**, **202**, and **203** (122 mg, 0.20 mmol) in Et_2O (5 mL) was added trimethylsilyl trifluoromethanesulfonate (40 μL , 0.22 mmol). The reaction mixture was stirred at room temperature for 10 min, and the volatiles were removed under vacuum. The resulting residue was redissolved in Et_2O and then filtered through a short plug of Celite. The product was further purified by recrystallization from Et_2O solution at room temperature overnight, yielding green needle-shaped crystals of **312** (96 mg, 66%). Orange block crystals were formed from Et_2O solution at -30 $^\circ\text{C}$, which represented the isomer **310**. In a freshly prepared solution of green needle crystals or orange block crystals, the two isomers **310** and **311** were observed in a $^{31}\text{P}\{^1\text{H}\}$ NMR spectrum with a ratio of 66:34 in C_6D_6 or 63:37 in CDCl_3 . The purity of the isolated mixture of **310** and **311** was gauged to be >95% by NMR spectroscopy. Data for **310** are as follows. $^{31}\text{P}\{^1\text{H}\}$ NMR (202 MHz, CDCl_3): δ 82.3 (d, $^1J_{\text{Rh-P}} = 193$ Hz). $^{11}\text{B}\{^1\text{H}\}$ NMR (128 MHz, CDCl_3): δ 22.6 (br). ^{19}F NMR (470 MHz, CDCl_3): δ -77.9 (s). ^1H NMR (500 MHz, CDCl_3): δ 7.55 (d, $^3J_{\text{H-H}} = 7.4$ Hz, 2H, Ar-*H*), 7.38 (m, 2H, Ar-*H*), 7.30 (t, $^3J_{\text{H-H}} = 7.4$ Hz, 2H, Ar-*H*), 7.14 (t, $^3J_{\text{H-H}} = 7.5$ Hz, 2H, Ar-*H*), 2.49 (m, 2H, CHMe_2), 2.02 (m, 2H, CHMe_2), 1.47 (dvt, $^3J_{\text{H-H}} \approx ^{3,5}J_{\text{H-P}} = 7.4$ Hz, 6H, CHMe_2), 1.39

(dvt, ${}^3J_{\text{H-H}} \approx {}^{3,5}J_{\text{H-P}} = 7.2$ Hz, 6H, CHMe_2), 1.27 (dvt, ${}^3J_{\text{H-H}} \approx {}^{3,5}J_{\text{H-P}} = 7.2$ Hz, 6H, CHMe_2), 0.99 (dvt, ${}^3J_{\text{H-H}} \approx {}^{3,5}J_{\text{H-P}} = 7.0$ Hz, 6H, CHMe_2). Five aromatic protons are obscured due to overlap with the signals from isomer **311**. Selected resonances of **310** are as follows. ${}^{13}\text{C}$ NMR (101 MHz, CDCl_3): δ 165.8 (br, $C_{\text{Ar-B}}$), 149.3 (br, $C_{\text{Ph-B}}$), 27.7 (m, CHMe_2 , 4C), 22.2 (s, CHMe_2), 20.1 (s, CHMe_2), 19.4 (s, CHMe_2), 17.4 (s, CHMe_2). The structure was further confirmed by single-crystal diffraction from an orange crystal. Data for **311** are as follows. ${}^{31}\text{P}\{^1\text{H}\}$ NMR (202 MHz, CDCl_3): δ 51.3 (d, ${}^1J_{\text{Rh-P}} = 130$ Hz). ${}^{11}\text{B}\{^1\text{H}\}$ NMR (128 MHz, CDCl_3): δ 95.6 (br). ${}^{19}\text{F}$ NMR (470 MHz, CDCl_3): δ -77.1 (s). ${}^1\text{H}$ NMR (500 MHz, CDCl_3): δ 8.21 (m, 2H, Ar-H), 8.18 (d, ${}^3J_{\text{H-H}} = 7.1$ Hz, 1H, Ph-H), 6.91 (br, 1H, Ph-H), 6.60 (t, ${}^3J_{\text{H-H}} = 7.2$ Hz, 1H, Ph-H), 6.31 (br, 1H, Ph-H), 5.58 (br, 1H, Ph-H), 3.01 (m, 2H, CHMe_2), 2.59 (m, 2H, CHMe_2), 1.32 (dvt, ${}^3J_{\text{H-H}} \approx {}^{3,5}J_{\text{H-P}} = 7.2$ Hz, 6H, CHMe_2), 1.21 (dvt, ${}^3J_{\text{H-H}} \approx {}^{3,5}J_{\text{H-P}} = 6.8$ Hz, 6H, CHMe_2), 0.65 (dvt, ${}^3J_{\text{H-H}} \approx {}^{3,5}J_{\text{H-P}} = 7.1$ Hz, 6H, CHMe_2), 0.15 (dvt, ${}^3J_{\text{H-H}} \approx {}^{3,5}J_{\text{H-P}} = 7.3$ Hz, 6H, CHMe_2). Six aromatic protons are obscured due to overlap with the signals from isomer **310**. Selected resonances of **311** are as follows. ${}^{13}\text{C}$ NMR (101 MHz, CDCl_3): δ 155.3 (br, $C_{\text{Ar-B}}$), 142.1 (vt, ${}^{1,3}J_{\text{P-C}} = 20$ Hz, $C_{\text{Ar-P}}$), 141.0 (dt, ${}^1J_{\text{Rh-C}} = 39$ Hz, ${}^2J_{\text{C-P}} = 8.5$ Hz, $C_{\text{Ph-B}}$), 132.6 (vt, $J_{\text{P-C}} = 9.2$ Hz), 23.67 (br, CHMe_2 , 4C), 20.1 (m, CHMe_2 , 6C), 17.17 (s, CHMe_2).

3.4.4 X-ray structural determination details

The X-ray crystal data (cifs) could be obtained by the follow link:

<http://pubsdc3.acs.org/doi/suppl/10.1021/acs.organomet.7b00070>

X-Ray data collection, solution, and refinement for 301. A yellow, multi-faceted block of suitable size (0.32 x 0.18 x 0.10 mm) and quality was selected from a representative sample of crystals of the same habit using an optical microscope, mounted onto a nylon loop and placed in a cold stream of nitrogen. Low temperature (110 K) X-ray data were obtained on a Bruker APEXII CCD based diffractometer (Mo sealed X-ray tube, $K_{\alpha} = 0.71073 \text{ \AA}$). All diffractometer manipulations, including data collection, integration and scaling were carried out using the Bruker APEXII software.¹⁵⁵ An absorption correction was applied using SADABS.¹⁵⁶ The space group was determined on the basis of systematic absences and intensity statistics and the structure was solved by direct methods and refined by full-matrix least squares on F^2 . The structure was solved in the triclinic $P-1$ space group using XS¹⁵⁷ (incorporated in SHELXTL). No additional symmetry was found using ADDSYM incorporated in PLATON program.¹⁵⁸ All non-hydrogen atoms were refined with anisotropic thermal parameters. All hydrogen atoms were placed in idealized positions and refined using riding model. The structure was refined (weighted least squares refinement on F^2) and the final least-squares refinement converged.

X-Ray data collection, solution, and refinement for 305. A pale yellow, multi-faceted block of suitable size (0.33 x 0.07 x 0.05 mm) and quality was selected from a representative sample of crystals of the same habit using an optical microscope, mounted onto a nylon loop and placed in a cold stream of nitrogen. Low temperature (110 K) X-ray data were obtained on a Bruker APEXII CCD based diffractometer (Mo sealed X-ray tube, $K_{\alpha} = 0.71073 \text{ \AA}$). All diffractometer manipulations, including data collection,

integration and scaling were carried out using the Bruker APEXII software.¹⁵⁵ An absorption correction was applied using SADABS.¹⁵⁶ The space group was determined on the basis of systematic absences and intensity statistics and the structure was solved by direct methods and refined by full-matrix least squares on F^2 . The structure was solved in the monoclinic P 21/n space group using XS¹⁵⁷ (incorporated in SHELXLE). No additional symmetry was found using ADDSYM incorporated in PLATON program.¹⁵⁸ The solution was then refined by full-matrix least squares on F^2 . All non-hydrogen atoms were refined with anisotropic thermal parameters. All hydrogen atoms were placed in idealized positions and refined using riding model. The structure was refined (weighted least squares refinement on F^2) and the final least-squares refinement converged.

X-Ray data collection, solution, and refinement for 308. A pale yellow, multi-faceted block of suitable size (0.18 x 0.07 x 0.05 mm) and quality was selected from a representative sample of crystals of the same habit using an optical microscope, mounted onto a nylon loop and placed in a cold stream of nitrogen. Low temperature (110 K) X-ray data were obtained on a Bruker APEXII CCD based diffractometer (Mo sealed X-ray tube, $K_{\alpha} = 0.71073 \text{ \AA}$). All diffractometer manipulations, including data collection, integration and scaling were carried out using the Bruker APEXII software.¹⁵⁵ An absorption correction was applied using SADABS.¹⁵⁶ The structure was initially solved by direct methods in the triclinic space group $P1$ using XS¹⁵⁷ (incorporated in SHELXLE). Additional symmetry was found and the solution was converted to the triclinic space group $P-1$ using PLATON – ADDSYM.¹⁵⁸ The solution was then refined by full-matrix least squares on F^2 . All non-hydrogen atoms were refined with anisotropic thermal parameters.

All hydrogen atoms were placed in idealized positions and refined using riding model. The structure was refined (weighted least squares refinement on F^2) and the final least-squares refinement converged.

X-Ray data collection, solution, and refinement for 310. An orange, multi-faceted needle of suitable size (0.90 x 0.12 x 0.06 mm) was selected from a representative sample of crystals of the same habit using an optical microscope and mounted onto a nylon loop. Low temperature (110 K) X-ray data were obtained on a Bruker APEXII CCD based diffractometer (Mo sealed X-ray tube, $K_{\alpha} = 0.71073 \text{ \AA}$). All diffractometer manipulations, including data collection, integration and scaling were carried out using the Bruker APEXII software.¹⁵⁵ An absorption correction was applied using SADABS.¹⁵⁶ The space group was determined on the basis of systematic absences and intensity statistics and the structure was solved by direct methods and refined by full-matrix least squares on F^2 . The structure was solved in the triclinic P21/c space group using XS¹⁵⁷ (incorporated in SHELXTL). No additional symmetry was found using ADDSYM incorporated in PLATON program.¹⁵⁸ All non-hydrogen atoms were refined with anisotropic thermal parameters. All hydrogen atoms were placed in idealized positions and refined using riding model. The structure was refined (weighted least squares refinement on F^2) and the final least-squares refinement converged.

X-Ray data collection, solution, and refinement for 312. A green, multi-faceted needle of suitable size (0.52 x 0.11 x 0.09 mm) was selected from a representative sample of crystals of the same habit using an optical microscope and mounted onto a nylon loop. Low temperature (150 K) X-ray data were obtained on a Bruker APEXII CCD based

diffractometer (Mo sealed X-ray tube, $K_{\alpha} = 0.71073 \text{ \AA}$). All diffractometer manipulations, including data collection, integration and scaling were carried out using the Bruker APEXII software.¹⁵⁵ An absorption correction was applied using SADABS.¹⁵⁶ The space group was determined on the basis of systematic absences and intensity statistics and the structure was solved by direct methods and refined by full-matrix least squares on F^2 . The structure was solved in the monoclinic P 21/n space group using XS¹⁵⁷ (incorporated in SHELXLE). No additional symmetry was found using ADDSYM incorporated in PLATON program.¹⁵⁸ All non-hydrogen atoms were refined with anisotropic thermal parameters. All hydrogen atoms were placed in idealized positions and refined using riding model. The structure was refined (weighted least squares refinement on F^2) and the final least-squares refinement converged.

3.4.5 Van't Hoff plot

NMR spectra have been collected in CDCl_3 at different temperatures to investigate the thermodynamics for the isomerization between **304** and **307**. **304/307** were picked as a model to study the intramolecular B–Ph bond activation process since the equilibrium between **304** and **307** was reached in a relatively short amount of time which made it easy to monitor by NMR spectroscopy. The equilibrium was reached and monitored by ^1H NMR spectroscopy at five different temperatures between $30 \text{ }^\circ\text{C}$ and $62 \text{ }^\circ\text{C}$. The ratio of **304** and **307** was determined by their integrations in the ^1H NMR spectra. The Van't Hoff analysis of the experimental data led to the determination of $\Delta H^\circ = 1.0(1) \text{ kcal/mol}$ and $\Delta S^\circ = 5.3(2) \text{ cal}\cdot\text{mol}^{-1}\cdot\text{K}^{-1}$ for the transformation from **304** to **307**.

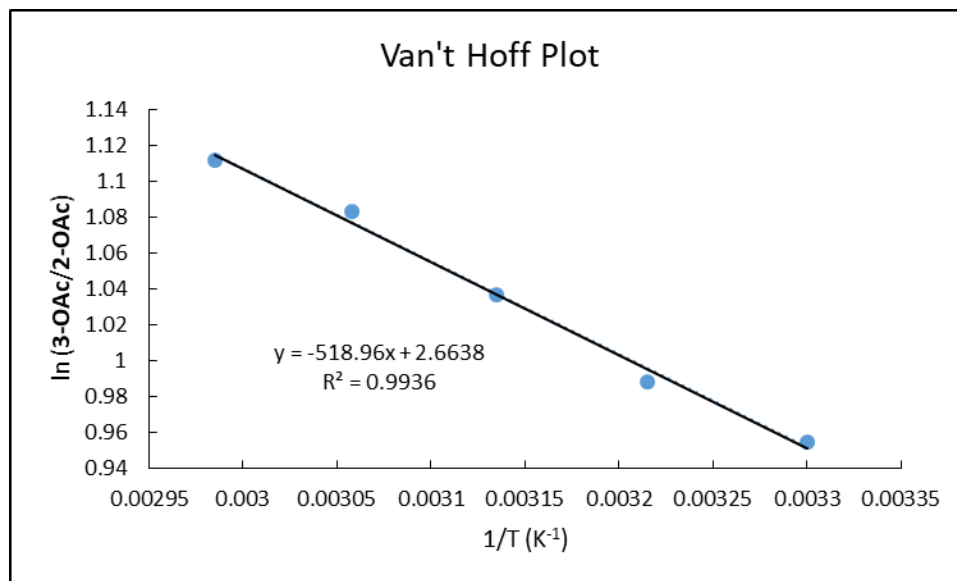
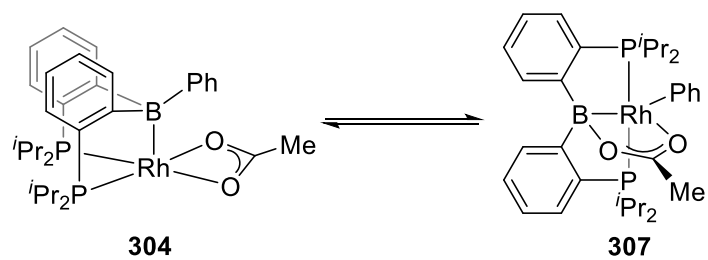


Figure III-11. Van't Hoff plot for the isomerization between **304** and **307**.

CHAPTER IV
SYNTHESIS AND CHARACTERIZATION OF PBP PINCER IRIIDIUM
COMPLEXES AND THEIR APPLICATION IN ALKANE TRANSFER
DEHYDROGENATION[‡]

4.1 Introduction

Pincer ligands are a particularly advantageous class of ancillary ligands in transition-metal chemistry that have allowed for the pursuit of well-defined fundamental reactivity as well as given rise to impressive catalytic applications.^{4-6,162,163} Alkane dehydrogenation and the associated catalytic transformations of hydrocarbons are among the most impressive accomplishments for pincers in catalysis.^{5,62,65,68,69,180-184}

Although diverse designs abound, the most common construction of a pincer ligand combines flanking phosphine side arms with a different central donor. Among these central donors, boryls have been among the latest to be introduced. Boryls are particularly interesting because they are arguably the most donating and the most trans influencing among donor ligands that can be incorporated into polydentate ligands. The first boryl/bis(phosphine) PBP pincer ligand was reported by Nozaki and Yamashita in 2009 (Figure IV-1).³⁷ In the following years, several groups accessed boryl-centered pincer ligands where the boryl donor is incorporated into an *m*-carborane cage (Figure

[‡] Reproduced in part from “Synthesis and Characterization of PBP Pincer Iridium Complexes and Their Application in Alkane Transfer Dehydrogenation” by Shih, W.-C.; Ozerov, O. V. *Organometallics* **2017**, *36*, 228. Copyright [2017] by The American Chemical Society.

IV-1).^{95,98,99,167} In 2015, Yamashita reported a study testing the utility of PBP* complexes of Ir in alkane dehydrogenation, and later in 2016 designed a new long-tethered PBP* complex to improve the catalytic reactivity, but both with modest success.^{72,166} Yamashita's PBP* ligand has also been used by other groups.^{86,87}

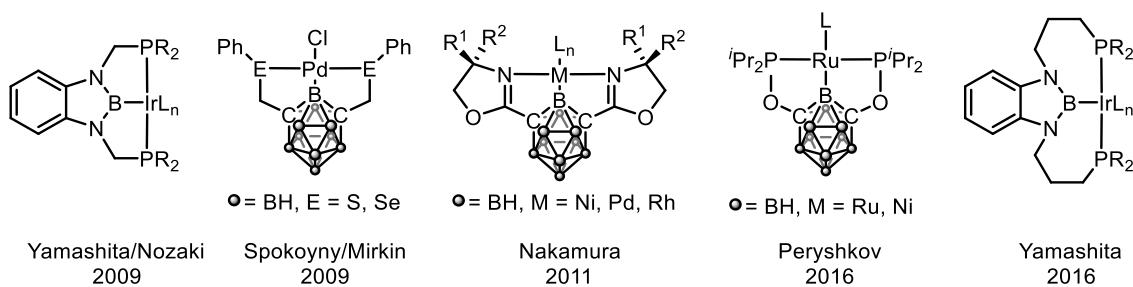
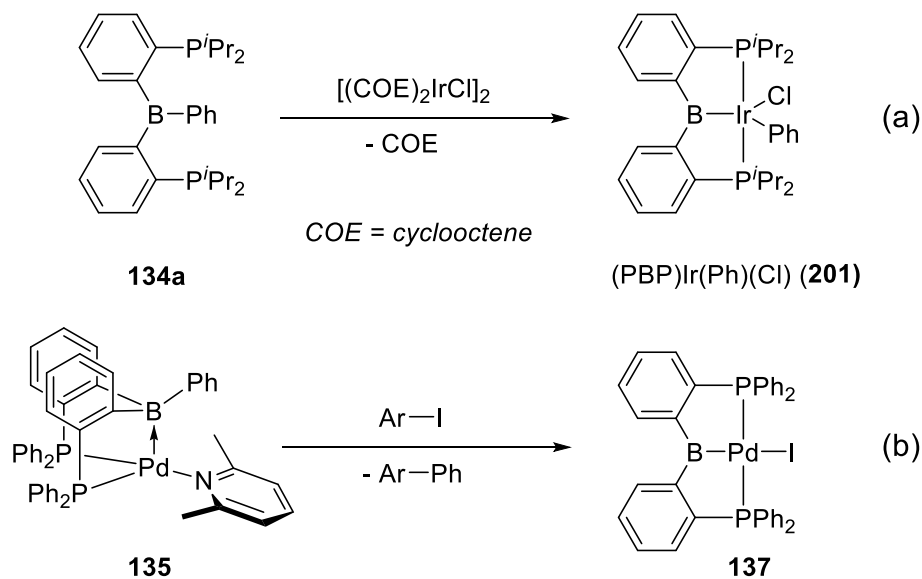
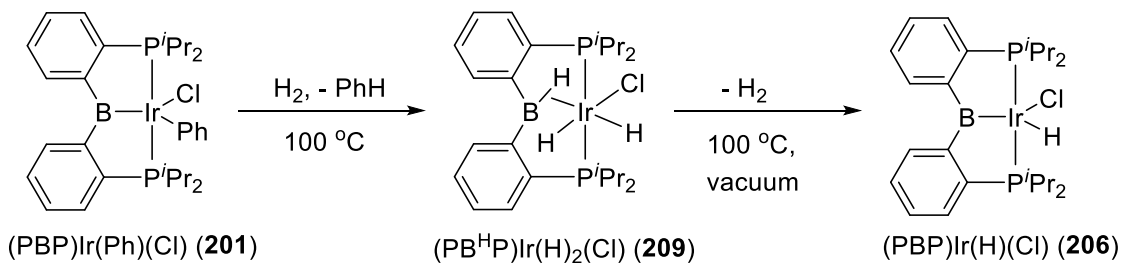


Figure IV-1. Previously reported pincer complexes with a central boryl donor.

In a previous publication,¹⁰² we showed how insertion of an Ir center into a B–Ph bond of a PB^{Ph}P precursor¹²⁷ provides access to the new boryl/bis(phosphine) complex (PBP)Ir(Ph)(Cl) (**201**) (Scheme IV-1a). Palladium complexes of this PBP pincer **137** were recently reported by Tauchert et al (Scheme IV-1b).²¹ We reported that complex **201** can be converted to the hydrido/chloride **206** via intermediacy of **209** in an overall hydrogenolysis reaction (Scheme IV-2). In order to evaluate the potential of the (PBP)Ir system in alkane dehydrogenation, we sought to prepare a (PBP)Ir polyhydride derivative. In addition, we envisaged synthesizing a carbonyl derivative for the purpose of comparing the apparent donor ability of the PBP ligand toward Ir in comparison with other pincer ligands. Herein we report the results of these pursuits.



Scheme IV-1. Synthesis of PBP Complex by Insertion of Metal into a B–Ph Bond or by C–C Bond Cross Coupling



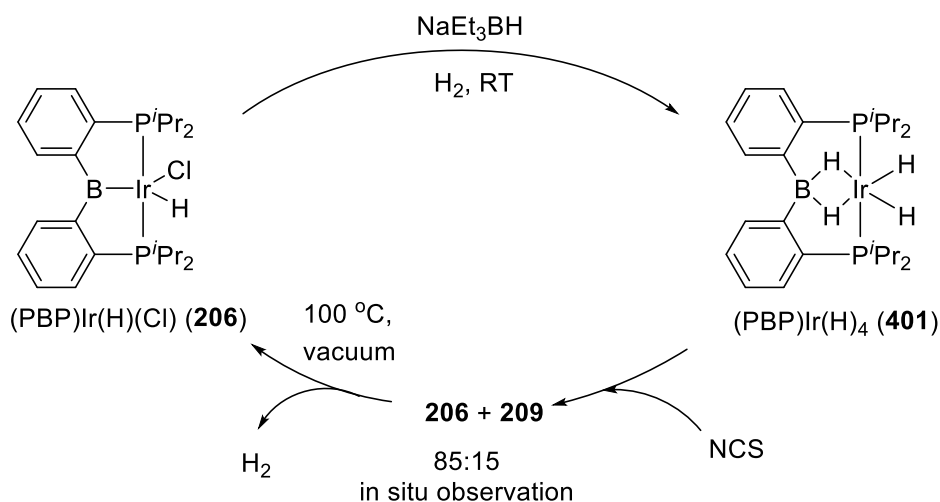
Scheme IV-2. Conversion of 201 to 206 from Intermediacy of 209

4.2 Results and Discussion

4.2.1 Synthesis and characterization of PBP-type pincer iridium complexes

Stirring **206** and sodium triethylborohydride in toluene or C_6D_6 at room temperature followed by placing the reaction mixture under 1 atm of H_2 afforded a pale yellow solution of $(\text{PBP})\text{IrH}_4$ (**401**), from which a 64% isolated yield was obtained upon

workup (Scheme IV-3).^{62,180} Treatment of solutions of **401** with 1.0 equiv of *N*-chlorosuccinimide (NCS) at room temperature was found to convert **401** back to **206**. The in situ mixture contained (PB^HP)Ir(H)₂(Cl) (**209**) and (PBP)Ir(H)(Cl) (**206**) in a 15:85 ratio, and the removal of volatiles at 100 °C under vacuum fully converted the mixture into **206**. Complex **401** displayed *C*_{2v} symmetry in its ¹H NMR spectrum, with two different hydride resonances apparent: a broad signal at δ -6.82 ppm and a triplet at δ -13.47 ppm (t, *J*_{H-P} = 12.7 Hz). We ascribe these resonances to the pair of bridging and terminal hydrides, respectively. A similar picture was observed in the hydride region by Lin and Peters for (PBP*)CoH₄,⁸⁶ albeit only at -90 °C and under an H₂ atmosphere (PBP* = Yamashita's PBP ligand).



Scheme IV-3. Synthesis of PBP Ir Polyhydrides (401) and Conversion of 401 back to 206

An X-ray diffraction study (Figure IV-2) of **401** permitted identification of the two bridging hydride ligands H1 and H2 and the two terminal hydride ligands H7 and H8, located via the Fourier difference map.

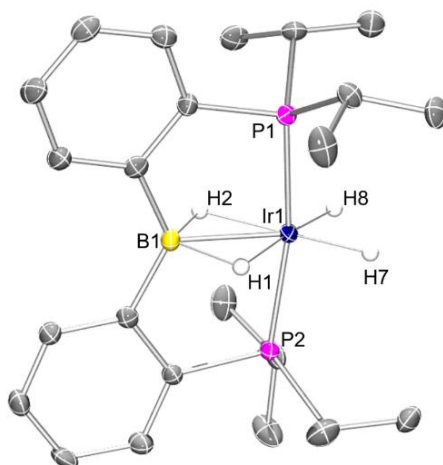


Figure IV-2. POV-Ray rendition of the ORTEP drawing (50% thermal ellipsoids) of **401** showing selected atom labeling. Hydrogen atoms are omitted, except for the hydrogens on Ir, for clarity. Selected bond distances (Å) and angles (deg): Ir1–B1, 2.159(3); Ir1–H1, 1.64(3); Ir1–H2, 1.71(3); Ir1–H7, 1.57(3); Ir1–H8, 1.50(3); B1–H1, 1.48(3); B1–H2, 1.34(3); Ir1–P1, 2.2840(7); Ir1–P2, 2.2804(7); B1–Ir1–H1, 43.3(10); B1–Ir1–H2, 38.3(10); B1–Ir1–H7, 138.6(11); B1–Ir1–H8, 139.9(10); H1–Ir1–H8, 176.0(14); H2–Ir1–H7, 176.0(13); H1–B1–H2, 101.5(17); H7–Ir1–H8, 81.5(15).

Radius, Braunschweig, et al. discussed the limiting structural motifs for complexes of $[R_2BH_2]^-$ fragments with transition metals (Figure IV-3).¹⁸⁵ They argued that a more Lewis acidic boron center favors structural type **A** (κ^2 -dihydroborate) over **B** (σ -B–H

complex of a metal hydride), whereas a more electron-rich metal would favor the higher valence type **C** (boryl/dihydride). It should be noted that type **B** may correspond to two degenerate forms (**B** and **B'**), which may average out to a more symmetric structure: for example, by NMR spectroscopy. These issues have been explored in detail by Sabo- Etienne and co-workers in Ru chemistry.^{186–188} In addition, **A** and **C** can be viewed as limiting structures at either end of a possible continuum of intermediate structures. In this vein, Yamashita et al. ascribed type **D** to the structures of (PBP*)(μ -H)₂RuX (where X = BH₄, OAc¹⁸⁹). These compounds possessed a Ru–B bond distance comparable to that of unambiguous 2c-2e Ru–B_{boryl} bonds yet clearly contained bridging hydrides. **D** can be viewed as either incomplete insertion of the metal into the pair of B–H bonds in type **A** or as a variation of **C** that retains B···H contacts.

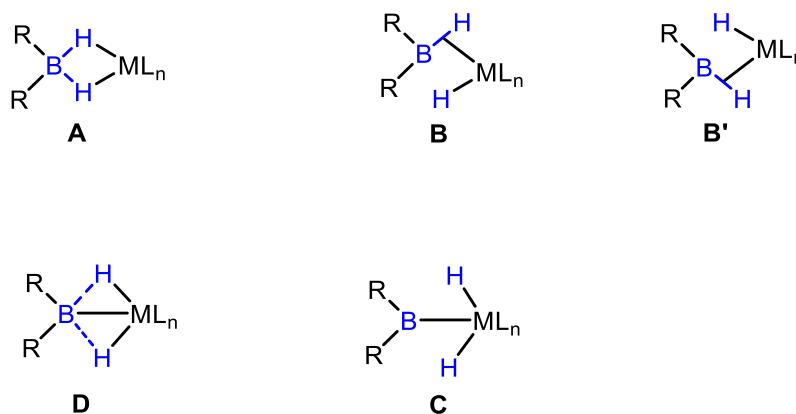


Figure IV-3. Different structural types for interaction of R₂BH₂ with a transition metal, as presented by Radius and Braunschweig (**A–C**), and Yamashita’s assignment of the intermediate structure **D**.

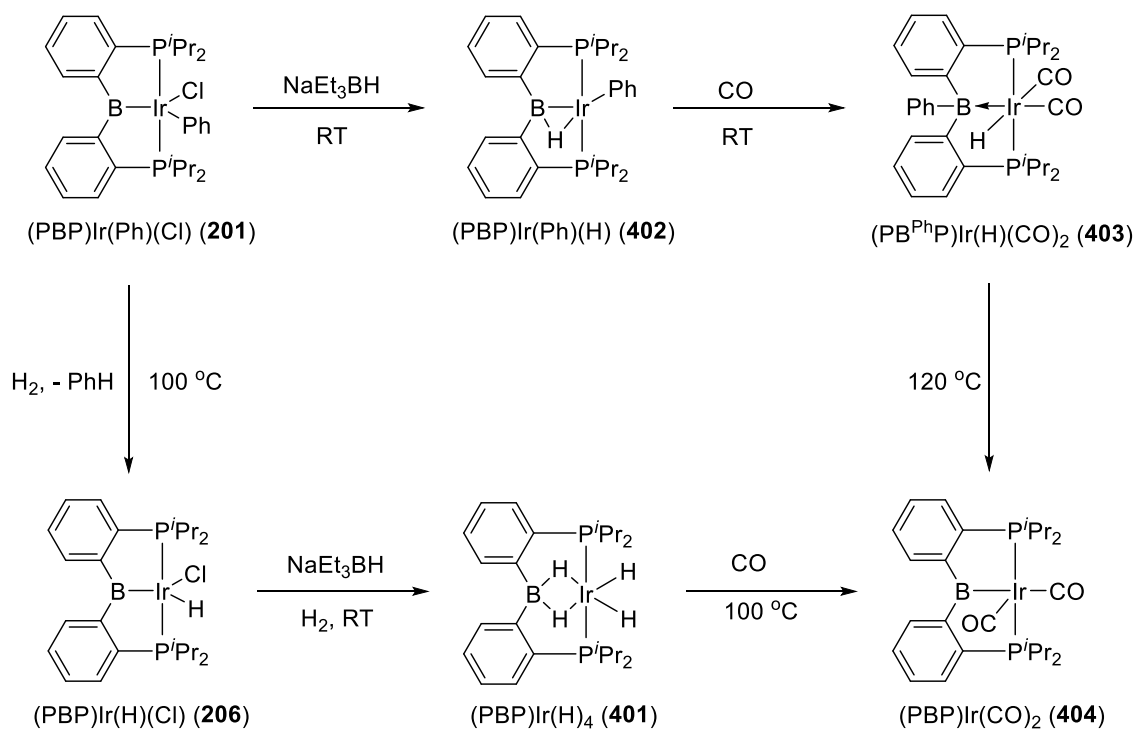
The Ir...B bond distance in **401** (2.159(3) Å) is shorter than the Ir...B_{borate} bond distances (2.19–2.28 Å) in the dihydrido borate iridium complexes. It is slightly longer than the Ir–B distances in **209** (2.135–2.137 Å) possessing a σ -B–H coordination mode.^{72,102,166} Although this distance is ca. 0.15 Å longer than the 2c-2e Ir–B bonds in **201** and **206**, it is only ca. 0.02 Å longer than the 2c-2e Ir–B distance in (PBP)Ir(CO)₂ (**404**) (vide infra). The ¹¹B{¹H} NMR chemical shift observed for **401** (45.6 ppm; Table IV-1) is decidedly upfield of that for the unambiguous boryl species but also clearly not upfield enough to fall in the region of sp³-hybridized B. On the basis of these observations, it seems reasonable to suggest that complex **401** lies somewhere along the continuum between **A** and **C**, and probably closer to type **A**. The fact that the solid-state structure is symmetric with respect to the B–Ir vector argues against **B** as the ground state, at least in the solid.

Table IV-1. Chemical Shifts in ¹¹B{¹H} NMR and ³¹P{¹H} NMR Spectra of Ir Complexes (in ppm)

	201	206	209	401	402	403	404	405
¹¹ B NMR	75.9	72.6	53.7	45.6	53.1	5.7	99.4	42.4
³¹ P NMR	44.9	61.9	53.5	65.4	56.8	51.7	61.0	66.2

Another potential transfer dehydrogenation precatalyst (PBP)Ir(Ph)(H) (**402**) was also successfully synthesized (Scheme IV-4). Stirring **201** and sodium triethylborohydride in toluene or C₆D₆ at room temperature resulted in an immediate formation of a dark red

solution. Solution multinuclear NMR analysis demonstrated the near-quantitative formation of complex **402**. Relative to **201** (75.9 ppm) or **206** (72.6 ppm), the ^{11}B NMR resonance of **402** (53.1 ppm) is shifted considerably upfield, and the hydride resonance (δ -11.51 ppm) is broad, which suggests a degree of interaction between B and H in **402** that is not present in **206**. This interaction is likely also responsible for the thermal stability of **402** with respect to reductive elimination of benzene, as it lowers the energy of **402** as a benzene addition product to (PBP)Ir. Without the auxiliary B–H interaction, elimination of benzene from **402** would be expected to be quite facile.³⁶



Scheme IV-4. Reactivity of PBP Complexes of Iridium

Exposure of a solution of **402** to 1 atm of CO led to the formation of a pale yellow solution of $(\text{PB}^{\text{Ph}}\text{P})\text{Ir}(\text{H})(\text{CO})_2$ (**403**) after a few minutes (Scheme IV-4). The presence of two carbonyl ligands was evident from the two downfield ^{13}C NMR resonances (179.0 and 168.5 ppm) as well as two bands in the IR spectrum (ν_{CO} 2015 and 1978 cm^{-1}). The ^{11}B NMR spectrum showed one upfield resonance at 5.7 ppm, consistent with an sp^3 -hybridized boron. One triplet peak at -10.66 ppm (t, $J_{\text{H-P}} = 15.0$ Hz, Ir–H) in the ^1H NMR spectrum showed no broadening from interaction with boron, consistent with a terminal Ir hydride. These observations suggest the structure of **403** as depicted in Scheme IV-2, with the triarylborane moiety acting as a Z-type ligand. Triarylboranes have been at the center of the development of new appreciation for Z-type ligands over the past decade or so.^{122,125,168,170,190,191} The formation of **403** can be viewed as CO-induced reductive elimination of a B–C bond from **402**.

Thermolysis of complex **402** at 120 °C under a CO atmosphere led to a gradual change in the color of the solution to dark-red, corresponding to the formation of the new complex $(\text{PBP})\text{Ir}(\text{CO})_2$ (**404**) (Scheme IV-4). Conversion of the intermediately formed **403** into **404** requires loss of benzene. While we have not ascertained the mechanism by which this happens, a likely scenario involves migration of Ph to Ir with loss of CO, followed by C–H reductive elimination of benzene and recoordination of CO.

The downfield ^{11}B NMR chemical shift (99.4 ppm; Table IV-1) confirmed the presence of an sp^2 -hybridized boryl central donor in **404**. Complex **404** displayed C_{2v} symmetry in solution on the NMR time scale at room temperature: a singlet resonance at 61.0 ppm in the $^{31}\text{P}\{^1\text{H}\}$ NMR spectrum, one methine resonance and two methyl

resonances from the isopropyl groups in the ^1H NMR spectrum, and one CO resonance in the $^{31}\text{C}\{^1\text{H}\}$ NMR spectrum. However, the solid-state IR spectrum revealed two CO stretching bands at 1960 and 1913 cm^{-1} . The presence of two coordinated carbonyls was confirmed in the course of an X-ray diffraction study on a single crystal of **404** (Figure IV-4). The geometry about Ir in **404** is distorted five-coordinate and is closer to square pyramidal than to trigonal bipyramidal (the τ parameter¹⁹² is 0.33). The solid-state structure is approximately C_s symmetric. The C_{2v} symmetry on the NMR time scale in solution suggests that rapid interconversion between the degenerate, less symmetric ground state forms takes place rapidly. The sum of angles about the boron center was found to be 360° , consistent with a trigonal-planar, sp^2 -hybridized boryl. However, the Ir–B distance (2.137 Å) was decidedly longer than typical PBP-type Ir–B_{boryl} distances (1.97–2.05 Å).^{37,72,102,166} The origin of this relative elongation in **404** is not clear.

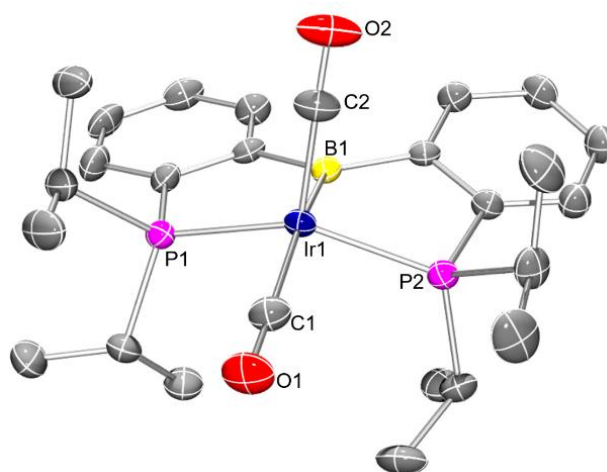


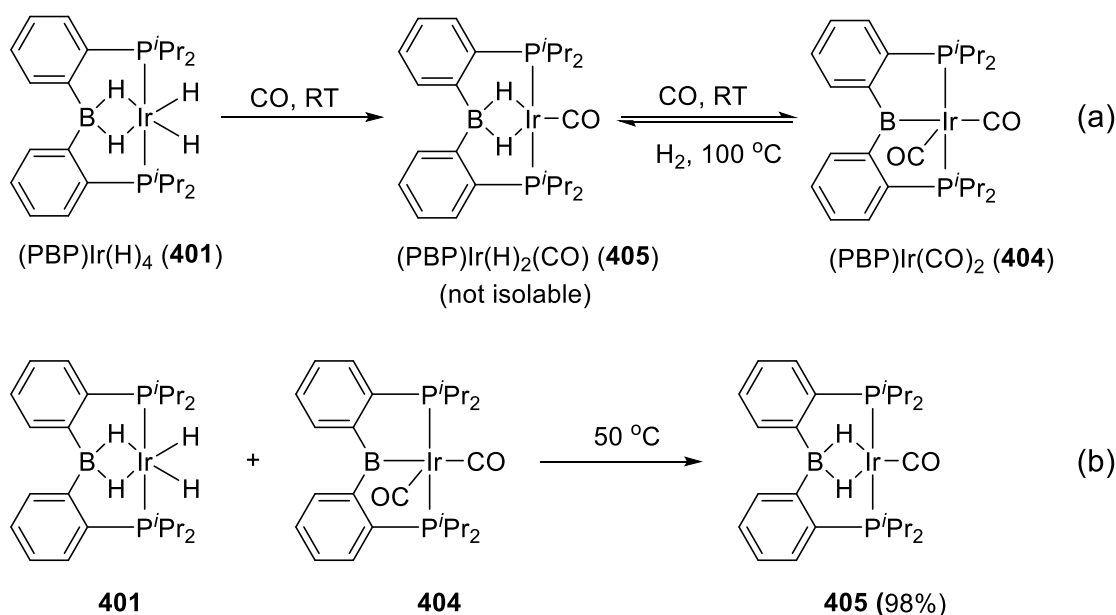
Figure IV-4. POV-Ray rendition of the ORTEP drawing (50% thermal ellipsoids) of **404** showing selected atom labeling. Hydrogen atoms are omitted for clarity. Selected

bond distances (Å) and angles (deg): Ir1–B1, 2.137(3); Ir1–C1, 1.935(3); Ir1–C2, 1.890(3); C1–O1, 1.144(4); C2–O2, 1.142(4); Ir1–P1, 2.3082(14); Ir1–P2, 2.2985(13); B1–Ir1–C1, 159.32(13); B1–Ir1–C2, 88.42(13); C1–Ir1–C2, 112.26(14); P1–Ir1–P2, 139.45(3); C2–Ir1–P1, 109.97(11); C2–Ir1–P2, 104.32(12).

Monovalent Ir complexed by PXP-type pincer ligands typically prefers to bind only a single carbonyl ligand. Although coordination of the second CO is possible, it is typically bound weakly and readily lost upon workup and/or exposure to vacuum.^{70,193} The fact that **404** persists as a dicarbonyl in solution in the absence of a CO atmosphere is thus rather unusual. It is possible that the strongly donating nature of the boryl ligand improves back-bonding to CO ligands, resulting in stronger bonds. On the other hand, it is also reasonable to suggest that the putative square planar monocarbonyl complex may be destabilized by the tenuous placement of the very strongly trans influencing boryl trans to CO.

Complex **404** can also be synthesized by addition of 1 atm of CO to a toluene solution of **401** at 100 °C overnight via loss of 2 equiv of H₂ (Scheme IV-4). When **401** was exposed to an atmosphere of CO at room temperature for 1 h, the new intermediate (PBP)Ir(H)₂(CO) (**405**) was observed to constitute 52% of the mixture, along with 22% of **401** and some other unidentifiable products (percentages of total ³¹P NMR intensity given). This reaction mixture gradually evolved into a dark red solution that contained 43% of **404** (³¹P NMR evidence) after 24 h (Scheme IV-5a). The reverse reaction was observed during the thermolysis of the C₆D₆ solution of **404** under 1 atm of

H₂ at 100 °C overnight, yielding a mixture of **405** and **404** in a ratio of 41 to 47, with the balance being due to two minor unidentified products. Although a pure bulk sample of **405** could not be isolated by the reaction of **401** with CO due to the facile conversion to **404**, it was easily synthesized by comproportionation of **401** and **404** at 50 °C in toluene (Scheme IV-5b). The signal in the ¹¹B{¹H} NMR spectrum and a broad resonance of the bridging hydrides in the ¹H NMR spectrum of **405** (42.4 and -6.26 ppm) are similar to those of compound **401** (45.6 and -6.82 ppm). It can be concluded that the same arguments (vide supra) regarding the nature of the apparent dihydroborate binding to Ir are applicable to **405** as well as **401**.

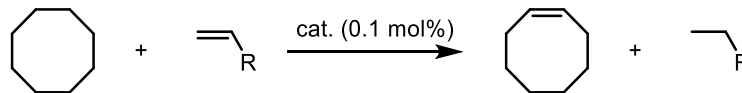


Scheme IV-5. Comproportionation of 401 and 404 into 405

4.2.2 Transfer dehydrogenation of COA to COE catalyzed by (PBP)Ir(H)₄ (401) and (PBP)Ir(Ph)(H) (402)

Complexes **401** and **402** were tested as precatalysts for transfer dehydrogenation of cyclooctane (COA) to cyclooctene (COE) with *tert*-butylethylene (TBE) or 1-hexene as the hydrogen acceptor (Table IV-2). A significant amount of work on related PCP/POCOP-type pincer complexes of Ir indicates that intermediacy of the monovalent [(pincer)Ir] fragment is crucial.⁵ **401** and **402** may be able to access a corresponding transient (PBP)Ir intermediate via reductive elimination of benzene or H₂ or by hydrogenation of the sacrificial olefin. Although there was no conversion at 100 °C (entry 1), a turnover number (TON) of 30 was achieved at 150 °C for 26 h (entry 2). The TONs were slightly increased to 43 upon elevation of the reaction temperature to 200 °C (entry 8), but it was clear that most of the TONs took place early in the reaction (entries 3–7). Utilization of the sterically less imposing 1-hexene instead of TBE as the hydrogen acceptor enhanced the obtained TONs to 78 at 150 °C and 221 at 200 °C (entries 9 and 10). Isomerization of 1-hexene into 2-hexene and 3-hexene was also observed in the reactions. Using complex **402** as the precatalyst with TBE or 1-hexene as the hydrogen acceptor gave TONs (entries 11–13) similar to those for use of **401** as the precatalyst. The activities of **401** and **402** as precatalysts for alkane transfer dehydrogenation are modestly higher than those of Yamashita's Ir complexes supported by the PBP* ligand.^{72,166} However, they fall significantly short of the best Ir examples utilizing pincer ligands of the aryl/bis(phosphine) type.^{5,68,184}

Table IV-2. TONs for Dehydrogenation of COA to COE Catalyzed by (PBP)Ir(H)₄ (401**) and (PBP)Ir(Ph)(H) (**402**)^a**



Entry	Cat.	R	T (°C)	Time (h)	TON
1	401	CMe ₃	100	26	0
2	401	CMe ₃	150	26	30
3	401	CMe ₃	200	0.5	32
4	401	CMe ₃	200	1	34
5	401	CMe ₃	200	2	36
6	401	CMe ₃	200	4	36
7	401	CMe ₃	200	6	36
8	401	CMe ₃	200	26	43
9	401	ⁿ Bu	150	26	78
10	401	ⁿ Bu	200	26	221
11	402	CMe ₃	150	26	38
12	402	CMe ₃	200	15	47
13	402	ⁿ Bu	200	26	158

a. TONs were calculated based on the formation of COE in ¹H NMR with mesitylene (3.59 mmol) as internal standard. COA (10.0 mmol), TBE or 1-hexene (10.0 mmol), Cat. **401** or **402** (0.01 mmol).

4.3 Conclusions

In summary, we report the preparation of new diarylboryl/bis(phosphine) PBP complexes of Ir that can serve as precatalysts for alkane transfer dehydrogenation. The activity displayed by this system was found to be modest. Structural and spectroscopic characterization of a series of PBP complexes enabled analysis of nonclassical BH/Ir interactions.

4.4 Experimental Section

4.4.1 General considerations

Unless specified otherwise, all manipulations were performed under an Ar atmosphere using standard Schlenk line or glovebox techniques. Screw-capped culture tubes with PTFE-lined phenolic caps were used to perform catalytic reactions. Toluene, pentane, and isooctane were dried and deoxygenated (by purging) using a solvent purification system (Innovative Technology Pure Solv MD-5 Solvent Purification System) and stored over molecular sieves in an Ar-filled glovebox. C₆D₆ was dried over NaK/Ph₂CO/18-crown-6, distilled or vacuum-transferred, and stored over molecular sieves in an Ar-filled glovebox. Hexamethyldisiloxane, COA, 1-hexene, and TBE were degassed by three freeze–pump–thaw cycles and stored over molecular sieves in an Ar-filled glovebox. (PBP)Ir(Ph)(Cl) (**201**), (PB^HP)Ir(H)₂(Cl) (**209**), and (PBP)Ir(H)(Cl) (**206**) were prepared via literature procedures.¹⁰² All other chemicals were used as received from commercial vendors.

4.4.2 Physical methods

NMR spectra were recorded on a Varian Inova 400 (¹H NMR, 399.535 MHz; ¹¹B NMR, 128.185 MHz; ³¹P NMR, 161.734 MHz) or a Varian Inova 500 (¹H NMR, 499.703 MHz; ¹³C NMR, 125.697 MHz; ³¹P NMR, 202.265 MHz) spectrometer. Chemical shifts are reported in δ (ppm). Coupling constant values in the ¹H NMR spectra should be interpreted with a 0.2 Hz uncertainty. For ¹H and ¹³C NMR spectra, the residual solvent peak was used as an internal reference (¹H NMR, δ 7.16 for C₆D₆; ¹³C NMR, δ 128.06 for

C₆D₆). ¹¹B NMR spectra were referenced externally with BF₃ etherate at δ 0. ³¹P NMR spectra were referenced externally with 85% phosphoric acid at δ 0. Elemental analyses were performed by CALI Laboratories, Inc. (Parsippany, NJ).

4.4.3 Synthesis and characterization of iridium complexes

(PBP)Ir(H)₄ (401): In a 25 mL Teflon screw-capped round-bottomed flask, NaEt₃BH (500 μL, 0.50 mmol, 1.0 M in toluene) was added to a toluene solution (2 mL) of (PBP)Ir(H)(Cl) (**206**; 313 mg, 0.50 mmol). The solution was degassed via freeze–pump–thaw, and the flask was refilled with H₂ (1 atm). The reaction mixture was stirred at room temperature for 1 h. During the stirring, the solution gradually changed from dark red to pale yellow. The solution was filtered through Celite, and the volatiles were removed under vacuum. The resulting solid was washed with isooctane, yielding a pale yellow solid (189 mg, 64%). ³¹P{¹H} NMR (202 MHz, C₆D₆): δ 65.4. ¹¹B NMR (128 MHz, C₆D₆): δ 45.6 (br). ¹H NMR (500 MHz, C₆D₆): δ 8.62 (d, *J*_{H,H} = 7.5 Hz, 2H, Ar–*H*), 7.43 (m, 2H, Ar–*H*), 7.30 (t, *J*_{H,H} = 7.4 Hz, 2H, Ar–*H*), 7.15 (m, 2H, Ar–*H*), 2.18 (m, 4H, CHMe₂), 1.24 (dvt, *J*_{H,H} ≈ *J*_{H,P} = 7.3 Hz, 12H, CHMe₂), 0.98 (dvt, *J*_{H,H} ≈ *J*_{H,P} = 7.1 Hz, 12H, CHMe₂), –6.82 (br s, 2H, B–H₂–Ir), –13.47 (t, *J*_{H,P} = 12.7 Hz, 2H, Ir–H₂). ¹³C{¹H} NMR (101 MHz, C₆D₆): δ 162.6 (br s, C–B), 149.3 (vt, *J*_{P,C} = 22.7 Hz, C–P), 131.5 (vt, *J*_{P,C} = 7.8 Hz), 130.5 (s), 130.3 (s), 126.2 (vt, *J*_{P,C} = 3.5 Hz), 26.6 (vt, *J*_{P,C} = 15.7 Hz, CHMe₂), 20.9 (t, *J*_{P,C} = 2.8 Hz, CHMe₂), 19.0 (s, CHMe₂). Anal. Calcd for C₂₄H₄₀BIrP₂: C, 48.57; H, 6.79. Found: C, 48.65; H, 6.59. Mp: 190 °C dec.

(PBP)Ir(H)(Ph) (402): In a 50 mL Schlenk flask, NaEt₃BH (1.00 mL, 1.00 mmol, 1.0 M in toluene) was added to a toluene solution (10 mL) of (PBP)Ir(Ph)(Cl) (**201**; 702 mg, 1.00 mmol). The reaction mixture was stirred at room temperature for 1 h. The solution was filtered through Celite, and the volatiles were removed under vacuum. The resulting solid was washed with hexamethyldisiloxane, yielding an orange solid (567 mg, 93%). ³¹P{¹H} NMR (202 MHz, C₆D₆): δ 56.8. ¹¹B NMR (128 MHz, C₆D₆): δ 53.1 (br). ¹H NMR (500 MHz, C₆D₆): δ 8.50 (d, *J*_{H,H} = 7.1 Hz, 2H), 7.43 (d, *J*_{H,H} = 6.7 Hz, 1H), 7.36 (m, 4H), 7.21 (m, 5H), 6.93 (t, *J*_{H,H} = 7.0 Hz, 1H), 2.57 (m, 2H, CHMe₂), 2.49 (m, 2H, CHMe₂), 1.18 (dvt, *J*_{H,H} ≈ *J*_{H,P} = 7.3 Hz, 6H, CHMe₂), 1.09 (dvt, *J*_{H,H} ≈ *J*_{H,P} = 7.3 Hz, 6H, CHMe₂), 0.94 (dvt, *J*_{H,H} ≈ *J*_{H,P} = 6.7 Hz, 6H, CHMe₂), 0.84 (dvt, *J*_{H,H} ≈ *J*_{H,P} = 7.3 Hz, 6H, CHMe₂), -11.51 (br s, 1H, Ir-H). ¹³C{¹H} NMR (101 MHz, C₆D₆): δ 165.0 (t, *J*_{P,C} = 8.6 Hz, Ir-C), 161.2 (br s, C-B), 145.3 (vt, *J*_{P,C} = 23.5 Hz, C-P), 138.1 (s), 130.4 (m), 129.9 (s), 128.6 (s), 126.9 (vt, *J*_{P,C} = 3.2 Hz), 125.0 (s), 121.5 (s), 25.5 (vt, *J*_{P,C} = 13.6 Hz, CHMe₂), 23.4 (vt, *J*_{P,C} = 14.5 Hz, CHMe₂), 20.5 (s, CHMe₂), 19.0 (s, CHMe₂), 18.8 (s, CHMe₂), 17.4 (s, CHMe₂). Anal. Calcd for C₃₀H₄₂BIrP₂: C, 53.97; H, 6.34. Found: C, 53.68; H, 6.46. Mp: 114 °C dec.

(PB^{Ph}P)Ir(H)(CO)₂ (403): In a 25 mL Teflon screw-capped round-bottomed flask, (PBP)Ir(H)(Ph) (**402**; 67 mg, 0.10 mmol) was dissolved in C₆H₆ (1.0 mL). The solution was degassed twice via freeze-pump-thaw, and the flask was refilled with CO (1 atm). After 10 min, the solution changed from orange to pale yellow. The volatiles were removed under vacuum, and the resulting solid was washed with cold pentane, yielding a pale yellow solid (52 mg, 72%). The purity of isolated samples of **403** was gauged to be

>95% by NMR spectroscopy. $^{31}\text{P}\{^1\text{H}\}$ NMR (202 MHz, C_6D_6): δ 51.7. ^{11}B NMR (128 MHz, C_6D_6): δ 5.7. ^1H NMR (500 MHz, C_6D_6): δ 7.81 (d, $J_{\text{H,H}} = 7.3$ Hz, 2H), 7.20 (t, $J_{\text{H,H}} = 7.3$ Hz, 2H), 7.16 (m, 2H), 7.12 (m, 2H), 7.03 (t, $J_{\text{H,H}} = 6.7$ Hz, 2H), 6.96 (t, $J_{\text{H,H}} = 7.2$ Hz, 1H), 6.89 (d, $J_{\text{H,H}} = 7.2$ Hz, 2H), 2.37 (m, 2H, CHMe_2), 2.27 (m, 2H, CHMe_2), 1.14 (dvt, $J_{\text{H,H}} \approx J_{\text{H,P}} = 7.2$ Hz, 6H, CHMe_2), 0.99 (m, 12H, CHMe_2), 0.69 (dvt, $J_{\text{H,H}} \approx J_{\text{H,P}} = 7.3$ Hz, 6H, CHMe_2), -10.66 (t, $J_{\text{H,P}} = 15.0$ Hz, 1H, Ir-H). $^{13}\text{C}\{^1\text{H}\}$ NMR (101 MHz, C_6D_6): δ 179.0 (s, CO), 174.2 (br, B-C_{Ar}), 168.5 (s, CO), 164.6 (br, B-C_{Ph}), 141.4 (vt, $J_{\text{P,C}} = 30.3$ Hz, C-P), 135.7 (s), 133.8 (vt, $J_{\text{P,C}} = 11.0$ Hz), 129.6 (s), 128.5 (vt, $J_{\text{P,C}} = 3.5$ Hz), 126.1 (s), 124.2 (vt, $J_{\text{P,C}} = 4.2$ Hz), 124.1 (s), 29.7 (vt, $J_{\text{P,C}} = 13.7$ Hz, CHMe_2), 27.9 (vt, $J_{\text{P,C}} = 17.9$ Hz, CHMe_2), 20.2 (s, CHMe_2), 20.1 (s, CHMe_2), 19.5 (s, CHMe_2), 18.6 (s, CHMe_2). IR (KBr), ν_{CO} 2015, 1978 cm^{-1} .

(PBP)Ir(CO)₂ (404): *Method A*. In a 25 mL Teflon screw-capped round-bottomed flask, (PBP)Ir(H)₄ (**3**; 89 mg, 0.15 mmol) was dissolved in toluene (2 mL). The solution was degassed twice via freeze-pump-thaw, and the flask was refilled with CO (1 atm). The reaction mixture was stirred at 100 °C overnight. During the heating, the color gradually changed from pale yellow to dark red. The volatiles were removed under vacuum, and the resulting solid was washed with cold pentane, yielding a dark red solid (80 mg, 83%). *Method B*. In a 25 mL Teflon screw-capped round-bottomed flask, (PBP)Ir(H)(Ph) (**402**; 134 mg, 0.20 mmol) was dissolved in toluene (2 mL). The solution was degassed twice via freeze-pump-thaw, and the flask was refilled with CO (1 atm). The reaction mixture was stirred at 120 °C for 3 days. The volatiles were removed under vacuum, and the resulting solid was washed with cold pentane, yielding a dark red solid

(98 mg, 76%). $^{31}\text{P}\{^1\text{H}\}$ NMR (202 MHz, C_6D_6): δ 61.0. ^{11}B NMR (128 MHz, C_6D_6): δ 99.4 (br). ^1H NMR (500 MHz, C_6D_6): 8.09 (d, $J_{\text{H,H}} = 7.4$ Hz, 2H), 7.38 (m, 2H), 7.20 (m, 2H), 7.11 (m, 2H), 2.31 (m, 4H, CHMe_2), 1.09 (dvt, $J_{\text{H,H}} \approx J_{\text{H,P}} = 6.9$ Hz, 12H, CHMe_2), 0.90 (dvt, $J_{\text{H,H}} \approx J_{\text{H,P}} = 6.9$ Hz, 12H, CHMe_2). $^{13}\text{C}\{^1\text{H}\}$ NMR (126 MHz, C_6D_6): δ 185.6 (s, CO), 163.2 (br s, C–B), 152.2 (vt, $J_{\text{P,C}} = 25.2$ Hz, C–P), 130.4 (vt, $J_{\text{P,C}} = 11.1$ Hz), 130.1 (s), 129.4 (s), 128.6 (s), 28.8 (vt, $J_{\text{P,C}} = 14.3$ Hz, CHMe_2), 19.74 (vt, $J_{\text{P,C}} = 2.4$ Hz, CHMe_2), 18.43 (s, CHMe_2). IR (KBr), ν_{CO} 1960, 1913 cm^{-1} . Anal. Calcd for $\text{C}_{26}\text{H}_{36}\text{BIrO}_2\text{P}_2$: C, 48.38; H, 5.62. Found: C, 48.76; H, 5.68.

(PBP)Ir(H)₂(CO) (405): In a 25 mL Teflon screw-capped round-bottomed flask, (PBP)Ir(H)₄ (**401**; 237 mg, 0.40 mmol) and (PBP)Ir(CO)₂ (**404**; 284 mg, 0.44 mmol) were dissolved in toluene (10 mL). The reaction mixture was stirred at 50 °C overnight. During the heating, the mixture gradually changed from dark red to orange. After the mixture was cooled to room temperature, the volatiles were removed under vacuum, and the resulting solid was redissolved in toluene, layered with pentane, and placed in a –35 °C freezer, yielding orange crystals (486 mg, 98%). The purity of isolated samples of **405** was gauged to be >95% by NMR spectroscopy. $^{31}\text{P}\{^1\text{H}\}$ NMR (202 MHz, C_6D_6): δ 66.2. ^{11}B NMR (128 MHz, C_6D_6): δ 42.4 (br). ^1H NMR (500 MHz, C_6D_6): 8.38 (d, $J_{\text{H,H}} = 7.5$ Hz, 2H), 7.31 (m, 2H), 7.27 (m, 2H), 7.09 (td, $J_{\text{H,H}} = 7.4$, $J_{\text{H,H}} = 1.2$ Hz, 2H), 2.22 (m, 4H, CHMe_2), 1.24 (dvt, $J_{\text{H,H}} \approx J_{\text{H,P}} = 6.9$ Hz, 12H, CHMe_2), 0.89 (dvt, $J_{\text{H,H}} \approx J_{\text{H,P}} = 7.0$ Hz, 12H, CHMe_2), –6.26 (br s, 2H, Ir–H). $^{13}\text{C}\{^1\text{H}\}$ NMR (126 MHz, C_6D_6) δ 187.0 (s, CO), 162.4 (br s, C–B), 146.9 (vt, $J_{\text{P,C}} = 25.8$ Hz, C–P), 132.0 (vt, $J_{\text{P,C}} = 8.6$ Hz), 130.3 (s), 130.0

(vt, $J_{P,C} = 2.3$ Hz), 126.1 (vt, $J_{P,C} = 3.9$ Hz), 28.1 (vt, $J_{P,C} = 15.7$ Hz, $CHMe_2$), 20.3 (vt, $J_{P,C} = 1.8$ Hz, $CHMe_2$), 18.9 (s, $CHMe_2$).

4.4.4 Catalytic transfer dehydrogenation of COA into COE

General Procedure of Transfer Dehydrogenation of COA using Complex 401.

In a screw-capped culture tube, complex **401** (5.9 mg, 0.01 mmol) was dissolved in a solution of COA (1.35 mL, 10.0 mmol) and a hydrogen acceptor (1.29 mL for TBE or 1.25 mL for 1-hexene, 10.0 mmol). The tube was sealed, and the reaction mixture was heated in a preheated oil bath at a suitable temperature for the required time (Table IV-2, entries 1–10). After the tube was cooled to room temperature, mesitylene (0.50 mL, 3.59 mmol) was added as internal standard and the TON was calculated on the basis of the formation of COE in the 1H NMR spectrum.

General Procedure of Transfer Dehydrogenation of COA using Complex 402.

In a screw-capped culture tube, complex **402** (6.7 mg for **402**, 0.01 mmol) was dissolved in a solution of COA (1.35 mL, 10.0 mmol) and a hydrogen acceptor (1.29 mL for TBE or 1.25 mL for 1-hexene, 10.0 mmol). The tube was sealed, and the reaction mixture was heated in a preheated oil bath at a suitable temperature for the required time (Table IV-2, entries 11–13). After the tube was cooled to room temperature, mesitylene (0.50 mL, 3.59 mmol) was added as internal standard and the TON was calculated on the basis of the formation of COE in the 1H NMR spectrum.

4.4.5 X-ray structural determination details

The X-ray crystal data (cifs) could be obtained by the follow link:

<http://pubs.acs.org/doi/suppl/10.1021/acs.organomet.6b00762>

X-ray Data Collection, Solution, and Refinement for (PBP)Ir(H)₄ (401). A colorless, multifaceted block of suitable size (0.26 × 0.09 × 0.04 mm) was selected from a representative sample of crystals of the same habit using an optical microscope and mounted onto a nylon loop. Low-temperature (110 K) X-ray data were obtained on a Bruker APEXII CCD-based diffractometer (Mo sealed X-ray tube, K α 0.71073 Å). All diffractometer manipulations, including data collection, integration, and scaling, were carried out using the Bruker APEXII software.¹⁵⁵ An absorption correction was applied using SADABS.¹⁵⁶ The space group was determined on the basis of systematic absences and intensity statistics, and the structure was solved by direct methods and refined by full-matrix least squares on F^2 . The structure was solved in the monoclinic $P2_1/c$ space group using XS¹⁵⁷ (incorporated in SHELXLE). All non-hydrogen atoms were refined with anisotropic thermal parameters. All hydrogen atoms were placed in idealized positions and refined using a riding model, with the exception of the hydrogen bound to iridium, which was located from the difference map. The structure was refined (weighted least-squares refinement on F^2), and the final least-squares refinement converged. No additional symmetry was found using ADDSYM incorporated in the PLATON program.¹⁵⁸

X-ray Data Collection, Solution, and Refinement for (PBP)Ir(CO)₂ (404). A red, multifaceted block of suitable size (0.20 × 0.16 × 0.04 mm) was selected from a

representative sample of crystals of the same habit using an optical microscope and mounted onto a nylon loop. Low-temperature (150 K) X-ray data were obtained on a Bruker APEXII CCD-based diffractometer (Mo sealed X-ray tube, $K\alpha = 0.71073 \text{ \AA}$). All diffractometer manipulations, including data collection, integration, and scaling, were carried out using the Bruker APEXII software.¹⁵⁵ An absorption correction was applied using SADABS.¹⁵⁶ The space group was determined on the basis of systematic absences and intensity statistics, and the structure was solved by direct methods and refined by full-matrix least squares on F^2 . The structure was solved in the monoclinic $P2_1/c$ space group using XS¹⁵⁷ (incorporated in SHELXLE). All non-hydrogen atoms were refined with anisotropic thermal parameters. All hydrogen atoms were placed in idealized positions and refined using a riding model. The structure was refined (weighted least-squares refinement on F^2) and the final least-squares refinement converged. No additional symmetry was found using ADDSYM incorporated in the PLATON program.¹⁵⁸

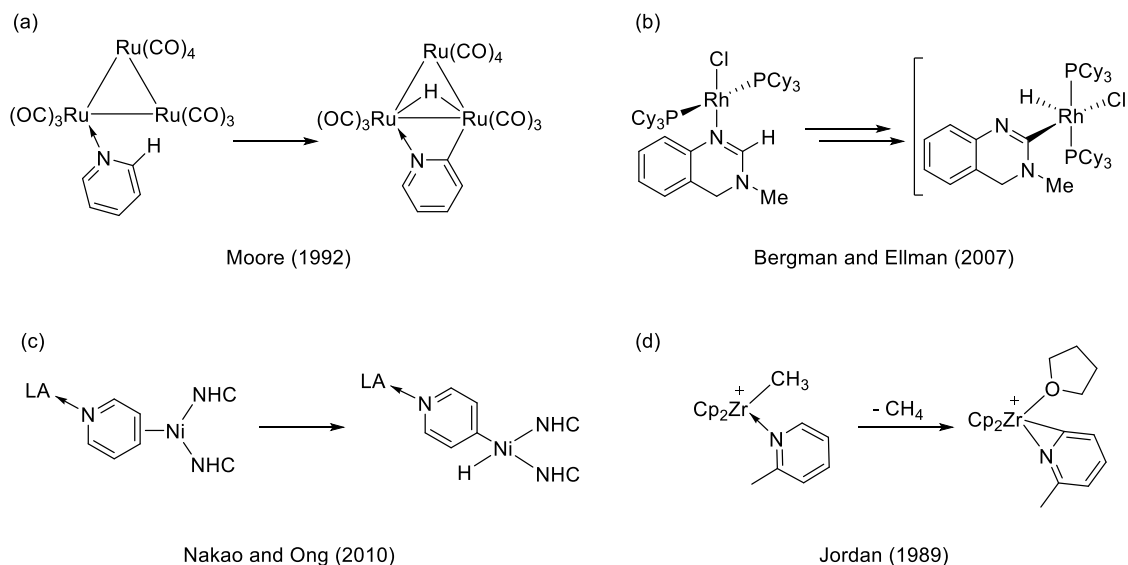
CHAPTER V

SELECTIVE *ORTHO* C–H ACTIVATION OF PYRIDINE DIRECTED BY LEWIS ACIDIC BORON OF PBP Pincer Iridium Complexes

5.1 Introduction

Selective C–H activation and functionalization of pyridine derivatives are of great interest because the pyridine moiety is an important building block for various areas including biochemistry, pharmaceuticals, and materials. The transition metal-mediated C–H activation and functionalization of pyridine and its derivatives are still proven to be challenging because the strong Lewis basic pyridine is known to poison metal catalyst. Many strategies have been reported in order to overcome this obstacle.¹⁹⁴ Triruthenium dodecacarbonyl ($\text{Ru}_3\text{CO}_{12}$) was an effective complex for C–H activation of pyridine that the nitrogen was bound to one Ru and C–H activation occurred on the other (Scheme V-1a).^{195–199} Bergman and Ellman reported the Rh-catalyzed C–H functionalization of *ortho*-substituted pyridines and emphasized the necessity of *ortho*-substituent to drive the equilibrium from an N-bound to C-bound Rh complex (Scheme V-1b).^{200,201} The C-2 and C-4 selective alkenylation or alkylation of pyridine was achieved by nickel/Lewis acid catalysis, and a structural evidence obtained by Ong revealed the electron-rich Ni(0) preferred to bind to the π -system of a AlMe_3 -activated pyridine (Scheme V-1c).^{202–204} Early transition metal²⁰⁵ and rare-earth metal^{206,207} demonstrated the coordination of pyridine group to metal was necessary and C–H abstraction (deprotonation) of pyridine occurred by metal alkyl or metal amido moiety to make an η^2 -pyridylmetal intermediate

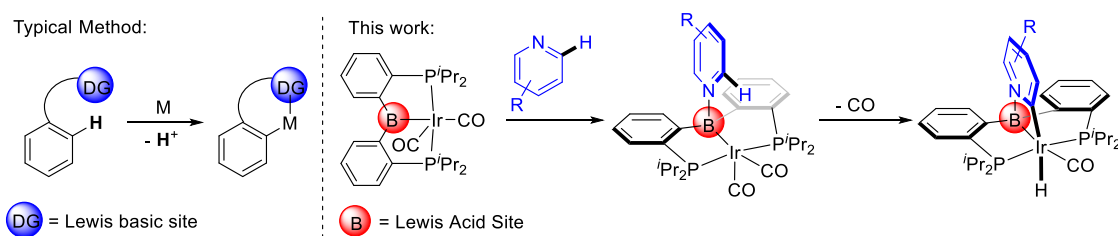
(Scheme V-1d). Other examples were also known by using metal complexes of Os,¹⁹⁸ Ir,^{208,209} and Co.^{210,211}



Scheme V-1. Strategies for C–H Activation of Pyridine

In most cases, they were still suffered from harsh conditions, low selectivity, and limited substrate scope. An alternative and unexplored strategy is to incorporate a Lewis acidic ligand on a metal complex for pyridine binding, which can avoid the deactivation of metal and serve as a directing group for *ortho*-selective C–H activation (Scheme V-2). Selective C–H activation assisted by a directing group has been studied for many decades and typically involved in the coordination of a Lewis basic functional group to a metal center to create suitable steric conformation, usually five- or six-membered metallacycle, for *ortho*-selective C–H functionalization.^{212–216} To our knowledge, there is no precedent example for the selective C–H activation directed by a Lewis acidic ligand. Recently, our

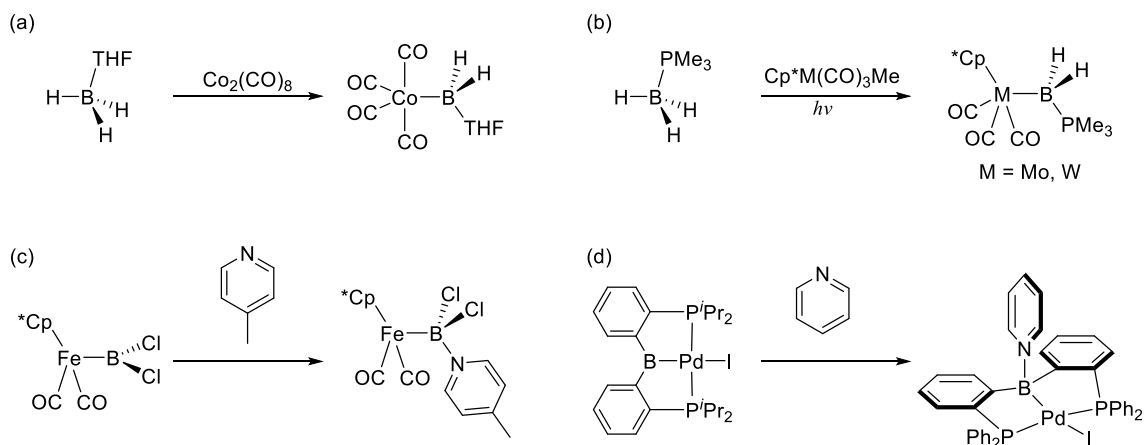
group has reported the synthesis of PBP pincer iridium and rhodium complexes and demonstrated their unique reactivity that the central boryl can be changed, reversibly, to borane or borate.¹⁰² With a proper design of PBP pincer iridium complexes, we envisaged pyridine can bind to the low-lying, accessible p orbital of boron instead of iridium center and result in the *ortho* C–H bond on the metal.



Scheme V-2. Lewis Acid Directed C–H Activation of Pyridine

Coordination of a Lewis base on a boron ligand is challenging because the vacant p orbital on the boron is easily stabilized by a long pair of electrons from adjacent atoms (typically N or O) and possible π -back donation from metal. Lewis bases can also bind to the unsaturated and electron-deficient metal center. Fehlner (Scheme V-3a)²¹⁷ and Kawano (Scheme V-3b)^{218,219} described the examples of a Lewis base such as THF or PMe_3 bind to the boryl BH_2 of a Co, Mo, or W complex, but the synthesis of these complexes required a stabilized borane precursor ($\text{BH}_3 \cdot \text{THF}$ or $\text{BH}_3 \cdot \text{PMe}_3$). Braunschweig and coworker demonstrated the first Lewis acid-base adduct formation involving an iron-dichloroboryl complex with 4-methylpyridine (Scheme V-3c).²²⁰ All of these examples conducted with a saturation of the metal center with at least two carbonyl

ligands, probably owing to exclude the binding of Lewis base on the metal and minimize the π -back donation of metal to boron.



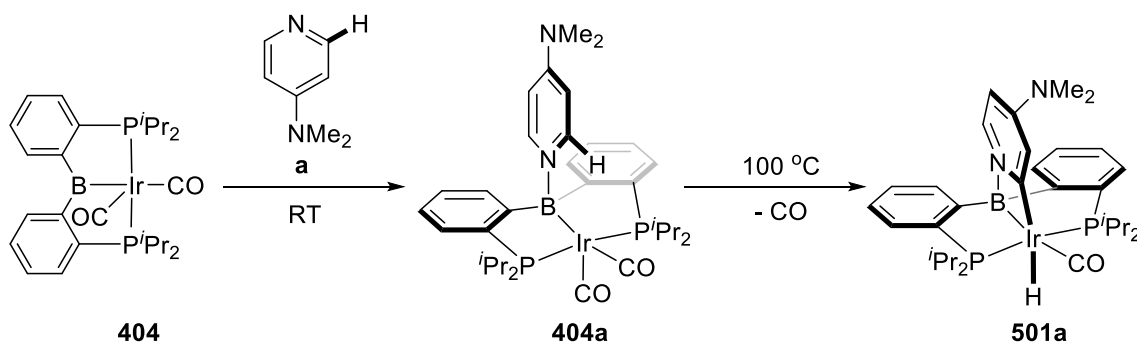
Scheme V-3. Lewis-base-stabilized Boryl Complexes

5.2 Results and Discussion

5.2.1 C–H activation of pyridine directed by (PBP)Ir(CO)₂

Previously, we have synthesized a series of PBP pincer complexes including (PBP)Ir(CO)₂ (**404**).²²¹ We surmised the coordination of Lewis base to the boron of **404** might be more favorable than to the metal because **404** has an 18-electron saturated Ir(I) center and the back donation from metal to boron could be decreased by two carbonyls. Addition of 1 equivalent of pyridine to the C₆D₆ solution of **404** showed only part of adduct formation evidenced by slight change of chemical shifts in ¹¹B{¹H} NMR (from 99.4 to 91.6 ppm) and ³¹P{¹H} NMR (from 61.0 to 60.2 ppm) spectra. We then tested the stronger Lewis base, dimethylaminopyridine (DMAP), and observed an upshift peak from

99.4 to 15.7 ppm in $^{11}\text{B}\{^1\text{H}\}$ NMR spectrum, apparently an sp^3 -hybridized boron formation from the coordination of a Lewis base to the boryl of PBP pincer complex (Scheme V-4). Two CO stretching frequencies at 1881 and 1937 cm^{-1} were observed in IR spectrum, indicating two carbonyls were attached on Ir of **404a**. The similar binding of pyridine to the boryl of diphenyl-PBP palladium has been reported by Tauchert and coworker recently (Scheme V-3d).²¹

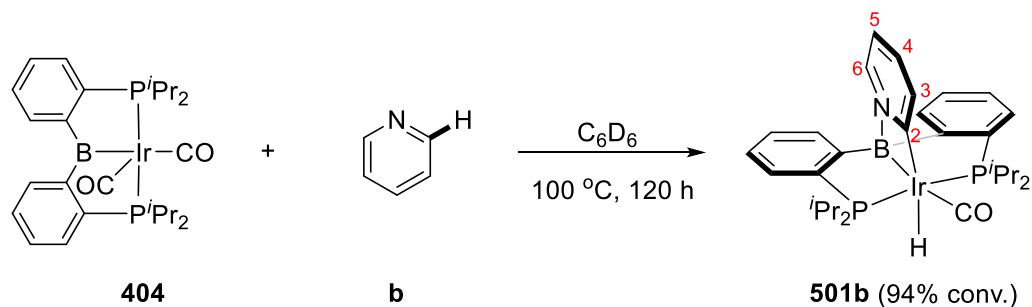


Scheme V-4. Coordination of DMAP to 404 and Selective C–H Activation of DMAP after Thermolysis

After thermolysis of **404a** at 100 °C for 18 h, 100% conversion to a new complex **501a** was achieved based on the $^{31}\text{P}\{^1\text{H}\}$ NMR spectrum (51.3 ppm) with a clear change in the color of the solution from dark red to pale yellow (Scheme V-4). One hydride resonance at -14.02 ppm (t, $J_{\text{H,P}} = 19.3$ Hz) and three aromatic proton resonances from pyridyl group at 7.06 (d, $J_{\text{H,H}} = 7.0$ Hz), 6.99 (d, $J_{\text{H,H}} = 3.0$ Hz), and 5.34 (dd, $J_{\text{H,H}} = 7.0$, $J_{\text{H,H}} = 3.0$ Hz) evidenced for the C–H bond activation of DMAP on the Ir center. **501a** displayed C_s symmetry in solution on the basis of two methine resonances and four methyl

resonances from $i\text{Pr}_2\text{P}$ groups in the ^1H NMR spectrum. The $^{11}\text{B}\{^1\text{H}\}$ NMR resonance of **501a** was further upshifted to 1.0 ppm and assigned as a four coordinate boron, suggesting the nitrogen of DMAP was still bound to the boron of PBP. Only one CO resonance at 179.9 ppm in $^{13}\text{C}\{^1\text{H}\}$ NMR spectrum and one CO stretching frequency at 1924 cm^{-1} in IR spectrum were observed, indicating the dissociation of one CO from 18-electron iridium of **404a** was involved in reaction.

C–H activation of pyridine was also achieved by the reaction of pyridine with **404** at $100\text{ }^\circ\text{C}$ nonetheless only small portion of pyridine adduct formation was observed at ambient temperature (Scheme V-5). Exclusive *ortho* C–H activation product **501b** was distinguished according to the ^1H NMR and 2D ^1H – ^1H COSY NMR spectroscopic data (Figure V-1). Four aromatic proton resonances from pyridyl group were observed at 7.59 (d, $J_{\text{H,H}} = 8.0\text{ Hz}$, C6–H), 7.22 (d, $J_{\text{H,H}} = 6.0\text{ Hz}$, C3–H), 6.48 (td, $J_{\text{H,H}} = 8.0$, $J_{\text{H,H}} = 1.5\text{ Hz}$, C5–H), and 5.91 (t, $J_{\text{H,H}} = 6.0\text{ Hz}$, C4–H) in ^1H NMR spectrum, with 3J or 4J correlations to each other in 2D ^1H – ^1H COSY spectrum.



Scheme V-5. Selective C–H Activation of Pyridine

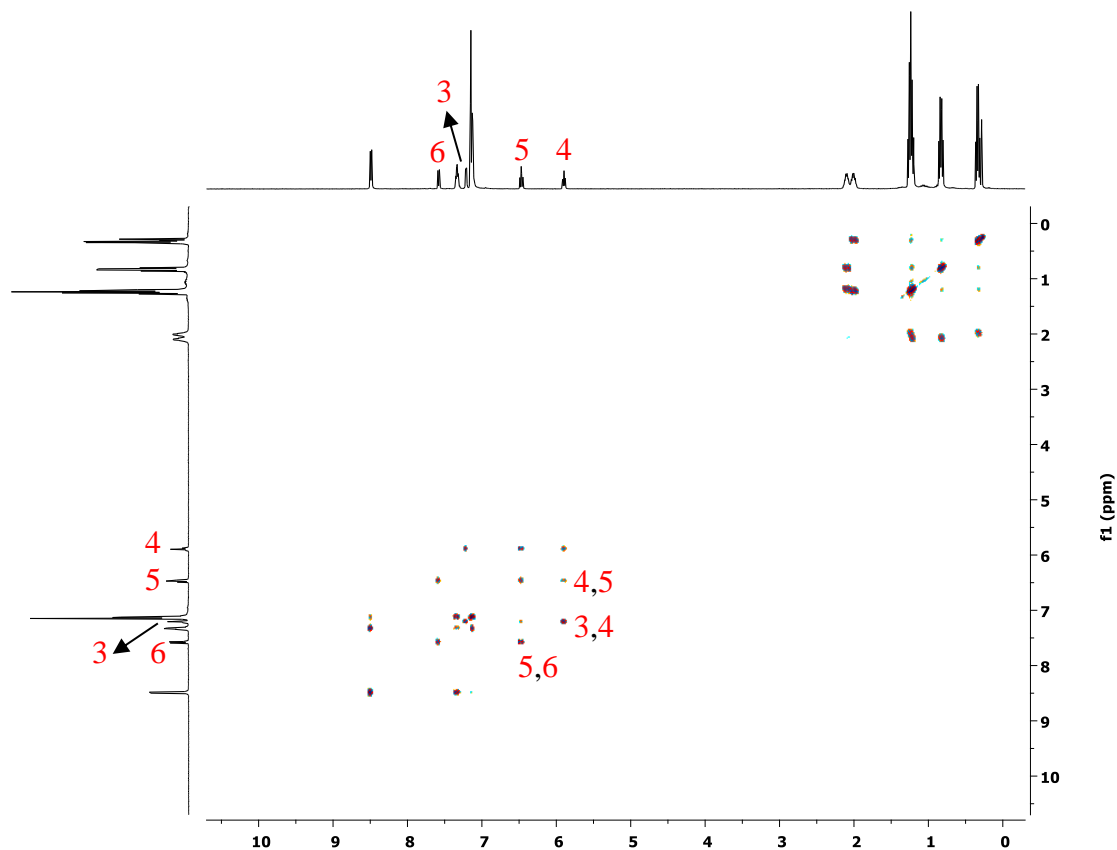


Figure V-1. 2D ^1H - ^1H COSY NMR spectrum of **501b** in C_6D_6 at room temperature, showing the correlation between H3-H4, H4-H5, and H5-H6 through bonds.

An X-ray diffraction study of **501b** further confirmed the proposed four-membered metallacycle with CO trans to the boron of PBP and pyridyl group trans to the hydride (Figure V-2). The N1-B1 distance (1.613(3) Å) is in the range of pyridine-triphenylborane adduct, but the Ir1-B1 distance (2.285(2) Å) is clearly longer than the Ir(III)-B_{boryl} distances (ca. 1.99–2.00 Å)¹⁰² and Ir(I)-B_{boryl} distance (2.14 Å)²²¹ in our previously reported examples. The elongation of the Ir-B distance in **501b** suggested a weak bond

strength between Ir and B, probably owing to the ring strain from four-membered metallacycle and stabilization of boron by pyridine coordination.

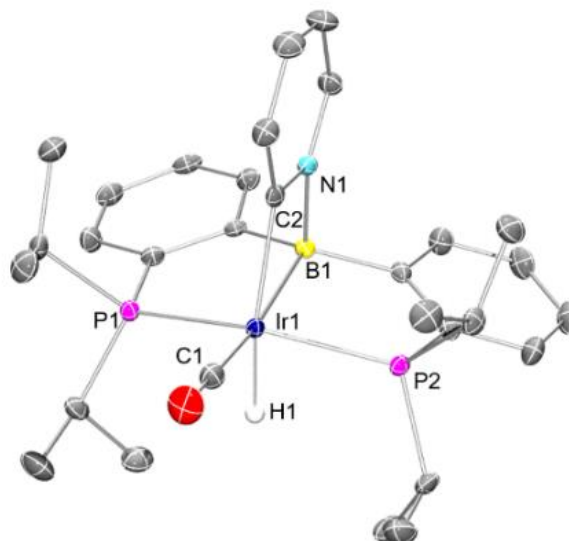
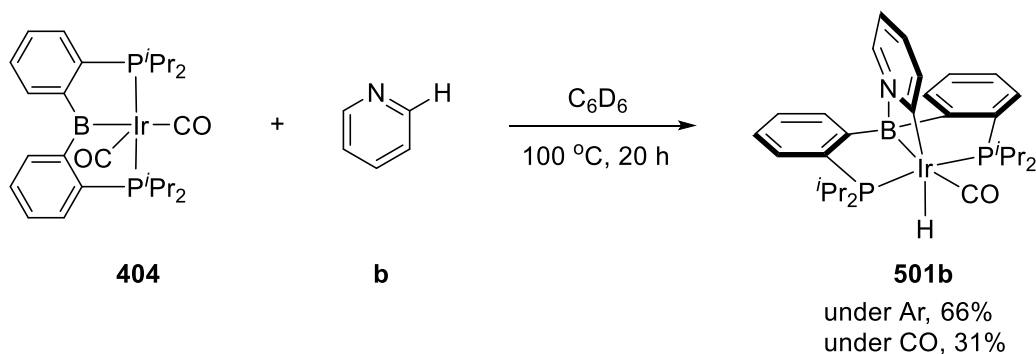


Figure V-2. POV-Ray rendition of the ORTEP drawing (50% thermal ellipsoids) of **501b** showing selected atom labeling. Hydrogen atoms are omitted for clarity with the exception of the hydrogen bound to iridium. Selected bond distances (Å) and angles (°): Ir1–B1, 2.285(2); Ir1–C1, 1.920(2); Ir1–C2, 2.078(2); Ir1–P1, 2.2797(6); Ir1–P2, 2.2849(6); C1–O1, 1.145(3); N1–C2, 1.360(3); N1–B1, 1.613(3); Ir1–H1, 1.50(3); B1–Ir1–C1, 168.22(8); B1–Ir1–C2, 64.71(8); C1–Ir1–C2, 103.51(8); C2–Ir1–P1, 96.56(5); C2–Ir1–P2, 95.06(5); P1–Ir1–P2, 152.371(18); N1–B1–Ir1, 87.72(11); N1–C2–Ir1, 103.93(13).

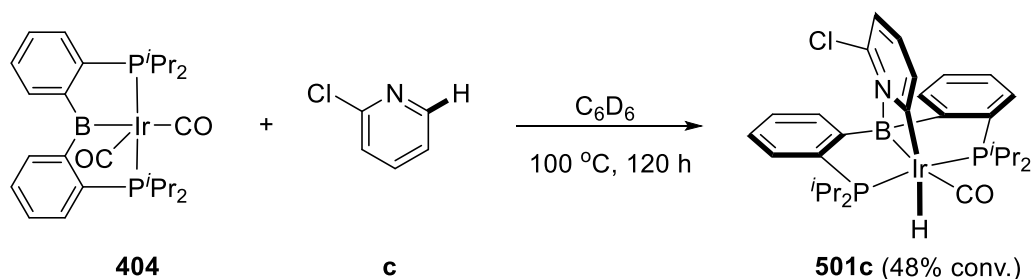
Although the selectivity of *ortho* C–H activation of pyridine was outstanding, the reaction rates were quite slow, presumably due to slow dissociation and gradual accumulation of CO in a reaction vessel. Moreover, thermolysis of **404** and pyridine at

100 °C for 20 h gave 66% conversion to the C–H activation product **501b** under Ar, whereas only 31% conversion was observed under 1 atm of CO (Scheme V-6). The notable decrease of product formation by introduction of CO atmosphere indicated CO dissociation was required before C–H activation occurred.



Scheme V-6. Decrease of Reaction Rate by Treatment with CO

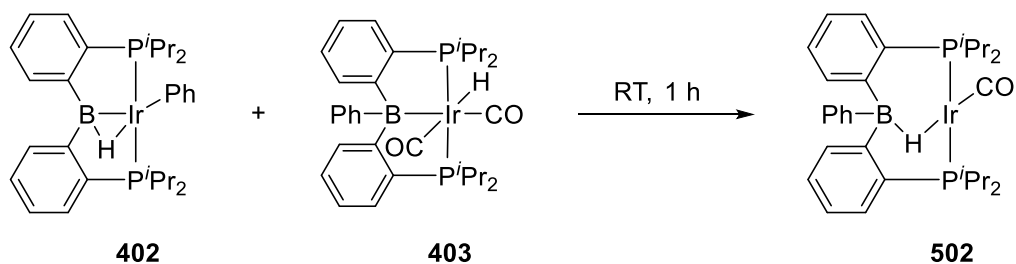
The reaction was even slower while using a substrate with weakly binding ability such as 2-chloropyridine and only 48% conversion to **501c** was observed after heating at 100 °C for 120 h (Scheme V-7). This difficulty also seriously discouraged a large-scale synthesis of complexes **501**. Therefore, we endeavored to further design and modify our PBP complex with only mono-carbonyl on Ir center. After several unsuccessful attempts of (PBP)Ir(CO) synthesis, we envisaged **502** was an alternative candidate because losing benzene from **502** might be feasible and facile during heating, leading to a reactive 16-electron mono-carbonyl intermediate.



Scheme V-7. Selective C–H Activation of 2-Chloropyridine

5.2.2 C–H activation of pyridine directed by $(\text{PB}^{\text{Ph}}\text{P})\text{Ir}(\text{H})(\text{CO})$

Previously, we have developed the synthesis of $(\text{PBP})\text{Ir}(\text{H})_2(\text{CO})$ by comproportionation of **404** with $(\text{PBP})\text{Ir}(\text{H})_4$.²²¹ Inspired by this result, complex **502** was successfully synthesized by comproportionation of $(\text{PBP})\text{Ir}(\text{H})(\text{Ph})$ (**402**) and $(\text{PB}^{\text{Ph}}\text{P})\text{Ir}(\text{H})(\text{CO})_2$ (**403**) through one CO transfer from **403** to **402** (Scheme V-8). The complex **502** displayed one phosphine resonance at 60.3 ppm in $^{31}\text{P}\{^1\text{H}\}$ NMR spectrum and one borate resonance at 1.4 ppm in $^{11}\text{B}\{^1\text{H}\}$ NMR spectrum. The hydride was bridged between Ir and B evidenced by a broad hydride peak at -4.09 ppm in ^1H NMR spectrum. One triplet from the CO at 185.5 ppm (t, $J_{\text{C,P}} = 8.2$ Hz) and one broad peak from the *ipso* carbon of Ph at 156.8 ppm were observed in ^{13}C NMR spectrum, suggesting the CO bound to the metal and the Ph connected to the boron, but it was not clear if there was an interaction between Ir and B by NMR data analysis.



Scheme V-8. Synthesis of Complex 502 by Comproportionation of 402 with 403

An X-ray diffraction study of **502** revealed the complex adopted square planar geometry with two phosphines trans to each other (P1–Ir1–P2, 161.10(2)°) and hydride trans to CO (C1–Ir1–H1, 164.4(10)°) (Figure V-3). The Ir center is monovalent with a hydride bridged between Ir and B, resulting in the highly pyramidalized boron center ($\Sigma B\alpha = 338^\circ$). There is no obvious interaction between Ir1–B1 because the distance (2.621(3) Å) is out of the range of Ir–B bond. The analogous structure of rhodium complex was previously reported by Nakazawa.¹⁰⁹

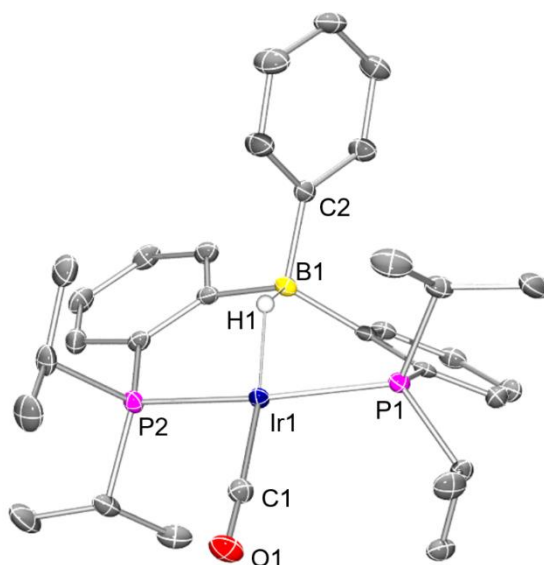
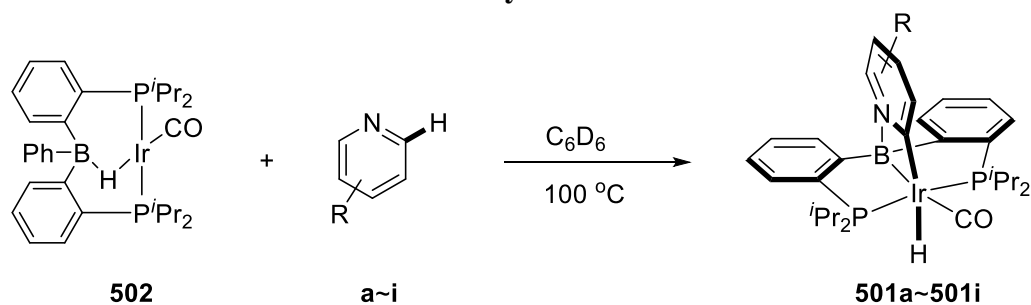


Figure V-3. POV-Ray rendition of the ORTEP drawing (50% thermal ellipsoids) of **502** showing selected atom labeling. Hydrogen atoms are omitted for clarity with the exception of the hydrogen bound to iridium. Selected bond distances (Å) and angles (°): Ir1–B1, 2.621(3); Ir1–C1, 1.824(3); Ir1–H1, 1.64(3); Ir1–P1, 2.2929(6); Ir1–P2, 2.2801(6); C1–O1, 1.151(3); B1–C2, 1.630(4); B1–H1, 1.33(3); C1–Ir1–H1, 164.4(10); B1–Ir1–H1, 24.8(10); Ir1–B1–H1, 31.2(13); P1–Ir1–P2, 161.10(2); C2–B1–C9, 111.4(2); C2–B1–C14, 110.3(2); C9–B1–C14, 116.0(2).

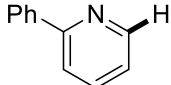
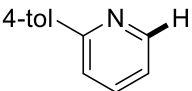
By treatment of **502** with DMAP at room temperature in C_6D_6 , the Lewis acid-base adduct was not observed, but the C–H activation product **501a** was observed after thermolysis at 100 °C for 2 h (Table V-1, entry 1). The complex **502** was proven to be a more effective complex than **404** for activation of *ortho* C–H bond of pyridine substrates since most of the reactions were completed within 2 h, compared to the reaction time (120 h or longer) required by using complex **404** (Scheme V-5 & Scheme V-7). This type of

reaction was highly selective for the formation of four-membered metalacycle products **501a~501i** (Table V-1).

Table V-1. Selective C–H Activation of Pyridines^a



entry	pyridines	product	time (h)	Yield (%) ^b
1		501a	2	95 (81) ^c
2		501b	2	99 (80) ^c
3		501c	2	79 (81) ^c
4		501d	2	93 (81) ^c
5		501e+501e'	2	98 [90:10] ^d
6		501f+501f'	2	99 [56:44] ^d
7		501g+501g'	2	99 [97:3] ^e

8		501h	6	83
9		501i	6	92

a. Reaction conditions: Ir complex **502** (0.02 mmol) and pyridine (0.02 mmol) in C₆D₆ at 100 °C. b. Yields were determined by ¹H NMR spectroscopy with hexamethyldisiloxane (0.01 mmol) as an internal standard. c. Isolated yield (0.20 mmol scale). d. The ratio of C6:C2 selectivity. e. The ratio of C2:C8 selectivity.

The activation of 2-chloropyridine occurred on *ortho* C–H bond with 79% yield of **501c** (entry 3), left the C–Cl bond intact. The reaction of 2-methylpyridine with **502** afforded **501d** with 93% yield via the activation of the sp²-hybridized *ortho* C–H bond on pyridine, and excluded the formation of a five-membered metallacycle via another possible activation of the sp³-hybridized methyl C–H bond (entry 4). This result somehow differed from the similar reaction that bond activation occurred on both methyl C–H bond and *o*-aryl C–H bond of the PN^(tol)P iridium complex.²²² For 3-trifluoromethylpyridine, both C6 and C2 C–H bonds were activated to form **501e** and **501e'** in a total 98% yield with a ratio of 90:10 (entry 5). We assumed the C6 C–H activation was a kinetic process owing to the less steric imposing position of C6, whereas C2 C–H activation was a thermodynamic process due to the more acidic C–H bond on C2. This assumption was supported by the increase of the thermodynamic product **501e'** (**501e**:**501e'** = 81:19) after heating the mixture of **501e** and **501e'** at 100 °C for another 18 h. Similarly, both C6 and C2 C–H bond activations of 3-ethylpyridine occurred in a total 99% yield with a ratio of 56:44 (entry 6). The ratio is approximately 1:1 probably because the electronic and steric properties were similar for both *ortho* C–H bonds of 3-ethylpyridine, but apparently

activation of C6 C–H bond was the thermodynamic and kinetic process. The four-membered metallacycle **501g** was formed by the reaction of quinoline with **5** via activation of C2 C–H bond with the formation of a minor five-membered metallacycle **501g'** via activation of C8 C–H bond in a total yield of 99% with a ratio of 97:3 (entry 7). An X-ray diffraction study of complex **501g** confirmed the major product is four-membered metallacycle structure (Figure V-4). 2-Phenylpyridine was used for decades as a model compound for the study of metal-mediated C–H bond activation and functionalization because pyridine served as an excellent directing group for activation of the *ortho* C–H bond on the phenyl, leading to a stable five-membered metallacycle.²¹⁶ In comparison, C6 C–H activation of 2-phenylpyridine was very rare. The reaction of 2-phenylpyridine and 2-tolylpyridine with **502** successfully afforded **501h** and **501i** with 83% and 92% yield, respectively (entry 8 and 9), albeit the steric hindrance of 2-phenylpyridine and 2-tolylpyridine might slightly influence the reactivity and the reaction required 6 h to achieve 100% conversion.

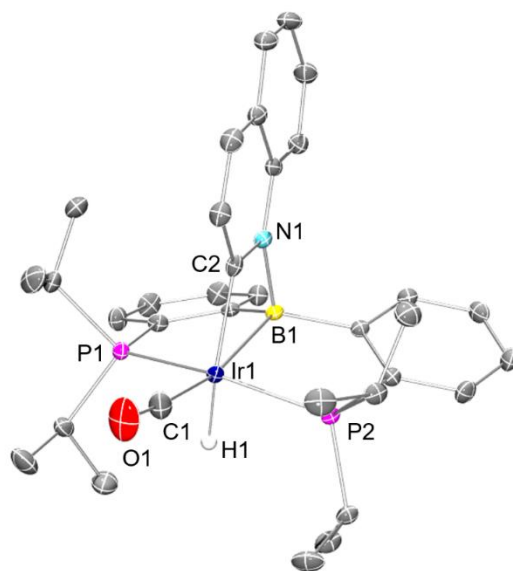


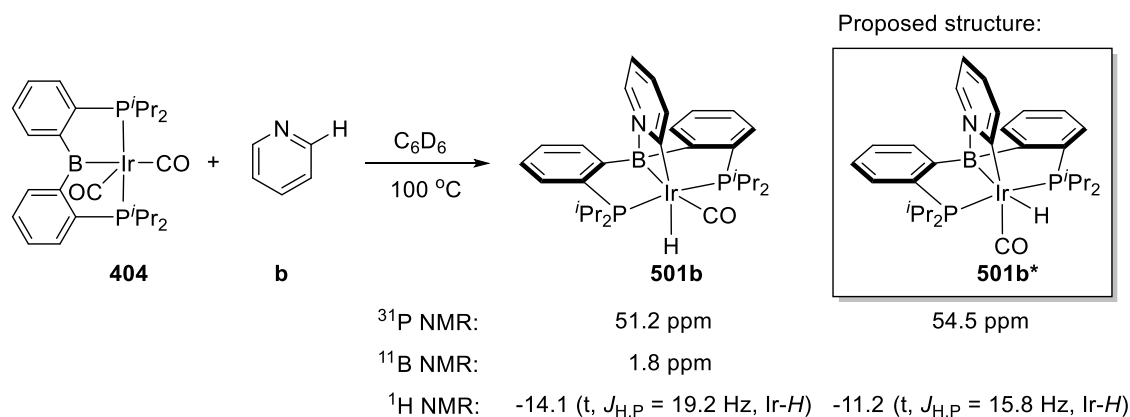
Figure V-4. POV-Ray rendition of the ORTEP drawing (50% thermal ellipsoids) of **501g** showing selected atom labeling. Hydrogen atoms are omitted for clarity with the exception of the hydrogen bound to iridium. Selected bond distances (Å) and angles (°): Ir1–B1, 2.280(2); Ir1–C1, 1.921(2); Ir1–C2, 2.061(2); Ir1–P1, 2.2969(5); Ir1–P2, 2.2861(6); C1–O1, 1.148(3); N1–C2, 1.344(2); N1–B1, 1.635(3); Ir1–H1, 1.46(3); B1–Ir1–C1, 166.13(9); B1–Ir1–C2, 64.17(7); C1–Ir1–C2, 102.09(9); C2–Ir1–P1, 93.96(5); C2–Ir1–P2, 97.02(5); P1–Ir1–P2, 154.193(17); N1–B1–Ir1, 87.47(10); N1–C2–Ir1, 105.98(12).

5.2.3 Mechanistic study

In complexes **501b**, the hydride was trans to the pyridyl group, suggesting rearrangement of cis hydridopyridyl complex **501b*** to **501b** may occur after C–H activation of pyridine. We were able to observe the formation of a new complex *in situ* by the reaction of **501b** with pyridine in C₆D₆ under CO atmosphere at 100 °C for 1 h (Table V-2, entry 4). One peak at 54.5 ppm in ³¹P{¹H} NMR spectrum and one hydride peak at

-11.2 ppm (t, $J_{H,P} = 15.8$ Hz) in ^1H NMR spectra suggested it is likely the complex **501b*** generated from the direct C2–H activation of pyridine by **404** before rearrangement into **501b**. The rate of rearrangement slightly decreased under CO compared to the similar reaction under argon (Table V-2, entry 4 vs. entry 1), probably due to the slower dissociation rate of CO from **501b*** under CO atmosphere. However, the isolation of **501b*** was unachievable because most of complex **501b*** still converted into **501b** after heating at 100 °C under CO for 4 h (Table V-2, entry 5).

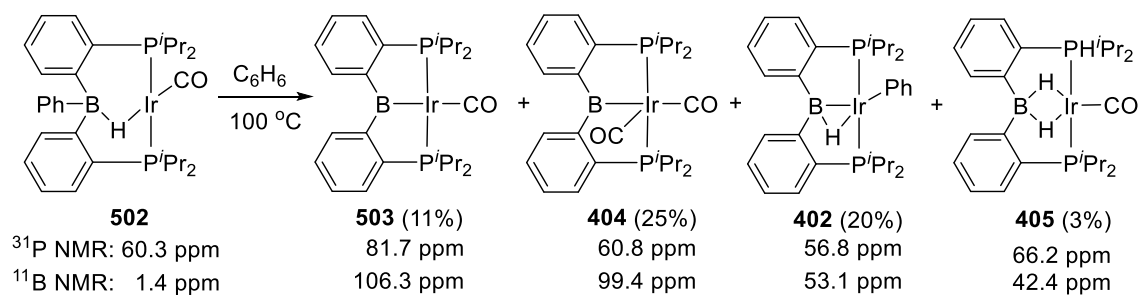
Table V-2. Reaction of Complex 404 with Pyridine under Ar or CO^a



Entry	Atmosphere (1 atm)	time (h)	404 : 501b: 501b* ^b
1	Ar	1	91 : 7 : 2
2	Ar	4	80 : 20 : 0
3	Ar	20	34 : 66 : 0
4	CO	1	87 : 0 : 13
5	CO	4	88 : 11 : 1
6	CO	20	69 : 31 : 0

a. The reaction was carried out using (PBP)Ir(CO)₂ (**404**; 0.02 mmol) and pyridine (0.02 mmol) in C₆D₆ at 100 °C a J. Young tube. b. Conversions were determined by $^{31}\text{P}\{^1\text{H}\}$ NMR spectroscopy.

For the C–H activation of pyridine mediated by **502**, the elimination of benzene from **502** might occur during heating to afford reactive mono-carbonyl complex (PBP)Ir(CO). Thermolysis of **502** in C₆H₆ without addition of pyridine at 100 °C for 2 h resulted in the remnant of 34% of **502** with the formation of 11% of **503**, 25% of **404**, 20% of **402**, 3% of (PBP)Ir(H)₂(CO) (**405**), and two other unidentifiable products (4% for each at 51.9 ppm and 34.7 ppm in ³¹P{¹H} NMR spectrum) (Scheme V-9 & Figure V-5). On the basis of the new downfield resonance at 106.3 ppm in ¹¹B{¹H} NMR spectrum (Figure V-6) and the balance of CO in the reaction (# of CO = 11% from **503** + 50% from **404** + 34% from **502** + 3% from **405** = 98% CO), we proposed the new complex **503** was mono-carbonyl complex (PBP)Ir(CO).



Scheme V-9. Thermolysis of Complex 502 at 100 °C in Benzene

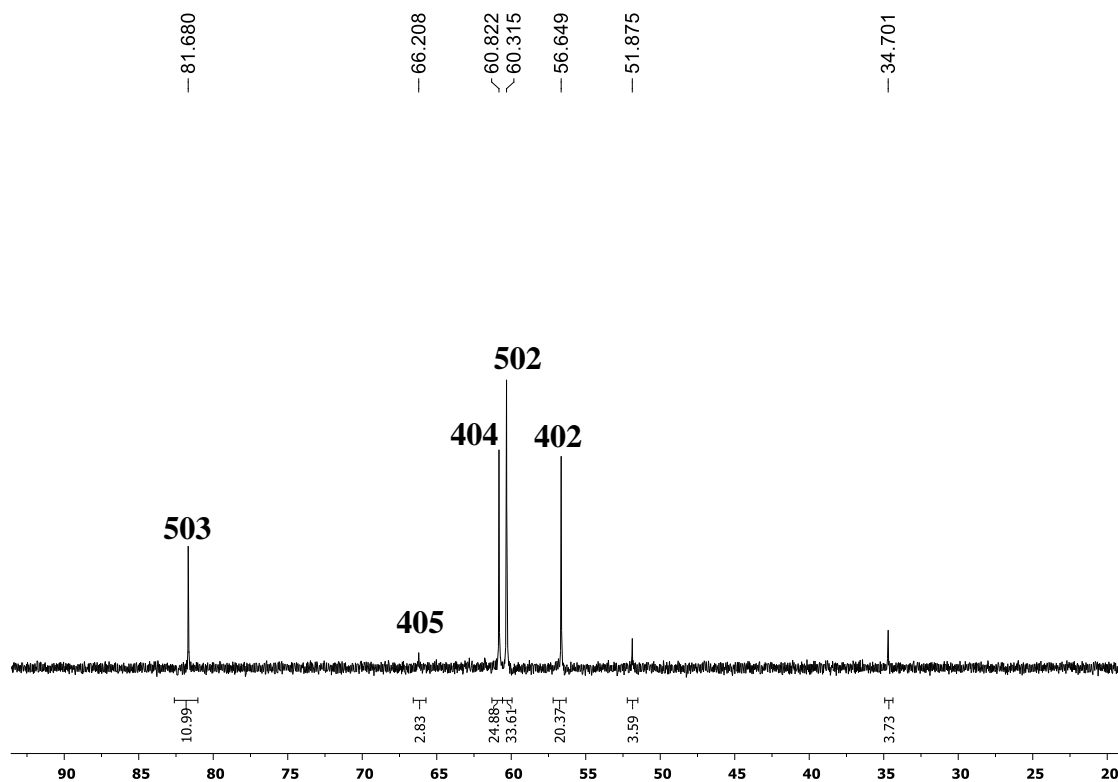


Figure V-5. $^{31}\text{P}\{^1\text{H}\}$ NMR spectrum of thermolysis of complex **502** in benzene for 2 h.

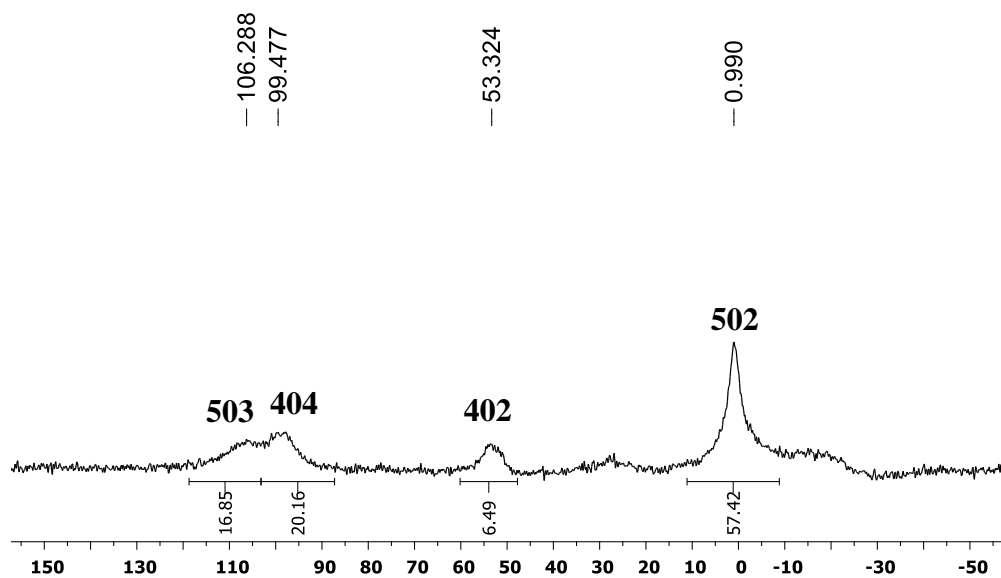
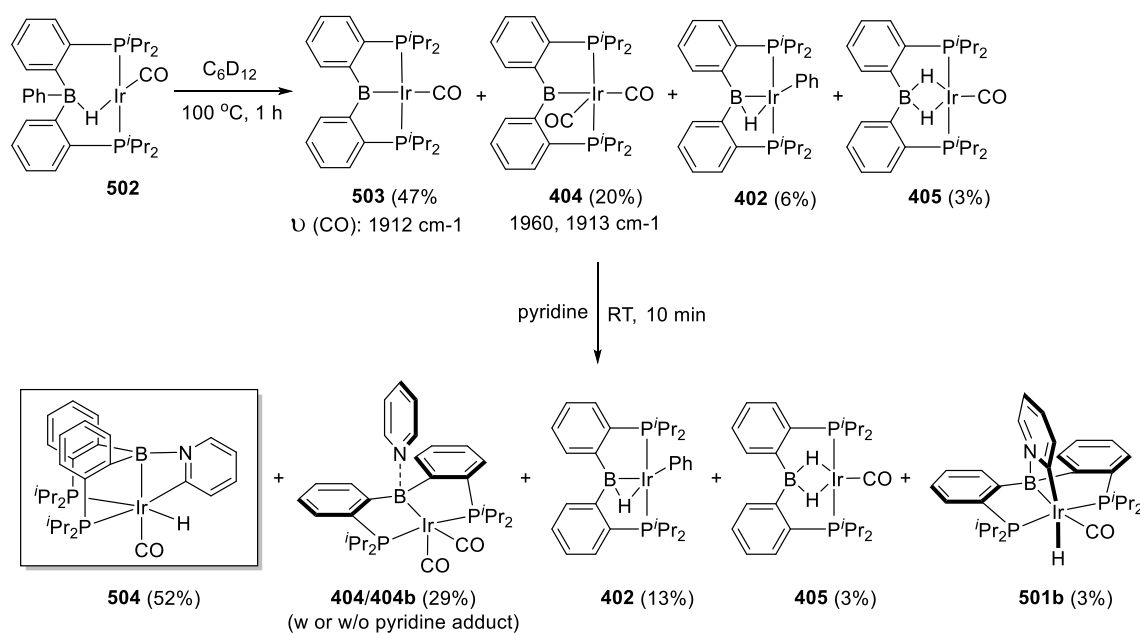


Figure V-6. $^{11}\text{B}\{^1\text{H}\}$ NMR spectrum of thermolysis of complex **502** in benzene for 2 h.

Thermolysis of **502** in C_6D_{12} without addition of pyridine at 100 °C for 1 h gave rise to the similar combination of products with 47% of **503** as a major compound (Scheme V-10). Subsequently addition of pyridine to the mixture resulted in the formation of pyridine C–H activation product. To our surprise, this product was not the same as **501b*** evidenced by the appearance of two peaks at 37.3 and 31.2 ppm in approximately 1:1 ratio in $^{31}P\{^1H\}$ NMR spectrum, one peak at -2.4 ppm in $^{11}B\{^1H\}$ NMR spectrum, and one doublet of doublets ($J_{H,P} = 109, 28$ Hz) at -10.70 ppm in 1H NMR spectrum. The hydride likely coupled to one trans phosphine and one cis phosphine and the boron was four coordinate with borate characteristics. On the basis of the observation in NMR spectroscopic data, we proposed the new compound was likely to be **504** (Scheme V-10).



Scheme V-10. Thermolysis of Complex 502 at 100 °C in C_6D_{12} and Subsequently Addition of Pyridine

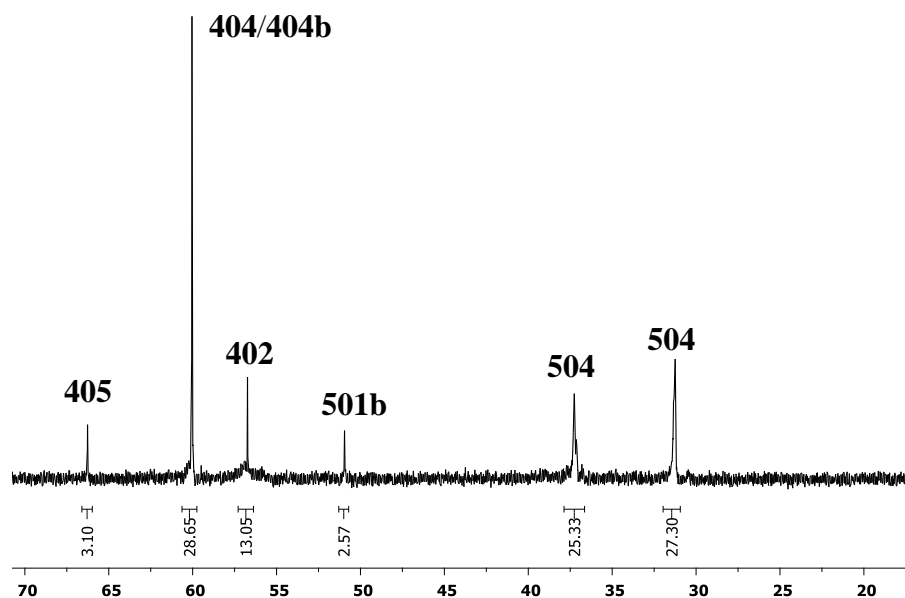


Figure V-7. $^{31}\text{P}\{^1\text{H}\}$ NMR spectrum after thermolysis of complex **502** for 1 h at 100 °C in C_6D_{12} followed by addition of pyridine.

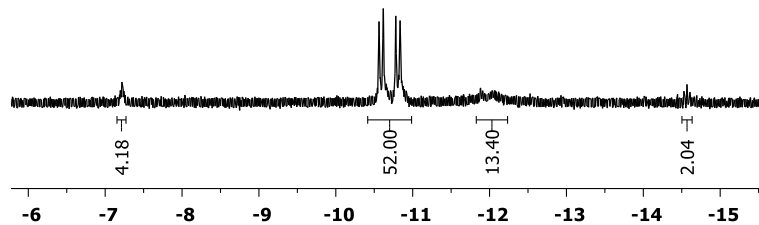
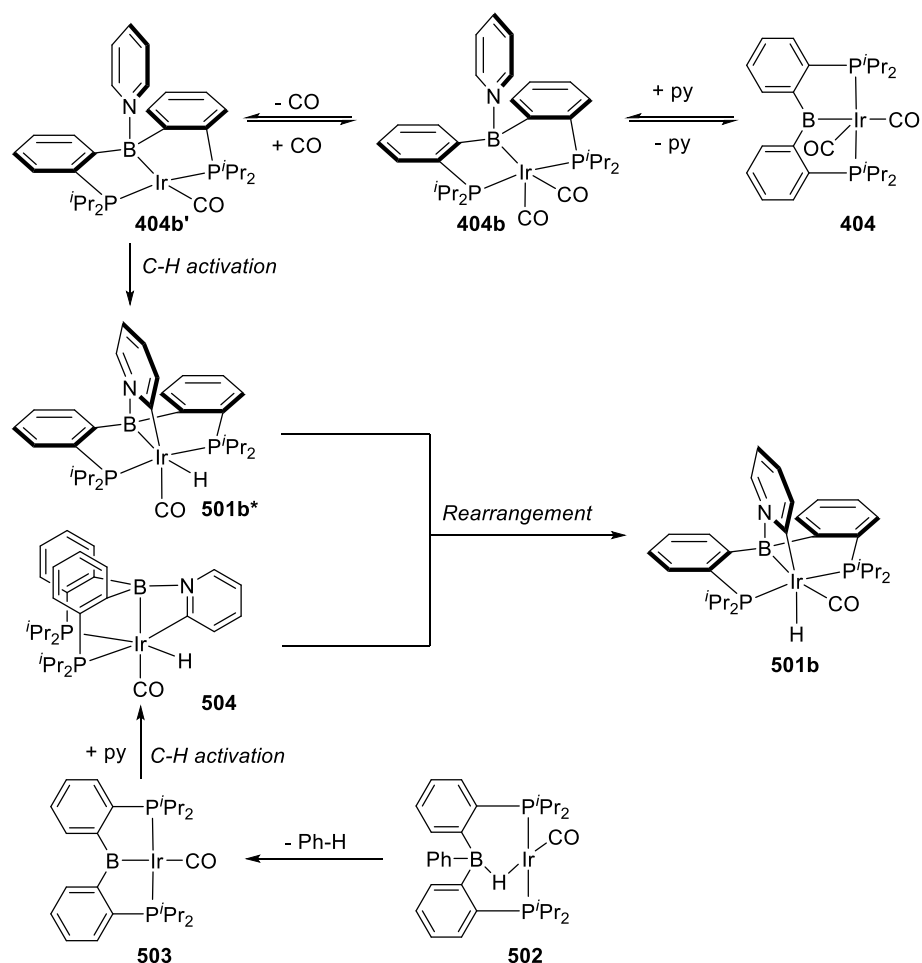


Figure V-8. Hydride region of ^1H NMR spectrum after thermolysis of complex **502** for 1 h at 100 °C in C_6D_{12} followed by addition of pyridine.

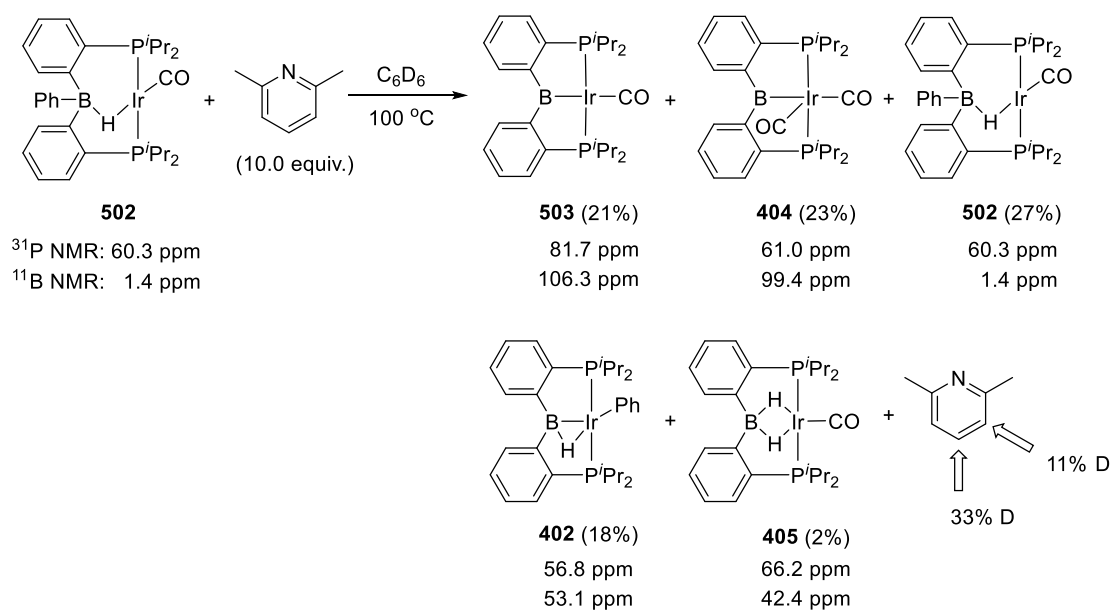
According to the reactivity observed above, we proposed the C–H activation of pyridine mediated by **404** and **502** might undergo two different pathways (Scheme V-11). The pyridine association and dissociation products **404b/404** was in equilibrium by treatment of **404** with pyridine at ambient temperature, but the dissociation of CO and C–H activation of pyridine required heating at 100 °C. After dissociation of CO from **404b**, **404b'** might undergo Lewis-acid-directed C–H activation of pyridine to form **501b***. Since the C–H activation on a square planar metal complex was generally unsuccessful, we surmised the distortion of **404b'** or the dissociation of second CO was necessary. Finally, the thermodynamically favorable complex **501b** was obtained after the rearrangement of **501b***.



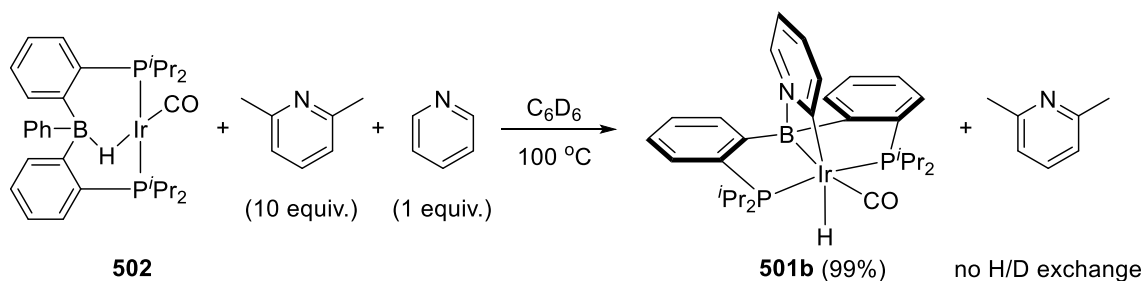
Scheme V-11. Proposed Mechanism of Pyridine C–H Activation by 404 or 502

In contrast, the coordination of pyridine on **502** was not observed owing to the borate character of central boron of PBP. However, thermolysis of **502** at 100 °C resulted in the elimination of benzene from **502** to afford **503**, which directly reacted with pyridine to give **504**. Again, distortion of **503** or dissociation of second CO might require for C–H activation. After rearrangement from **504**, the same final product **501b** was obtained (Scheme V-11).

We surmised whether the C–H activation of pyridine was achievable without coordination of pyridine on boron, and therefore we tested the reaction with 2,6-lutidine. Thermolysis of **502** with 2,6-lutidine in C₆D₆ at 100 °C for 2 h resulted in the remnant of **502** (27%) with the formation of many products including **404** (23%), **402** (18%), **405** (2%) and **503** (21%) on the basis of ³¹P{¹H} NMR spectroscopic data (Scheme V-12). The observable H/D exchange on the *meta* (11%) and *para* (33%) positions of 2,6-lutidine in ¹H NMR spectrum suggested the C–H activation occurred, but the complexes were unstable without the nitrogen binding to the boron of PBP complex. The competition reaction by thermolysis of **502** with 10 equivalent of 2,6-lutidine and 1 equivalent of pyridine in C₆D₆ at 100 °C gave rise to the formation of **501b** without any H/D exchange on 2,6-lutidine, indicating the C–H activation of pyridine was faster than H/D exchange of 2,6-lutidine (Scheme V-13).



Scheme V-12. Thermolysis of Complex 502 with 2,6-Lutidine at 100 °C in C₆D₆

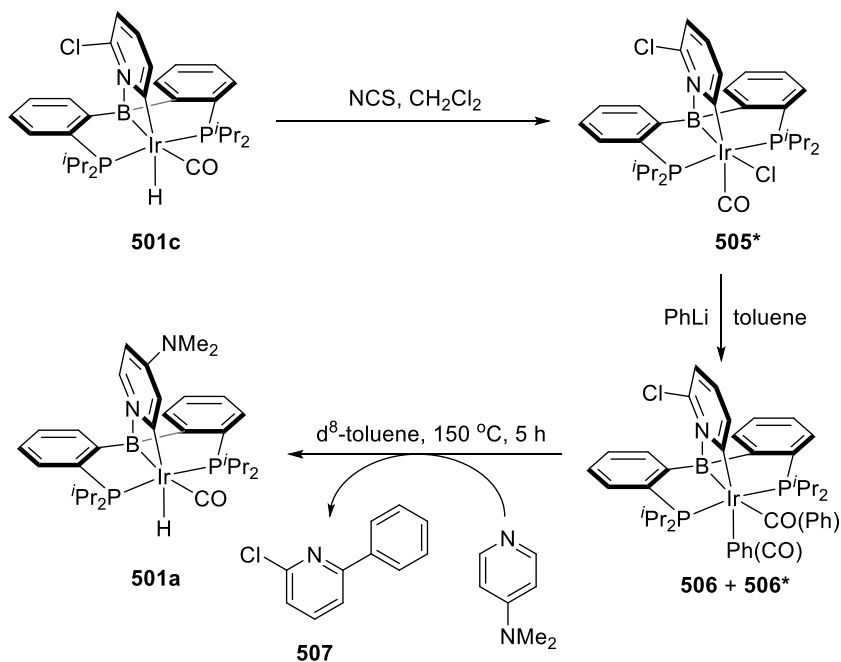


Scheme V-13. Competition Reaction between Pyridine and 2,6-Lutidine

5.2.3 Arylation of pyridine

C–H arylation of pyridine on the *ortho*-position has been reported previously by using Rh,²⁰¹ Au,²²³ Ag,²²⁴ Fe,²²⁵ Ni,²²⁶ but the reactions were usually suffered from the harsh conditions with poor functional group tolerance and selectivity. Herein, we report the C–H phenylation of 2-chloropyridine by C–C reductive elimination (Scheme V-14). The conversion of complex **501c** into **505*** was achieved by treatment of **501c** with 1.1 equiv. of *N*-chlorosuccinimide in CH₂Cl₂ at room temperature. The disappearance of hydride peak in ¹H NMR spectrum and appearance of new phosphorus peak at 21.5 ppm in ³¹P{¹H} NMR spectrum indicated the hydride was replaced by chloride, likely via the radical pathway. After introducing 1.2 equiv. of PhLi into **505***, two complexes **506** and **506*** were observed *in situ* in ¹H and ³¹P{¹H} NMR spectra with approximately 1:9 ratio. Thermolysis of the mixture of **506** and **506*** in the presence of DMAP in d₈-toluene at 150 °C gave rise to product **507** and complex **501a** in 97% and 96% NMR yields, respectively. This reaction has demonstrated the C–H arylation of pyridine was feasible stoichiometrically in our PBP Ir system with excellent yield and selectivity. Moreover, it

has displayed the vulnerable C–Cl bond was intact during the heating and might be used in the next step for further functionalization.



Scheme V-14. C–H Arylation of Pyridine from Complex 501c

5.3 Conclusions

In conclusion, we have demonstrated the first example of Lewis-acid-directed C–H activation of pyridines by the PBP-type iridium complex **404** or **502**. The selectivity was excessively toward the *ortho* position of pyridine displayed by various substrates. The mechanistic study showed two possible pathways for C–H activation of pyridine mediated by **404** or **502**. The C–H functionalization of complex **501c** was accomplished by the stoichiometric reactions with quantitative yield. The study on catalytic reactions by PBP metal complexes is undergoing.

5.4 Experimental Section

5.4.1 General considerations

Unless specified otherwise, all manipulations were performed under an Ar atmosphere using standard Schlenk line or glovebox techniques. Toluene and pentane were dried and deoxygenated (by purging) using a solvent purification system (Innovative Technology Pure Solv MD-5 Solvent Purification System) and stored over molecular sieves in an Ar-filled glove box. C₆D₆ was dried over NaK/Ph₂CO/18-crown-6, distilled or vacuum transferred and stored over molecular sieves in an Ar-filled glovebox. Acetonitrile was dried over CaH₂, distilled or vacuum transferred and stored over molecular sieves in an Ar-filled glove box. Pyridine, its derivatives and hexamethyldisiloxane were degassed by three freeze-pump-thaw cycles and stored over molecular sieves in an Ar-filled glovebox. (PBP)Ir(CO)₂ (**404**), (PBP)Ir(H)(Ph) (**402**), and (PB^{Ph}P)Ir(H)(CO)₂ (**403**) were prepared via literature procedures.²²¹ All other chemicals were used as received from commercial vendors.

5.4.2 Physical methods

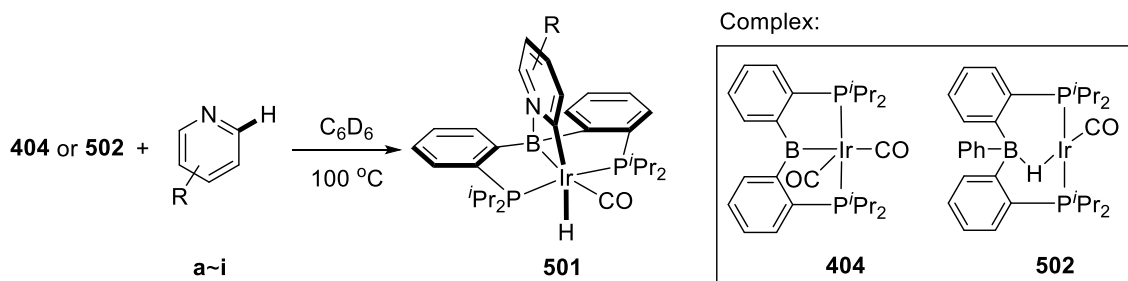
NMR spectra were recorded on a Varian Inova 400, a Bruker Avance III 400 (¹H NMR, 399.535 MHz; ¹¹B NMR, 128.185 MHz; ³¹P NMR, 161.734 MHz), or a Varian Inova 500 (¹H NMR, 499.703 MHz; ¹³C NMR, 125.697 MHz; ³¹P NMR, 202.265 MHz) spectrometer. Chemical shifts are reported in δ (ppm). For ¹H and ¹³C NMR spectra, the residual solvent peak was used as an internal reference (¹H NMR: δ 7.16 for C₆D₆; ¹³C NMR: δ 128.06 for C₆D₆). ¹¹B NMR spectra were referenced externally with BF₃ etherate

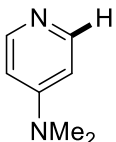
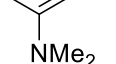
at δ 0. ^{31}P NMR spectra were referenced externally with 85% phosphoric acid at δ 0. Elemental analyses were performed by CALI Labs, Inc. (Parsippany, NJ).

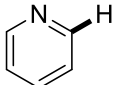
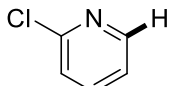
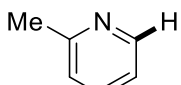
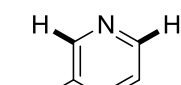
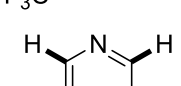
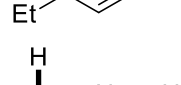
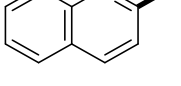
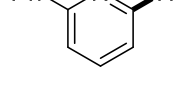
5.4.3 Reactivity of complex 404 or 502 toward C–H activation of pyridine

In-situ observation of the formation of 501a~501i by the reaction of complex 404 with pyridine. In a J. Young NMR tube, to a C_6D_6 solution of $(\text{PBP})\text{Ir}(\text{CO})_2$ (**404**; 200 μL , 0.1 M in C_6D_6 , 0.02 mmol) was added a pyridine substrate (**a~i**; 20 μL , 0.1 M in C_6D_6 , 0.02 mmol) and hexamethyldisiloxane (400 μL , 0.025 M in C_6D_6 , 0.01 mmol) as an internal standard. After heating at 100 $^\circ\text{C}$ for the required time, the conversion was determined by ^1H and $^{31}\text{P}\{^1\text{H}\}$ NMR spectroscopy and the yield was determined by ^1H NMR spectroscopy with hexamethyldisiloxane (0.01 mmol) as an internal standard (Table V-3).

Table V-3. Selective C–H Activation of Pyridines by complex 404 or 502^a



entry	pyridines	Ir^{I}	product	time (h)	Conv. (%) ^b	Yield (%) ^c
1		404	501a	18	100	99
		502	501a	2	100	99

2		404	501b	120	94	94
		502	501b	2	100	95
3		404	501c	120	48	47
		502	501c	2	100	93
4		404	501d	120	100	99
		502	501d	2	100	79
5		404	501e + 501e'	120	99	99 (73:27) ^d
		502	501e + 501e'	2	100	98 (88:12) ^d
6		404	501f + 501f'	120	91	88 (59:41) ^d
		502	501f + 501f'	2	100	99 (56:44) ^d
7		404	501g + 501g'	120	98	95 (85:15) ^e
		502	501g + 501g'	2	100	99 (97:3) ^e
8		404	501h	120	34	33
		502	501h	6	100	83
9		502	501i	6	95	92

a. Reaction conditions: Ir complex **404** or **502** (0.02 mmol) and pyridine (0.02 mmol) in C₆D₆ at 100 °C. b. Conversions were determined by ¹H and ³¹P{¹H} NMR spectroscopy. c. Yields were determined by ¹H NMR spectroscopy with hexamethyldisiloxane (0.01 mmol) as an internal standard. d. The ratio of C2:C6 selectivity. e. The ratio of C2:C8 selectivity.

In-situ observation of the formation of 501a~h by the reaction of complex 502 with pyridine. In a J. Young NMR tube, to a C₆D₆ solution of (PB^{Ph}P)Ir(H)(CO) (**502**; 200 μL, 0.1 M in C₆D₆, 0.02 mmol) was added a pyridine substrate (**a~i**; 20 μL, 0.1 M in C₆D₆, 0.02 mmol) and hexamethyldisiloxane (400 μL, 0.025 M in C₆D₆, 0.01 mmol) as an internal standard. After heating at 100 °C for the required time, the conversion was determined by ¹H and ³¹P{¹H} NMR spectroscopy and the yield was determined by ¹H

NMR spectroscopy with hexamethyldisiloxane (0.01 mmol) as an internal standard (Table V-3).

5.4.4 Reactivity of complex 404 with pyridine under Ar or CO₂

In-situ observation of the formation of 501b and possible 501b* by the reaction of complex 404 with pyridine under Ar. In an Ar-filled glove box, (PBP)Ir(CO)₂ (**404**; 200 μL, 0.1 M in C₆D₆, 0.02 mmol), pyridine (**a**; 20 μL, 0.1 M in C₆D₆, 0.02 mmol), and C₆D₆ (300 μL) were added into a J. Young tube. After heating at 100 °C for the required time, the product yields were determined by ³¹P{¹H} NMR spectroscopy (Table V-2, entry 1~3).

In-situ observation of the formation of 501b and possible 501b* by the reaction of complex 404 with pyridine under CO. In an Ar-filled glove box, (PBP)Ir(CO)₂ (**404**; 200 μL, 0.1 M in C₆D₆, 0.02 mmol), pyridine (**a**; 20 μL, 0.1 M in C₆D₆, 0.02 mmol), and C₆D₆ (300 μL) were added into a J. Young tube. The mixture was degassed via freeze-pump-thaw, and then the flask was refilled with CO (1 atm). After heating at 100 °C for the required time, the product yields were determined by ³¹P{¹H} NMR spectroscopy (Table V-2, entry 4~6).

The C2–H activation of pyridine was clearly inhibited by CO atmosphere, indicating the CO dissociation from **404** was required before C–H activation occurred (entry 3 vs. entry 6). A new peak at 54.5 ppm in ³¹P{¹H} NMR spectra and a new hydride at –11.2 ppm (t, *J*_{H,P} = 15.8 Hz) in ¹H NMR spectra were observed after the reaction was heating at 100 °C for 1 h under CO (entry 4), and we proposed it is likely the complex

501b* generated from the direct C2–H activation of pyridine by **404** before rearrangement into **501b**.

5.4.5 Thermolysis of complex 502 at 100 °C in benzene

In-situ observation of the thermolysis of complex 502. In an Ar-filled glove box, (PB^{Ph}P)Ir(H)(CO) (**502**; 14 mg, 0.02 mmol) and C₆H₆ (500 μL) were added into a J. Young tube. After heating at 100 °C for 2 h, the product yields were determined by ³¹P{¹H} NMR spectroscopy. The complex **502** remained 34% (60.3 ppm) with the formation of 11% of **503** (81.7 ppm), 25% of **404** (60.8 ppm), 20% of **402** (56.8 ppm), 3% of **405** (66.2 ppm), and two other unidentifiable products (4% for each at 51.9 ppm and 34.7 ppm) (Scheme V-9 & Figure V-5). On the basis of a new downfield resonance at 106.3 ppm in ¹¹B{¹H} NMR spectrum (Figure V-6) and the balance of CO in the reaction (# of CO = 11% from **503** + 50% from **404** + 34% from **502** + 3% from **405** = 98% CO), we proposed the new complex **503** was (PBP)Ir(CO).

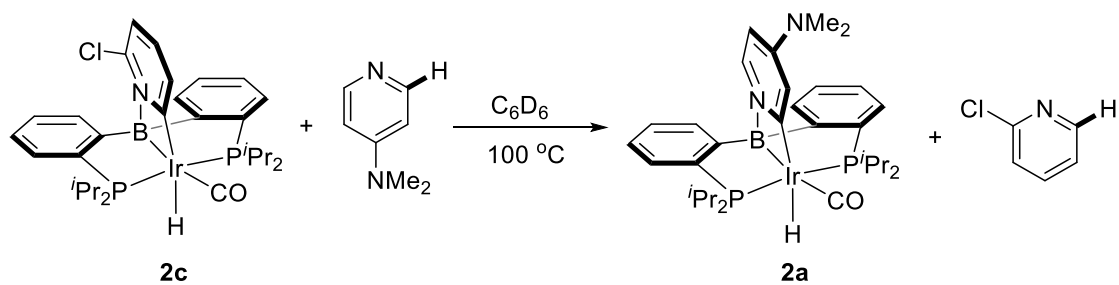
5.4.6 Thermolysis of complex 502 with 2,6-lutidine at 100 °C in C₆D₆

In-situ observation of the thermolysis of complex 502 with 2,6-lutidine. In an Ar-filled glove box, (PB^{Ph}P)Ir(H)(CO) (**502**; 14 mg, 0.02 mmol), 2,6-lutidine (10 μL, 0.10 mmol), and C₆H₆ (500 μL) were added into a J. Young tube. After heating at 100 °C for 2 h, the product yields were determined by ³¹P{¹H} NMR spectroscopy. The complex **502** remained 34% (60.3 ppm) with the formation of 11% of **503** (81.7 ppm), 25% of **404** (60.8 ppm), 20% of **402** (56.8 ppm), 3% of **405** (66.2 ppm), and two other unidentifiable

products (4% for each at 51.9 ppm and 34.7 ppm) (Scheme V-12). The observable H/D exchange on the *meta* (11%) and *para* (33%) positions of 2,6-lutidine in ^1H NMR spectrum suggested the C–H activation occurred, but the complexes were unstable without the nitrogen binding to the boron of PBP complex.

5.4.7 Exchange reaction of 501c to 501a in the presence of DMAP at 100 °C in C_6D_6

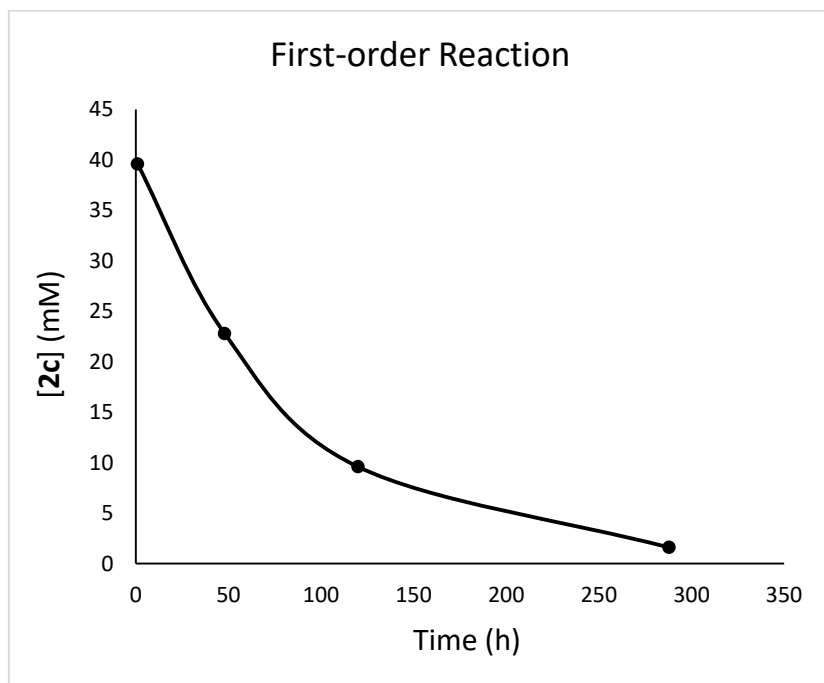
In a J. Young NMR tube, to a C_6D_6 solution of **501c** (15 mg, 0.02 mmol) was added DMAP (48 μL , 0.5 M in C_6D_6 , 0.024 mmol). After heating at 100 °C for the required time, the complex **501c** was slowly converted to **501a** and the conversions was determined by ^1H and $^{31}\text{P}\{^1\text{H}\}$ NMR spectroscopy (Table V-4). On the basis of kinetic plots (Figure V-9), the exchange reaction is first-order dependent to the concentration of **501c**. The rate constant $k = 0.0112 \text{ h}^{-1}$, and the half-life $t_{1/2} \approx 62 \text{ h}$.

Table V-4. Exchange Reaction of 501c to 501a^a

Entry	Time (h)	501a:501c^b	[501c] (mM)	ln [501c] (mM)
1	1	01:99	39.6	3.68
2	48	43:57	22.8	3.13
3	120	76:24	9.6	2.26
4	288	96:4	1.6	0.47

a. Reaction conditions: Ir complex **2c** (0.020 mmol) and DAMP (0.024 mmol) in C₆D₆ at 100 °C. b. Ratios were determined by ³¹P{¹H} NMR spectroscopy.

(a)



(b)

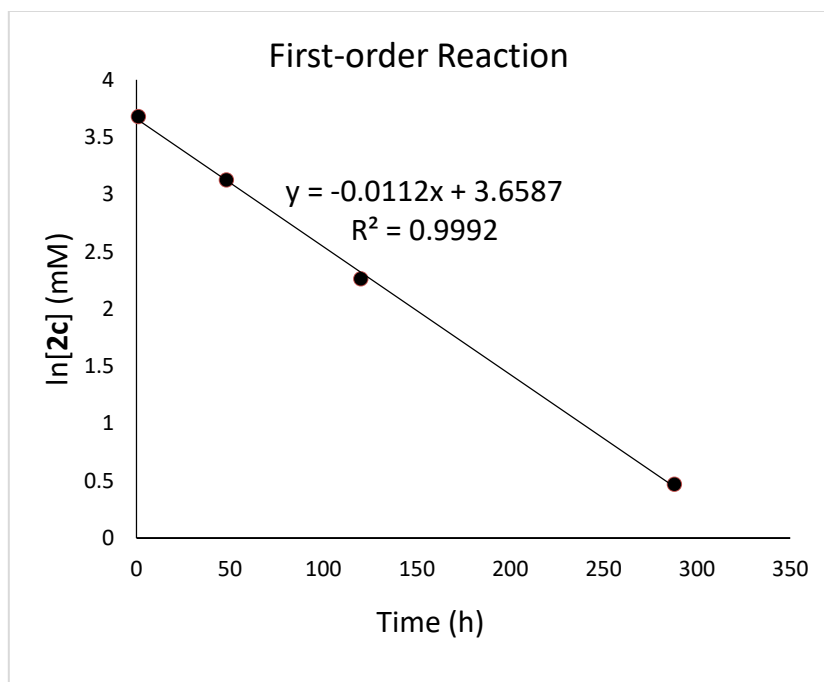


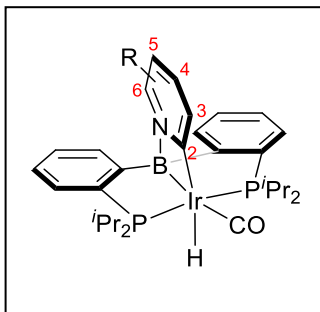
Figure V-9. Kinetic plots of (a) $[501c]$ vs. time; (b) $\ln[501c]$ vs. time.

5.4.8 Synthesis and characterization of iridium complexes

Table V-5. $^{11}\text{B}\{^1\text{H}\}$ NMR, $^{31}\text{P}\{^1\text{H}\}$ NMR, ^1H NMR of Ir–H, and $^{13}\text{C}\{^1\text{H}\}$ NMR of CO Chemical Shifts of Ir Complexes (in ppm), J Values (in Hz), and CO Stretching Frequencies (in cm^{-1})

Compound	^{11}B	^{31}P	^1H NMR of Ir–H (J)	^{13}C NMR of CO	νCO
501a	1.0	51.3	-14.02 (t, $J_{\text{H,P}} = 19.3$ Hz)	179.9	1924
501b	1.8	51.2	-14.15 (t, $J_{\text{H,P}} = 19.1$ Hz)	179.1	1938
501c	4.7	50.5	-13.92 (t, $J_{\text{H,P}} = 18.8$ Hz)	178.7	1952
501d	3.3	50.0	-13.78 (t, $J_{\text{H,P}} = 18.7$ Hz)	179.1	1938
501e	2.7	51.3	-14.19 (t, $J_{\text{H,P}} = 19.2$ Hz)	178.5	1953
501e'	--	47.9	-15.03 (t, $J_{\text{H,P}} = 19.3$ Hz)	--	--
501f	1.8	50.8	-14.10 (t, $J_{\text{H,P}} = 19.1$ Hz)	179.3	1938
501f'	0.7	49.8	-14.54 (t, $J_{\text{H,P}} = 19.2$ Hz)	--	--
501g	3.2	50.3	-13.83 (t, $J_{\text{H,P}} = 19.0$ Hz)	179.3	1938
501g'	--	51.3	-12.72 (t, $J_{\text{H,P}} = 19.1$ Hz)	--	--
501h	4.9	50.1	-13.75 (t, $J_{\text{H,P}} = 18.6$ Hz)	179.6	1950
501i	4.9	50.1	-13.73 (t, $J_{\text{H,P}} = 18.7$ Hz)	179.6	1950

Table V-6. ^1H NMR Chemical Shifts of C3–H, C4–H, C5–H, and C6–H in Ir Complexes (in ppm) and J Values (in Hz)



Compound	C3–H	C4–H	C5–H	C6–H
501a	6.99 (d, $J_{\text{H,H}} = 2.8$ Hz)	--	5.34 (dd, $J_{\text{H,H}} = 6.8, J_{\text{H,H}} = 2.8$ Hz)	7.06 (d, $J_{\text{H,H}} = 6.8$ Hz)
501b	7.22 (d, $J_{\text{H,H}} = 5.7$ Hz)	5.91 (t, $J_{\text{H,H}} = 6.5$ Hz)	6.48 (td, $J_{\text{H,H}} = 7.6, J_{\text{H,H}} = 1.5$ Hz)	7.59 (d, $J_{\text{H,H}} = 7.6$ Hz)
501c	7.51 (d, $J_{\text{H,H}} = 7.7$ Hz)	6.27 (t, $J_{\text{H,H}} = 7.7$ Hz)	6.01 (dd, $J_{\text{H,H}} = 7.7, J_{\text{H,H}} = 0.8$ Hz)	--
501d	7.59 (d, $J_{\text{H,H}} = 7.6$ Hz)	6.50 (t, $J_{\text{H,H}} = 7.6$ Hz)	5.82 (d, $J_{\text{H,H}} = 7.6$ Hz)	--
501e	7.58 (d, $J_{\text{H,H}} = 8.1$ Hz)	6.70 (d, $J_{\text{H,H}} = 8.1$ Hz)	--	7.85 (s)
501f	7.61 (d, $J_{\text{H,H}} = 7.8$ Hz)	6.49 (d, $J_{\text{H,H}} = 7.8$ Hz)	--	7.34 (s, 1H)
501f'	--	6.66 (d, $J_{\text{H,H}} = 7.6$ Hz)	6.05 (t, $J_{\text{H,H}} = 6.6$ Hz)	7.22 (d, $J_{\text{H,H}} = 5.4$ Hz)
501h	7.75 (d, $J_{\text{H,H}} = 7.5$ Hz)	N.D.	6.10 (d, $J_{\text{H,H}} = 7.5$ Hz)	--
501i	7.75 (d, $J_{\text{H,H}} = 7.5$ Hz)	6.61 (t, $J_{\text{H,H}} = 7.5$ Hz)	6.15 (d, $J_{\text{H,H}} = 7.5$ Hz)	--

In-situ observation of 404a. In a J. Young tube, to a C₆D₆ solution of (PBP)Ir(CO)₂ (32 mg, 0.05 mmol) was added 4-dimethylaminopyridine (DMAP) (6 mg, 0.05 mmol). The solution color was changed from dark red to dark orange immediately with 100% conversion based on ³¹P{¹H} NMR spectrum. **Synthesis and isolation of 404a.** In a 25 mL Schlenk flask, to a toluene solution of (PBP)Ir(CO)₂ (64 mg, 0.10 mmol) was added 4-dimethylaminopyridine (DMAP) (12 mg, 0.10 mmol). The reaction was stirred at room temperature for 10 minutes. After removing the volatiles, the residues were washed with pentane, yielding a yellow solid (54 mg, 71%). ³¹P{¹H} NMR (202 MHz, C₆D₆): δ 54.8. ¹¹B NMR (128 MHz, C₆D₆): δ 15.7. ¹H NMR (500 MHz, C₆D₆): δ 7.87 (d, *J*_{H,H} = 5.8 Hz, 2H, Py-*H*), 7.68 (d, *J*_{H,H} = 7.5 Hz, 2H, Ar-*H*), 7.43 (m, 2H, Ar-*H*), 7.24 (t, *J*_{H,H} = 7.3 Hz, 2H, Ar-*H*), 7.12 (t, *J*_{H,H} = 7.3 Hz, 2H, Ar-*H*), 5.54 (d, *J*_{H,H} = 6.1 Hz, 2H, Py-*H*), 2.33 (m, 4H, CHMe₂), 1.91 (s, 6H, NMe₂), 1.26 (dvt, *J*_{H,H} ≈ *J*_{H,P} = 6.9 Hz, 12H, CHMe₂), 1.05 (dvt, *J*_{H,H} ≈ *J*_{H,P} = 6.9 Hz, 12H, CHMe₂). ¹³C NMR (126 MHz, C₆D₆) δ 188.7 (br s, CO), 169.2 (br s, B-C), 153.2 (s), 148.9 (vt, *J*_{P,C} = 22.3 Hz, C-P), 147.4 (s), 131.7 (vt, *J*_{P,C} = 12.0 Hz), 128.6 (s), 128.4 (s), 124.9 (vt, *J*_{P,C} = 2.3 Hz), 105.2 (s), 37.8 (s, NMe₂), 30.9 (s, CHMe₂), 19.8 (s, CHMe₂). ATR-IR: ν_{CO} 1881, 1937 cm⁻¹. Elem. Anal. Calcd for C₃₃H₄₆BIrN₂O₂P₂: C, 51.63; H, 6.04. Found: C, 51.46; H, 6.09.

Synthesis of 501a. In a screw-capped culture tube, to a toluene solution (2 mL) of complex **502** (139 mg, 0.20 mmol) was added DMAP (30 mg, 0.25 mmol). The reaction was stirred at 100 °C for 2 h, and the solution was filtered over a pad of silica gel and washed through with toluene. After the volatiles were removed under vacuum, and the resulting solid was washed with acetonitrile, yielding a pale yellow orange solid (118 mg,

81%). $^{31}\text{P}\{^1\text{H}\}$ NMR (202 MHz, C_6D_6): δ 51.3. ^{11}B NMR (128 MHz, C_6D_6): δ 1.0. ^1H NMR (500 MHz, C_6D_6): δ 8.59 (d, $J_{\text{H,H}} = 7.6$ Hz, 2H, Ar-*H*), 7.39 (t, $J_{\text{H,H}} = 7.3$ Hz, 2H, Ar-*H*), 7.20 (m, 2H, Ar-*H*), 7.16 (m, 2H, Ar-*H*), 7.06 (d, $J_{\text{H,H}} = 6.8$ Hz, 1H, Py-*H*), 6.99 (d, $J_{\text{H,H}} = 2.7$ Hz, 1H, Py-*H*), 5.34 (dd, $J_{\text{H,H}} = 6.8$, $J_{\text{H,H}} = 2.8$ Hz, 1H, Py-*H*), 2.17 (m, 2H, *CHMe*₂), 2.14 (s, 6H, *NMe*₂), 2.11 (m, 2H, *CHMe*₂), 1.39 (dvt, $J_{\text{H,H}} \approx J_{\text{H,P}} = 6.9$ Hz, 6H, *CHMe*₂), 1.30 (dvt, $J_{\text{H,H}} \approx J_{\text{H,P}} = 6.8$ Hz, 6H, *CHMe*₂), 0.91 (dvt, $J_{\text{H,H}} \approx J_{\text{H,P}} = 6.9$ Hz, 6H, *CHMe*₂), 0.61 (dvt, $J_{\text{H,H}} \approx J_{\text{H,P}} = 6.9$ Hz, 6H, *CHMe*₂), -14.02 (t, $J_{\text{H,P}} = 19.3$ Hz, 1H, Ir-*H*). ^{13}C NMR (126 MHz, C_6D_6) δ 179.9 (s, CO), 165.0 (br s, B-*C*), 158.2 (br s, Ir-*C*), 151.6 (s), 147.4 (vt, $J_{\text{P,C}} = 26.2$ Hz, C-*P*), 140.5 (d, $J_{\text{P,C}} = 6.5$ Hz), 132.0 (vt, $J_{\text{P,C}} = 10.7$ Hz), 129.9 (s), 129.0 (s), 125.6 (s), 119.4 (s), 100.9 (d, $J_{\text{P,C}} = 7.8$ Hz), 38.4 (s), 31.5 (vt, $J_{\text{P,C}} = 13.4$ Hz, *CHMe*₂), 30.6 (vtd, $J_{\text{P,C}} = 18.5$, 5.2 Hz, *CHMe*₂), 20.7 (s, *CHMe*₂), 20.5 (s, *CHMe*₂), 19.3 (s, *CHMe*₂). ATR-IR: ν_{CO} 1924 cm^{-1} . Elem. Anal. Calcd for $\text{C}_{32}\text{H}_{46}\text{BIrN}_2\text{OP}_2$: C, 51.96; H, 6.27; N, 3.79. Found: C, 51.82; H, 6.31; N, 3.71.

Synthesis of 501b. In a screw-capped culture tube, to a toluene solution (2 mL) of complex **502** (139 mg, 0.20 mmol) was added pyridine (20 μL , 0.25 mmol). The reaction was stirred at 100 °C for 2 h, and the solution was filtered over a pad of silica gel and washed through with toluene. After the volatiles were removed under vacuum, the resulting solid was washed with acetonitrile, yielding a pale yellow solid (112 mg, 80%). $^{31}\text{P}\{^1\text{H}\}$ NMR (202 MHz, C_6D_6): δ 51.2. ^{11}B NMR (128 MHz, C_6D_6): δ 1.8. ^1H NMR (400 MHz, C_6D_6): δ 8.50 (d, $J_{\text{H,H}} = 7.6$ Hz, 2H, Ar-*H*), 7.59 (d, $J_{\text{H,H}} = 7.7$ Hz, 1H, Py-*H*), 7.34 (m, 2H, Ar-*H*), 7.22 (d, $J_{\text{H,H}} = 5.7$ Hz, 1H, Py-*H*), 7.14 (m, 4H, Ar-*H*), 6.48 (td, $J_{\text{H,H}} = 7.6$, $J_{\text{H,H}} = 1.5$ Hz, 1H, Py-*H*), 5.91 (t, $J_{\text{H,H}} = 6.5$ Hz, 1H, Py-*H*), 2.11 (m, 2H, *CHMe*₂),

2.03 (m, 2H, CHMe₂), 1.25 (m, 12H, CHMe₂), 0.84 (dvt, $J_{H,H} \approx J_{H,P} = 6.9$ Hz, 6H, CHMe₂), 0.35 (dvt, $J_{H,H} \approx J_{H,P} = 7.2$ Hz, 6H, CHMe₂), -14.15 (t, $J_{H,P} = 19.1$ Hz, 1H, Ir-H). ¹³C NMR (126 MHz, C₆D₆) δ 179.1 (s, CO), 164.9 (br, Ir-C), 164.0 (br, B-C), 147.2 (vt, $J_{P,C} = 26.3$ Hz, C-P), 141.3 (s), 139.1 (s), 132.6 (s), 132.0 (vt, $J_{P,C} = 10.6$ Hz), 129.9 (s), 129.1 (s), 126.0 (vt, $J_{P,C} = 3.9$ Hz), 115.3 (s), 31.5 (vt, $J_{P,C} = 13.5$ Hz, CHMe₂), 30.7 (vtd, $J_{P,C} = 18.7$, 4.5 Hz, CHMe₂), 20.7 (vt, $J_{P,C} = 2.3$ Hz, CHMe₂), 20.5 (s, CHMe₂), 20.0 (s, CHMe₂), 19.3 (s, CHMe₂). Elem. Anal. Calcd for C₃₀H₄₁BIrNOP₂: C, 51.72; H, 5.93; N, 2.01. Found: C, 51.77; H, 5.84; N, 1.87.

Synthesis of 501c. In a screw-capped culture tube, to a toluene solution (2 mL) of complex **502** (139 mg, 0.20 mmol) was added 2-chloropyridine (20 μL, 0.26 mmol). The reaction was stirred at 100 °C for 2 h, and the solution was filtered over a pad of silica gel and washed through with toluene. After the volatiles were removed under vacuum, the resulting solid was washed with acetonitrile, yielding an off-white solid (119 mg, 81%). The purity of isolated samples of **501c** was gauged to be >95% by NMR spectroscopy. ³¹P{¹H} NMR (202 MHz, C₆D₆): δ 50.5. ¹¹B NMR (128 MHz, C₆D₆): δ 4.7. ¹H NMR (500 MHz, C₆D₆): δ 8.94 (d, $J_{H,H} = 7.8$ Hz, 2H, Ar-H), 7.51 (d, $J_{H,H} = 7.6$ Hz, 1H, Py-H), 7.40 (t, $J_{H,H} = 7.3$ Hz, 2H, Ar-H), 7.17 (m, 4H, Ar-H), 6.27 (t, $J_{H,H} = 7.7$ Hz, 1H, Py-H), 6.01 (dd, $J_{H,H} = 7.8$, $J_{H,H} = 0.8$ Hz, 1H, Py-H), 2.10 (m, 2H, CHMe₂), 2.04 (m, 2H, CHMe₂), 1.26 (m, 12H, CHMe₂), 0.82 (dvt, $J_{H,H} \approx J_{H,P} = 6.9$ Hz, 6H, CHMe₂), 0.41 (dvt, $J_{H,H} \approx J_{H,P} = 7.2$ Hz, 6H, CHMe₂), -13.92 (t, $J_{H,P} = 18.8$ Hz, 1H, Ir-H). ¹³C NMR (101 MHz, C₆D₆) δ 178.7 (s, CO), 173.9 (s, Ir-C), 161.7 (br s, B-C), 147.3 (vt, $J_{P,C} = 26.4$ Hz, C-P), 146.5 (s), 137.7 (s), 135.0 (vt, $J_{P,C} = 10.3$ Hz), 134.0 (s), 129.5 (s), 128.8 (s), 126.2 (s), 116.0 (s),

31.6 (vt, $J_{P,C} = 13.5$ Hz, $CHMe_2$), 30.6 (vt, $J_{P,C} = 18.9$ Hz, $CHMe_2$), 20.7 (s, $CHMe_2$), 20.5 (s, $CHMe_2$), 20.2 (s, $CHMe_2$), 19.2 (s, $CHMe_2$). ATR-IR: ν_{CO} 1952 cm^{-1} .

Synthesis of 501d. In a screw-capped culture tube, to a toluene solution (2 mL) of complex **502** (139 mg, 0.20 mmol) was added 2-methylpyridine (25 μ L, 0.25 mmol). The reaction was stirred at 100 °C for 2 h, and the solution was filtered over a pad of silica gel and washed through with toluene. After the volatiles were removed under vacuum, the resulting solid was washed with acetonitrile, yielding a yellow solid (115 mg, 81%). $^{31}P\{^1H\}$ NMR (202 MHz, C_6D_6): δ 50.0. ^{11}B NMR (128 MHz, C_6D_6): δ 3.3. 1H NMR (500 MHz, C_6D_6): δ 8.63 (d, $J_{H,H} = 7.8$ Hz, 2H, Ar-*H*), 7.59 (d, $J_{H,H} = 7.6$ Hz, 1H, Py-*H*), 7.31 (m, 2H, Ar-*H*), 7.13 (m, 4H, Ar-*H*), 6.50 (t, $J_{H,H} = 7.6$ Hz, 1H, Py-*H*), 5.82 (d, $J_{H,H} = 7.6$ Hz, 1H, Py-*H*), 2.07 (m, 2H, $CHMe_2$), 2.01 (m, 2H, $CHMe_2$), 2.00 (s, 3H, Py-*Me*), 1.27 (m, 12H, $CHMe_2$), 0.79 (dvt, $J_{H,H} \approx J_{H,P} = 6.8$ Hz, 6H, $CHMe_2$), 0.42 (dvt, $J_{H,H} \approx J_{H,P} = 7.2$ Hz, 6H, $CHMe_2$), -13.78 (t, $J_{H,P} = 18.7$ Hz, 1H, Ir-*H*). ^{13}C NMR (126 MHz, C_6D_6) δ 179.1 (s, CO), 167.0 (m, Ir-*C*), 162.8 (br s, B-*C*), 153.5 (s), 147.9 (vt, $J_{P,C} = 26.4$ Hz, C-*P*), 137.2 (s), 133.8 (vt, $J_{P,C} = 10.5$ Hz), 132.9 (s), 130.1 (s), 128.5 (s), 125.8 (vt, $J_{P,C} = 3.9$ Hz), 116.5 (s), 31.5 (vt, $J_{P,C} = 13.7$ Hz, $CHMe_2$), 30.6 (vt, $J_{P,C} = 17.9$ Hz, $CHMe_2$), 20.8 (vt, $J_{P,C} = 2.1$ Hz, $CHMe_2$), 20.5 (vt, $J_{P,C} = 2.0$ Hz, $CHMe_2$), 20.3 (s, $CHMe_2$), 19.2 (s, $CHMe_2$), 18.7 (s, Py-*Me*). ATR-IR: ν_{CO} 1938 cm^{-1} . Elem. Anal. Calcd for $C_{31}H_{43}BIrNOP_2$: C, 52.39; H, 6.10; N, 1.97. Found: C, 52.65; H, 5.89; N, 1.83.

Synthesis of the mixture of 501e and 501e'. In a screw-capped culture tube, to a toluene solution (2 mL) of complex **502** (139 mg, 0.20 mmol) was added 3-(trifluoromethyl)pyridine (30 μ L, 0.26 mmol). The reaction was stirred at 100 °C for 2 h,

and the solution was filtered over a pad of silica gel and washed through with toluene. The volatiles were removed under vacuum, yielding a pale yellow solid (138 mg, 90%). Two isomers **501e** and **501e'** were observed in $^{31}\text{P}\{^1\text{H}\}$ NMR (51.3 and 47.9 ppm), ^{19}F NMR (-63.5 and -62.0 ppm) and ^1H NMR (-14.19 ppm [t, $J_{\text{H,P}} = 19.2$ Hz, Ir-*H*] and -15.03 ppm [t, $J_{\text{H,P}} = 19.3$ Hz, Ir-*H*]) spectra with a ratio of 90:10. Only the data from **501e** was reported below. $^{31}\text{P}\{^1\text{H}\}$ NMR (202 MHz, C_6D_6): δ 51.3. ^{11}B NMR (128 MHz, C_6D_6): δ 2.7. ^{19}F NMR (470 MHz, C_6D_6) δ -63.5 . ^1H NMR (400 MHz, C_6D_6): δ 8.40 (d, $J_{\text{H,H}} = 7.5$ Hz, 2H, Ar-*H*), 7.85 (s, 1H, Py-*H*), 7.58 (d, $J_{\text{H,H}} = 8.1$ Hz, 1H, Py-*H*), 7.28 (t, $J_{\text{H,H}} = 7.0$ Hz, 2H, Ar-*H*), 7.08 (m, 4H, Ar-*H*), 6.70 (d, $J_{\text{H,H}} = 8.1$ Hz, 1H, Py-*H*), 2.07 (m, 2H, *CHMe*₂), 2.00 (m, 2H, *CHMe*₂), 1.18 (m, 12H, *CHMe*₂), 0.78 (dvt, $J_{\text{H,H}} \approx J_{\text{H,P}} = 7.2$ Hz, 4H), 0.26 (dvt, $J_{\text{H,H}} \approx J_{\text{H,P}} = 7.2$ Hz, 3H), -14.19 (t, $J_{\text{H,P}} = 19.2$ Hz, 1H, Ir-*H*). ^{13}C NMR (101 MHz, C_6D_6) δ 178.5 (s, CO), 176.3 (s, Ir-*C*), 162.7 (br s, B-*C*), 146.6 (vt, $J_{\text{P,C}} = 26.6$ Hz, C-*P*), 139.6 (s), 137.8 (d, $J_{\text{P,C}} = 4.3$ Hz), 131.9 (vt, $J_{\text{P,C}} = 10.5$ Hz), 129.9 (s), 129.6 (s), 129.3 (s), 126.5 (vt, $J_{\text{P,C}} = 3.8$ Hz), 119.4 (q, $J_{\text{F,C}} = 33.9$ Hz), 31.5 (vt, $J_{\text{P,C}} = 13.6$ Hz, *CHMe*₂), 30.8 (vt, $J_{\text{P,C}} = 19.0$ Hz, *CHMe*₂), 20.5 (vt, $J_{\text{P,C}} = 2.0$ Hz, *CHMe*₂), 20.4 (s, *CHMe*₂), 19.8 (s, *CHMe*₂), 19.1 (s, *CHMe*₂). One aromatic carbon signal was missing likely due to the overlap with solvent peak. ATR-IR: ν_{CO} 1953 cm^{-1} . Elem. Anal. Calcd for $\text{C}_{31}\text{H}_{40}\text{BF}_3\text{IrNOP}_2$: C, 48.70; H, 5.27; N, 1.83. Found: C, 48.70; H, 5.35; N, 1.80.

Synthesis of the mixture of 501f and 501f'. In a screw-capped culture tube, to a toluene solution (2 mL) of complex **502** (139 mg, 0.20 mmol) was added 3-ethylpyridine (25 μL , 0.22 mmol). The reaction was stirred at 100 °C for 2 h, and the solution was filtered over a pad of silica gel and washed through with toluene. The volatiles were removed under

vacuum, yielding a pale yellow solid (131 mg, 90%). Two isomers **501f** and **501f'** were observed in $^{31}\text{P}\{^1\text{H}\}$ NMR (50.8 and 49.8 ppm) and ^1H NMR (-14.10 ppm [t, $J_{\text{H,P}} = 19.1$ Hz, Ir-H] and -14.54 ppm [t, $J_{\text{H,P}} = 19.2$ Hz, Ir-H]) spectra with a ratio of 56:44.

501f: $^{31}\text{P}\{^1\text{H}\}$ NMR (202 MHz, C_6D_6): δ 50.8. ^{11}B NMR (128 MHz, C_6D_6): δ 1.8. ^1H NMR (400 MHz, C_6D_6): δ 8.59 (d, $J_{\text{H,H}} = 7.6$ Hz, 2H, Ar-H), 7.61 (d, $J_{\text{H,H}} = 7.9$ Hz, 1H, Py-H), 7.36 (m, 2H, Ar-H), 7.22 (d, $J_{\text{H,H}} = 5.4$ Hz, 1H, Py-H), 7.14 (m, 4H, Ar-H), 6.49 (d, $J_{\text{H,H}} = 7.8$ Hz, 1H, Py-H), 2.12 (m, 4H, CHMe₂), 1.72 (q, $J_{\text{H,H}} = 7.6$ Hz, 2H, CH₂CH₃), 1.17 (dvt, $J_{\text{H,H}} \approx J_{\text{H,P}} = 7.8$ Hz, 6H, CHMe₂), 0.84 (m, 12H, CHMe₂), 0.55 (t, $J_{\text{H,H}} = 7.6$ Hz, 3H, CH₂CH₃), 0.40 (dvt, $J_{\text{H,H}} \approx J_{\text{H,P}} = 7.2$ Hz, 6H, CHMe₂), -14.10 (t, $J_{\text{H,P}} = 19.1$ Hz, 1H, Ir-H).

501f': $^{31}\text{P}\{^1\text{H}\}$ NMR (202 MHz, C_6D_6): δ 49.8. ^{11}B NMR (128 MHz, C_6D_6): δ 0.7. ^1H NMR (400 MHz, C_6D_6): δ 8.53 (d, $J_{\text{H,H}} = 7.6$ Hz, 2H, Ar-H), 7.36 (m, 3H, Ar-H + Py-H), 7.14 (m, 4H, Ar-H), 6.66 (d, $J_{\text{H,H}} = 7.6$ Hz, 1H, Py-H), 6.05 (t, $J_{\text{H,H}} = 6.6$ Hz, 1H, Py-H), 3.10 (q, $J_{\text{H,H}} = 7.5$ Hz, 2H, CH₂CH₃), 2.12 (m, 4H, CHMe₂), 1.27 (m, 21H, CHMe₂ + CH₂CH₃), 0.25 (dvt, $J_{\text{H,H}} \approx J_{\text{H,P}} = 7.2$ Hz, 6H, CHMe₂), -14.54 (t, $J_{\text{H,P}} = 19.2$ Hz, 1H, Ir-H).

^{13}C NMR (126 MHz, C_6D_6) of **501f** + **501f'**: δ 179.3 (s, CO), 167.5 (s, Ir-C), 164.3 (br s, B-C), 160.1 (s), 148.9 (s), 147.4 (vt, $J_{\text{P,C}} = 26.2$ Hz, C-P of **501f**), 147.2 (vt, $J_{\text{P,C}} = 26.5$ Hz, C-P of **501f'**), 140.5 (d, $J_{\text{P,C}} J = 4.9$ Hz), 139.0 (d, $J = 4.6$ Hz), 138.9 (s), 133.5 (d, $J_{\text{P,C}} = 5.3$ Hz), 132.3 – 131.8 (m), 131.4 (s), 130.0 (s), 129.7 (s), 129.3 (s), 129.1 (s), 126.0 (d, $J_{\text{P,C}} = 3.8$ Hz), 116.4 (d, $J_{\text{P,C}} = 5.9$ Hz), 31.8 (vt, $J_{\text{P,C}} = 13.4$ Hz, CHMe₂ of **501f'**), 31.4 (vt, $J_{\text{P,C}} = 13.5$ Hz, CHMe₂ of **501f**), 31.4 (vtd, $J_{\text{P,C}} = 19.0$ Hz, 3.2 Hz, CHMe₂ of

501f'), 30.7 (vtd, $J_{P,C} = 18.6, 3.2$ Hz, $CHMe_2$ of **501f**), 29.5 (s, CH_2CH_3 of **501f'**), 25.4 (s, CH_2CH_3 of **501f**), 20.9 (s, $CHMe_2$), 20.7 (s, $CHMe_2$), 20.5 (s, $CHMe_2$), 20.0 (s, $CHMe_2$), 19.3 (s, $CHMe_2$), 19.3 (s, $CHMe_2$), 19.2 (s, $CHMe_2$), 14.7 (s, CH_2CH_3 of **501f**), 13.4 (s, CH_2CH_3 of **501f'**). ATR-IR: ν_{CO} 1938 cm^{-1} .

Synthesis of 501g. In a screw-capped culture tube, to a toluene solution (2 mL) of complex **502** (139 mg, 0.20 mmol) was added quinoline (30 μ L, 0.25 mmol). The reaction was stirred at 100 °C for 2 h, and the solution was filtered over a pad of silica gel and washed through with toluene. After the volatiles were removed under vacuum, the resulting solid was recrystallized in a concentrated toluene solution at -35 °C, yielding a pale yellow solid (104 mg, 70%). $^{31}P\{^1H\}$ NMR (202 MHz, C_6D_6): δ 50.3. ^{11}B NMR (128 MHz, C_6D_6): δ 3.2. 1H NMR (500 MHz, C_6D_6) δ 8.89 (d, $J_{H,H} = 7.7$ Hz, 2H), 8.38 (d, $J_{H,H} = 8.5$ Hz, 1H), 7.85 (d, $J_{H,H} = 8.3$ Hz, 1H), 7.34 (m, 2H), 7.07 (m, 6H), 6.93 (d, $J_{H,H} = 8.2$ Hz, 1H), 6.76 (m, 1H), 2.09 (m, 2H, $CHMe_2$), 1.95 (m, 2H, $CHMe_2$), 1.22 (m, 12H, $CHMe_2$), 0.83 (dvt, $J_{H,H} \approx J_{H,P} = 6.9$ Hz, 6H, $CHMe_2$), 0.34 (dvt, $J_{H,H} \approx J_{H,P} = 7.2$ Hz, 6H, $CHMe_2$), -13.83 (t, $J_{H,P} = 19.0$ Hz, 1H, Ir-H). ^{13}C NMR (126 MHz, C_6D_6) δ 179.3 (s, CO), 176.4 (m, Ir-C), 163.2 (br s, B-C), 147.6 (vt, $J_{P,C} = 26.3$ Hz, C-P), 143.8 (s), 137.5 (s), 133.4 (vt, $J_{P,C} = 10.3$ Hz), 131.4 (s), 130.2 (s), 129.3 (s), 128.9 (d, $J_{P,C} = 2.9$ Hz), 128.4 (s), 125.9 (vt, $J_{P,C} = 4.0$ Hz), 124.6 (s), 123.8 (s), 119.1 (s), 31.2 (vt, $J_{P,C} = 13.5$ Hz, $CHMe_2$), 30.6 (vt, $J_{P,C} = 20.2$ Hz, $CHMe_2$), 20.4 (s, $CHMe_2$), 20.3 (s, $CHMe_2$), 19.1 (s, $CHMe_2$). ATR-IR: ν_{CO} 1938 cm^{-1} .

Synthesis of 501h. In a screw-capped culture tube, to a toluene solution (2 mL) of complex **502** (139 mg, 0.20 mmol) was added 2-phenylpyridine (35 μ L, 0.24 mmol). The

reaction was stirred at 100 °C for 6 h, and the solution was filtered over a pad of silica gel and washed through with toluene. After the volatiles were removed under vacuum, the resulting solid was washed with acetonitrile, yielding a pale yellow solid (125 mg, 81%). $^{31}\text{P}\{^1\text{H}\}$ NMR (202 MHz, C_6D_6): δ 50.1. ^{11}B NMR (128 MHz, C_6D_6): δ 4.9. ^1H NMR (400 MHz, C_6D_6) δ 7.75 (d, $J_{\text{H,H}} = 7.7$ Hz, 1H), 7.47 (d, $J_{\text{H,H}} = 6.8$ Hz, 2H), 7.18 (m, 1H), 7.12 (m, 2H), 7.08 (m, 4H), 7.02 (t, $J_{\text{H,H}} = 7.6$ Hz, 2H), 6.59 (m, 3H), 6.10 (d, $J_{\text{H,H}} = 7.5$ Hz, 1H), 2.12 (m, 2H, CHMe_2), 2.08 (m, 2H, CHMe_2), 1.32 (dvt, $J_{\text{H,H}} \approx J_{\text{H,P}} = 7.1$ Hz, 6H, CHMe_2), 1.21 (dvt, $J_{\text{H,H}} \approx J_{\text{H,P}} = 7.0$ Hz, 6H, CHMe_2), 0.76 (dvt, $J_{\text{H,H}} \approx J_{\text{H,P}} = 7.0$ Hz, 6H, CHMe_2), 0.59 (dvt, $J_{\text{H,H}} \approx J_{\text{H,P}} = 7.2$ Hz, 6H, CHMe_2), -13.75 (t, $J_{\text{H,P}} = 18.6$ Hz, 1H, Ir- H). ^{13}C NMR (101 MHz, C_6D_6) δ 179.6 (s, CO), 169.7 (s, Ir-C), 164.1 (br s, B-C), 156.6 (s), 146.7 (vt, $J_{\text{P,C}} = 26.2$ Hz, C-P), 138.7 (s), 136.7 (s), 134.2 (vt, $J_{\text{P,C}} = 10.4$ Hz), 132.5 (s), 130.5 (s), 129.5 (s), 128.8 (s), 128.2 (s), 125.9 (vt, $J_{\text{P,C}} = 3.9$ Hz), 117.9 (s), 31.1 (vt, $J_{\text{P,C}} = 13.4$ Hz, CHMe_2), 30.7 (vt, $J_{\text{P,C}} = 18.8$ Hz, CHMe_2), 20.46 (s, CHMe_2), 20.42 (s, CHMe_2), 20.32 (s, CHMe_2), 19.07 (s, CHMe_2). ATR-IR: ν_{CO} 1950 cm^{-1} .

Synthesis of 501i. In a screw-capped culture tube, to a toluene solution (2 mL) of complex **502** (139 mg, 0.20 mmol) was added 2-(*p*-tolyl)pyridine (45 μL , 0.26 mmol). The reaction was stirred at 100 °C for 6 h, and the solution was filtered over a pad of silica gel and washed through with toluene. After the volatiles were removed under vacuum, the resulting solid was washed with acetonitrile, yielding an off-white solid (144 mg, 92%). $^{31}\text{P}\{^1\text{H}\}$ NMR (202 MHz, C_6D_6): δ 50.1. ^{11}B NMR (128 MHz, C_6D_6): δ 4.9. ^1H NMR (500 MHz, C_6D_6) δ 7.75 (d, $J_{\text{H,H}} = 7.6$ Hz, 1H, Py- H), 7.57 (m, 2H, Ar- H), 7.10 (m, 6H, Ar- H), 6.89 (d, $J_{\text{H,H}} = 7.7$ Hz, 2H, tolyl- H), 6.61 (t, $J_{\text{H,H}} = 7.6$ Hz, 1H, Py- H), 6.53 (d, $J_{\text{H,H}} =$

8.0 Hz, 2H, tolyl-*H*), 6.15 (d, $J_{H,H} = 7.5$ Hz, 1H, Py-*H*), 2.15 (s, 3H, CH_3), 2.11 (m, 4H, $CHMe_2$), 1.32 (dvt, $J_{H,H} \approx J_{H,P} = 7.0$ Hz, 6H, $CHMe_2$), 1.22 (dvt, $J_{H,H} \approx J_{H,P} = 6.9$ Hz, 6H, $CHMe_2$), 0.77 (dvt, $J_{H,H} \approx J_{H,P} = 6.9$ Hz, 6H, $CHMe_2$), 0.60 (dvt, $J_{H,H} \approx J_{H,P} = 7.2$ Hz, 6H, $CHMe_2$), -13.73 (t, $J_{H,P} = 18.7$ Hz, 1H, Ir-*H*). ^{13}C NMR (126 MHz, C_6D_6): δ 179.6 (s, CO), 169.5 (s, Ir-C), 164.1 br s, B-C), 156.7 (s), 146.7 (vt, $J_{P,C} = 26.3$ Hz, C-P), 138.6 (s), 138.5 (d, $J_{P,C} = 5.3$ Hz), 134.2 (td, $J_{P,C} = 10.4, 5.8$ Hz), 134.1 (s), 132.5 (d, $J_{P,C} = 5.3$ Hz), 130.5 (d, $J_{P,C} = 5.0$ Hz), 129.5 (s), 128.5 (s), 125.8 (d, $J_{P,C} = 3.2$ Hz), 118.0 (d, $J_{P,C} = 9.6$ Hz), 31.0 (vt, $J_{P,C} = 13.4$ Hz, $CHMe_2$), 30.6 (vt, $J_{P,C} = 18.8$ Hz, $CHMe_2$), 21.4 (d, $J_{P,C} = 2.8$ Hz, $CHMe_2$), 20.45 (s, $CHMe_2$), 20.33 (d, $J_{P,C} = 1.8$ Hz, $CHMe_2$), 19.09 (s, $CHMe_2$). ATR-IR: ν_{CO} 1950 cm^{-1} .

Synthesis of (PB^{Ph}P)Ir(H)(CO) (502). In a 50 mL Teflon screw-capped round-bottomed flask, the toluene solution (10 mL) of (PBP)Ir(Ph)(H) (**402**; 768 mg, 1.15 mmol) was degassed by freeze-pump-thaw, and the flask was refilled with CO (1 atm) to *in situ* generate complex **403**. After stirring at room temperature for 1 h, the CO atmosphere was removed under vacuum, and the solution was added to a toluene solution (5 mL) of (PBP)Ir(Ph)(H) (**402**; 768 mg, 1.15 mmol). The mixture was stirred at room temperature for another 1 h. The volatiles were removed under vacuum, and the resulting solid was washed with cold pentane, yielding an orange brown solid (1.19 g, 74%). $^{31}P\{^1H\}$ NMR (202 MHz, C_6D_6): δ 60.3. ^{11}B NMR (128 MHz, C_6D_6): δ 1.4. 1H NMR (400 MHz, C_6D_6) δ 7.59 (d, $J = 7.5$ Hz, 2H), 7.17 (m, 6H), 7.07 (m, 5H), 2.46 (m, 2H, $CHMe_2$), 2.21 (m, 2H, $CHMe_2$), 1.09 (m, 18H, $CHMe_2$), 0.94 (vtd, $J_{H,H} \approx J_{P,C} = 7.5$ Hz, 6H, $CHMe_2$), -4.09 (br s, 1H, Ir-*H*). ^{13}C NMR (101 MHz, C_6D_6) δ 185.5 (t, $J_{P,C} = 8.2$ Hz, CO), 160.9 (br, B-

C_{Ar}), 156.8 (br, B- C_{Ph}), 136.2 (vt, $J = 25.3$ Hz, C-P), 135.4 (vt, $J_{P,C} = 8.0$ Hz), 134.9 (s), 129.8 (s), 127.6 (s), 125.6 (vt, $J_{P,C} = 3.8$ Hz, $CHMe_2$), 28.1 (vt, $J_{P,C} = 14.0$ Hz, $CHMe_2$, 2C), 25.1 (vt, $J_{P,C} = 16.2$ Hz, 2C), 19.9 (vt, $J_{P,C} = 2.0$ Hz, $CHMe_2$, 2C), 19.24 (s, $CHMe_2$, 4C), 18.57 (s, $CHMe_2$, 2C). Two aromatic carbons were missing probably due to overlap. Elem. Anal. Calcd for $C_{31}H_{42}BIrOP_2$: C, 53.52; H, 6.09. Found: C, 53.48; H, 5.65.

Synthesis of 505*. In a 50 mL Schlenk flask, to a dichloromethane solution (3 mL) of complex **501c** (136 mg, 0.19 mmol) was added *N*-chlorosuccinimide (27 mg, 0.20 mmol). The reaction was stirred at room temperature for 1 h, and the solution was filtered over a pad of silica gel and washed through with dichloromethane. After the volatiles were removed under vacuum, the resulting solid was washed with Et_2O , yielding an off-white solid (111 mg, 76%). $^{31}P\{^1H\}$ NMR (202 MHz, $CDCl_3$): δ 21.5. ^{11}B NMR (128 MHz, $CDCl_3$): δ 1.7. 1H NMR (500 MHz, $CDCl_3$) δ 8.72 (d, $J_{H,H} = 7.7$ Hz, 2H, Ar- H), 8.08 (d, $J_{H,H} = 7.7$ Hz, 1H, Py- H), 7.40 (t, $J_{H,H} = 7.4$ Hz, 2H, Ar- H), 7.32 (m, 3H, Ar- H + Py- H), 7.24 (t, $J_{H,H} = 7.6$ Hz, 2H, Ar- H), 6.74 (d, $J = 7.9$ Hz, 1H, Py- H), 3.07 (m, 2H, $CHMe_2$), 1.67 (vtd, $J_{H,H} \approx J_{P,C} = 7.8$ Hz, 6H, $CHMe_2$), 1.64 (m, 2H, $CHMe_2$), 1.15 (m, 12H, $CHMe_2$), 0.88 (vtd, $J_{H,H} \approx J_{P,C} = 7.0$ Hz, 6H, $CHMe_2$). ^{13}C NMR (126 MHz, $CDCl_3$) δ 180.8 (t, $J_{P,C} = 10.8$ Hz, CO), 176.6 (t, $J_{P,C} = 12.0$ Hz, Ir-C), 158.2 (br, B- C_{Ar}), 144.8 (s), 141.6 (vt, $J_{P,C} = 25.0$ Hz, C-P), 136.6 (s), 133.6 (vt, $J_{P,C} = 8.7$ Hz), 132.6 (s), 132.0 (vt, $J_{P,C} = 2.0$ Hz), 128.9 (s), 126.0 (vt, $J_{P,C} = 3.9$ Hz), 119.2 (s), 28.0 (vt, $J_{P,C} = 14.5$ Hz, $CHMe_2$), 25.9 (vt, $J_{P,C} = 14.8$ Hz, $CHMe_2$), 20.9 (vt, $J_{P,C} = 2.1$ Hz, $CHMe_2$), 20.52 (s, $CHMe_2$), 19.99 (s, $CHMe_2$), 18.74 (s, $CHMe_2$).

Observation of the mixture of 506 and 506*. In a 50 mL Schlenk flask, to a 2 mL toluene suspension of complex **505*** (77 mg, 0.10 mmol) was added PhLi (67 μ L, 1.8 M, 0.12 mmol) dropwise, and the suspension turned to clear, orange solution immediately. The reaction was stirred at room temperature for 10 min, and the solution was filtered over a pad of silica gel and washed through with toluene. After the volatiles were nearly removed under vacuum for 30 min, yielding an orange solid assigned as the mixture of **506** and **506*** in a ratio of 1:9 on the basis of $^{31}\text{P}\{^1\text{H}\}$ NMR spectroscopic data (35.7 ppm for **506** and 18.8 ppm for **506***). The mixture was gradually decomposed under vacuum for 3 h. For complex **506***: $^{31}\text{P}\{^1\text{H}\}$ NMR (202 MHz, C_6D_6): δ 18.8. ^1H NMR (500 MHz, C_6D_6) δ 8.93 (d, $J_{\text{H,H}} = 7.7$ Hz, 2H, Ar-*H*), 8.56 (d, $J_{\text{H,H}} = 6.5$ Hz, 2H, Ph-*H*), 8.22 (d, $J_{\text{H,H}} = 7.9$ Hz, 1H, Py-*H*), 7.41 (t, $J_{\text{H,H}} = 7.4$ Hz, 2H, Ar-*H*), 7.36 (t, $J_{\text{H,H}} = 7.1$ Hz, 2H, Ar-*H*), 7.27 (t, $J = 7.2$ Hz, 1H, Ph-*H*), 7.05 (m, 4H, Ar-*H* + Ph-*H*), 6.41 (t, $J_{\text{H,H}} = 7.9$ Hz, 1H, Py-*H*), 6.01 (dd, $J_{\text{H,H}} = 7.9, 1.0$ Hz, 1H, Py-*H*), 2.73 (m, 2H, CHMe_2), 1.87 (m, 2H, CHMe_2), 1.02 (m, 12H, CHMe_2), 0.77 (vtd, $J_{\text{H,H}} \approx J_{\text{P,C}} = 7.2$ Hz, 6H, CHMe_2), 0.67 (vtd, $J_{\text{H,H}} \approx J_{\text{P,C}} = 7.0$ Hz, 6H, CHMe_2).

Formation of 507 via C–C reductive elimination from 506 and 506*. In a J-Young NMR tube, to a 0.5 mL d_8 -toluene solution of **506** and **506*** (32 mg, 0.04 mmol) was added DMAP (100 μ L, 0.5 M, 0.05 mmol) and hexamethyldisiloxane (100 μ L, 0.025 M, 0.0025 mmol) as an internal standard. After heating at 150 $^\circ\text{C}$ for 5 h, the mixture of **506** and **506*** was converted into the complex **501a** with 96% NMR yield and the C–C coupling product **507** was detected with 97% NMR yield. The product **507** is a known compound: CAS-RN 13382-54-2. ^1H NMR (500 MHz, CDCl_3) δ 7.96 (dd, $J_{\text{H,H}} = 8.0, 1.0$

Hz, 2H, Ph-*H*), 7.65 (t, $J_{\text{H,H}} = 8.0$ Hz, 1H, Py-*H*), 7.60 (d, $J_{\text{H,H}} = 8.0$ Hz, 1H, Py-*H*), 7.42 (m, 3H, Ph-*H*), 7.21 (m, 1H, Py-*H*). ^{13}C NMR (126 MHz, CDCl_3) δ 158.1 (C, C_{Py}), 151.4 (C, C_{Py}), 139.3 (CH, C_{Py}), 137.7 (C, C_{Ph}), 129.6 (CH, C_{Ph}), 128.8 (CH, C_{Ph}), 127.0 (CH, C_{Ph}), 122.5 (CH, C_{Py}), 118.6 (CH, C_{Py}). GC-MS: $m/z = 188.94$. Spectroscopic data were consistent with those previously reported in the literature.²²⁷

5.4.9 X-Ray structural determination details

The X-ray crystal data (CCDC 1557040 for **501b**, CCDC 1557042 for **501g**, and CCDC 1557043 for **502**) could be obtained by The Cambridge Structural Database (CSD).

X-Ray data collection, solution, and refinement for 501b. A colorless, multi-faceted block of suitable size (0.23 x 0.18 x 0.03 mm) was selected from a representative sample of crystals of the same habit using an optical microscope and mounted onto a nylon loop. Low temperature (110 K) X-ray data were obtained on a Bruker APEXII CCD based diffractometer (Mo sealed X-ray tube, $K_{\alpha} = 0.71073$ Å). All diffractometer manipulations, including data collection, integration and scaling were carried out using the Bruker APEXII software.¹⁵⁵ An absorption correction was applied using SADABS.¹⁵⁶ The space group was determined on the basis of systematic absences and intensity statistics and the structure was solved by direct methods and refined by full-matrix least squares on F^2 . The structure was solved in the monoclinic $P 2_1/n$ space group using XS¹⁵⁷ (incorporated in SHELXLE). All non-hydrogen atoms were refined with anisotropic thermal parameters. All hydrogen atoms were placed in idealized positions and refined using riding model with

the exception of the hydrogen bound to iridium which was located from the difference map. The structure was refined (weighted least squares refinement on F^2) and the final least-squares refinement converged. No additional symmetry was found using ADDSYM incorporated in PLATON program.¹⁵⁸

X-Ray data collection, solution, and refinement for 501g. A yellow, multi-faceted block of suitable size (0.75 x 0.57 x 0.25 mm) was selected from a representative sample of crystals of the same habit using an optical microscope and mounted onto a nylon loop. Low temperature (110 K) X-ray data were obtained on a Bruker APEXII CCD based diffractometer (Mo sealed X-ray tube, $K_{\alpha} = 0.71073 \text{ \AA}$). All diffractometer manipulations, including data collection, integration and scaling were carried out using the Bruker APEXII software.¹⁵⁵ An absorption correction was applied using SADABS.¹⁵⁶ The space group was determined on the basis of systematic absences and intensity statistics and the structure was solved by direct methods and refined by full-matrix least squares on F^2 . The structure was solved in the triclinic P 1 space group using XS¹⁵⁷ (incorporated in SHELXLE). All non-hydrogen atoms were refined with anisotropic thermal parameters. All hydrogen atoms were placed in idealized positions and refined using riding model with the exception of the hydrogen bound to iridium which was located from the difference map. The structure was refined (weighted least squares refinement on F^2) and the final least-squares refinement converged. Additional symmetry triclinic P -1 was found using ADDSYM incorporated in PLATON program.¹⁵⁸

X-Ray data collection, solution, and refinement for (PB^{Ph}P)Ir(H)(CO) (502). A yellow, multi-faceted block of suitable size (0.55 x 0.25 x 0.12 mm) was selected from

a representative sample of crystals of the same habit using an optical microscope and mounted onto a nylon loop. Low temperature (110 K) X-ray data were obtained on a Bruker APEXII CCD based diffractometer (Mo sealed X-ray tube, $K_{\alpha} = 0.71073 \text{ \AA}$). All diffractometer manipulations, including data collection, integration and scaling were carried out using the Bruker APEXII software.¹⁵⁵ An absorption correction was applied using SADABS.¹⁵⁶ The space group was determined on the basis of systematic absences and intensity statistics and the structure was solved by direct methods and refined by full-matrix least squares on F^2 . The structure was solved in the monoclinic $P 2_1/c$ space group using XS¹⁵⁷ (incorporated in SHELXLE). All non-hydrogen atoms were refined with anisotropic thermal parameters. All hydrogen atoms were placed in idealized positions and refined using riding model with the exception of the hydrogen bound to iridium which was located from the difference map. The structure was refined (weighted least squares refinement on F^2) and the final least-squares refinement converged. No additional symmetry was found using ADDSYM incorporated in PLATON program.¹⁵⁸

CHAPTER VI

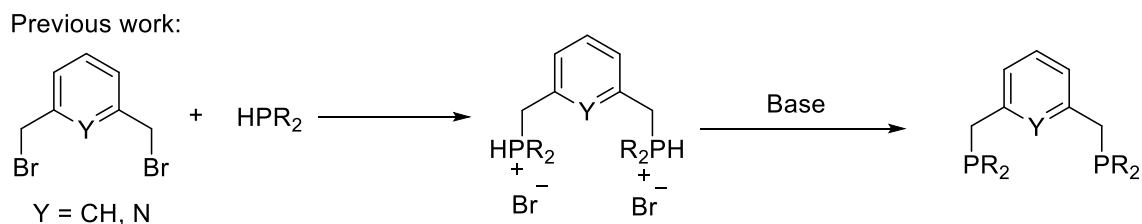
ONE-POT SYNTHESIS OF 1,3-BIS(PHOSPHINOMETHYL)ARENE PCP/PNP

PINCER LIGANDS AND THEIR NICKEL COMPLEXES[§]

6.1 Introduction

Pincer ligands are broadly used in organometallic chemistry.^{1,3-5} They are typically defined as ligands that preferentially bind to transition metals in a tridentate, meridional fashion. Pincer complexes often possess exceptional thermal stability, which may permit homogeneous catalysis at unusually high temperatures.⁶⁴ They are also prized for the opportunity to position the desired types of donors about the metal center in a predictable and persistent fashion. Among the many families of pincers, PCP and PNP ligands based on the bis(phosphinomethyl)benzene or -pyridine (Scheme VI-1, simply PCP and PNP from here on) frameworks hold a particularly venerated place. This is in part due to their historical significance,⁹ but also to the number of groundbreaking discoveries in which they have been instrumental.²²⁸⁻²³⁰

[§] Reproduced in part from “One-Pot Synthesis of 1,3-Bis(phosphinomethyl)arene PCP/PNP Pincer Ligands and Their Nickel Complexes” by Shih, W.-C.; Ozerov, O. V. *Organometallics* **2015**, *34*, 4591. Copyright [2015] by The American Chemical Society.

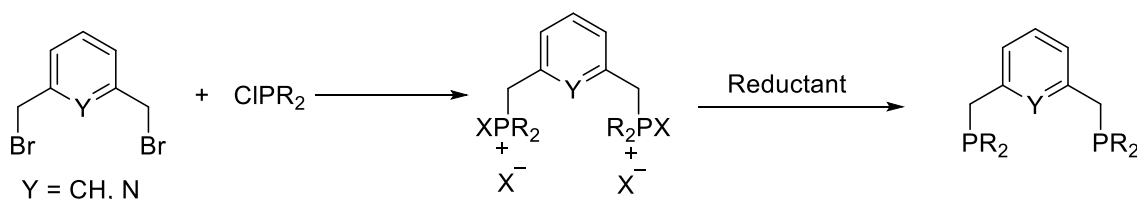


Scheme VI-1. Traditional Synthesis of PCP or PNP Ligands

The traditional synthesis of these ligands involves an S_N2 reaction of a secondary phosphine (HPR_2) with bis(bromomethyl)benzene or -pyridine, followed by deprotonation of the resultant bis(phosphonium) salt (Scheme VI-1).^{231–234} This type of synthesis works very well, but the reliance on the HPR_2 starting material is not ideal. Secondary phosphines of modest molecular weight are pyrophoric liquids, and the selection of commercially available secondary phosphines is rather limited. An equally reliable PCP/PNP synthesis utilizing chlorodiorganyl phosphines ($ClPR_2$) would be preferable because $ClPR_2$ are generally not pyrophoric (although still quite air- and moisture-sensitive), because a somewhat large variety of $ClPR_2$ compounds is commercially available, and because $ClPR_2$ compounds tend to be cheaper than their HPR_2 counterparts. The latter is understandable since most HPR_2 compounds are prepared by $LiAlH_4$ reduction of $ClPR_2$,^{235–237} a rather hazardous procedure on many counts.

We surmised that if $ClPR_2$ could successfully undergo an S_N2 reaction with halomethylarenes, then there should be a practical way to reduce the resultant halophosphonium salt to the desired phosphine (Scheme VI-2). $ClPR_2$ should possess reduced nucleophilicity compared to HPR_2 , but the reaction still appeared plausible. This report describes its successful implementation leading to a reliable method of preparation

of a series of PCP/PNP pincer ligands that obviates the need for secondary phosphines. We also describe the incorporation of this method into one-pot synthesis of PCP and PNP nickel complexes, inspired by the one-pot synthesis of related POCOP complexes of Ni by Zargarian et al.²³⁸



Scheme VI-2. New Method of Synthesis of PCP or PNP Ligands by Using ClPR₂

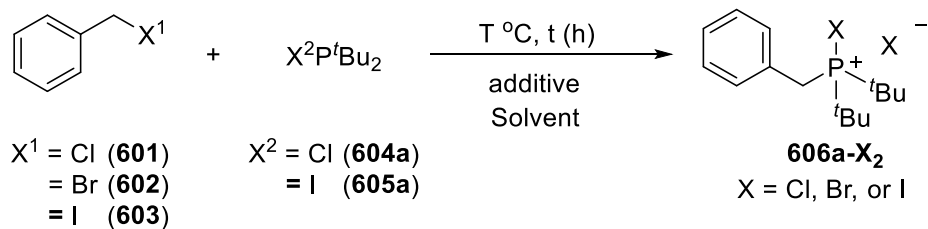
6.2 Results and Discussion

6.2.1 Synthesis of benzylphosphonium salts (606-X₂) and benzylphosphines (606)

To the best of our knowledge, the only precedent for the preparation of quaternary phosphonium salts by reactions of halodiorganyl phosphines with alkyl halides is the succinct report of Kabachnik et al.,²³⁹ in which iododiisopropylphosphine was shown to react with methyl, allyl, and benzyl halides. That work reported that chloro- and bromodialkylphosphines did not react, but without providing any details. We were eager to explore this reaction in greater depth in the context of the proposed phosphine ligand synthesis. Although alkyl chlorides are typically less expensive, many simple alkyl bromides and iodides are also commercially available. On the other hand, iododialkylphosphines are not, and the ability to use chlorodialkylphosphines would be strongly advantageous.

Instead of the bis(halomethyl)arenes required for pincer synthesis, we chose to explore benzyl halides (PhCH₂X, **601**~**603**) as simpler model substrates. We initially focused on their reactions²⁴⁰ with di-*tert*-butylchlorophosphine (**604a**), which we expected to be more challenging compared to smaller dialkylhalophosphines (Table VI-1). Gratifyingly, the reaction of PhCH₂Br (**602**) with **604a** proceeded to give the product of S_N2 addition in both CD₃CN and C₆D₆ as solvents (entries 1 and 2). The product formation was accelerated in the more polar acetonitrile (consistent with Hughes–Ingold rules for S_N2 reactions),²⁴¹ and further optimization was conducted in this solvent. Using benzyl chloride (**601**) as substrate resulted in a much lower conversion than with benzyl bromide (**602**) or benzyl iodide (**603**) (entries 2–4). The highest reactivity can be achieved by the reaction of benzyl iodide (**603**) with di-*tert*-butyliodophosphine (**605a**)²⁴² to afford 100% conversion in 15 h at room temperature (entry 5).

Table VI-1. Screening and Optimization of the Reaction of Benzyl Halide with Halodi-*tert*-butylphosphine^a



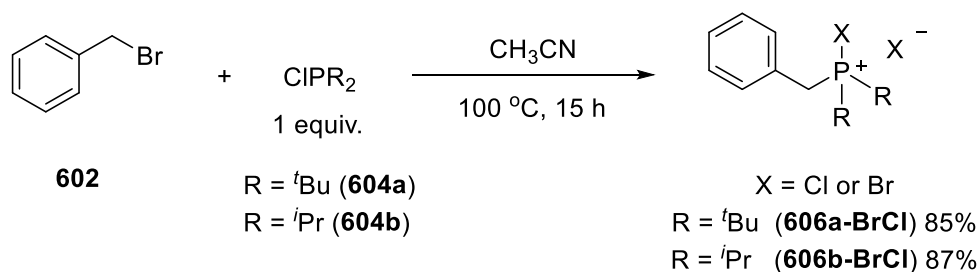
Entry	X ¹	X ²	additive	T (°C)	t (h)	Solvent	606a-X₂ (%) ^b
1	Br	Cl	--	50	15	C ₆ D ₆	22
2	Br	Cl	--	50	15	CD ₃ CN	90
3	Cl	Cl	--	50	15	CD ₃ CN	2
4	I	Cl	--	50	15	CD ₃ CN	100
5	I	I	--	r.t.	15	CD ₃ CN	100
6	Br	Cl	--	100	15	CD ₃ CN	100
7 ^c	Cl	Cl	NaI	50	15	CD ₃ CN	86
8 ^d	Cl	Cl	NaI	50	15	CD ₃ CN	100
9 ^e	Cl	Cl	NaI	50	20	CD ₃ CN	26
10 ^c	Cl	Cl	LiBr	50	15	CD ₃ CN	66

a. The reaction was carried out using **601~603** (0.2 mmol) and **604a~605a** (0.2 mmol) in C₆D₆ or CD₃CN in a J. Young NMR tube. b. The conversion was determined by ³¹P NMR and ¹H NMR. c. 1.0 equivalent of additive was added. d. 2.0 equivalent of additive was added. e. 0.1 equivalent of additive was added.

By using commercially available **602** and **604a**, the reaction can be brought to completion in 15 h at 100 °C (entry 6). Addition of 1 equiv of sodium iodide or lithium bromide accelerated the reaction between **601** and **604a**, leading to 86% or 66% conversion (entries 7 and 10) vs 2% without additives (entry 3). The use of 2 equiv of sodium iodide further improved the conversion under the same conditions to 100% (entry 8). Addition of 0.1 equiv of sodium iodide gave lower conversion, but the observed 26%

yield (entry 9) indicated that NaI accelerates the reaction as a catalyst. Both chlorides **601** and **604a** can undergo halide exchange with sodium iodide to form iodo-substituted compounds **603** and **605a**. Since **603** is a better S_N2 electrophile, access to it and regeneration of iodide anion upon S_N2 substitution is likely the mechanism of acceleration.

On the preparative scale (2 mmol), thermolysis of **602** and **604a** for 15 h at 100 °C led to **606a-BrCl** in 85% isolated yield. Analogously, the reaction of **602** with diisopropylchlorophosphine **604b** under the same conditions led to **606b-BrCl** in 87% isolated yield (Scheme VI-3). Available literature evidence indicates that R_3PX_2 (R = alkyl and X = Cl, Br, or I) are ionic compounds as $[R_3PX][X^-]$ with approximately tetrahedral phosphonium centers.^{243–245} We assume **606a-BrCl** and **606b-BrCl** are also ionic because of their poor solubility in benzene, toluene, diethyl ether, and THF.

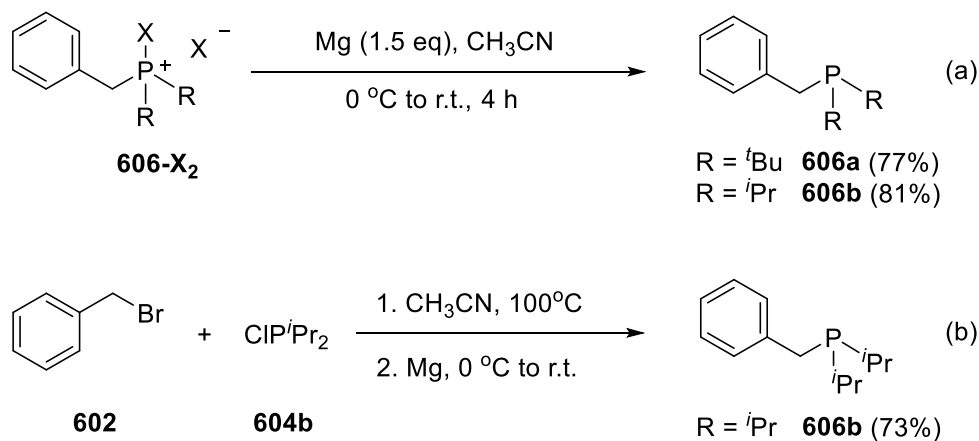


Scheme VI-3. Synthesis of Phosphonium Salts (**606-X₂**) from **604**

606a-BrCl showed two resonances at 115.8 and 117.1 ppm in a 1:9 ratio in the ³¹P NMR spectrum, which are presumed to be isomeric products with either a bromine or chlorine atom attached to the phosphorus atom. **606b-BrCl** showed only one broad

resonance at 111.2 ppm. This may be due to a stronger preference for one halide or a more rapid halide exchange. The observation of doublet signals for the benzylic protons of **606a-BrCl** (δ 4.69 ppm, $^2J_{\text{P-H}} = 7.3$ Hz) and **606b-BrCl** (δ 4.86 ppm, $^2J_{\text{P-H}} = 10$ Hz) in the ^1H NMR spectra was in agreement with the formation of benzylic C–P bonds.

Pure **606a-BrCl** and **606b-BrCl** were reduced by the reactions of **606-X₂** with magnesium powder in acetonitrile at 0 °C for 2 h. The reactions were allowed to stir at room temperature for another 2 h, affording benzyldialkylphosphines **606a** and **606b** in 77% and 81% isolated yields, respectively (Scheme VI-4a). A 73% overall isolated yield of **606b** was obtained by the reaction of **602** with **604b** followed by reduction in situ (Scheme VI-4b), showing that isolation of pure **606a-BrCl/606b-BrCl** was not necessary. Pure products **606a** and **606b** were obtained simply by pentane extraction from the crude mixture in acetonitrile. Two immiscible layers were formed, and the acetonitrile layer fortuitously retained not only magnesium halides but also the small amounts of various unidentified side products.



Scheme VI-4. Synthesis of Benzyldialkylphosphines (606) from 606-X₂

6.2.2 Synthesis of PCP and PNP ligands (610)

Having optimized the synthesis of benzyldialkylphosphines, we set out to tackle the one-pot synthesis of PCP or PNP pincer ligands from chlorophosphines **604** (Table VI-2). The reaction of 1,3-bis(bromomethyl)benzene (**607**) with **604b** in acetonitrile at 100 °C for 15 h produced a copious amount of a poorly soluble product, which is assumed to be the corresponding bis-phosphonium salt **610b-Br₂Cl₂**; it resonated at a frequency (δ 110.9 ppm) similar to **606b-BrCl** by ³¹P NMR spectroscopy. Reduction of this bis-phosphonium salt with magnesium powder in situ at 0 °C followed by gradual warming to ambient temperature gave the ⁱPr(PCP)H ligand **610b** in 70% overall isolated yield (entry 1). The analogous synthesis of the bulkier ^tBu(PCP)H (**610a**) from **607** and **604a** afforded a yellow, viscous oil in 76% yield, but only with ~75% purity. Attempts to purify **610a** by chromatography or recrystallization were unsuccessful. However, reaction of **608** and **604a** with 4 equiv of sodium iodide followed by reduction with Mg led to a pure off-white powder of **610a** in 64% isolated yield (entry 2, 0.5 g scale). On a larger scale, analogous preparation yielded 4.1 g as a 52% isolated yield of **610a**.

Table VI-2. Synthesis of Various PCP and PNP Ligands^a

$\text{X} = \text{Br}, \text{Y} = \text{CH}$ (**607**)
 $\text{X} = \text{Cl}, \text{Y} = \text{CH}$ (**608**)
 $\text{X} = \text{Br}, \text{Y} = \text{N}$ (**609**)

604 $\text{X} = \text{Cl or Br}$ (**610-X₄**) **610**

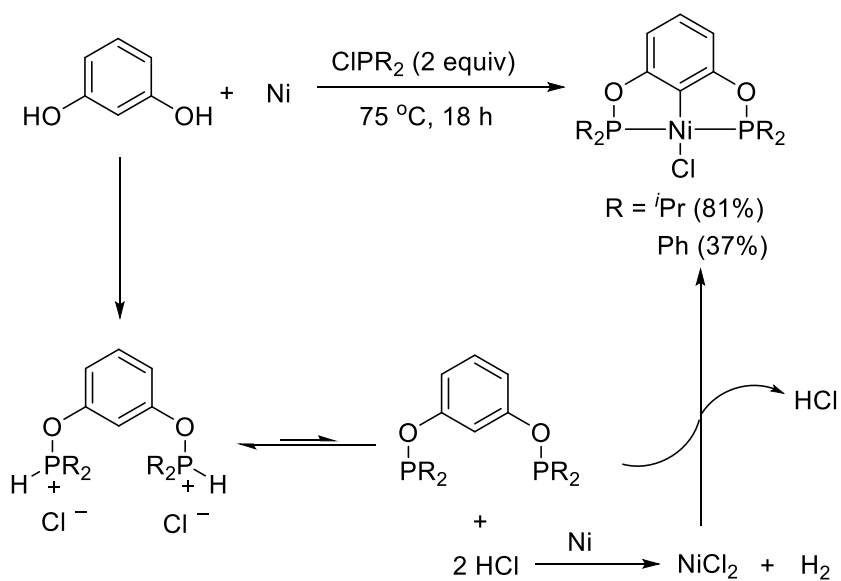
Entry	607~609	604	Product	Yield (%) ^b
1	607	ClP ^t Pr ₂ 604b	 610b	70
2 ^c	608	ClP ^t Bu ₂ 604a	 610a	64 (52) ^d
3	607	ClPEt ₂ 604c	 610c	78
4	607	ClPPh ₂ 604d	 610d	42
5	609	604b	 610e + 610e'	72:7

^a. General conditions: **607~609** (2.0 mmol) and **604** (4.0 mmol) in CH₃CN was stirred at 100 °C for 15 h, and then Mg powder (4.0-5.0 mmol) was added to the mixture. See Experimental Section for procedure details. ^b. Isolated yield. ^c. Sodium iodide (8.0 mmol) was added. ^d. Larger scale preparation: **608** (20.0 mmol) and **604a** (40.0 mmol) in CH₃CN with NaI was refluxed for 15 h, and then Mg powder (40.0 mmol) was added to the mixture. See Experimental Section for procedure details.

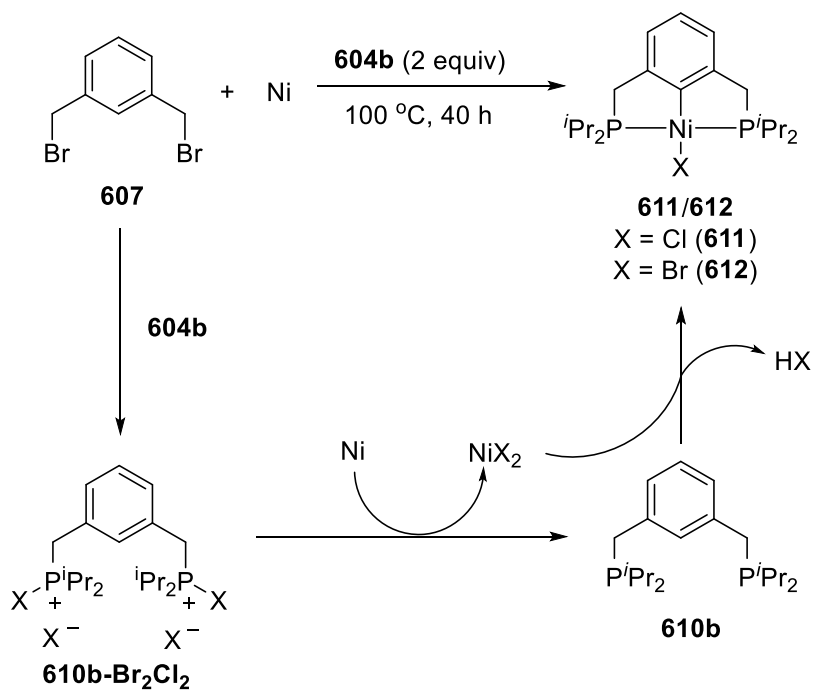
The less sterically imposing ligand $\text{Et}(\text{PCP})\text{H}$ (**610c**) was successfully isolated in 78% yield starting from **607** and **604c** (entry 3). Benzyl C–P bond cleavage was observed in the synthesis of $\text{Ph}(\text{PCP})\text{H}$ **610d** and $i\text{Pr}(\text{PNP})$ **610e**, which gave rise to the formation of (3-methylbenzyl)diphenylphosphine (**610d'**) and **610e'** as side products. The oily nature of **610e** and **610e'** precluded their separation (entry 5), but it proved possible to obtain pure **610d** in 42% yield by recrystallization (entry 4). The lower isolated yield of **610d** is due to lower conversion to **610d** and the need for an extra workup step to separate it from **610d'**.

6.2.3 Synthesis of PCP and PNP nickel complexes (611/612 and 614)

We envisaged that metallic powders other than Mg might be suitable for reduction of phosphonium salts and through it generate precursors for the formation of pincer complexes. This line of thought was inspired by the similar one-pot concept of synthesis of $\text{P}^{\text{O}}\text{C}^{\text{O}}\text{P}$ -type nickel complexes from metallic nickel powder, resorcinol, and **604b** reported by the Zargarian group (Scheme VI-5).²³⁸ In the Zargarian synthesis, the interaction of the ligand precursors can be viewed to produce HCl equivalents, which react with Ni(0) to give NiCl_2 for the metalation. On the other hand, our syntheses (Scheme VI-6) here can be viewed to produce formal dihalogen (X_2) equivalents that then give rise to NiX_2 .

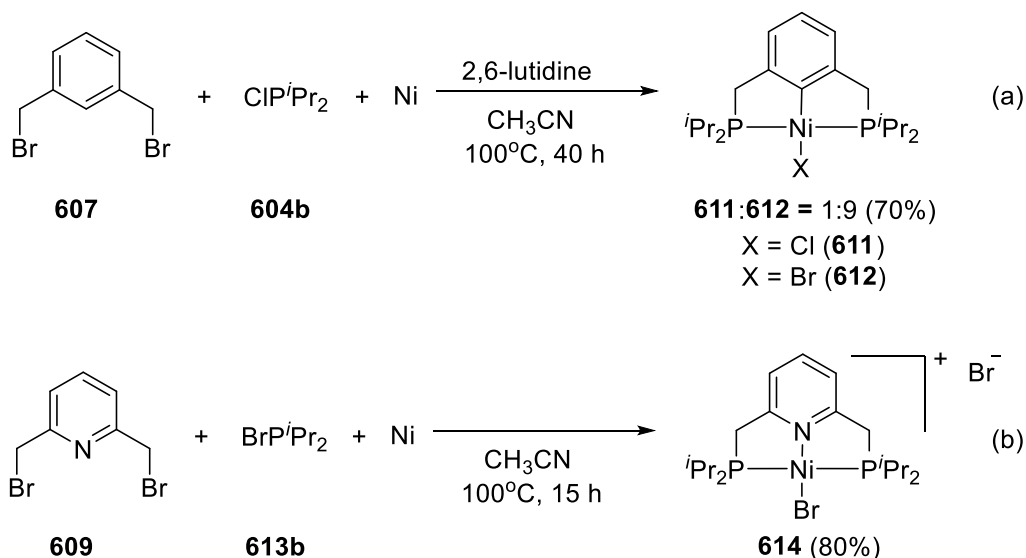


Scheme VI-5. Proposed Mechanism of (P^OC^OP)NiCl Formation in the Study by Zargarian et al.²³⁸



Scheme VI-6. Proposed Mechanism of (PCP)NiX Formation

When the mixture of **607**, **604b**, and metallic nickel powder in acetonitrile was heated at 100 °C for 40 h, the metalated products **611**²⁴⁶ and **612**^{247–249} were isolated in 50% combined yield. The reaction yield was increased to 70% by the addition of 1.0 equiv of 2,6-lutidine as base to the mixture of **604b**, **607**, and Ni prior to thermolysis (Scheme VI-7a). The ratio of **612** and **611** was ca. 9:1 based on the ³¹P NMR spectrum (**612**: δ 61.7 ppm, **611**: δ 60.6 ppm). The mixture could be fully converted to **612** by treatment with 2 equiv of lithium bromide in toluene at room temperature overnight. Most likely, the bis(halophosphonium) salt **610b-Br₂Cl₂** is formed first and then was reduced by Ni metal to give rise to **610a**, which undergoes metalation to **611/612** with NiX₂ formed in the reduction of **610b-Br₂Cl₂** (Scheme VII-6). The analogous [ⁱPr(PNP)NiBr][Br] complex **614** was also synthesized by the reaction of **609** and **613b**²⁵⁰ without base (Scheme VI-7b). In control experiments, Ni powder did not react with **604b** in CD₃CN (100 °C, 15 h) and gave only ca. 30% conversion of **607** under analogous conditions to benzyl radical coupling products containing Ar-CH₂-CH₂-Ar moieties (as evidenced by ¹H NMR resonances in the 2.8–3.0 ppm region). These products were not observed in the one-pot syntheses of **611/612**. It is worth noting that Ni powder can be added to the reaction mixture from the start, while Mg has to be added only after the formation of halophosphonium salts is allowed to take place.



Scheme VI-7. Synthesis of $^i\text{Pr}(\text{PCP})\text{NiX}$ (611/612**) and $[\text{}^i\text{Pr}(\text{PNP})\text{NiBr}][\text{Br}]$ (**614**)**

6.3 Conclusions

The synthesis of PCP- and PNP-type pincer ligands and their nickel complexes was achieved via utilization of inexpensive and commercially available chlorophosphines. Due to the electron-withdrawing nature of the chlorine atom on the phosphorus, chlorophosphines are weaker nucleophiles but safer reactants than secondary phosphines, particularly for the phosphines containing less sterically imposing alkyl groups. Moreover, we discovered metallic nickel powder was not only a suitable reagent for the reduction of halophosponium salts to phosphine ligands but also the nickel precursor for the formation of PCP and PNP nickel complexes. This synthetic strategy permits one-pot synthesis of PCP and PNP nickel complexes from commercially available, nonpyrophoric²⁵¹ materials.

6.4 Experimental Section

6.4.1 General considerations

Unless otherwise noted, all manipulations were performed under argon, using standard glovebox or Schlenk line techniques. Screw-cap culture tubes with PTFE-lined phenolic caps were used to perform reactions. Toluene, THF, pentane, and diethyl ether were dried and deoxygenated (by purging) using a solvent purification system (Innovative Technology Pure Solv MD-5 solvent purification system) and stored over molecular sieves in an Ar-filled glovebox. C₆D₆ was dried over NaK/Ph₂CO/18-crown-6, distilled, and stored over molecular sieves in an Ar-filled glovebox. Acetonitrile, CD₃CN, CDCl₃, CH₂Cl₂, CD₂Cl₂, and 2,6-lutidine were dried over CaH₂, distilled or vacuum transferred, and stored over molecular sieves in an Ar-filled glovebox. Benzyl chloride, benzyl bromide, and benzyl iodide were degassed by freeze–pump–thaw and stored over molecular sieves in an Ar-filled glovebox. Sodium iodide was purified by recrystallization in acetone and dried under vacuum at 70 °C for 12 h. Celite and silica gel were dried at 200 °C overnight under vacuum and then stored inside a glovebox. All other chemicals were used as received from commercial vendors.

6.4.2 Physical methods

NMR spectra were recorded on a Varian Inova 300, Mercury 300 (¹H NMR, 299.952 MHz; ¹³C NMR, 75.421 MHz; ³¹P NMR, 121.422 MHz), and Inova NMR 500 (¹H NMR, 499.703 MHz; ¹³C NMR, 125.697 MHz; ³¹P NMR, 202.265 MHz) spectrometers. Chemical shifts are reported in δ (ppm). For ¹H and ¹³C NMR, the residual

solvent peak was used to reference the spectra (^1H NMR: δ 7.16 for C_6D_6 , 7.26 for CDCl_3 , 5.32 for CD_2Cl_2 , and 1.94 for CD_3CN ; ^{13}C NMR: δ 128.06 for C_6D_6 , 77.16 for CDCl_3 , 53.84 for CD_2Cl_2 , and 118.26 for CD_3CN).

6.4.3 Synthesis and characterization

Synthesis of Di-*tert*-butyliodophosphine (605a): *Method A.* In a 25 mL Schlenk flask, to the toluene solution (10 mL) of di-*tert*-butylchlorophosphine (**604a**, 1.80 g, 10.0 mmol) was added sodium iodide (3.00 g, 20.0 mmol), and the reaction mixture was stirred at room temperature for 24 h. After the solution was quickly filtered through a short pad of Celite and silica gel, the filtrate was collected and the volatiles were removed under vacuum, yielding a yellow liquid that appeared ca. 95% pure by NMR spectroscopy. Isolated yield: 2.24 g, 82%. *Method B.* In a 10 mL Schlenk flask, to the pentane solution (1 mL) of di-*tert*-butylchlorophosphine (**604a**, 90 mg, 0.50 mmol) was added trimethylsilyl iodide (200 mg, 1.00 mmol), and the reaction mixture was stirred at room temperature for 10 min. After the solution was filtered through a pad of Celite, the filtrate was collected and the volatiles were removed under vacuum, yielding a yellow liquid (129 mg, 95%) that appeared >98% pure by NMR spectroscopy. ^1H NMR (500 MHz, C_6D_6): δ 1.19 (d, $J_{\text{H-P}} = 12.0$ Hz, 18 H). $^{13}\text{C}\{^1\text{H}\}$ NMR (126 MHz, C_6D_6): δ 33.1 (d, $J_{\text{P-C}} = 47.0$ Hz), 29.7 (d, $J_{\text{P-C}} = 16.4$ Hz). $^{31}\text{P}\{^1\text{H}\}$ NMR (202 MHz, C_6D_6): δ 135.8.

Synthesis of Bromodiisopropylphosphine (613b): In a 25 mL Schlenk flask, to the toluene solution (10 mL) of chlorodiisopropylphosphine (**604b**, 1.53 g, 10.0 mmol) was added lithium bromide (1.74 g, 20.0 mmol), and the reaction mixture was stirred at

room temperature for 24 h. After the solution was filtered through a pad of Celite and silica gel, the filtrate was collected and the volatiles were removed under vacuum, yielding a colorless liquid. Isolated yield: 1.58 g, 80%. ^1H NMR (500 MHz, C_6D_6): δ 1.70 (m, 2 H), 0.98 (dd, $J_{\text{H-H}} = 13$ Hz, $J_{\text{H-P}} = 6.8$ Hz, 12 H). $^{13}\text{C}\{^1\text{H}\}$ NMR (126 MHz, C_6D_6): δ 28.1 (d, $J_{\text{P-C}} = 34$ Hz), 18.6 (d, $J_{\text{P-C}} = 14$ Hz). $^{31}\text{P}\{^1\text{H}\}$ NMR (202 MHz, C_6D_6): δ 134.7. HRMS (ESI): calcd for $\text{C}_6\text{H}_{14}\text{BrLiP}$ ($\text{M} + \text{Li}$) $^+$ 203.0177, found 203.0178.

Synthesis of 606a-BrCl: In a screw-cap culture tube, to the acetonitrile solution (10 mL) of benzyl bromide (342 mg, 2.00 mmol) was added **604a** (361 mg, 2.00 mmol), and the reaction mixture was stirred at 100 °C for 15 h. After cooling to room temperature, the volatiles were removed under vacuum, and the product was washed with pentane, yielding a white solid. Isolated yield: 597 mg, 85%. The product was a mixture of two isomers in ca. 9:1 ratio based on ^{31}P NMR (117.1 and 115.8 ppm) and ^1H NMR spectra. The spectroscopic data for the major isomer follow. ^1H NMR (500 MHz, CD_3CN): δ 7.61 (m, 2 H), 7.41 (m, 3 H), 4.69 (d, $J_{\text{P-H}} = 7.3$ Hz, 2 H), 1.52 (d, $J_{\text{P-H}} = 19$ Hz, 18 H). $^{13}\text{C}\{^1\text{H}\}$ NMR (126 MHz, CD_3CN): δ 132.2 (d, $J_{\text{P-C}} = 5.7$ Hz), 130.0 (s), 129.7 (m), 129.5 (d, $J_{\text{P-C}} = 11$ Hz), 42.3 (d, $J_{\text{P-C}} = 23$ Hz), 29.5 (d, $J_{\text{P-C}} = 27$ Hz), 27.0 (d, $J_{\text{P-C}} = 4.8$ Hz). $^{31}\text{P}\{^1\text{H}\}$ NMR (202 MHz, CD_3CN): δ 117.1. HRMS (MALDI): calcd for $\text{C}_{15}\text{H}_{25}\text{ClP}$ ($\text{M} - \text{Br}$) $^+$ 271.1376, found 271.1360.

Synthesis of 606b-BrCl: In a screw-cap culture tube, to the acetonitrile solution (10 mL) of benzyl bromide (342 mg, 2.00 mmol) was added **604b** (305 mg, 2.00 mmol), and the reaction mixture was stirred at 100 °C for 15 h. After cooling to room temperature, the volatiles were removed under vacuum, and the product was washed with pentane,

yielding a white solid. Isolated yield: 560 mg, 87%. ^1H NMR (500 MHz, CD_3CN): δ 7.57 (m, 2 H), 7.40 (m, 3 H), 4.86 (d, $J_{\text{P-H}} = 10$ Hz, 2 H), 3.43 (m, 2 H), 1.32 (dd, $J_{\text{P-H}} = 21$ Hz, $J_{\text{H-H}} = 7.0$ Hz, 12 H). $^{13}\text{C}\{^1\text{H}\}$ NMR (126 MHz, CD_3CN): δ 131.8 (d, $J_{\text{P-C}} = 5.9$ Hz), 130.2 (d, $J_{\text{P-C}} = 2.7$ Hz), 129.8 (m), 128.4 (d, $J_{\text{P-C}} = 10$ Hz), 31.4 (d, $J_{\text{P-C}} = 32$ Hz), 28.4 (d, $J_{\text{P-C}} = 33$ Hz), 16.5 (s). $^{31}\text{P}\{^1\text{H}\}$ NMR (202 MHz, CD_3CN): δ 111.2 (br s).

Synthesis of $\text{PhCH}_2\text{P}^i\text{Bu}_2$ (606a): In a screw-cap culture tube, to the acetonitrile solution (5 mL) of **606a-BrCl** (352 mg, 1.00 mmol) was added magnesium powder (37 mg, 1.50 mmol), and the reaction mixture was stirred at 0 °C for 2 h. The reaction was allowed to warm to room temperature and stirred for another 2 h. The product was extracted with pentane (3×10 mL), and the volatiles were removed under vacuum, yielding a yellow oil. Isolated yield: 191 mg, 81%. ^1H NMR (500 MHz, CDCl_3): δ 7.32 (d, $J_{\text{H-H}} = 7.5$ Hz, 2 H), 7.21 (t, $J_{\text{H-H}} = 7.6$ Hz, 2 H), 7.09 (t, $J_{\text{H-H}} = 7.2$ Hz, 1 H), 2.83 (d, $J_{\text{P-H}} = 3.0$ Hz, 2 H), 1.12 (d, $J_{\text{P-H}} = 11$ Hz, 18 H). $^{13}\text{C}\{^1\text{H}\}$ NMR (126 MHz, CDCl_3): δ 141.5 (d, $J_{\text{P-C}} = 12$ Hz), 129.5 (d, $J_{\text{P-C}} = 8.5$ Hz), 128.2, 125.3 (d, $J_{\text{P-C}} = 2.1$ Hz), 31.8 (d, $J_{\text{P-C}} = 22$ Hz), 29.8 (d, $J_{\text{P-C}} = 13$ Hz), 28.5 (d, $J_{\text{P-C}} = 24$ Hz). $^{31}\text{P}\{^1\text{H}\}$ NMR (202 MHz, CDCl_3): δ 35.9. NMR spectroscopic data were consistent with those previously reported in the literature.^{233,252}

Synthesis of $\text{PhCH}_2\text{P}^i\text{Pr}_2$ (606b): In a screw-cap culture tube, to the acetonitrile solution (5 mL) of **606b-BrCl** (324 mg, 1.00 mmol) was added magnesium powder (37 mg, 1.50 mmol), and the reaction mixture was stirred at 0 °C for 2 h. The reaction was allowed to warm to room temperature and stirred for another 2 h. The product was extracted with pentane (3×5 mL), and the volatiles were removed under vacuum, yielding

a colorless oil. Isolated yield: 161 mg, 77%. ^1H NMR (500 MHz, CD_2Cl_2): δ 7.29 (m, 4 H), 7.17 (m, 1 H), 2.82 (d, $J_{\text{P-H}} = 1.6$ Hz, 2 H), 1.78 (dsp, $J_{\text{P-H}} = 2.0$ Hz, $J_{\text{H-H}} = 7.1$ Hz, 2 H), 1.09 (m, 12 H). $^{13}\text{C}\{^1\text{H}\}$ NMR (126 MHz, CD_2Cl_2): δ 141.0 (d, $J_{\text{P-C}} = 8.5$ Hz), 129.8 (d, $J_{\text{P-C}} = 6.9$ Hz), 128.7 (d, $J_{\text{P-C}} = 0.8$ Hz), 125.8 (d, $J_{\text{P-C}} = 2.2$ Hz), 30.1 (d, $J_{\text{P-C}} = 21$ Hz), 23.9 (d, $J_{\text{P-C}} = 15$ Hz), 20.0 (d, $J_{\text{P-C}} = 14$ Hz), 19.5 (d, $J_{\text{P-C}} = 11$ Hz). $^{31}\text{P}\{^1\text{H}\}$ NMR (202 MHz, CD_2Cl_2): δ 12.2. NMR spectroscopic data were consistent with those previously reported in the literature.¹⁷⁹

One-Pot Synthesis of $\text{PhCH}_2\text{P}^i\text{Pr}_2$ (606b): In a screw-cap culture tube, to the acetonitrile solution (10 mL) of benzyl bromide (342 mg, 2.00 mmol) was added **604b** (305 mg, 2.00 mmol), and the reaction mixture was stirred at 100 °C for 15 h. After cooling to room temperature, magnesium powder (73 mg, 3.00 mmol) was added under argon, and the reaction mixture was stirred at 0 °C for 2 h. The reaction was allowed to warm to room temperature and stirred for another 2 h. The product was extracted by pentane (3×20 mL), and the volatiles were removed under vacuum, yielding a yellow oil. Isolated yield: 305 mg, 73%. ^1H NMR (500 MHz, CD_2Cl_2): δ 7.29 (m, 4 H), 7.17 (m, 1 H), 2.82 (d, $J_{\text{P-H}} = 1.6$ Hz, 2 H), 1.78 (dsp, $J_{\text{P-H}} = 2.0$ Hz, $J_{\text{H-H}} = 7.1$ Hz, 2 H), 1.09 (m, 12 H). $^{13}\text{C}\{^1\text{H}\}$ NMR (126 MHz, CD_2Cl_2): δ 141.0 (d, $J_{\text{P-C}} = 8.5$ Hz), 129.8 (d, $J_{\text{P-C}} = 6.9$ Hz), 128.7 (d, $J_{\text{P-C}} = 0.8$ Hz), 125.8 (d, $J_{\text{P-C}} = 2.2$ Hz), 30.1 (d, $J_{\text{P-C}} = 21$ Hz), 23.9 (d, $J_{\text{P-C}} = 15$ Hz), 20.0 (d, $J_{\text{P-C}} = 14$ Hz), 19.5 (d, $J_{\text{P-C}} = 11$ Hz). $^{31}\text{P}\{^1\text{H}\}$ NMR (202 MHz, CD_2Cl_2): δ 12.2. NMR spectroscopic data were consistent with those previously reported in the literature.¹⁷⁹

Synthesis of ⁱPr(PCP)H (610b): In a screw-cap culture tube, to the acetonitrile solution (10 mL) of *m*-xylylene dibromide (**607**) (528 mg, 2.00 mmol) was added **604b** (610 mg, 4.00 mmol), and the reaction mixture was stirred at 100 °C for 15 h. After cooling to room temperature, magnesium powder (122 mg, 5.00 mmol) was added under argon, and the reaction mixture was stirred at 0 °C for 2 h. The reaction was allowed to warm to room temperature and stirred for another 2 h. The product was extracted with pentane (3 × 20 mL), and the volatiles were removed under vacuum, yielding a yellow oil. Isolated yield: 472 mg, 70%. ¹H NMR (300 MHz, C₆D₆): δ 7.47 (br s, 1 H), 7.18 (m, 3 H), 2.70 (br s, 4 H), 1.62 (dsp, *J*_{P-H} = 1.9 Hz, *J*_{H-H} = 7.1 Hz, 4 H), 1.04 (d, *J*_{H-H} = 7.0 Hz, 12 H), 1.00 (dd, *J*_{P-H} = 0.9 Hz, *J*_{H-H} = 7.0 Hz, 12 H). ¹³C{¹H} NMR (126 MHz, C₆D₆): δ 140.5 (d, *J*_{P-C} = 7.4 Hz), 130.9 (vt, *J*_{P-C} = 7.0 Hz), 128.6 (s), 127.0 (dd, *J*_{P-C} = 7.2 Hz, *J*_{P-C} = 2.1 Hz), 30.3 (d, *J*_{P-C} = 22 Hz), 23.8 (d, *J*_{P-C} = 16 Hz), 19.9 (d, *J*_{P-C} = 14 Hz), 19.5 (d, *J*_{P-C} = 12 Hz). ³¹P{¹H} NMR (121 MHz, C₆D₆): δ 10.3. NMR spectroscopic data were consistent with those previously reported in the literature.²⁵³

Synthesis of ^tBu(PCP)H (610a): In a screw-cap culture tube, to the acetonitrile solution (10 mL) of *m*-xylylene dichloride (**608**) (350 mg, 2.00 mmol) were added **604a** (723 mg, 4.00 mmol) and sodium iodide (1.20 g, 8.00 mmol), and the reaction mixture was stirred at 100 °C for 15 h. After cooling to room temperature, magnesium powder (97 mg, 4.00 mmol) was added under argon, and the reaction mixture was stirred at room temperature for 36 h. The product was extracted with pentane (3 × 20 mL), and the volatiles were removed under vacuum, yielding an off-white solid. Isolated yield: 507 mg, 64%. ¹H NMR (500 MHz, C₆D₆): δ 7.59 (br s, 1 H), 7.26 (d, *J*_{P-H} = 7.5 Hz, 2 H), 7.14

(m, 1 H), 2.76 (d, $J_{\text{P-H}} = 2.0$ Hz, 4 H), 1.06 (d, $J_{\text{P-H}} = 11$ Hz, 36 H). $^{13}\text{C}\{^1\text{H}\}$ NMR (126 MHz, C_6D_6): δ 141.7 (d, $J_{\text{P-C}} = 12$ Hz), 131.5 (vt, $J_{\text{P-C}} = 8.4$ Hz), 128.4 (s), 127.2 (dd, $J_{\text{P-C}} = 9.2$ Hz, $J_{\text{P-C}} = 1.8$ Hz), 31.8 (d, $J_{\text{P-C}} = 25$ Hz), 30.1 (d, $J_{\text{P-C}} = 14$ Hz), 29.2 (d, $J_{\text{P-C}} = 26$ Hz). $^{31}\text{P}\{^1\text{H}\}$ NMR (202 MHz, C_6D_6): δ 33.6. NMR spectroscopic data were consistent with those previously reported in the literature.²³⁵

Larger Scale Preparation of $^t\text{Bu}(\text{PCP})\text{H}$ (610a): In a 250 mL Schlenk flask, to the acetonitrile solution (100 mL) of *m*-xylylene dichloride (**608**) (3.50 g, 20.0 mmol) were added **604a** (7.23 g, 40.0 mmol) and sodium iodide (12.0 g, 80.0 mmol), and the reaction mixture was refluxed under argon for 15 h. After cooling to room temperature, magnesium powder (0.97 g, 40.0 mmol) was added under argon, and the reaction mixture was stirred at room temperature for 36 h. The reaction was filtered through a pad of silica gel, and the product was extracted with pentane (3×75 mL). The volatiles were removed under vacuum, yielding an off-white solid. Isolated yield: 4.10 g, 52%. ^1H NMR (500 MHz, C_6D_6): δ 7.59 (br s, 1 H), 7.26 (d, $J_{\text{P-H}} = 7.5$ Hz, 2 H), 7.14 (m, 1 H), 2.76 (d, $J_{\text{P-H}} = 2.0$ Hz, 4 H), 1.06 (d, $J_{\text{P-H}} = 11$ Hz, 36 H). $^{13}\text{C}\{^1\text{H}\}$ NMR (126 MHz, C_6D_6): δ 141.7 (d, $J_{\text{P-C}} = 12$ Hz), 131.5 (vt, $J_{\text{P-C}} = 8.4$ Hz), 128.4 (s), 127.2 (dd, $J_{\text{P-C}} = 9.2$ Hz, $J_{\text{P-C}} = 1.8$ Hz), 31.8 (d, $J_{\text{P-C}} = 25$ Hz), 30.1 (d, $J_{\text{P-C}} = 14$ Hz), 29.2 (d, $J_{\text{P-C}} = 26$ Hz). $^{31}\text{P}\{^1\text{H}\}$ NMR (202 MHz, C_6D_6): δ 33.6. NMR spectroscopic data were consistent with those previously reported in the literature.²³⁵

Synthesis of $^{\text{Et}}(\text{PCP})\text{H}$ (610c): In a screw-cap culture tube, to the acetonitrile solution (10 mL) of **607** (528 mg, 2.00 mmol) was added diethylchlorophosphine (**604c**, 498 mg, 4.00 mmol), and the reaction mixture was stirred at 100 °C for 15 h. After cooling

to room temperature, magnesium powder (122 mg, 5.00 mmol) was added under argon, and the reaction mixture was stirred at 0 °C for 2 h. The reaction was allowed to warm to room temperature and stirred for another 2 h. The product was extracted with pentane (3 × 20 mL), and the volatiles were removed under vacuum, yielding a colorless oil. Isolated yield: 440 mg, 78%. ¹H NMR (500 MHz, C₆D₆): δ 7.11 (t, *J*_{H-H} = 8.0 Hz, 1 H), 7.08 (m, 1 H), 6.97 (m, 2 H), 2.61 (s, 4 H), 1.21 (m, 8 H), 0.96 (t, *J*_{H-H} = 7.1 Hz, 6 H), 0.93 (t, *J*_{H-H} = 7.1 Hz, 6 H). ¹³C{¹H} NMR (126 MHz, C₆D₆): δ 138.8 (dd, *J*_{P-C} = 3.9 Hz, *J*_{P-C} = 1.2 Hz), 130.4 (vt, *J*_{P-C} = 5.4 Hz), 128.5 (vt, *J*_{P-C} = 1.0 Hz), 126.8 (dd, *J*_{P-C} = 5.3 Hz, *J*_{P-C} = 2.0 Hz), 34.3 (d, *J*_{P-C} = 19 Hz), 19.3 (d, *J*_{P-C} = 15 Hz), 10.0 (d, *J*_{P-C} = 14 Hz). ³¹P{¹H} NMR (202 MHz, C₆D₆): δ -15.9. HRMS (ESI): calcd for C₁₆H₂₉P₂ (M + H)⁺ 283.1745, found 283.1746.

Synthesis of Ph(PCP)H (610d): In a screw-cap culture tube, to the acetonitrile solution (10 mL) of **607** (528 mg, 2.00 mmol) was added diphenylchlorophosphine (**604d**, 882 mg, 4.00 mmol), and the reaction mixture was stirred at 100 °C for 20 h. After cooling to room temperature, magnesium powder (97.2 mg, 4.00 mmol) was added under argon, and the reaction mixture was stirred at 0 °C for 2 h. The reaction was allowed to warm to room temperature and stirred for another 2 h. The volatiles were removed under vacuum, and then the product was extracted with THF and filtered through Celite. The filtrate was layered with pentane and placed in the freezer (-35 °C) overnight, yielding a white crystalline solid. Isolated yield: 400 mg, 42%. ¹H NMR (500 MHz, C₆D₆): δ 7.35 (m, 8 H), 7.05 (m, 13 H), 6.87 (t, *J*_{H-H} = 7.5 Hz, 1 H), 6.80 (m, 2 H) 3.20 (s, 4 H). ¹³C{¹H} NMR (126 MHz, C₆D₆): δ 139.2 (d, *J*_{P-C} = 17 Hz), 137.9 (dd, *J*_{P-C} = 8.2 Hz, *J*_{P-C} = 1.6 Hz),

133.3 (d, $J_{P-C} = 19$ Hz), 131.0 (vt, $J_{P-C} = 7.1$ Hz), 128.8 (s), 128.6 (d, $J_{P-C} = 6.5$ Hz), 128.4 (s), 127.4 (dd, $J_{P-C} = 6.9$ Hz, $J_{P-C} = 2.5$ Hz), 36.3 (d, $J_{P-C} = 17$ Hz). $^{31}\text{P}\{^1\text{H}\}$ NMR (202 MHz, C_6D_6): δ -9.9. NMR spectroscopic data were consistent with those previously reported in the literature.²⁵⁴

Synthesis of $^{i\text{Pr}}(\text{PNP})$ (610e): In a screw-cap culture tube, to the acetonitrile solution (10 mL) of 2,6-bis(bromomethyl)pyridine (**609**, 532 mg, 2.00 mmol) was added **604b** (610 mg, 4.00 mmol), and the reaction mixture was stirred at 100 °C for 15 h. After cooling to room temperature, magnesium powder (97.2 mg, 4.00 mmol) was added under argon, and the reaction mixture was stirred at 0 °C for 2 h. The reaction was allowed to warm to room temperature and stirred for 2 h. The product was extracted with pentane (3×20 mL), and the volatiles were removed under vacuum, yielding a yellow oil. The product was a mixture of **610e** and **610e'**, and the ratio was about 9:1 based on the ^1H NMR spectrum. Total yield: 519 mg, 79%. The NMR spectroscopic data for **610e** follow. ^1H NMR (500 MHz, CDCl_3): δ 7.42 (t, $J_{H-H} = 8.0$ Hz, 1 H), 7.07 (d, $J_{H-H} = 8.0$ Hz, 2 H), 2.92 (d, $J_{P-H} = 2.2$ Hz, 4 H), 1.77 (dsp, $J_{P-H} = 2.0$ Hz, $J_{H-H} = 7.0$ Hz, 4 H), 1.03 (m, 24 H). $^{13}\text{C}\{^1\text{H}\}$ NMR (126 MHz, CDCl_3): δ 159.9 (d, $J_{P-C} = 9.0$ Hz), 136.2 (s), 120.5 (d, $J_{P-C} = 7.7$ Hz), 32.5 (d, $J_{P-C} = 21$ Hz), 23.6 (d, $J_{P-C} = 14$ Hz), 19.8 (d, $J_{P-C} = 15$ Hz), 19.2 (d, $J_{P-C} = 11$ Hz). $^{31}\text{P}\{^1\text{H}\}$ NMR (202 MHz, CDCl_3): δ 12.7. NMR spectroscopic data were consistent with those previously reported in the literature.²⁵⁵

Synthesis of $^{i\text{Pr}}(\text{PCP})\text{NiBr}$ (612): In a screw-cap culture tube, to the acetonitrile solution (10 mL) of **607** (528 mg, 2.00 mmol) were added nickel powder (294 mg, 5.00 mmol), **604b** (610 mg, 4.00 mmol), and 2,6-lutidine (214 mg, 2.00 mmol). The reaction

mixture was stirred at 100 °C for 40 h. After cooling to room temperature, diethyl ether (3 × 10 mL) was added and the mixture was filtered through silica gel. The filtrate was collected, and the volatiles were removed under vacuum, yielding a yellow solid. Isolated yield: 659 mg, 70%. The product was a mixture of **612** and **611**, and the ratio was about 9:1 based on the ³¹P NMR spectrum (61.7 ppm for **612** and 60.6 ppm for **611**). The mixture can be fully converted to **612** by reacting the mixture with 2 equiv of lithium bromide in toluene at rt overnight. The NMR spectroscopic data for **612** follow. ¹H NMR (500 MHz, CD₂Cl₂): δ 6.91 (br s, 3 H), 3.09 (vt, $J_{P-H} = 4.0$ Hz, 4 H), 2.37 (m, 4 H), 1.45 (dvt, $J_{H-H} \approx J_{P-H} \approx 7.8$ Hz, 12 H), 1.18 (dvt, $J_{H-H} \approx J_{P-H} \approx 7.0$ Hz, 12 H). ¹³C{¹H} NMR (126 MHz, CD₂Cl₂): δ 159.5 (vt, $J_{P-C} = 16$ Hz), 152.8 (vt, $J_{P-C} = 13$ Hz), 125.5 (s), 122.5 (vt, $J_{P-C} = 8.9$ Hz), 33.1 (vt, $J_{P-C} = 13$ Hz), 24.2 (vt, $J_{P-C} = 11$ Hz), 19.1 (s), 18.3 (s). ³¹P{¹H} NMR (202 MHz, CD₂Cl₂): δ 61.7. NMR spectroscopic data were consistent with those previously reported in the literature.²⁴⁹

Synthesis of [ⁱPr(PNP)NiBr][Br] (614**):** In a screw-cap culture tube, to the acetonitrile solution (2 mL) of **609** (53 mg, 0.20 mmol) were added nickel powder (29 mg, 0.50 mmol) and **613b** (90 mg, 0.40 mmol). The reaction mixture was stirred at 100 °C for 15 h. After cooling to room temperature, the volatiles were removed under vacuum, and the product was extracted with CH₂Cl₂ and filtered through Celite. The filtrate was collected, and the volatiles were removed under vacuum. The resulting residue was washed with THF and then dried under vacuum, yielding a brown solid. Isolated yield: 94 mg, 80%. ¹H NMR (500 MHz, CD₃CN): δ 8.09 (br, 1 H), 7.78 (d, $J_{H-H} = 6.7$ Hz, 2 H), 3.79 (s, 4 H), 2.50 (br s, 4 H), 1.53 (dvt, $J_{H-H} \approx J_{P-H} \approx 8.0$ Hz, 12 H), 1.38 (dvt, $J_{H-H} \approx J_{P-}$

$\text{H} \approx 7.3$ Hz, 12 H). ^1H NMR (500 MHz, CDCl_3): δ 11.23 (br s, 2 H), 9.72 (br s, 1 H), 5.17 (br s, 4 H), 2.99 (br s, 4 H), 2.09 (br s, 12 H), 1.92 (br s, 12 H). $^{13}\text{C}\{^1\text{H}\}$ NMR (126 MHz, CDCl_3): δ 165.4, 147.5, 125.5, 36.2, 25.6 (vt, $J_{\text{P-C}} = 13$ Hz), 25.0, 20.3. $^{31}\text{P}\{^1\text{H}\}$ NMR (202 MHz, CD_3CN): δ 50.5. $^{31}\text{P}\{^1\text{H}\}$ NMR (202 MHz, CDCl_3): 50.3. NMR spectroscopic data were similar to $[\text{iPr}(\text{PNP})\text{NiCl}][\text{Cl}]$ previously reported in the literature.²⁵⁶

6.4.4 General procedure for screening and optimization of synthesis of Phosphonium

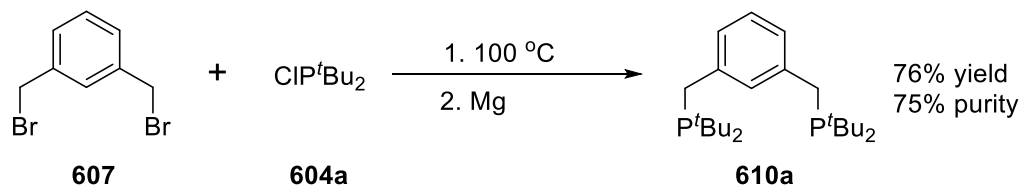
Salts (606a-X₂)

Table VI-1, Entry 1~6: In a J. Young NMR tube, the reactin of **601~603** (0.20 mmol, 23.0 μL for **601**, 24.0 μL for **602**, and 43.6 mg for **603**) and **604a~605a** (0.20 mmol, 38.0 μL for **604a** and 54.4 mg for **605a**) in 0.7 mL of C_6D_6 (Entry 1) or CD_3CN (Entry 2~6) was heated at the required temperature as indicated in Table 1 for 15 h. After the reaction was cooled to room temperature, the conversion was determined by ^{31}P NMR and ^1H NMR.

Table VI-1, Entry 7~10: In a J. Young NMR tube, to the CD_3CN (0.7 mL) solution of **601** (23.0 μL , 0.20 mmol) and **604a** (38.0 μL , 0.20 mmol) was added sodium iodide (30.0 mg, 0.20 mmol for Entry 7; 60.0 mg, 0.40 mmol for Entry 8; 3.00 mg, 0.02 mmol for Entry 9) or lithium bromide (17.4 mg, 0.20 mmol for Entry 10). The mixture was heated at 50 °C for 15 h (Entry 7, 8, and 10) or 20 h (Entry 9). After the reaction was cooled to room temperature, the conversion was determined by ^{31}P NMR and ^1H NMR.

6.4.5 Synthesis of ^tBu(PCP)H by different methods

In a Screw cap culture tube, to the acetonitrile solution (10 mL) of *m*-xylylene dibromide (**607**, 528 mg, 2.00 mmol) was added di-*tert*-butylchlorophosphine (**604a**, 723 mg, 4.00 mmol), and the reaction mixture was stirred at 100 °C for 15 h. After cooling down to room temperature, magnesium powder (122 mg, 5.00 mmol) was added under argon, and the reaction mixture was stirred at 0 °C for 2 h. The reaction was allowed to warm to room temperature and stirred overnight. The product was extracted by pentane (3 × 20 mL), and the volatiles were removed under vacuum, yielding a yellow oil. Isolated yield: 600 mg, 76% (75% purity; Scheme VI-8 & Figure VI-1).



Scheme VI-8. Synthesis of ^tBu(PCP)H by using ClP^tBu₂

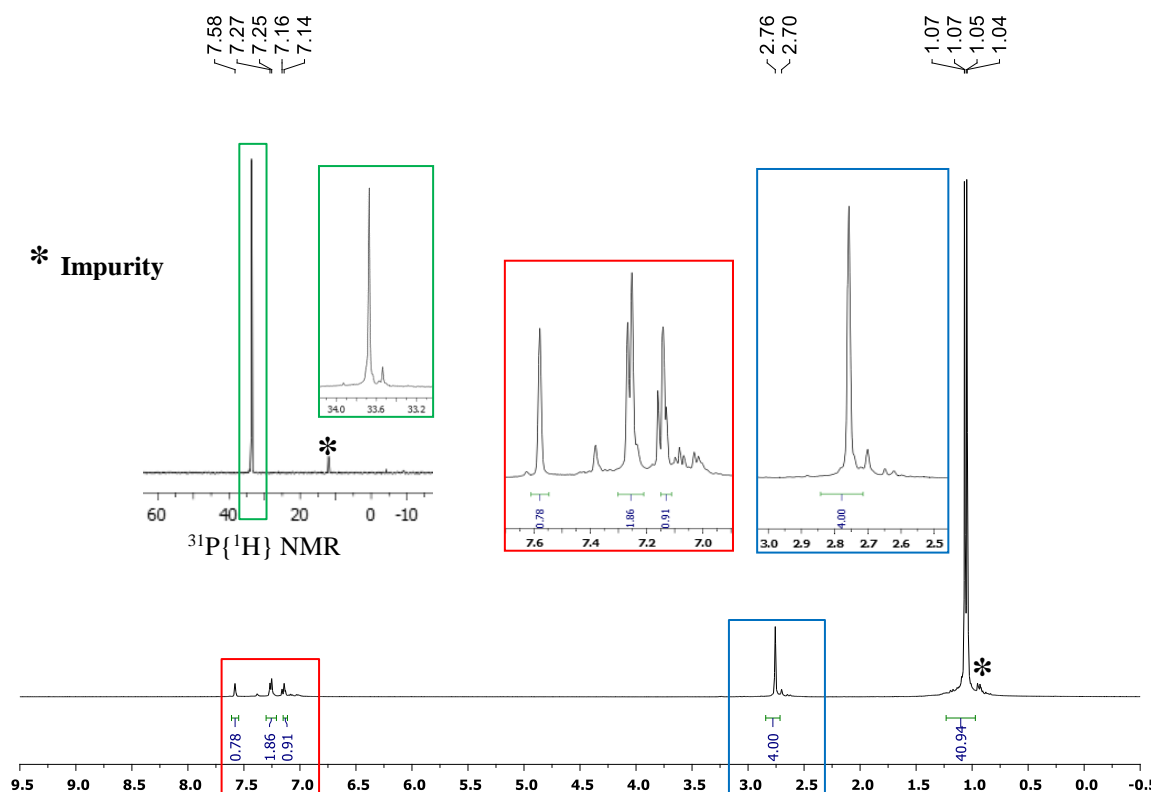
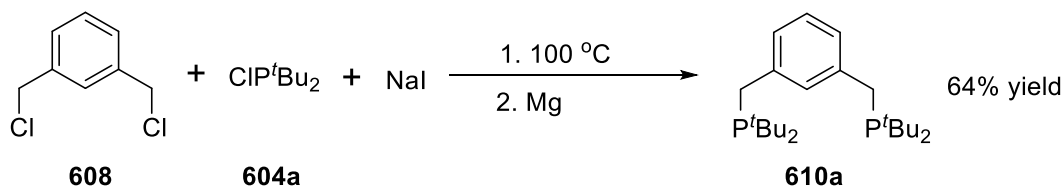


Figure VI-1. 1H NMR and $^{31}P\{^1H\}$ NMR spectra of **610a** in C_6D_6 at RT measured on a 500 MHz Varian NMR spectrometer.

In a screw cap culture tube, to the acetonitrile solution (10 mL) of *m*-xylylene dichloride (**608**, 350 mg, 2.00 mmol) was added **604a** (723 mg, 4.00 mmol) and sodium iodide (1.20g, 8.00 mmol), and the reaction mixture was stirred at 100 °C for 15 h. After cooling down to room temperature, magnesium powder (97 mg, 4.00 mmol) was added under argon, and the reaction mixture was stirred at room temperature for 36 h. The product was extracted by pentane (3×20 mL), and the volatiles were removed under vacuum, yielding an off white solid. Isolated yield: 507 mg, 64% (Scheme VI-9 & Figure VI-2).



Scheme VI-9. Synthesis of ^tBu(PCP)H by using CIP^tBu₂ and NaI

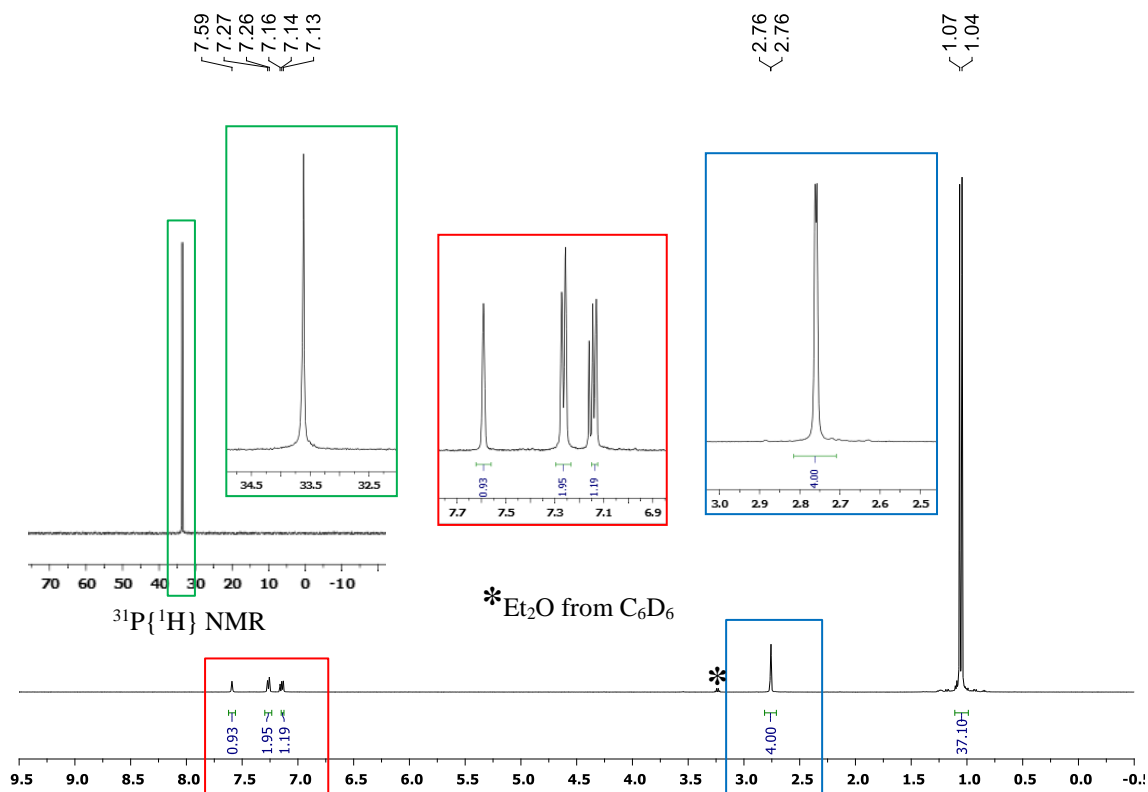


Figure VI-2. ¹H NMR and ³¹P{¹H} NMR spectra of **610a** in C₆D₆ at RT measured on a 500 MHz Varian NMR spectrometer.

6.4.6 C–P bond cleavage observation in ^{Ph}(PCP)H and ^{iPr}(PNP) synthesis

The benzyl C–P bond cleavage was observed in the synthesis of ^{Ph}(PCP)H (**610d**) and ^{iPr}(PNP) (**610e**), which gave rise to the formation of (3-

methylbenzyl)diphenylphosphine (**610d'**) and 2-((diisopropylphosphanyl)methyl)-6-methylpyridine (**610e'**) as side products. The following two ^1H NMR spectra showed the identification of these side products. In the synthesis of **610d**, two small peaks were observed at 3.24 ppm and 2.02 ppm (Figure VI-3), which corresponded to the benzylic protons and methyl protons of **610d'**.

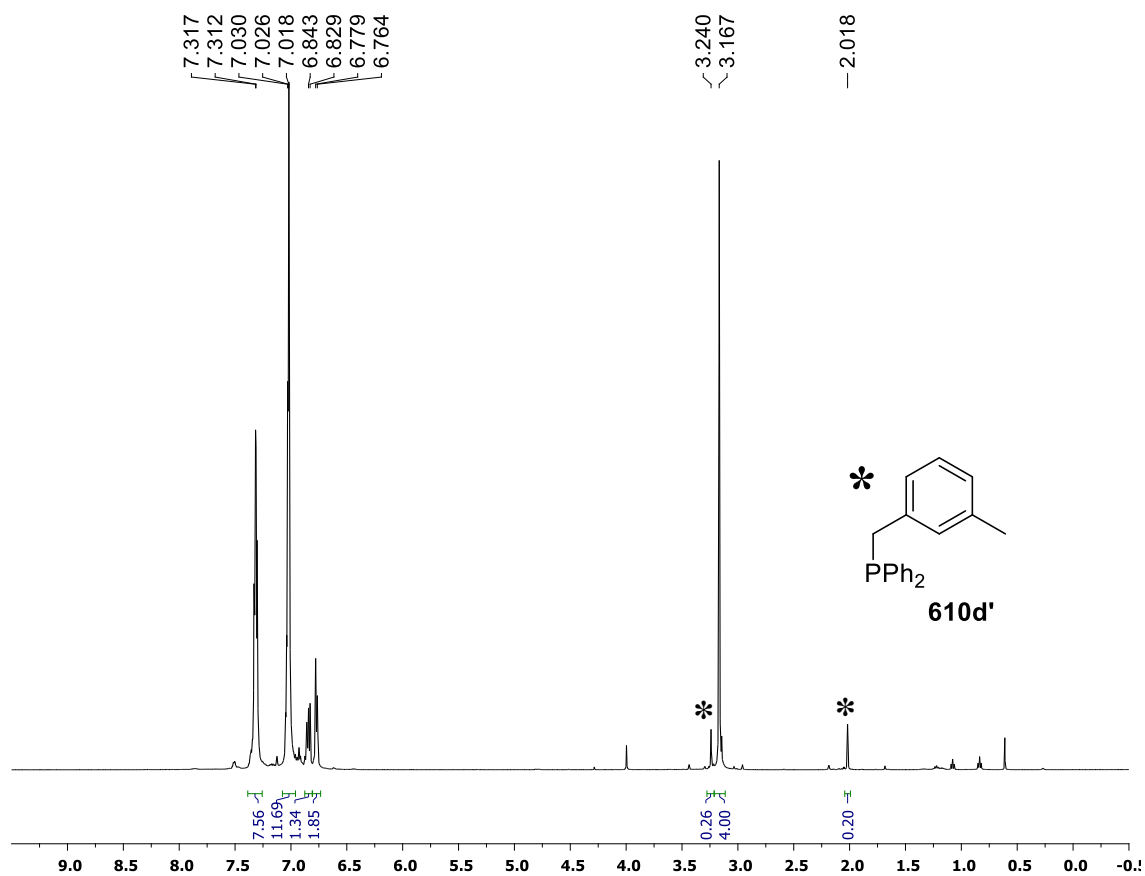


Figure VI-3. ^1H NMR spectrum of **610d** and **610d'** in C_6D_6 at RT measured on a 500 MHz Varian NMR spectrometer.

Analogously, in the synthesis of **610e**, two small peaks were observed at 2.99 ppm (d, $J_{H-P} = 1.5$ Hz) and 2.40 ppm (s) (Figure VI-4), which corresponded to the benzylic protons and methyl protons of **610e'**.

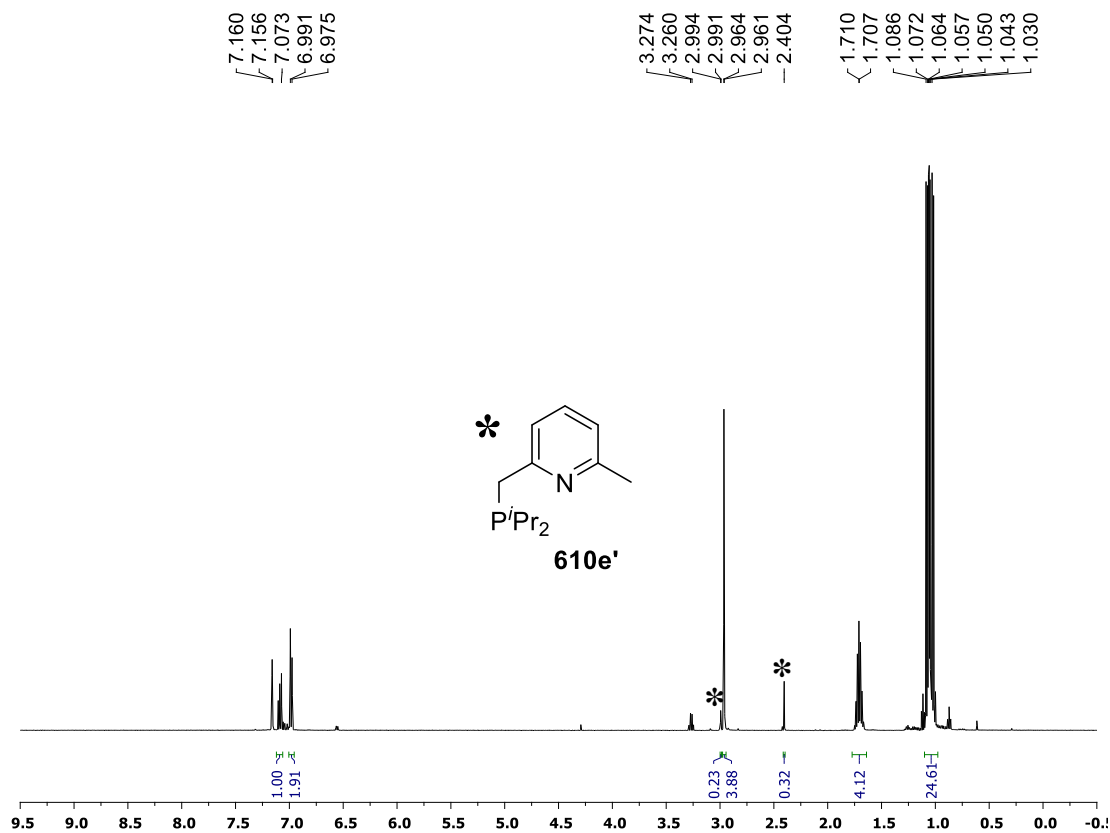


Figure VI-4. 1H NMR spectrum of **610e** and **610e'** in C_6D_6 at RT measured on a 500 MHz Varian NMR spectrometer.

6.4.7 Control reactions related to the synthesis of $iPr(PCP)NiX$ (611/612)

Reaction of di-*iso*-propylchlorophosphine (604b) with nickel powder. In a screw cap culture tube, to the CD₃CN solution (2 mL) of **604b** (61 mg, 0.40 mmol) was added nickel powder (29 mg, 0.50 mmol). The reaction mixture was stirred at 100 °C for 15 h. After cooling down to room temperature, the mixture was filtered through a pad of Celite. The filtrate was analyzed by ¹H NMR and ³¹P NMR spectroscopy, showing only unreacted **604b** was present.

Reaction of xylylene dibromide (607) with nickel powder. In a screw cap culture tube, to the CD₃CN solution (2 mL) of **607** (53 mg, 0.20 mmol) was added nickel powder (29 mg, 0.50 mmol). The reaction mixture was stirred at 100 °C for 15 h. After cooling down to room temperature, the mixture was filtered through a pad of Celite. The filtrate was analyzed by ¹H NMR spectroscopy, showing 72% of unreacted **607** along with new resonances attributable to compounds containing Ar-CH₂CH₂-Ar' linkages from the likely benzyl-benzyl coupling (Figure VI-5).

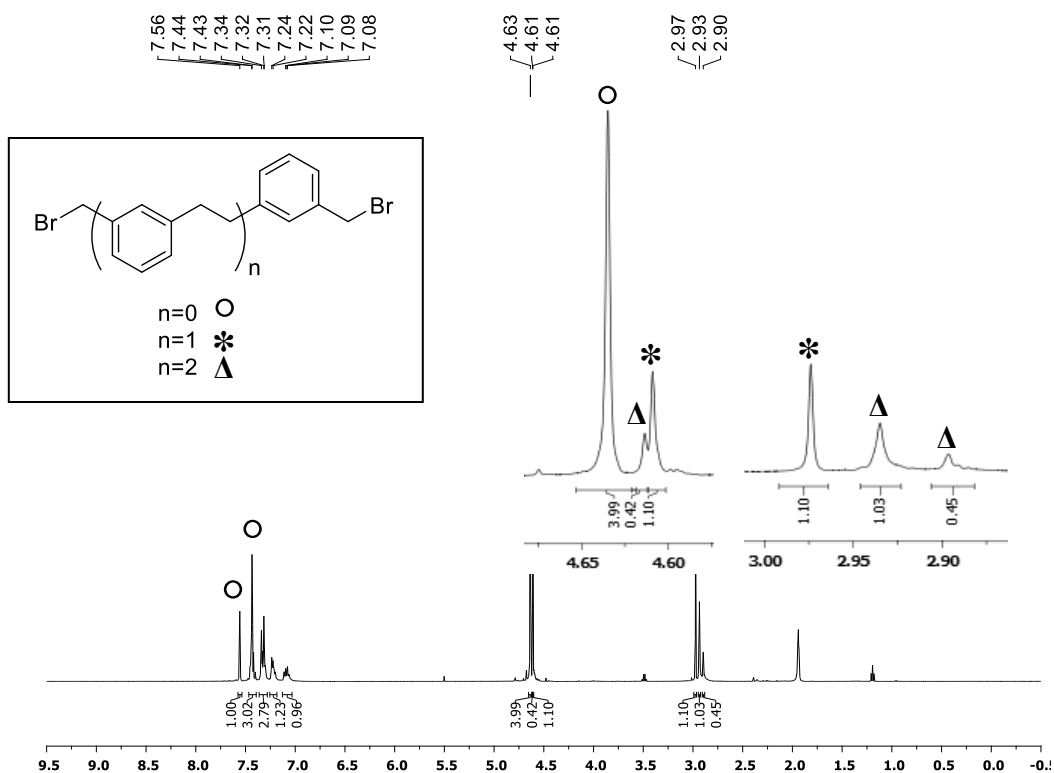


Figure VI-5. ^1H NMR spectrum of the mixture resulting after treatment of **607**, with Ni powder in CD_3CN at $100\text{ }^\circ\text{C}$ for 15 h. The spectrum was measured at ambient temperature on a 500 MHz Varian NMR spectrometer. Signals corresponding to **607** (72% unreacted) and to tentatively assigned products highlighted.

CHAPTER VII
SYNTHESIS OF BIS-PINCER PALLADIUM/NICKEL COMPLEXES AND
APPLICATION IN CATALYTIC NITRILE HYDRATION

7.1 Introduction

The intramolecular cooperation of two metal centers in hetero- and homo-binuclear metal complexes mediates a wide range of molecule transformations, which could be challenging to achieve by monomeric complexes. This type of reactions is typically catalyzed by metalloenzymes including urease,²⁵⁷ hydrogenase,^{258,259} and nitrogenase²⁶⁰⁻²⁶³ (Figure VII-1). The binuclear metalloenzymes provide suitable pockets for covalent or noncovalent interactions with specific substrate and catalyze numerous reactions under mild conditions. The two separate metal centers generally play different roles and cooperate with each other in the catalytic process in order to activate the substrate and carry out bond formation or cleavage with accelerated rate and high selectivity.²⁶⁴ For example, the hydroxide-bridged binuclear nickel complex found in urease from *Klebsiella aerogenes* displayed a high reactivity for hydrolysis of urea.²⁵⁷ One nickel center acted as a Lewis acid for urea binding and activation, and the other nickel center carried a hydroxide group as a nucleophile to attack carbonyl group of urea, resulting in the formation of bridging carbamate and release one equivalent of ammonia. The subsequent hydrolysis of bridging carbamate gave rise to CO₂ and ammonia as final products and regenerate hydroxide-bridged binuclear nickel complex (Figure VII-2).²⁶⁵⁻²⁶⁸

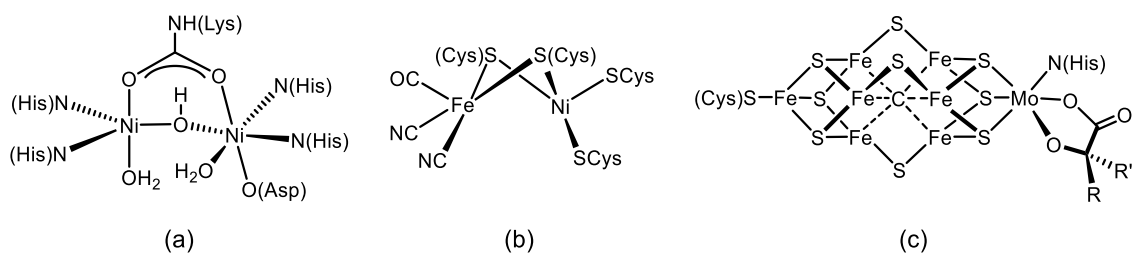


Figure VII-1. (a) Active site of urease. (b) Active site of [NiFe]-hydrogenase. (c) Active site of the FeMo cofactor from nitrogenase.

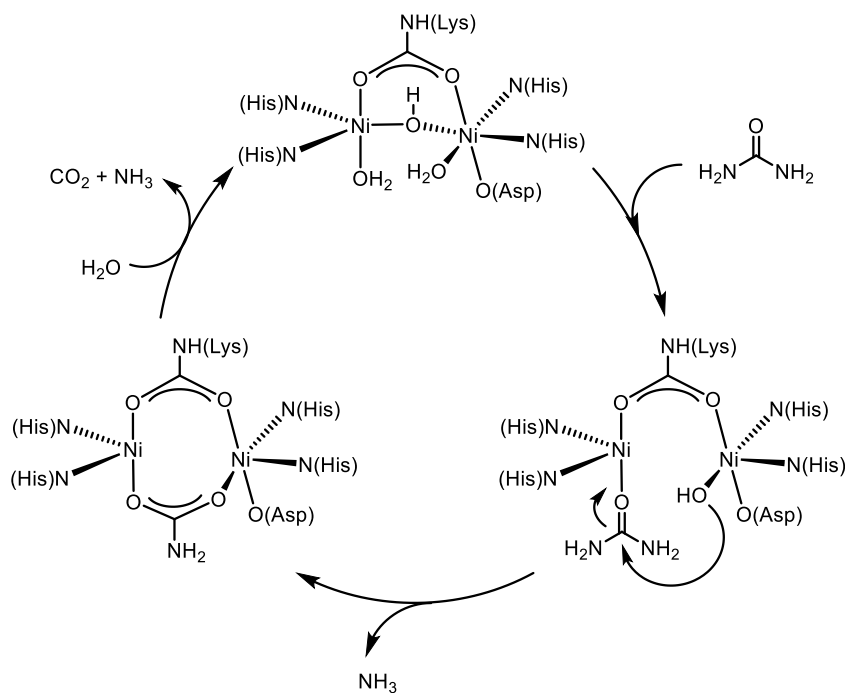


Figure VII-2. Hydrolysis of urea mediated by hydroxide-bridged binuclear nickel complex.²⁶⁵

Inspired by unique reactivity of metalloenzymes, organometallic chemists have focused on designing various ligand frameworks to support metal complexes in order to

study the collaboration between two metal sites and discover new reactivity and catalysis.²⁶⁹⁻²⁷¹ Therefore, the ligand design and synthesis are influential in this chemistry. As shown in Figure VII-3, our strategy was to tie two LX^1P -type pincer ligands together with a linker, and force the two metal centers to interact with the same substrate. The length and rigidity of linker may affect the size of pocket between two pincer complexes in order to selectively activate specific incoming substrate. By introducing an “ X^2 abstractor”, two different metal centers could be generated: one metal center acts as Lewis acid for substrate binding and the other provides X^2 as a transferring group for bond cleavage and formation reaction. Recently, the Ozerov group reported binuclear palladium complexes supported by bridged PNN and PCN bis-pincer ligands.²⁷² Herein, we describe the synthesis of POCS bis-pincer ligands and the reactivity of their metal complexes for the hydration of nitriles.

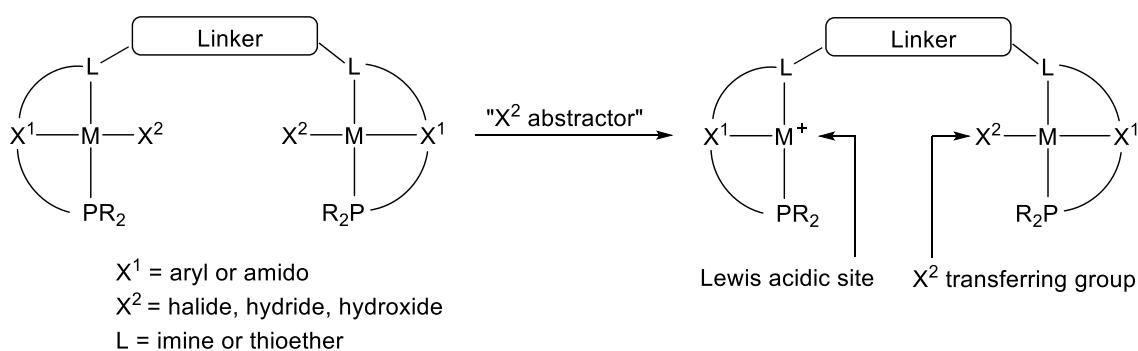
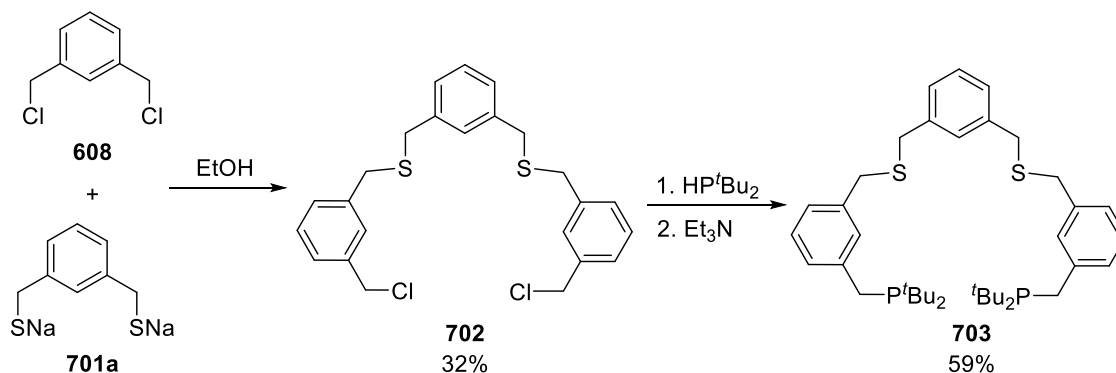


Figure VII-3. Strategy of making binuclear bis-pincer complex with two non-equivalent metal centers.

7.2 Results and Discussion

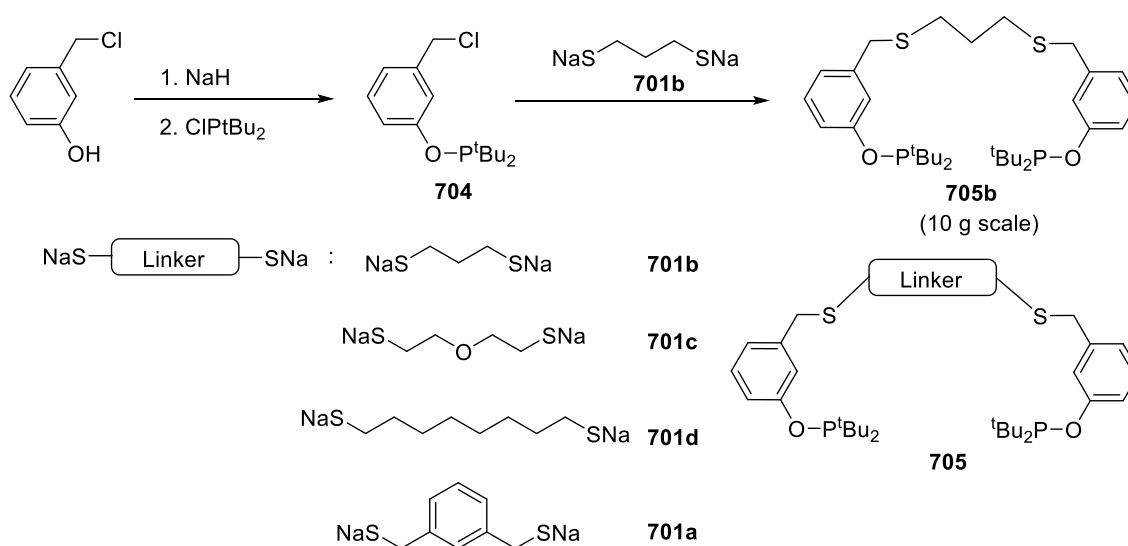
7.2.1 Synthesis of PCS and POCS bis-pincer ligands

The synthesis of target PCS bis-pincer ligand **703** was achieved by the reaction of bis-thiolate **701a** with *m*-xylylene dichloride **608** to afford compound **702**, which was further phosphinated to give the bis-pincer ligand **703**. Selective formation of compound **702** was achieved by slow addition of a low concentration solution of **701a** (0.10 M in EtOH) to a high concentration solution of **608** (1.00 M in EtOH). The resulting compound **702** was immediately precipitated from ethanol solution due to the poor solubility, which inhibited the formation of oligomers, polymers, or cyclic compounds. The reaction of compound **702** with HP^tBu_2 resulted in the formation of PCS bis-pincer ligand **703** (Scheme VII-1). Although the synthesis of **703** only required two steps, the reaction and purification procedure of **702** was tedious and the overall yield was moderate. Thus, we sought another simple and scalable method for synthesizing bis-pincer ligands.



Scheme VII-1. Synthesis of PCS Bis-pincer Ligand

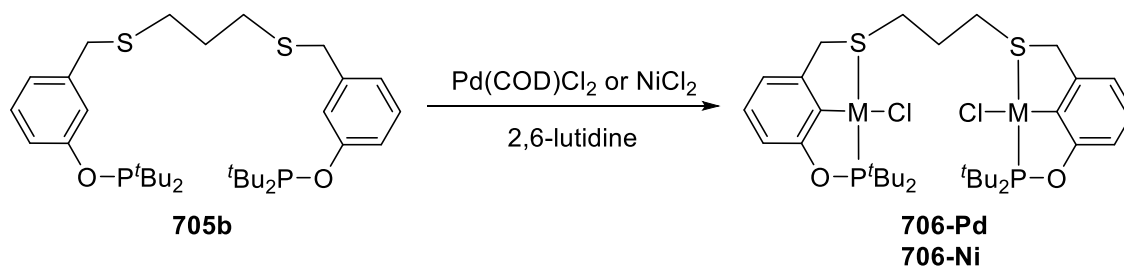
Synthesis of POCS bis-pincer ligand **705b** was developed by Dr. Loren Press in the Ozerov group.²⁷³ We first attempted the direct addition of dithiolato linker **701b** to 3-(chloromethyl)phenol. In this reaction, the hydroxyl group was partially deprotonated by thiolates to form many side products. In order to install the linker, the protection of the hydroxyl group on 3-(chloromethyl)phenol was necessary. Protection by silyl groups and then deprotection by fluoride sources was achievable, albeit with a moderate yield. Therefore, the alternative pathway was to install the phosphine on 3-(chloromethyl)phenol as a protecting group to afford compound **704** followed by reacting with linker **701b** to give POCS bis-pincer ligand **705b** (Scheme 2). This procedure was simple and can be scaled up to 10 grams. It is noteworthy that the bulky di-*tert*-butylphosphine group acted as a good protecting group in the reaction, but the less sterically imposing diethylphosphine group was directly attacked by **701b** to form P–O bond cleavage byproducts. With this synthetic strategy in hand, the ligands **705a-d** were obtained by the reaction of compound **704** with various thiolato linkers **701a~701d**.



Scheme VII-2. Synthesis of POCS Bis-pincer Ligands

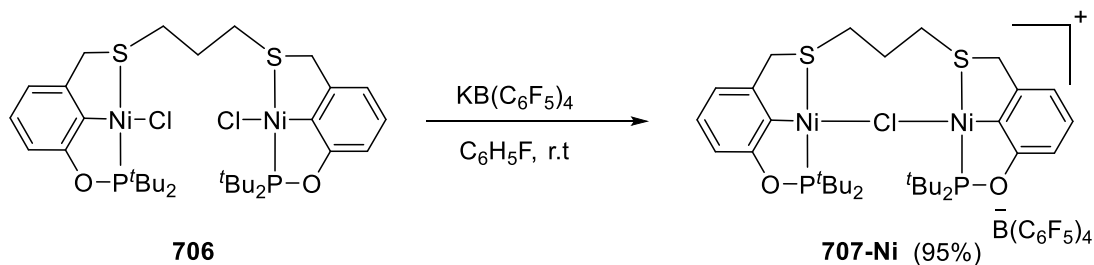
7.2.2 Synthesis and reactivity of binuclear palladium and nickel complexes

The reaction of ligand **705b** with Pd(COD)Cl₂ in the presence of 2,6-lutidine in toluene at 130 °C afforded complex **706-Pd** (Scheme VII-3). The high reaction temperature was required for C–H bond activation of arenes and production of thermodynamically favorable pincer complex. The reaction of **705b** and nickel chloride was conducted in 1,4-dioxane as solvent in the presence of 2,6-lutidine to afford **706-Ni** with good yield. Both complexes **706-Pd** and **706-Ni** displayed C_{2v} symmetry in the solution evidenced by one phosphine resonance in ³¹P NMR spectrum (202.0 ppm for **706-Pd** and 198.2 ppm for **706-Ni**) and one *tert*-butyl resonance in ¹H NMR spectrum (1.33 ppm, d, J_{P,H} = 15.3 Hz for **706-Pd** and 1.43 ppm, d, J_{P,H} = 14.3 Hz for **706-Ni**).

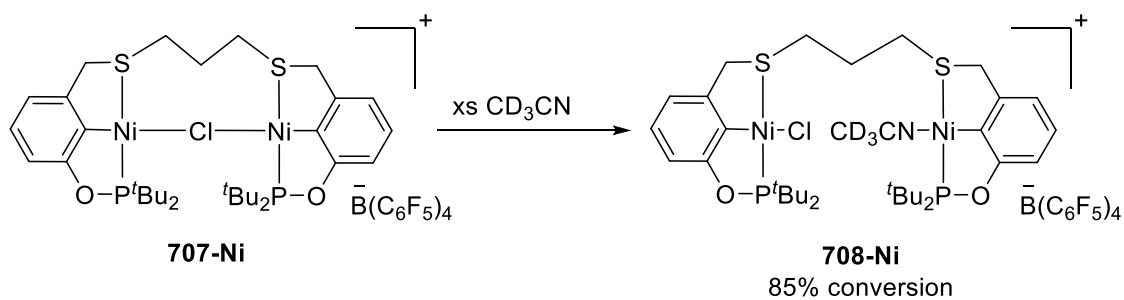


Scheme VII-3. Synthesis of POCS Bis-pincer Complexes of Pd and Ni (706)

The abstraction of one chloride from complex **706-Ni** was achieved by addition of one equivalent of $\text{K}[\text{B}(\text{C}_6\text{F}_5)_4]$ (Scheme VII-4). Instead of producing two different metal centers, the chloro-bridged complex **707-Ni** was afforded in the benzene solution demonstrated by only one phosphine resonance shown at 200.4 ppm in ^{31}P NMR spectrum. Although the bridging complex **707-Ni** contained two identical metal centers, the bridge can be simply cleaved by addition of excess of strongly donating ligand such as acetonitrile to form complex **708-Ni** (Scheme VII-5). On the basis of ^{31}P NMR spectrum, 85% of chloro-bridged complex **707-Ni** was converted into a new complex **708-Ni** with two non-equivalent phosphine resonances at 206.1 and 199.7 ppm with 1:1 ratio (Figure VII-4).



Scheme VII-4. Synthesis of Chloro-bridged Complex of Ni (707-Ni)



Scheme VII-5. Synthesis of Bis-pincer Complex of Ni with Non-equivalent Metal Centers

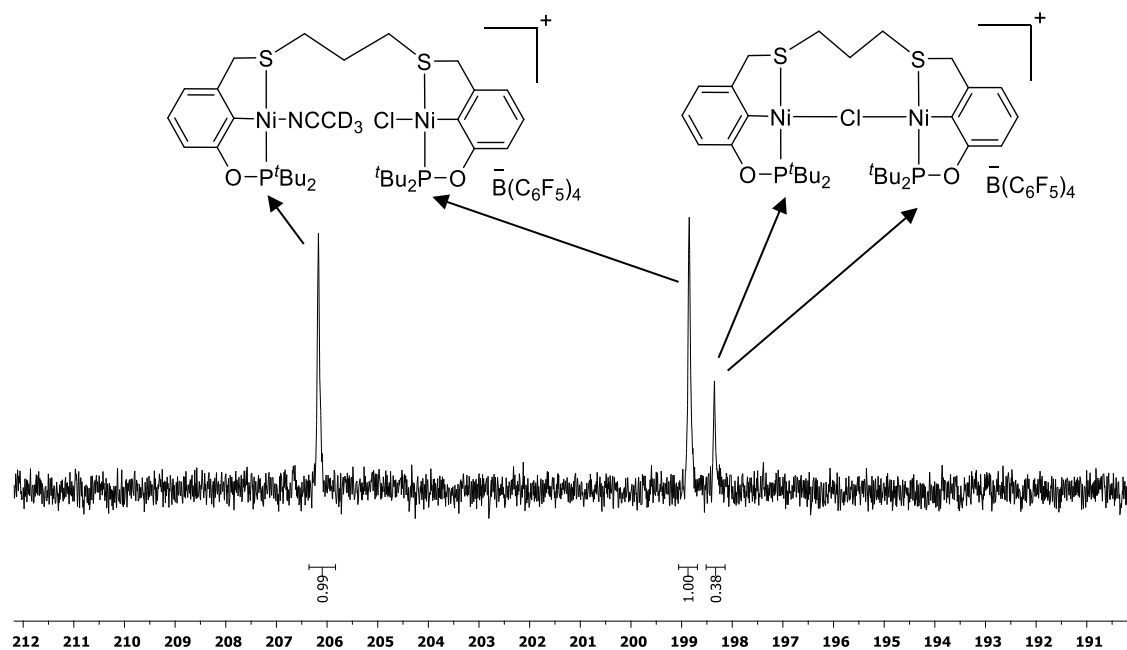
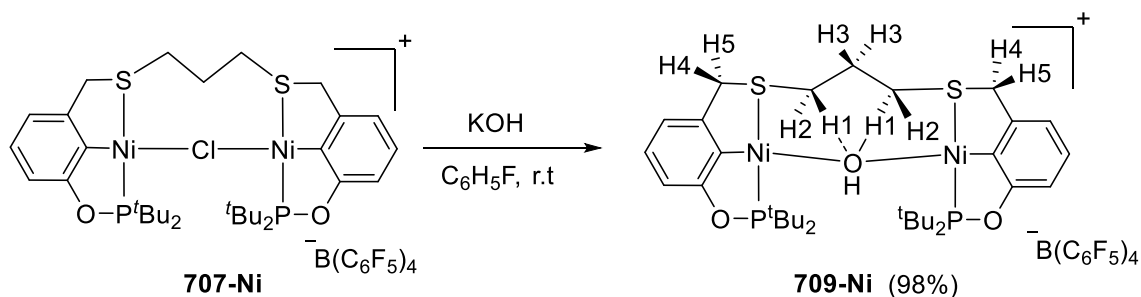


Figure VII-4. ^{31}P NMR spectrum of complex **708-Ni** and **707-Ni** in an 85:15 ratio.

The bridging chloride in **707-Ni** was further replaced with hydroxo group by treatment of **707-Ni** with KOH in $\text{C}_6\text{H}_5\text{F}$, resulting in the formation of hydroxo-bridged

complex **709-Ni** in 98% yield (Scheme VII-6). One phosphine resonance at 192.0 ppm in ^{31}P NMR spectrum and one broad hydrogen resonance at -4.78 ppm in ^1H NMR spectrum, indicating the hydroxide group bridged on two equivalent nickel centers. Complex **709-Ni** displayed C_2 symmetry in its ^1H NMR spectrum, determined by two *tert*-butyl resonances at 1.54 ppm (d, $J_{\text{H,P}} = 15.0$ Hz) and 1.45 ppm (d, $J_{\text{H,P}} = 15.0$ Hz). One hydrogen chemical shift from the propylene linker was anomalous downfield at 5.79 ppm, probably owing to $\text{CH}\cdots\text{O}$ hydrogen bonds between the protons and bridging hydroxide. On the basis of the 2D ^1H - ^1H gCOSY and NOESY spectroscopic data, we assumed this downfield resonance was from H1 in **709-Ni** (Scheme VII-6) because H1 displayed correlations with H2 and H3 through bonds in the gCOSY spectrum (Figure VII-5) and a correlation with H2 in the NOESY spectrum (Figure VII-6).



Scheme VII-6. Synthesis of Hydroxo-bridged Complex of Ni (709-Ni)

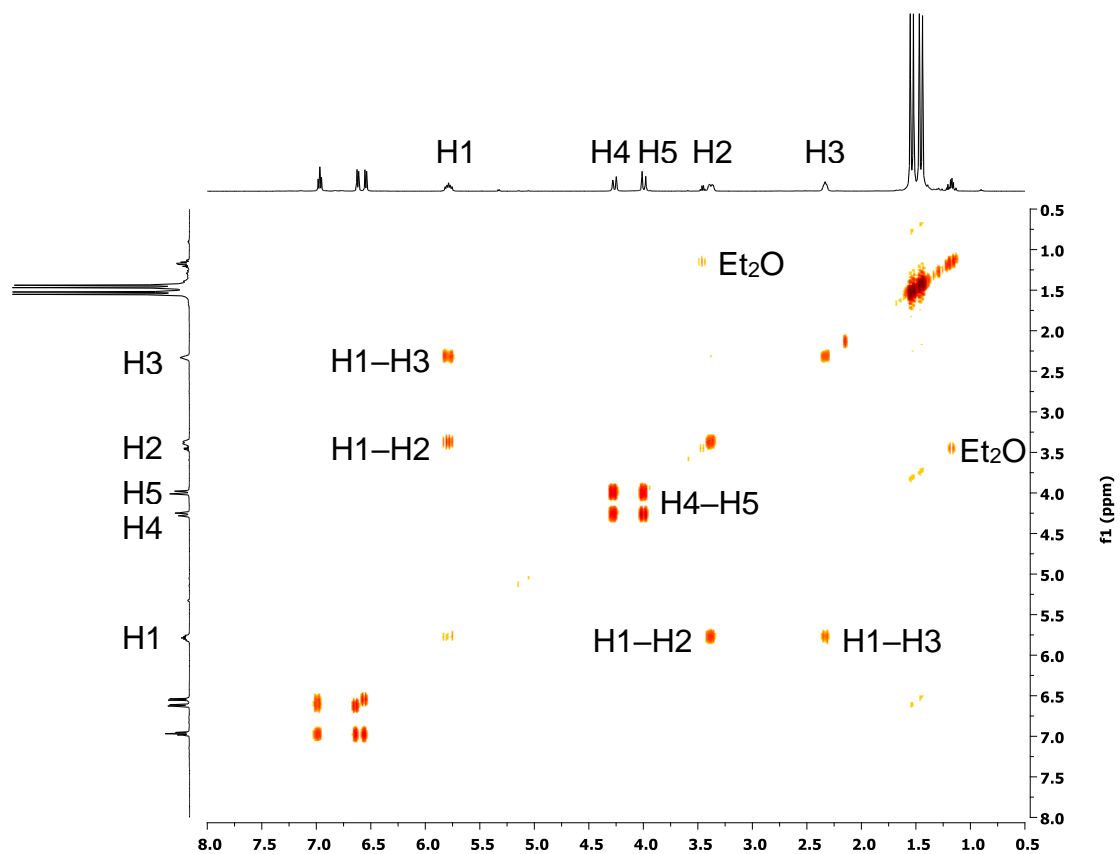


Figure VII-5. 2D ^1H - ^1H gCOSY spectrum of **709-Ni** showing ^1H - ^1H correlations through bonds.

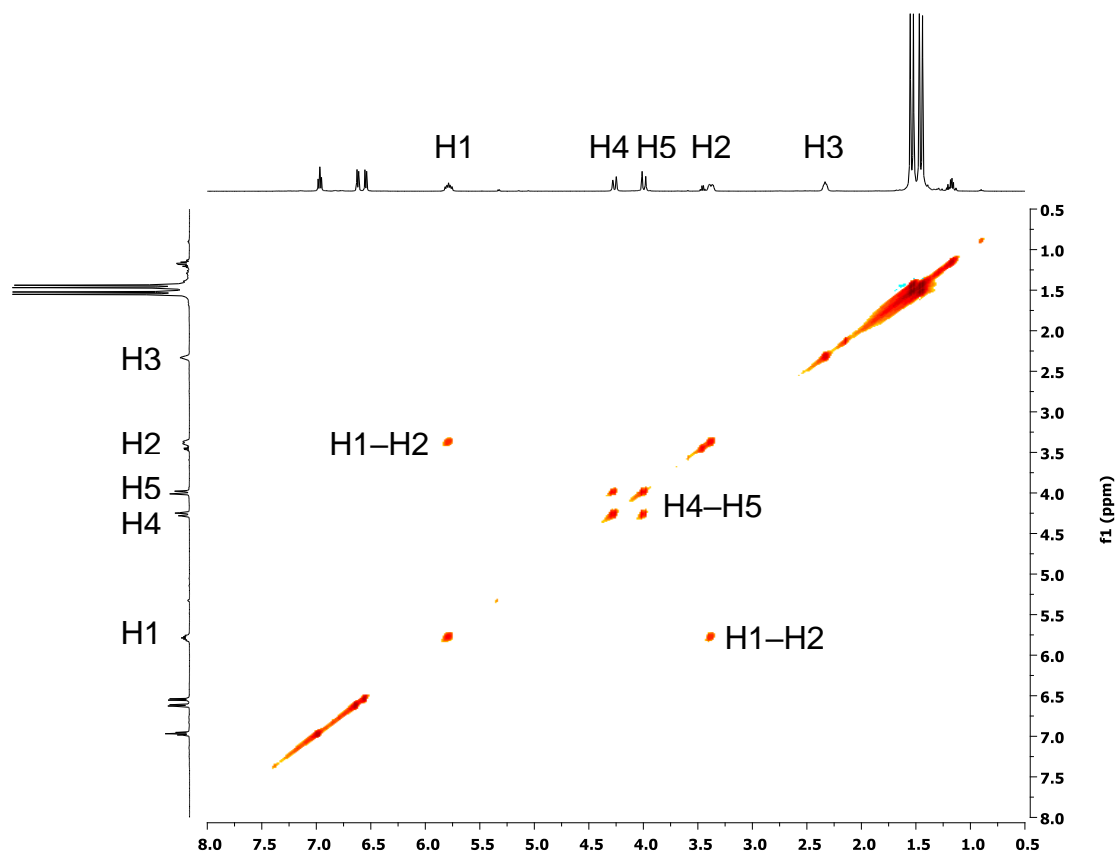
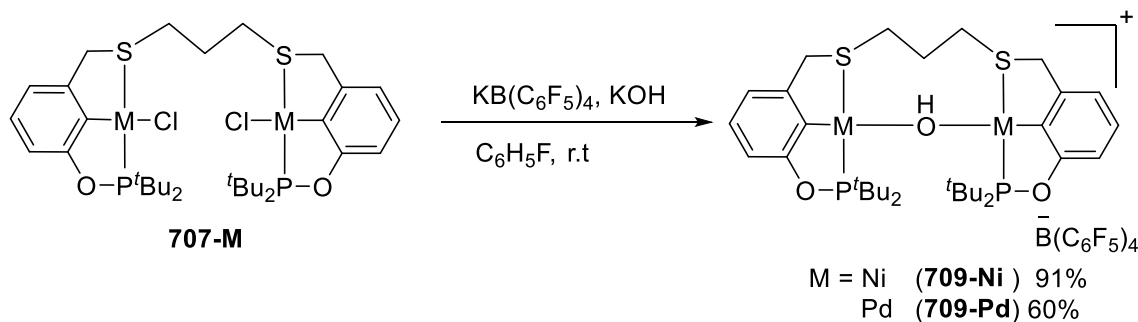


Figure VII-6. 2D ^1H - ^1H NOESY spectrum of **709-Ni** showing ^1H - ^1H correlations through space.

Hydroxo-bridged complex **709-Ni** can be obtained in one pot by treatment of **706-Ni** with $\text{K}[\text{B}(\text{C}_6\text{F}_5)_4]$ and KOH (Scheme VII-7). The synthesis of **709-Pd** was also achieved by the similar reaction with **706-Pd** as the starting precursor, albeit with lower yield. Complex **709-Pd** displayed C_{2v} symmetry evidenced by appearance of one *tert*-butyl resonance at 1.43 ppm (d, $J_{\text{H,P}} = 15.5$ Hz) and one benzyl CH_2 group at 4.23 ppm in ^1H NMR spectrum. Unlike the possible hydrogen bonds observed in **709-Ni**, the propylene linker of **709-Pd** exhibited two chemical shifts at 3.84 ppm (br, $\text{CH}_2\text{CH}_2\text{CH}_2$) and 2.38

ppm (m, CH₂CH₂CH₂) with 2:1 integration ratio in ¹H NMR spectrum, suggesting no hydrogen bond between protons of linker and bridging hydroxide.



Scheme VII-7. Synthesis of Hydroxo-bridged Complexes of Pd and Ni (709)

The complexes **709-Ni** and **709-Pd** were structurally characterized by single X-ray analysis (Figure VII-7 & Figure VII-8). Both pincer complex moieties in complex **709-Ni** adopted distorted square-planar geometry with similar bond distances between Ni1–O3 (1.9270(18) Å) and Ni2–O3 (1.9300(19) Å), indicating the two nickel centers were nearly equivalent. The bond distances of H(C16)⋯O3 and H(C18)⋯O3 were 3.114 and 3.180 Å and the bond distances of C16⋯O3 and C18⋯O3 were 3.480 and 3.535 Å, suggesting a potential CH⋯O hydrogen bonds²⁷⁴ in complex **709-Ni**, which was consistent with NMR spectroscopic data. The bond distances of Pd1–O3 (2.097(2) Å) and Pd2–O3 (2.089(2) Å) in complex **709-Pd** were slightly shorter than the Pd–O bond distances (2.149(7) Å and 2.113(6) Å) in [(^tBuPCO)Pd]₂(μ-OH)[B(Ar^F)₄] reported by Goldberg,²⁷⁵ and the angle of Pd1–O3–Pd2 (120.98(11)°) in **709-Pd** was significantly smaller than the

one ($142.2(3)^\circ$) in $[(t\text{BuPCO})\text{Pd}]_2(\mu\text{-OH})[\text{B}(\text{Ar}^{\text{F}})_4]$, presumably owing to the restricted rotation in **709-Pd** resulted from the propylene linker.

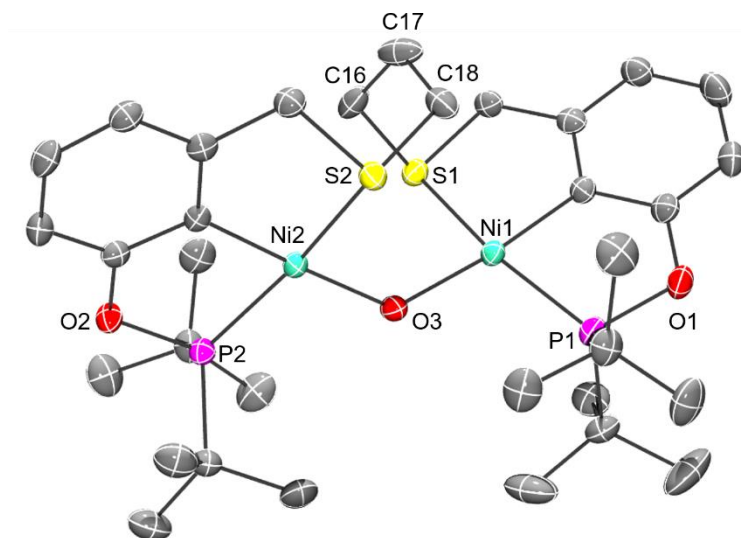


Figure VII-7. POV-Ray rendition of the ORTEP drawing (50% thermal ellipsoids) of **709-Ni** showing selected atom labeling. Hydrogen atoms and $\text{B}(\text{C}_6\text{F}_5)_4^-$ anion are omitted for clarity. Selected bond distances (\AA) and angles (deg): Ni1–O3, 1.9270(18); Ni2–O3, 1.9300(19); Ni1–P1, 2.1647(10); Ni2–P2, 2.1683(12); Ni1–S1, 2.2223(12); Ni2–S2, 2.2238(13); Ni1–O3–Ni2, 131.19(10); P1–Ni1–S1, 166.05(3); P2–Ni2–S2, 164.99(3); O3–Ni1–S1, 89.85(6); O3–Ni2–S2, 93.08(5); O3–Ni1–P1, 101.86(7); O3–Ni2–P2, 99.07(6).

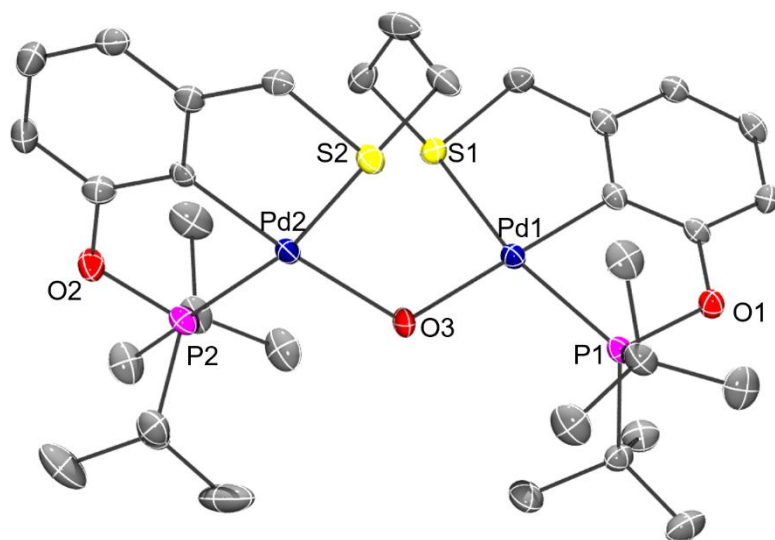
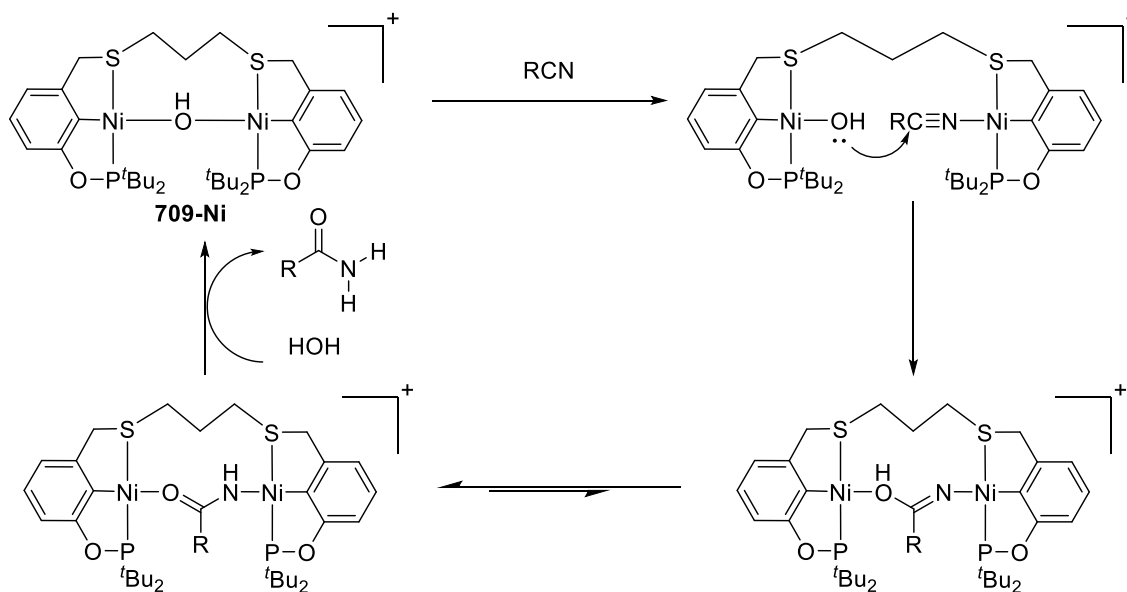


Figure VII-8. POV-Ray rendition of the ORTEP drawing (50% thermal ellipsoids) of **709-Pd** showing selected atom labeling. Hydrogen atoms and $\text{B}(\text{C}_6\text{F}_5)_4^-$ anion are omitted for clarity. Selected bond distances (\AA) and angles (deg): Pd1–O3, 2.097(2); Pd2–O3, 2.089(2); Pd1–P1, 2.2255(11); Pd2–P2, 2.2261(10); Pd1–S1, 2.3593(11); Pd2–S2, 2.3491(11); Pd2–O3–Pd1, 120.98(11); P1–Pd1–S1, 163.54(3); P2–Pd2–S2, 165.27(4); O3–Pd1–S1, 97.30(7); O3–Pd2–S2, 90.67(7); O3–Pd1–P1, 97.91(7); O3–Pd2–P2, 103.45(7).

7.2.3 Nitrile hydration catalyzed by binuclear complexes

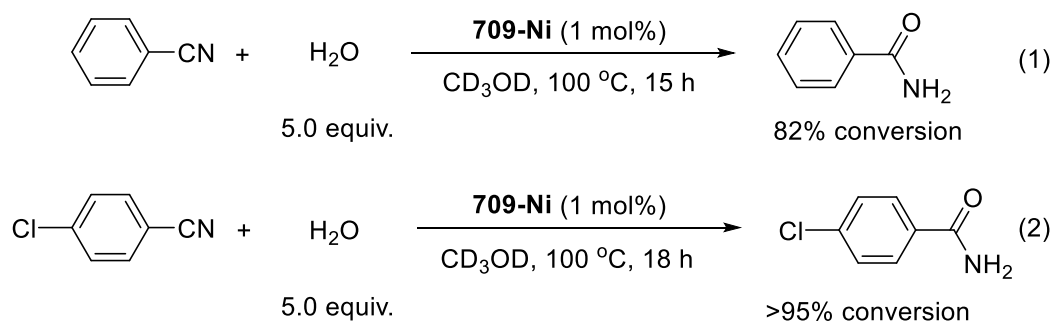
Unlike the chloro-bridged complex **707-Ni**, the bridging hydroxide on **709-Ni** cannot be cleaved by addition of acetonitrile at room temperature. We proposed the bridge can still be broken at higher temperature, which may generate the nickel cation as a Lewis acid on one side and the nickel hydroxide on the other side. Once nitrile binds to the nickel cation, it can be attacked by the nucleophilic nickel hydroxide followed by a proton

transfer from oxygen to nitrogen to form an amido-bridged complex. Finally, protonation of the bridging amide by water affords an amide product and regenerates the hydroxo-bridged catalyst (Scheme VII-8).



Scheme VII-8. Proposed Mechanism of Nitrile Hydration by Complex 709-Ni

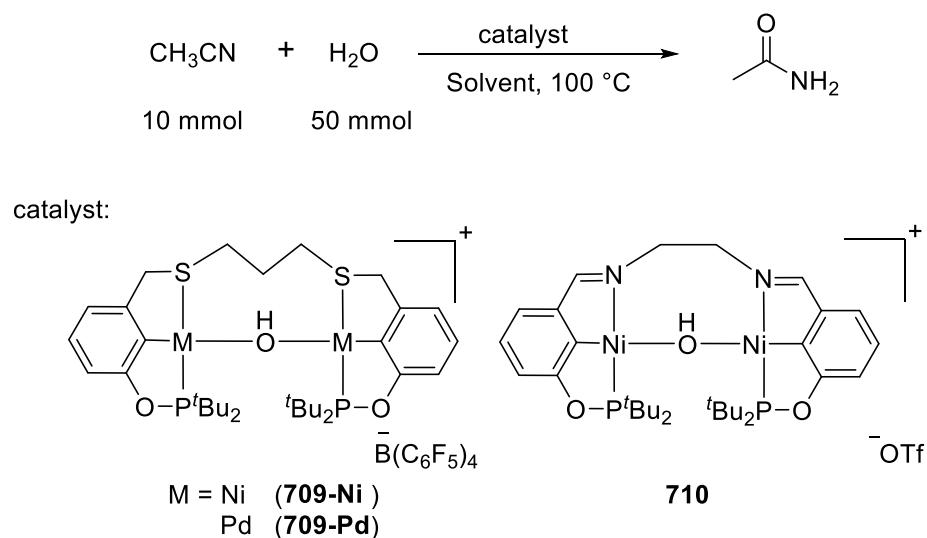
The reaction of benzonitrile or 4-chlorobenzonitrile with water in the presence of 1 mol% **709-Ni** afforded benzamide and 4-chlorobenzamide with 82% and >95% conversion, respectively (Scheme VII-9, eq. 1 and 2).



Scheme VII-9. Nitrile Hydration Catalyzed by 709-Ni

In order to test the efficiency of bis-pincer complexes for nitrile hydration catalysis, acetonitrile was used as model substrate and reacted with water in the presence of bis-pincer complexes as catalysts (Table VII-1). The acetonitrile hydration was achieved with a turnover number of 220 by using 0.1 mol% of **709-Ni** as catalyst (entry 1). In contrast, **709-Pd** was totally inactive in the nitrile hydration reaction under same condition (entry 2). We surmised **709-Pd** might be decomposed in ethanol, and therefore without adding solvent, **709-Pd** catalyzed the nitrile hydration in neat acetonitrile and water with a turnover number of 60 (entry 3). By reacting the acetonitrile with water in the presence of 0.01 mol% of **709-Ni** for 72 h, turnover numbers can be increased up to 1250 (entry 6). Unlike **709-Pd**, **709-Ni** was inactive without addition of ethanol as solvent (entry 7). Using PCN bis-pincer complex (**710**)²⁷² as catalyst, a turnover number of 100 was obtained (entry 8).

Table VII-1. Nitrile Hydration Catalyzed by Bis-pincer Complexes^a

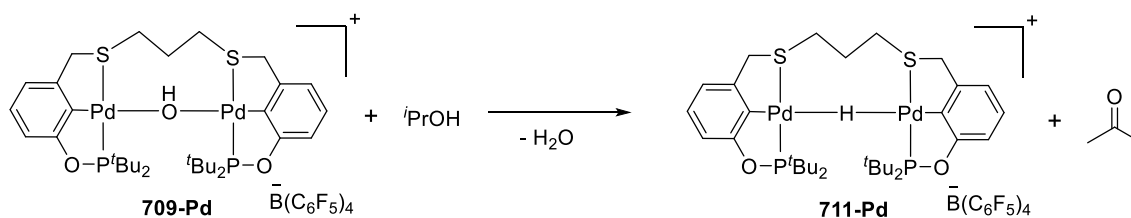


Entry	catalyst	cat. loading	t (h)	Solvent	Conv. (%) ^b	TON ^c	TOF (h ⁻¹) ^d
1	709-Ni	0.1 mol%	24	EtOH	44	220	9
2	709-Pd	0.1 mol%	24	EtOH	0	0	0
3	709-Pd	0.1 mol%	24	----	12	60	3
4	709-Ni	0.01 mol%	15	EtOH	13	650	43
5	709-Ni	0.01 mol%	24	EtOH	16	800	33
6	709-Ni	0.01 mol%	48	EtOH	23	1150	24
7	709-Ni	0.01 mol%	72	EtOH	25	1250	17
8	709-Ni	0.01 mol%	24	----	0	0	0
9	710	0.01 mol%	24	EtOH	2	100	4

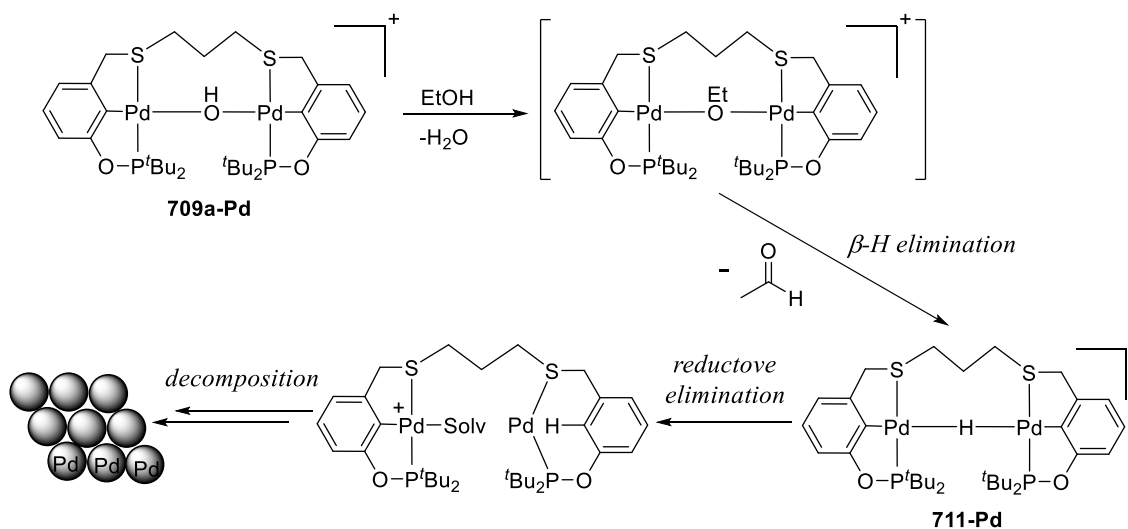
a. The reaction was carried out using CH₃CN (10 mmol), water (50 mmol), and catalyst (0.1 mol% or 0.01 mol%) in ethanol (2.0 mL) at 100 °C in a culture tube. b. Conversions were calculated based on the formation of CH₃CN in ¹H NMR spectra with 1,4-dioxane (4.0 mmol) as an internal standard. c. TONs were calculated by Conv./M (M = Ni or Pd). d. TOFs were calculated by TON/h.

To study the possible pathway for the decomposition of **709-Pd** in ethanol, the reaction of **709-Pd** with isopropanol in C₆D₆ at 100 °C resulted in the formation of hydrido-bridged complex **711-Pd** and ketone (Scheme VII-10). The dehydrogenation of alcohols is possibly resulted from the formation of alkoxo-bridged intermediate by

replacement of hydroxide with alkoxide, followed by β -hydrogen elimination to afford an aldehyde/ketone and complex **711-Pd**. During heating, **711-Pd** gradually decomposed and the formation of palladium black coating on the reaction tube was observed. It was likely the reductive elimination of C–H bond between bridging hydride and pincer backbone in **711-Pd** resulted in the formation of Pd(0) followed by dissociation from the ligand (Scheme VII-11). The decomposition was also detected by the reaction of **709-Ni** in alcohol, but the decomposition rate was much slower than **709-Pd**. To avoid the decomposition of catalyst **709-Ni** in alcohol, various solvents were tested in the reaction. *N,N*-dimethyl formamide, propylene carbonate, and toluene were ineffective solvents, while only trace amounts of acetamide were obtained in 1,4-dioxane or fluorobenzene solvent systems. The only effective solvents were methanol and ethanol, but the decomposition of **709-Ni** in these solvents makes the improvement of turnover number difficult to be achieved.



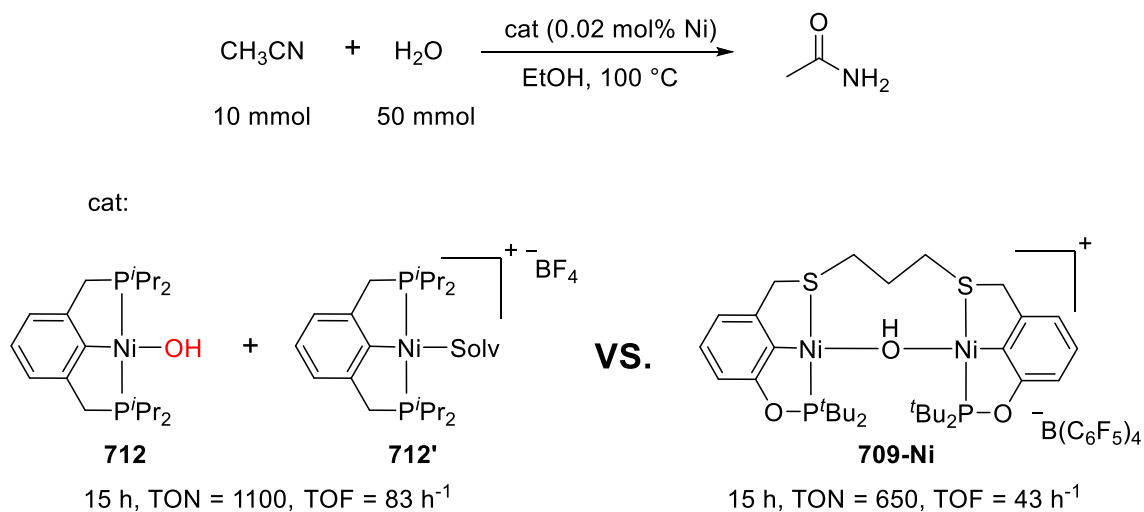
Scheme VII-10. Dehydrogenation of Isopropanol by 709-Pd



Scheme VII-11. Possible Decomposition Pathway of Complex 709-Pd in Ethanol

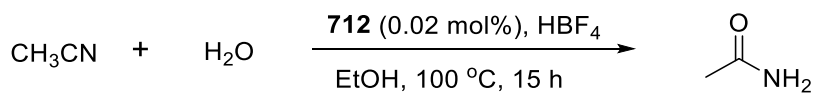
7.2.4 Nitrile hydration catalyzed via monomeric nickel complexes

In order to test whether the linker on **709-Ni** was necessary to facilitate binuclear metal cooperation for nitrile hydration, one equivalent of HBF₄ was added to two equivalents of monomeric nickel complex **712** to *in situ* generate complex pair with two nickel centers: one Lewis acidic nickel cation in **712'** and one nickel hydroxide in **712** as a possible nucleophile transfer source for the nitrile hydration catalyst (Scheme VII-12). With this complex pair, the turnover numbers and turnover frequencies of nitrile hydration were higher than those obtained with **709-Ni** (Table VII-4, entry 7). This result indicates the linker is not necessary in this reaction, albeit a direct comparison may not be appropriate because the electronic and steric properties were different between the complex pair (**712**, **712'**) and **709-Ni**.



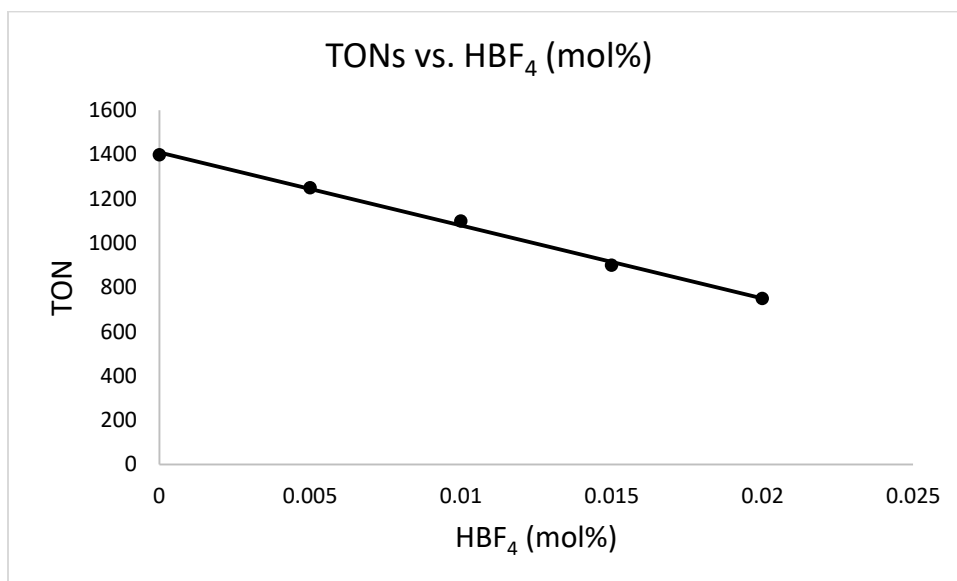
Scheme VII-12. Nitrile Hydration Catalyzed by Monomeric Pincer Complex Pair

We further tested the catalytic activity of **712** with various amounts of HBF₄ (Table VII-2). To our surprise, the catalytic activity gradually decreased when introducing increased amounts of HBF₄ (entry 1~5). The highest activity with a turnover number of 1400 was observed in the experiment without addition of acid (entry 1). It showed the catalytic activity of nitrile hydration catalyzed by complex **712** was pH dependent with a linear correlation between turnover numbers and added amounts of acid (Figure VII-9). The turnover numbers were lower under more acidic conditions. Thus, we surmised addition of base might further improve the conversion of acetonitrile to acetamide.

Table VII-2. Catalytic Activity with Various Amounts of HBF₄^a

Entry	HBF ₄ (mol%)	Conversion (%) ^b	TON ^c	TOF (h ⁻¹) ^d
1	0.000	28	1400	93
2	0.005	25	1250	83
3	0.010	22	1100	73
4	0.015	18	900	60
5	0.020	15	750	50

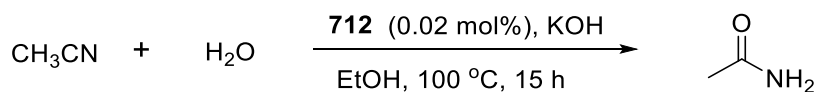
a. The reaction was carried out using CH₃CN (10 mmol), water (50 mmol), **712** (0.02 mol%), and HBF₄ in ethanol (2.0 mL) at 100 °C in a culture tube. b. Conversions were calculated based on the formation of CH₃CN in ¹H NMR spectra with 1,4-dioxane (4.0 mmol) as an internal standard. c. TONs were calculated by Conversion/Ni. d. TOFs were calculated by TON/h.

**Figure VII-9.** Catalytic activity with various amounts of HBF₄.

The data in Table VII-3 showed that the turnover numbers were gradually increased with increased amounts of KOH from 0.00 mol% to 0.20 mol% (entry 1~5), and

the turnover number up to 3050 was achieved at the rate of 203 turnover h⁻¹ (entry 5). The TON dropped to 2600 when 0.40 mol% of KOH was used (entry 6) and remained similar for added amounts KOH beyond 0.40 mol% to 1.00 mol% (entry 6~8). The reactions were pH dependent under basic conditions, but the activity was not linearly correlated with added amount of base (Figure VII-10). Without addition of catalyst **712**, only a turnover number of 300 was obtained by the reaction of acetonitrile with water in the presence of 0.1 mol% of KOH (entry 9), whereas a turnover number of 2750 was achieved under the similar conditions with addition of **712** (entry 4).

Table VII-3. Catalytic Activity with Various Amounts of KOH^a



Entry	HOH (mol%)	Conversion (%) ^b	TON ^c	TOF (h ⁻¹) ^d
1	0.00	28	1400	93
2	0.02	40	2000	133
3	0.05	50	2500	167
4	0.10	55	2750	183
5	0.20	61	3050	203
6	0.40	52	2600	173
7	0.80	54	2700	180
8	1.00	55	2750	183
9	0.10	6	300	20

a. The reaction was carried out using CH₃CN (10 mmol), water (50 mmol), **712** (0.02 mol%), and KOH in ethanol (2.0 mL) at 100 °C in a culture tube. b. Conversions were calculated based on the formation of CH₃CN in ¹H NMR spectra with 1,4-dioxane (4.0 mmol) as an internal standard. c. TONs were calculated by Conversion/Ni. d. TOFs were calculated by TON/h.

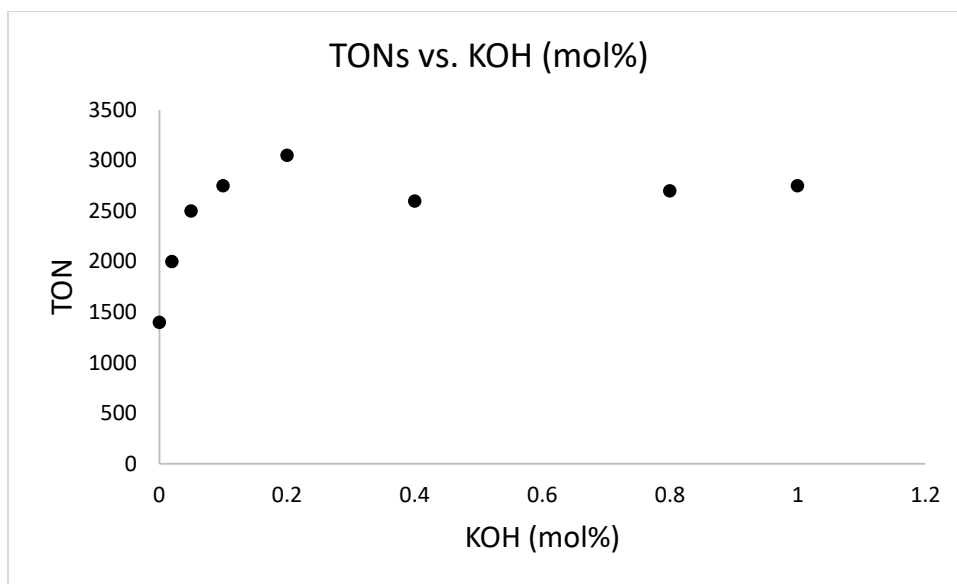
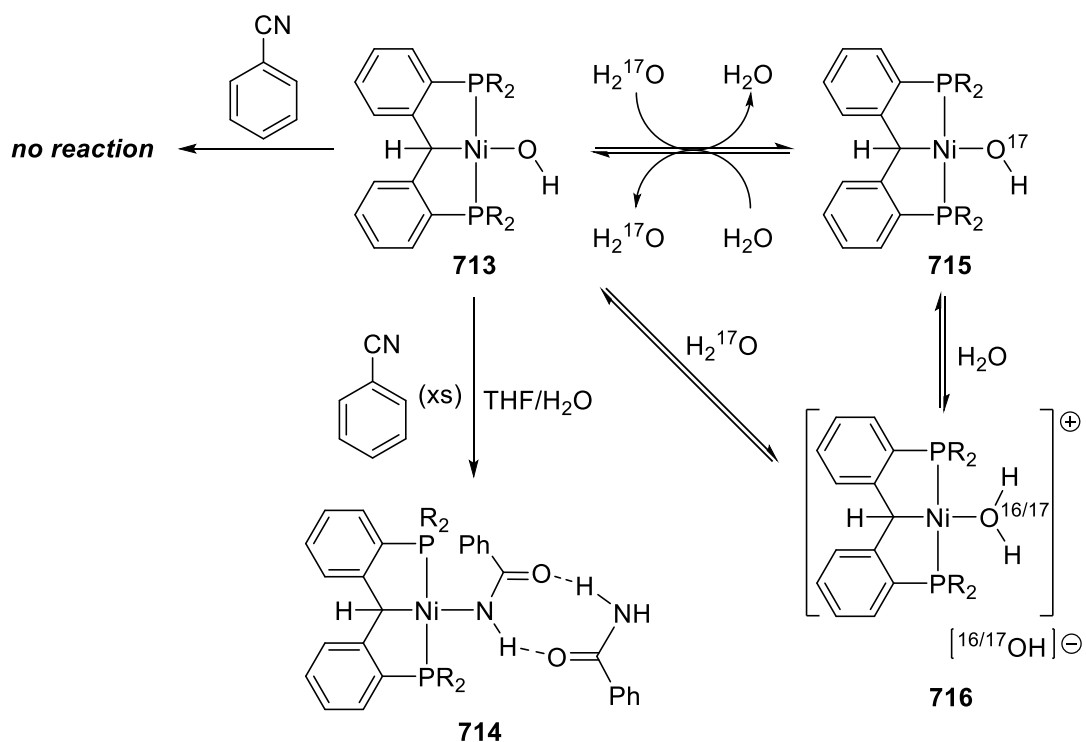


Figure VII-10. Catalytic activity with various amounts of KOH.

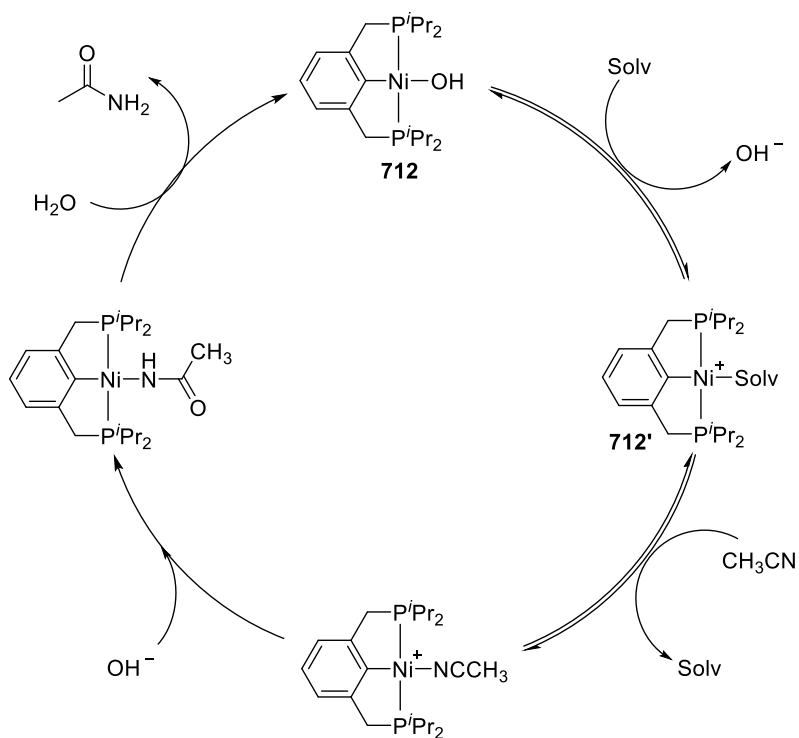
Nitrile hydration catalyzed by monomeric PC(sp³)P nickel hydroxide complex **713** was also reported by Piers.²⁷⁶ In the mechanistic study, no reaction was observed by treatment of **713** with an excess of benzonitrile in THF, whereas the formation of **714** rapidly proceeded after addition of water in this solution, suggesting dissociation of hydroxo group might be facilitated by water and likely produced a key intermediate for nitrile hydration (Scheme VII-13). When introducing H₂O to ¹⁷O labeled complex **715**, decrease of **715** and increase of **713** were observed, indicating the exchange reaction occurred through **716** as the possible intermediate. This intermediate **716** was proposed as the active catalyst for nitrile hydration in the presence of nitrile substrates.



Scheme VII-13. Hydration of Benzonitrile using 713 and Exchange Reaction with Water in the Study by Piers et. al.²⁷⁶

On the basis of study presented by Piers, we proposed the similar mechanism for nitrile hydration catalyzed by monomeric nickel hydroxide complex **712** (Scheme VII-14). First, the hydroxo group on **712** might be directly dissociated from nickel or protonated by water to generate a Lewis acidic nickel cation and free hydroxide anion. The nickel cation could be coordinated by acetonitrile, ethanol, or water, while hydroxide anion could be stabilized by water and alcohol by the formation of hydrogen bonds. The alcohol solvent may provide hydrogen bond donors to facilitate dissociation of hydroxide, and it may explain the reaction only worked effectively with alcohol solvent systems. Secondly,

the bound acetonitrile was nucleophilically attacked by external hydroxide anion followed by hydration to form the acetamide product. According to this proposed mechanism, our previous proposed binuclear cooperation for the bis-pincer complex catalyzed nitrile hydration described in Scheme VII-8 may not be entirely necessary. Since the nitrile hydration can be easily achieved by simple complex **712**, it is more applicable by using **712** than **709-Ni**.



Scheme VII-14. Proposed Mechanism of Nitrile Hydration Catalyzed by Monomeric Pincer Complex 712

Compared to the efficiencies of acetonitrile hydration catalyzed by various metal complexes, **712** showed much higher reactivity than trans-[Ir(OH)(CO)(PPh₃)₂],²⁷⁷ trans-[Rh(OH)(CO)(PPh₃)₂],²⁷⁷ [(Cp*₂Mo(OH)(OH)₂]⁺,²⁷⁸ [{Ni(dippe)(μ-H)}₂],²⁷⁹ and [PC(sp³)P]Ni(OH)²⁷⁶ (Figure VII-11). Although the most reactive catalysts for nitrile hydration were platinum complexes,^{280,281} the scarcity and expensive price of platinum made them challenging for industrial production. The problem of nitrile hydration catalyzed by complex **712** was decomposition of **712** in ethanol. Our future goal is to synthesize and develop water-soluble or alcohol-resistant complexes in order to improve the stability of nickel catalyst.

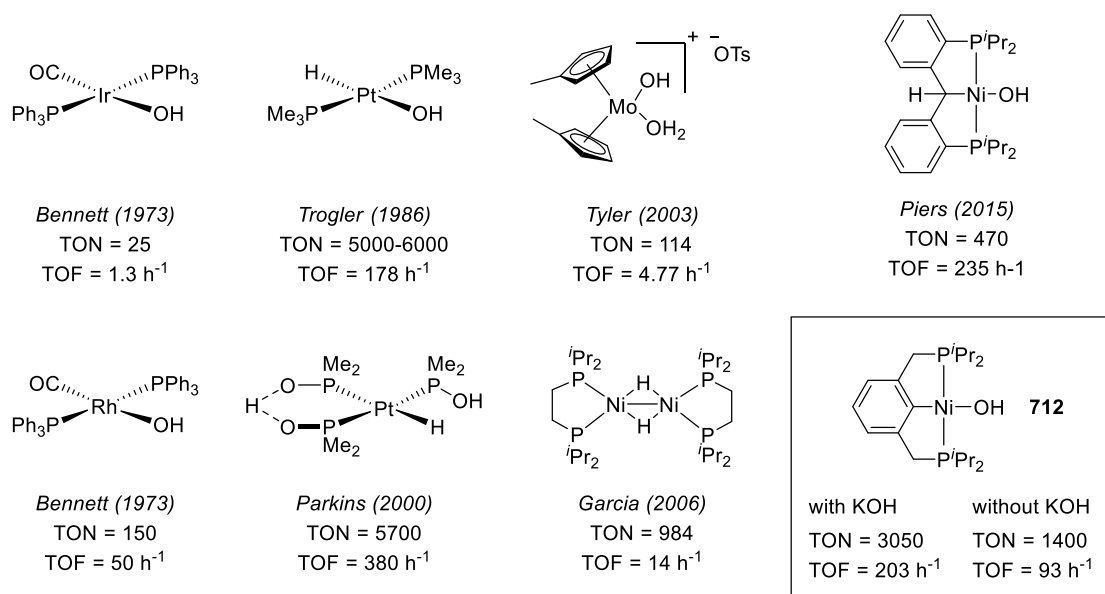


Figure VII-11. Comparison of efficiencies for hydration of acetonitrile catalyzed by various metal complexes.

7.3 Conclusions

The synthesis and reactivity of POCS bis-pincer palladium and nickel complexes were successfully developed. Abstraction of one chloride from **706** was accessed by addition of $\text{K}[\text{B}(\text{C}_6\text{F}_5)_4]$ to afford chloro-bridged complexes **707**, which could be converted into hydroxo-bridged complexes **709** by treatment of KOH. Instead of the formation of two different metal centers, binuclear metal cations (**707**, **709**, and **711**) tends to form bridging complexes evidenced by NMR spectroscopic data and X-ray diffraction studies. The chloro-bridged nickel complex (**707-Ni**) can be cleaved by acetonitrile at room temperature, whereas the hydroxo-bridged complex (**709-Ni**) was more resistant to be broken. **709-Ni** showed good catalytic activity toward nitrile hydration, but the concept of binuclear cooperation via two different metal centers was not confirmed due to the better reactivity catalyzed by a monomeric PCP pincer nickel hydroxide complex **712**. With the addition of catalytic amount of KOH, nitrile hydration catalyzed by **712** was achieved with up to a turnover number of 3050.

7.4 Experimental Section

7.4.1 General considerations

Unless specified otherwise, all manipulations were performed under an Ar atmosphere using standard Schlenk line or glovebox techniques. Toluene, diethyl ether, pentane, THF, and isooctane were dried and deoxygenated (by purging) using a solvent purification system (Innovative Technology Pure Solv MD-5 Solvent Purification System) and stored over molecular sieves in an Ar-filled glove box. C_6D_6 was dried over

NaK/Ph₂CO/18-crown-6, distilled or vacuum transferred and stored over molecular sieves in an Ar-filled glovebox. CH₂Cl₂, CDCl₃, cyclohexane, and C₆D₁₂ were dried over CaH₂, distilled or vacuum transferred and stored over molecular sieves in an Ar-filled glove box. The linker precursor 1,3-bis(mercaptomethyl)benzene²⁸² was prepared via the procedures reported in previous literature. Compounds 3-hydroxybenzyl chloride, **704**, sodium propane-1,3-bis(thiolate) **701b**, POCS bis-pincer ligand **705b**, [(POCS)PdCl]₂ **706-Pd**, and [(POCS)NiCl]₂ **706-Ni** were prepared via the procedures reported in Dr. Press dissertation.²⁷³ All other chemicals were used as received from commercial vendors.

7.4.2 Physical methods

NMR spectra were recorded on a Varian Inova 300, Mercury 300 (¹H NMR, 299.952 MHz; ¹³C NMR, 75.421 MHz; ³¹P NMR, 121.422 MHz), a Varian Inova 400 (¹H NMR, 399.535 MHz; ¹³C NMR, 100.467 MHz; ³¹P NMR, 161.734 MHz), and Varian Inova 500 (¹H NMR, 499.703 MHz; ¹³C NMR, 125.697 MHz; ³¹P NMR, 202.265 MHz) spectrometer. Chemical shifts are reported in δ (ppm). For ¹H and ¹³C NMR spectra, the residual solvent peak was used as an internal reference (¹H NMR: δ 7.16 for C₆D₆, 7.26 for CDCl₃, and 5.32 for CD₂Cl₂; ¹³C NMR: δ 128.06 for C₆D₆, 77.16 for CDCl₃, and 53.84 for CD₂Cl₂). ³¹P NMR spectra were referenced using 85% H₃PO₄ at δ 0 ppm. ¹⁹F NMR spectra were referenced using CF₃CO₂H at δ -78.5 ppm. ¹⁹F NMR signals (-133.9, -164.5, -168.4 ppm in CD₂Cl₂) and ¹³C{¹H} NMR signals (149.7, 147.7, 139.7, 137.8, 135.8, 124.6 ppm in CD₂Cl₂) for [B(C₆F₅)₄]⁻ were consistent between spectra and are not included below. Elemental analyses were performed by CALI Labs, Inc. (Parsippany, NJ).

7.4.3 Synthesis and characterization of palladium and nickel complexes

701a: In a 100 mL flask, the THF solution (10 mL) of 1,3-bis(mercaptomethyl)-benzene (4.26 g, 25.0 mmol) was added to a THF solution (30 mL) of NaO^tBu (5.29 g, 55.0 mmol). The mixture was stirred at room temperature overnight. The precipitate was collected on a frit, washed with THF, and dried under vacuum, yielding a white solid (5.01 g, 94%). ¹H NMR (499 MHz, CD₃OD): δ 7.22 (s, 1H, Ar-*H*), 7.10 (m, 2H, Ar-*H*), 7.04 (m, 1H, Ar-*H*), 3.63 (s, 4H, ArCH₂SH). ¹³C{¹H} NMR (126 MHz, CD₃OD): δ 148.7 (s), 129.0 (s), 128.5 (s), 126.1 (s), 30.6 (s, ArCH₂SH).

702: The reaction was conducted under air. In a 500 mL flask, a EtOH (100 mL) solution of sodium 1,3-phenylenedimethanethiolate **701a** (4.29 g, 20.0 mmol) was added dropwise to a EtOH solution (15 mL) of xylylene dichloride (**608**; 7.88 g, 45.0 mmol). The reaction mixture was stirred at room temperature overnight, and the white solid slowly precipitated from the solution over time. The solids were collected on a frit, washed with hexane, and further purified by extraction in Et₂O (300 mL × 3). The solution was dried by MgSO₄ and the volatiles were removed under vacuum, yielding a white solid (2.86 g, 32%). ¹H NMR (300 MHz, CDCl₃): δ 7.26 (m, 12H, Ar-*H*), 4.57 (s, 4H, ArCH₂Cl), 3.60 (s, 4H, ArCH₂S), 3.59 (s, 4H, ArCH₂S). ¹³C NMR (75 MHz, CDCl₃): δ 138.7 (s), 138.2 (s), 137.7 (s), 129.7 (s), 129.2 (s), 129.0 (s), 128.9 (s), 128.7 (s), 127.7 (s), 127.2 (s), 46.2 (s, ArCH₂Cl), 35.6 (s, ArCH₂S), 35.4 (s, ArCH₂S).

PCS bis-pincer ligand 703: In a 50 mL Schlenk flask, HP^tBu₂ (366 mg, 2.50 mmol) was added to a CH₃CN solution (10 mL) of **702** (448 mg, 1.00 mmol), and the reaction mixture was stirred at 80 °C overnight. After cooling to the room temperature,

Et₃N (223 mg, 2.20 mmol) was added and the reaction was stirred at room temperature for 1 h. The solution was removed under vacuum, and the corresponding residues were dissolved in Et₂O and filtered through silica gel. The volatiles were removed under, yielding a white solid (396 mg, 59%). ¹H NMR (300 MHz, CDCl₃): δ 7.25 (m, 10H, Ar-*H*), 7.09 (d, *J* = 7.2 Hz, 2H, Ar-*H*), 3.60 (s, 4H, ArCH₂S), 3.59 (s, 4H, ArCH₂S), 2.87 (d, *J*_{H,P} = 3.0 Hz, 4H, ArCH₂P), 1.17 (d, *J*_{H,P} = 10.8 Hz, 36H, CMe₃). ¹³C NMR (75 MHz, CDCl₃): δ 142.0 (d, *J*_{C,P} = 12.0 Hz), 138.6 (s), 138.1 (s), 130.3 (d, *J*_{C,P} = 8.1 Hz), 129.8 (s), 128.6 (s), 128.5 (s), 128.4 (s), 127.8 (s), 126.2 (d, *J*_{C,P} = 2.1 Hz), 35.8 (s, ArCH₂S), 35.5 (s, ArCH₂S), 32.0 (d, *J*_{C,P} = 21.9 Hz, CMe₃), 29.9 (d, *J*_{C,P} = 13.2 Hz, CMe₃), 28.6 (d, *J*_{C,P} = 23.4 Hz, ArCH₂P).

[(POCS)Ni]₂Cl[B(C₆F₅)₄] (707-Ni): In a 25 mL Schlenk flask, KB(C₆F₅)₄ (490 mg, 0.68 mmol) was added to a C₆H₅F solution (52 mL) of [(POCS)NiCl]₂ (**706-Ni**; 493 mg, 0.62 mmol). The reaction mixture was stirred at room temperature overnight. The solution was filtered through Celite, and the volatiles were removed under vacuum at 100 °C. The resulting solid was washed with pentane, yielding a yellow solid (856 mg, 95%). ³¹P{¹H} NMR (202 MHz, CD₂Cl₂): δ 200.4. ¹H NMR (499 MHz, CD₂Cl₂): δ 7.06 (td, *J*_{H,H} = 8.0, *J*_{H,P} = 1.0 Hz, 2H, Ar-*H*), 6.73 (d, *J*_{H,H} = 8.0 Hz, 2H, Ar-*H*), 6.68 (dd, *J*_{H,H} = 8.0, *J*_{H,P} = 1.0 Hz, 2H, Ar-*H*), 4.31 (br, 4H, CH₂CH₂CH₂), 4.19 (s, 4H, ArCH₂), 2.30 (m, 2H, CH₂CH₂CH₂), 1.53 (d, *J*_{H,P} = 15.0 Hz, 36H, CMe₃). ¹³C{¹H} NMR (126 MHz, CD₂Cl₂): δ 168.4 (d, *J*_{C,P} = 9.0 Hz), 152.1 (d, *J*_{C,P} = 1.0 Hz), 134.2 (d, *J*_{C,P} = 23.0 Hz), 129.0 (s), 118.7 (s), 110.6 (d, *J*_{C,P} = 13.0 Hz), 41.0 (s, ArCH₂), 40.3 (d, *J*_{C,P} = 16.0 Hz, CMe₃), 31.6 (s, CH₂CH₂CH₂), 28.1 (s, CMe₃), 19.8 (s, CH₂CH₂CH₂).

$[\{(POCS)Ni\}_2OH][B(C_6F_5)_4]$ (**709-Ni**): *Method A*. In a 25 mL Schlenk flask, $KB(C_6F_5)_4$ (790 mg, 1.10 mmol) and KOH (112 mg, 2.00 mmol) were added to a C_6H_5F solution (5 mL) of $[(POCS)NiCl]_2$ (**706-Ni**; 795 mg, 1.00 mmol). The reaction mixture was stirred at room temperature overnight. The solution was filtered through Celite, and the volatiles were removed under vacuum at 100 °C. The resulting solid was washed with pentane, yielding an orange solid (1396 mg, 98%). *Method B*. In a 25 mL Schlenk flask, KOH (11 mg, 0.20 mmol) was added to a C_6H_5F solution (2 mL) of $[\{(POCS)Ni\}_2Cl][B(C_6F_5)_4]$ (**707-Ni**; 137 mg, 0.10 mmol). The reaction mixture was stirred at room temperature overnight. The solution was filtered through Celite, and the volatiles were removed under vacuum at 100 °C. The resulting solid was washed with pentane, yielding an orange solid (123 mg, 91%). $^{31}P\{^1H\}$ NMR (202 MHz, CD_2Cl_2): δ 192.0. 1H NMR (499 MHz, CD_2Cl_2): δ 6.97 (t, $J_{H,H} = 8.0$ Hz, 2H, Ar-H), 6.62 (d, $J_{H,H} = 8.0$ Hz, 2H, Ar-H), 6.55 (d, $J_{H,H} = 8.0$ Hz, 2H, Ar-H), 5.79 (m, 2H, $CH_2CH_2CH_2$), 4.26 (d, $J_{H,H} = 16.0$ Hz, 2H, Ar CH_2), 3.99 (d, $J_{H,H} = 16.0$ Hz, 2H, Ar CH_2), 3.38 (m, 2H, $CH_2CH_2CH_2$), 2.33 (m, 2H, $CH_2CH_2CH_2$), 1.54 (d, $J_{H,P} = 15.0$ Hz, 18H, CMe_3), 1.45 (d, $J_{H,P} = 15.0$ Hz, 18H, CMe_3), -4.8 (br s, 1H, OH). $^{13}C\{^1H\}$ NMR (126 MHz, CD_2Cl_2): δ 168.3 (d, $J_{C,P} = 8.5$ Hz), 152.7 (d, $J_{C,P} = 2.0$ Hz), 130.9 (d, $J_{C,P} = 26.0$ Hz), 128.4 (s), 118.5 (d, $J_{C,P} = 12.0$ Hz), 110.1 (m), 40.1 (d, $J_{C,P} = 15.0$ Hz, CMe_3), 39.8 (s, Ar CH_2), 38.9 (d, $J_{C,P} = 16.0$ Hz, CMe_3), 32.4 (s, $CH_2CH_2CH_2$), 28.6 (s, CMe_3), 27.6 (s, CMe_3), 19.0 (s, $CH_2CH_2CH_2$). Anal. Calcd for $C_{57}H_{53}BF_{20}Ni_2O_3P_2S_2$: C, 48.20; H, 3.76. Found: C, 48.36; H, 3.84.

[(POCS)Pd]₂OH][B(C₆F₅)₄] (709-Pd): In a 25 mL Schlenk flask, KB(C₆F₅)₄ (151 mg, 0.21 mmol) and KOH (22 mg, 0.40 mmol) were added to a C₆H₅F solution (5 mL) of [(POCS)PdCl]₂ (**706-Pd**; 178 mg, 0.20 mmol). The reaction mixture was stirred at room temperature overnight. The solution was filtered through Celite, and the volatiles were removed under vacuum at 100 °C. The resulting solid was washed with pentane, yielding a white solid (182 mg, 60%). ³¹P{¹H} NMR (202 MHz, CD₂Cl₂): δ 196.9. ¹H NMR (499 MHz, CD₂Cl₂): δ 6.99 (t, *J*_{H,H} = 8.0 Hz, 2H, Ar-H), 6.76 (d, *J*_{H,H} = 8.0 Hz, 2H, Ar-H), 6.73 (d, *J*_{H,H} = 8.0 Hz, 2H, Ar-H), 4.23 (s, 4H, ArCH₂), 3.84 (br s, 4H, CH₂CH₂CH₂), 2.38 (m, 2H, CH₂CH₂CH₂), 1.43 (d, *J*_{H,P} = 15.5 Hz, 36H, CMe₃), -2.40 (s, OH).

In situ observation of [(POCS)Pd]₂H[B(C₆F₅)₄] (711-Pd): In a J. Young tube, isopropanol (5.0 μL, 0.07 mmol) was added to a solution (C₆D₆/C₆H₅F [1/1, 0.5 mL]) of **709-Pd** (30 mg, 0.02 mmol). After thermolysis of the mixture at 60 °C for 60 h, 85% conversion of **711-Pd** was detected in ³¹P{¹H} NMR spectrum. ³¹P{¹H} NMR (202 MHz, C₆D₆/C₆H₅F=1/1): δ 215.2. Hydride resonance in ¹H NMR (499 MHz, C₆D₆/C₆H₅F=1/1): δ -8.96 (t, *J*_{H,H} = 14 Hz, 1H, Pd-H-Pd).

In situ decomposition of 709-Pd in ethanol: In a J. Young tube, ethanol (0.5 mL) was added to **709-Pd** (30 mg, 0.02 mmol). After thermolysis of the mixture at 100 °C for 24 h, the metallic palladium was generated and coating to the wall of J. Young tube. No resonance was observed in ³¹P{¹H} NMR spectrum.

7.4.4 Catalytic nitrile hydration

General Procedure of Nitrile Hydration Catalyzed by Bis-pincer Complexes (Table VII-1). In a screw-capped culture tube, bis-pincer complex **709-Ni**, **709-Pd**, or **710** (0.01 M, 1 mL or 100 μ L, 0.1 mol% or 0.01 mol%) was added to a solution of acetonitrile (520 μ L, 10.0 mmol), water (900 μ L, 50.0 mmol), and an internal standard 1,4-dioxane (340 μ L, 4.00 mmol). The tube was sealed, and the reaction mixture was stirred at 100 °C for required time (Table VII-1). After the tube was cooled to room temperature, TONs were calculated on the basis of the formation of acetamide in the ^1H NMR spectrum.

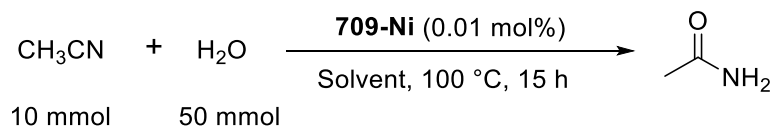
General Procedure of Nitrile Hydration Catalyzed by 712 in the Presence of HBF₄ (Table VII-2). In a screw-capped culture tube, complex **712** (0.02 M, 100 μ L, 0.02 mol%) was added to a solution of acetonitrile (520 μ L, 10.0 mmol), water (900 μ L, 50.0 mmol), and an internal standard 1,4-dioxane (340 μ L, 4.00 mmol). The mixture was subsequently introduced with required amount of HBF₄ (0.016 M, Table VII-2). The tube was sealed, and the reaction mixture was stirred at 100 °C for 15 h. After the tube was cooled to room temperature, TONs were calculated on the basis of the formation of acetamide in the ^1H NMR spectrum.

General Procedure of Nitrile Hydration Catalyzed by 712 in the Presence of KOH (Table VII-3). In a screw-capped culture tube, complex **712** (0.02 M, 100 μ L, 0.02 mol%) was added to a solution of acetonitrile (520 μ L, 10.0 mmol), water (900 μ L, 50.0 mmol), and an internal standard 1,4-dioxane (340 μ L, 4.00 mmol). The mixture was subsequently introduced with required amount of KOH (0.111 M, Table VII-3). The tube

was sealed, and the reaction mixture was stirred at 100 °C for 15 h. After the tube was cooled to room temperature, TONs were calculated on the basis of the formation of acetamide in the ¹H NMR spectrum.

Solvent Test for Nitrile Hydration Catalyzed by 709-Ni (Table VII-4). In a screw-capped culture tube, bis-pincer complex **709-Ni** (100 μL, 0.01 M, 0.01 mol%) was added to acetonitrile (520 μL, 10.0 mmol), water (900 μL, 50.0 mmol), and an internal standard 1,4-dioxane (340 μL, 4.00 mmol). The mixture was subsequently introduced with required solvent (Table VII-4). The tube was sealed, and the reaction mixture was stirred at 100 °C for 15 h. After the tube was cooled to room temperature, TONs were calculated on the basis of the formation of acetamide in the ¹H NMR spectrum.

Table VII-4. Solvent Test for Nitrile Hydration Catalyzed by 709-Ni^a



Entry	Solvent	Conversion (%) ^b	TON ^c	TOF (h ⁻¹) ^d
1	1,4-dioxane	1	50	3
2	DMF	0	0	0
3	toluene	0	0	0
4	propylene carbonate	0	0	0
5	C ₆ H ₅ F	trace	—	—
6	^t BuOH	1	50	3
7	EtOH	13	650	43

a. The reaction was carried out using CH₃CN (10 mmol), water (50 mmol), and **709-Ni** (0.01 mol%) in required solvent (2.0 mL) at 100 °C for 15 h in a culture tube. b. Conversions were calculated based on the formation of CH₃CN in ¹H NMR spectra with 1,4-dioxane (4.0 mmol) as an internal standard. c. TONs were calculated by Conv./M (M = Ni or Pd). d. TOFs were calculated by TON/h.

7.4.5 X-ray structural determination details

The X-ray crystal data (oz420 for **709-Ni** and oz421 for **709-Pd**) could be obtained by Ozerov group server.

X-ray Data Collection, Solution, and Refinement for 709-Ni. A yellow, multi-faceted block of suitable size (0.50 x 0.45 x 0.20 mm) was selected from a representative sample of crystals of the same habit using an optical microscope and mounted onto a nylon loop. Low temperature (110 K) X-ray data were obtained on a Bruker APEXII CCD based diffractometer (Mo sealed X-ray tube, $K_{\alpha} = 0.71073 \text{ \AA}$). All diffractometer manipulations, including data collection, integration and scaling were carried out using the Bruker APEXII software.¹⁵⁵ An absorption correction was applied using SADABS.¹⁵⁶ The space group was determined on the basis of systematic absences and intensity statistics and the structure was solved by direct methods and refined by full-matrix least squares on F^2 . The structure was solved in the triclinic P-1 space group using XS¹⁵⁷ (incorporated in SHELXTL). All non-hydrogen atoms were refined with anisotropic thermal parameters. All hydrogen atoms were placed in idealized positions and refined using riding model. The structure was refined (weighted least squares refinement on F^2) and the final least-squares refinement converged. The SQUEEZE protocol included in PLATON¹⁵⁸ was used to account for disordered solvent molecules found in the crystal lattice that could not be satisfactorily modeled.

X-ray Data Collection, Solution, and Refinement for 709-Pd. A colorless, multi-faceted block of suitable size (0.65 x 0.50 x 0.30 mm) was selected from a representative

sample of crystals of the same habit using an optical microscope and mounted onto a nylon loop. Low temperature (110 K) X-ray data were obtained on a Bruker APEXII CCD based diffractometer (Mo sealed X-ray tube, $K_{\alpha} = 0.71073 \text{ \AA}$). All diffractometer manipulations, including data collection, integration and scaling were carried out using the Bruker APEXII software.¹⁵⁵ An absorption correction was applied using SADABS.¹⁵⁶ The space group was determined on the basis of systematic absences and intensity statistics and the structure was solved by direct methods and refined by full-matrix least squares on F^2 . The structure was solved in the triclinic P-1 space group using XS¹⁵⁷ (incorporated in SHELXTL). All non-hydrogen atoms were refined with anisotropic thermal parameters. All hydrogen atoms were placed in idealized positions and refined using riding model. Although the proton of bridging hydroxide ligand couldn't be located in the crystal structure confidently, its presence is indicated both by ^1H NMR spectroscopic data and was needed for balancing the charges. The structure was refined (weighted least squares refinement on F^2) and the final least-squares refinement converged. The SQUEEZE protocol included in PLATON¹⁵⁸ was used to account for disordered solvent molecules found in the crystal lattice that could not be satisfactorily modeled.

CHAPTER VIII

SUMMARY

The synthesis of new PBP-type pincer complexes of iridium and rhodium has been developed. The borane-containing ligand $\text{PB}^{\text{Ph}}\text{P}$ has been typically treated as a robust Z-type ligand for studying its ability to accept two electrons from metal. Here, we have revealed a new type of binding, X-type boryl PBP pincer complexes, by facile insertion of rhodium and iridium into the B–Ph bond of $\text{PB}^{\text{Ph}}\text{P}$. This reactivity has demonstrated the first example of B–C oxidative addition, which has not been previously observed for classical B–C bonds. Compared to the carborane-derived PBP complexes or the diamino-boryl PBP complexes, this type of PBP complexes has a lower-lying empty orbital at boron with a higher degree of Lewis acidity. This unique property allows the boron of PBP ligand to cooperate with iridium center for bond formation/cleavage and interconvert between the boryl (R_2B^-)/borane (R_3B)/borate (R_4B^-) central functionality in the reactions with dihydrogen. Moreover, new PBP complexes of Ir that can serve as precatalysts for alkane transfer dehydrogenation have been developed. Although the activity of this system displayed the modest turnover numbers (up to 221), the structural and spectroscopic characterization of this series of PBP complexes enabled analysis of nonclassical BH/Ir interactions.

Unlike the synthesis of PBP complex of Ir, the analogous reaction of $\text{PB}^{\text{Ph}}\text{P}$ ligand with Rh precursor resulted in a mixture of complexes containing a Z-type borane interaction, a boryl pincer, and a $\eta^2\text{-B,C}$ binding to Rh. The similar mixture were accessible by replacement of chloride with potentially bidentate acetylacetonate,

carboxylate, and trifluoromethanesulfonate ligands. A new type of binding was observed by complexes with acetate and pivalate ligands, where the carboxylate bridges between Rh and B. All of these types of complexes are isomeric and the preference for the particular isomers for different anionic ligands varies. These isomers differ and are related by a change in the coordination mode of the oxygenous ligands and the migration of the Ph group between B and Rh.

The *ortho*-selective C–H activation of pyridines directed by Lewis acidic boron center of PBP pincer Ir complex has been developed. Transition metal-mediated C–H activation and functionalization of pyridines are still proven to be challenging because the oxidative addition of non-polar C–H bond generally involves two-electron vacant site, which is easily coordinated by the strong Lewis basic pyridine to inhibit the reactivity. With the proper design of PBP pincer Ir complexes, pyridine can bind to the Lewis acidic boron instead of iridium center. This special binding mode creates a required steric conformation sufficiently to activate the *ortho* C–H bond of pyridine selectively. The formation of four-membered products was achieved with several pyridine substrates. The C–H functionalization of 2-chloropyridine was also accomplished by the stoichiometric reactions with quantitative yield.

The synthesis of PCP- and PNP-type pincer ligands and their nickel complexes has been developed via utilization of inexpensive and commercially available chlorophosphines. The metallic nickel powder was not only a suitable reagent for the reduction of halophosphonium salts to phosphine ligands but also the nickel precursor for the formation of PCP and PNP nickel complexes. This synthetic strategy permits one-pot

synthesis of PCP and PNP nickel complexes from commercially available, nonpyrophoric materials. The PCP-type pincer Ni complexes were further applied to catalytic nitrile hydration and up to a turnover number of 3050 was achieved, which was more efficient than our newly designed POCS bis-pincer complexes of nickel and palladium.

REFERENCES

- (1) Morales-Morales, D., Jensen, C. M., Eds.; *The chemistry of pincer compounds*, 1st ed.; Elsevier: Amsterdam, 2007.
- (2) Szabó, K. J., Wendt, O. F., Eds.; *Pincer and pincer-type complexes: applications in organic synthesis and catalysis*; Wiley-VCH: Weinheim, 2014.
- (3) Koten, G. van, Milstein, D., Eds.; *Organometallic pincer chemistry*; Springer: Berlin, 2013.
- (4) van der Boom, M. E.; Milstein, D. *Chem. Rev.* **2003**, *103*, 1759–1792.
- (5) Choi, J.; MacArthur, A. H. R.; Brookhart, M.; Goldman, A. S. *Chem. Rev.* **2011**, *111*, 1761–1779.
- (6) Selander, N.; Szabó, K. *Chem. Rev.* **2011**, *111*, 2048–2076.
- (7) Gunanathan, C.; Milstein, D. *Science* **2013**, *341*, 1229712–1229712.
- (8) Gunanathan, C.; Milstein, D. *Chem. Rev.* **2014**, *114*, 12024–12087.
- (9) Moulton, C. J.; Shaw, B. L. *J. Chem. Soc., Dalton Trans.* **1976**, 1020.
- (10) Al-Salem, N. A.; Empsall, H. D.; Markham, R.; Shaw, B. L.; Weeks, B. *J. Chem. Soc., Dalton Trans.* **1979**, 1972–1982.
- (11) Green, M. L. H. *J. Organomet. Chem.* **1995**, *500*, 127–148.
- (12) Martin, C.; Mallet-Ladeira, S.; Miqueu, K.; Bouhadir, G.; Bourissou, D. *Organometallics* **2014**, *33*, 571–577.
- (13) Braunschweig, H.; Brenner, P.; Müller, A.; Radacki, K.; Rais, D.; Uttinger, K. *Chem. - Eur. J.* **2007**, *13*, 7171–7176.
- (14) Coe, B. J.; Glenwright, S. J. *Coord. Chem. Rev.* **2000**, *203*, 5–80.

- (15) Anderson, K. M.; Orpen, A. G. *Chem. Commun.* **2001**, 2682–2683.
- (16) Takaya, J.; Nakamura, S.; Iwasawa, N. *Chem. Lett.* **2012**, *41*, 967–969.
- (17) Comanescu, C. C.; Vyushkova, M.; Iluc, V. M. *Chem. Sci.* **2015**, *6*, 4570–4579.
- (18) Suh, H.-W.; Balcells, D.; Edwards, A. J.; Guard, L. M.; Hazari, N.; Mader, E. A.; Mercado, B. Q.; Repisky, M. *Inorg. Chem.* **2015**, *54*, 11411–11422.
- (19) Fan, L.; Foxman, B. M.; Ozerov, O. V. *Organometallics* **2004**, *23*, 326–328.
- (20) Mazzeo, M.; Lamberti, M.; Massa, A.; Scettri, A.; Pellicchia, C.; Peters, J. C. *Organometallics* **2008**, *27*, 5741–5743.
- (21) Schuhknecht, D.; Ritter, F.; Tauchert, M. E. *Chem. Commun.* **2016**, *52*, 11823–11826.
- (22) Olsson, D.; Nilsson, P.; El Masnaouy, M.; Wendt, O. F. *Dalton Trans.* **2005**, 1924–1929.
- (23) Zhu, J.; Lin, Z.; Marder, T. B. *Inorg. Chem.* **2005**, *44*, 9384–9390.
- (24) Morales-Morales, D.; Lee, D. W.; Wang, Z.; Jensen, C. M. *Organometallics* **2001**, *20*, 1144–1147.
- (25) Kanzelberger, M.; Zhang, X.; Emge, T. J.; Goldman, A. S.; Zhao, J.; Incarvito, C.; Hartwig, J. F. *J. Am. Chem. Soc.* **2003**, *125*, 13644–13645.
- (26) Zhao, J.; Goldman, A. S.; Hartwig, J. F. *Science* **2005**, *307*, 1080–1082.
- (27) Lee, D. W.; Kaska, W. C.; Jensen, C. M. *Organometallics* **1998**, *17*, 1–3.
- (28) Lee, D. W.; Jensen, C. M.; Morales-Morales, D. *Organometallics* **2003**, *22*, 4744–4749.

- (29) Kanzelberger, M.; Singh, B.; Czerw, M.; Krogh-Jespersen, K.; Goldman, A. S. *J. Am. Chem. Soc.* **2000**, *122*, 11017–11018.
- (30) Fan, L.; Parkin, S.; Ozerov, O. V. *J. Am. Chem. Soc.* **2005**, *127*, 16772–16773.
- (31) Göttker-Schnetmann, I.; White, P. S.; Brookhart, M. *Organometallics* **2004**, *23*, 1766–1776.
- (32) Gatard, S.; Çelenligil-Çetin, R.; Guo, C.; Foxman, B. M.; Ozerov, O. V. *J. Am. Chem. Soc.* **2006**, *128*, 2808–2809.
- (33) Hasegawa, M.; Segawa, Y.; Yamashita, M.; Nozaki, K. *Angew. Chem. Int. Ed.* **2012**, *51*, 6956–6960.
- (34) Masuda, Y.; Hasegawa, M.; Yamashita, M.; Nozaki, K.; Ishida, N.; Murakami, M. *J. Am. Chem. Soc.* **2013**, *135*, 7142–7145.
- (35) Cundari, T. R. *J. Am. Chem. Soc.* **1994**, *116*, 340–347.
- (36) Wang, D. Y.; Choliy, Y.; Haibach, M. C.; Hartwig, J. F.; Krogh-Jespersen, K.; Goldman, A. S. *J. Am. Chem. Soc.* **2016**, *138*, 149–163.
- (37) Segawa, Y.; Yamashita, M.; Nozaki, K. *J. Am. Chem. Soc.* **2009**, *131*, 9201–9203.
- (38) Morgan, E.; MacLean, D. F.; McDonald, R.; Turculet, L. *J. Am. Chem. Soc.* **2009**, *131*, 14234–14236.
- (39) Galli, P.; Vecellio, G. *Prog. Polym. Sci.* **2001**, *26*, 1287–1336.
- (40) Alt, H. G.; Köppl, A. *Chem. Rev.* **2000**, *100*, 1205–1222.
- (41) Chen, E. Y.-X.; Marks, T. J. *Chem. Rev.* **2000**, *100*, 1391–1434.
- (42) Hlatky, G. G. *Chem. Rev.* **2000**, *100*, 1347–1376.
- (43) Gibson, V. C.; Spitzmesser, S. K. *Chem. Rev.* **2003**, *103*, 283–316.

- (44) Baier, M. C.; Zuideveld, M. A.; Mecking, S. *Angew. Chem. Int. Ed.* **2014**, *53*, 9722–9744.
- (45) Ojima, I.; Tsai, C.-Y.; Tzamarioudaki, M.; Bonafoux, D. In *Organic Reactions*; John Wiley & Sons, Inc., Ed.; John Wiley & Sons, Inc.: Hoboken, NJ, USA, 2000; pp 1–354.
- (46) Eilbracht, P.; Bärfacker, L.; Buss, C.; Hollmann, C.; Kitsos-Rzychon, B. E.; Kranemann, C. L.; Rische, T.; Roggenbuck, R.; Schmidt, A. *Chem. Rev.* **1999**, *99*, 3329–3366.
- (47) Franke, R.; Selent, D.; Börner, A. *Chem. Rev.* **2012**, *112*, 5675–5732.
- (48) Skupinska, J. *Chem. Rev.* **1991**, *91*, 613–648.
- (49) McGuinness, D. S. *Chem. Rev.* **2011**, *111*, 2321–2341.
- (50) Weissermel, K.; Arpe, H.-J. *Industrial organic chemistry*, 3rd completely rev. ed.; VCH: Weinheim, 1997.
- (51) Weckhuysen, B. M.; Schoonheydt, R. A. *Catal. Today* **1999**, *51*, 223–232.
- (52) Weckhuysen, B. M.; Wachs, I. E.; Schoonheydt, R. A. *Chem. Rev.* **1996**, *96*, 3327–3350.
- (53) Baudry, D.; Ephritikhine, M.; Felkin, H.; Holmes-Smith, R. *J. Chem. Soc., Chem. Commun.* **1983**, 788.
- (54) Felkin, H.; Fillebeen-Khan, T.; Gault, Y.; Holmes-Smith, R.; Zakrzewski, J. *Tetrahedron Lett.* **1984**, *25*, 1279–1282.
- (55) Felkin, H.; Fillebeen-khan, T.; Holmes-Smith, R.; Yingrui, L. *Tetrahedron Lett.* **1985**, *26*, 1999–2000.

- (56) Burk, M. J.; Crabtree, R. H.; Parnell, C. P.; Uriarte, R. J. *Organometallics* **1984**, *3*, 816–817.
- (57) Burk, M. J.; Crabtree, R. H.; McGrath, D. V. *J. Chem. Soc., Chem. Commun.* **1985**, 1829.
- (58) Burk, M. J.; Crabtree, R. H. *J. Am. Chem. Soc.* **1987**, *109*, 8025–8032.
- (59) Crabtree, R. H.; Mihelcic, J. M.; Quirk, J. M. *J. Am. Chem. Soc.* **1979**, *101*, 7738–7740.
- (60) Crabtree, R. H.; Mellea, M. F.; Mihelcic, J. M.; Quirk, J. M. *J. Am. Chem. Soc.* **1982**, *104*, 107–113.
- (61) Belli, J.; Jensen, C. M. *Organometallics* **1996**, *15*, 1532–1534.
- (62) Gupta, M.; Hagen, C.; Flesher, R. J.; Kaska, W. C.; Jensen, C. M. *Chem. Commun.* **1996**, 2083–2084.
- (63) Punji, B.; Emge, T. J.; Goldman, A. S. *Organometallics* **2010**, *29*, 2702–2709.
- (64) Haenel, M. W.; Oevers, S.; Angermund, K.; Kaska, W. C.; Fan, H.-J.; Hall, M. B. *Angew. Chem. Int. Ed.* **2001**, *40*, 3596.
- (65) Göttker-Schnetmann, I.; White, P.; Brookhart, M. *J. Am. Chem. Soc.* **2004**, *126*, 1804–1811.
- (66) Kuklin, S. A.; Sheloumov, A. M.; Dolgushin, F. M.; Ezernitskaya, M. G.; Peregudov, A. S.; Petrovskii, P. V.; Koridze, A. A. *Organometallics* **2006**, *25*, 5466–5476.
- (67) Shi, Y.; Suguri, T.; Dohi, C.; Yamada, H.; Kojima, S.; Yamamoto, Y. *Chem. - Eur. J.* **2013**, *19*, 10672–10689.

- (68) Yao, W.; Zhang, Y.; Jia, X.; Huang, Z. *Angew. Chem. Int. Ed.* **2014**, *53*, 1390–1394.
- (69) Renkema, K. B.; Kissin, Y. V.; Goldman, A. S. *J. Am. Chem. Soc.* **2003**, *125*, 7770–7771.
- (70) Bézier, D.; Brookhart, M. *ACS Catal.* **2014**, *4*, 3411–3420.
- (71) Polukeev, A. V.; Wendt, O. F. *Organometallics* **2017**, *36*, 639–649.
- (72) Tanoue, K.; Yamashita, M. *Organometallics* **2015**, *34*, 4011–4017.
- (73) Kwan, E. H.; Kawai, Y. J.; Kamakura, S.; Yamashita, M. *Dalton Trans.* **2016**.
- (74) Kwan, E. H.; Ogawa, H.; Yamashita, M. *ChemCatChem* **2017**, *9*, 2457–2462.
- (75) Segawa, Y.; Yamashita, M.; Nozaki, K. *Organometallics* **2009**, *28*, 6234–6242.
- (76) Masuda, Y.; Hasegawa, M.; Yamashita, M.; Nozaki, K.; Ishida, N.; Murakami, M. *J. Am. Chem. Soc.* **2013**, *135*, 7142–7145.
- (77) MacLean, D. F.; McDonald, R.; Ferguson, M. J.; Caddell, A. J.; Turculet, L. *Chem. Commun.* **2008**, 5146–5148.
- (78) Shimada, S.; Batsanov, A. S.; Howard, J. A. K.; Marder, T. B. *Angew. Chem. Int. Ed.* **2001**, *40*, 2168–2171.
- (79) Lachaize, S.; Sabo-Etienne, S. *Eur. J. Inorg. Chem.* **2006**, *2006*, 2115–2127.
- (80) Lam, W. H.; Shimada, S.; Batsanov, A. S.; Lin, Z.; Marder, T. B.; Cowan, J. A.; Howard, J. A. K.; Mason, S. A.; McIntyre, G. J. *Organometallics* **2003**, *22*, 4557–4568.
- (81) Montiel-Palma, V.; Lumbierres, M.; Donnadiou, B.; Sabo-Etienne, S.; Chaudret, B. *J. Am. Chem. Soc.* **2002**, *124*, 5624–5625.

- (82) Hebden, T. J.; Denney, M. C.; Pons, V.; Piccoli, P. M. B.; Koetzle, T. F.; Schultz, A. J.; Kaminsky, W.; Goldberg, K. I.; Heinekey, D. M. *J. Am. Chem. Soc.* **2008**, *130*, 10812–10820.
- (83) Douglas, T. M.; Chaplin, A. B.; Weller, A. S.; Yang, X.; Hall, M. B. *J. Am. Chem. Soc.* **2009**, *131*, 15440–15456.
- (84) Alcaraz, G.; Chaplin, A. B.; Stevens, C. J.; Clot, E.; Vendier, L.; Weller, A. S.; Sabo-Etienne, S. *Organometallics* **2010**, *29*, 5591–5595.
- (85) Lin, T.-P.; Peters, J. C. *J. Am. Chem. Soc.* **2013**, *135*, 15310–15313.
- (86) Lin, T.-P.; Peters, J. C. *J. Am. Chem. Soc.* **2014**, *136*, 13672–13683.
- (87) Hill, A. F.; McQueen, C. M. A. *Organometallics* **2014**, *33*, 1977–1985.
- (88) Miyada, T.; Yamashita, M. *Organometallics* **2013**, *32*, 5281–5284.
- (89) Miyada, T.; Huang Kwan, E.; Yamashita, M. *Organometallics* **2014**, *33*, 6760–6770.
- (90) Hill, A. F.; McQueen, C. M. A. *Organometallics* **2014**, *33*, 1977–1985.
- (91) Hill, A. F.; Lee, S. B.; Park, J.; Shang, R.; Willis, A. C. *Organometallics* **2010**, *29*, 5661–5669.
- (92) Ogawa, H.; Yamashita, M. *Dalton Trans.* **2013**, *42*, 625–629.
- (93) Ogawa, H.; Yamashita, M. *Chem. Lett.* **2014**, *43*, 664–666.
- (94) Curado, N.; Maya, C.; López-Serrano, J.; Rodríguez, A. *Chem. Commun.* **2014**, *50*, 15718–15721.
- (95) Spokoyny, A. M.; Reuter, M. G.; Stern, C. L.; Ratner, M. A.; Seideman, T.; Mirkin, C. A. *J. Am. Chem. Soc.* **2009**, *131*, 9482–9483.

- (96) El-Zaria, M. E.; Arai, H.; Nakamura, H. *Inorg. Chem.* **2011**, *50*, 4149–4161.
- (97) Eleazer, B. J.; Smith, M. D.; Peryshkov, D. V. *Organometallics* **2016**, *35*, 106–112.
- (98) Eleazer, B. J.; Smith, M. D.; Popov, A. A.; Peryshkov, D. V. *J. Am. Chem. Soc.* **2016**, *138*, 10531–10538.
- (99) Eleazer, B. J.; Smith, M. D.; Peryshkov, D. V. *J. Organomet. Chem.* **2017**, *829*, 42–47.
- (100) Ohta, K.; Goto, T.; Yamazaki, H.; Pichierri, F.; Endo, Y. *Inorg. Chem.* **2007**, *46*, 3966–3970.
- (101) Quan, Y.; Xie, Z. *J. Am. Chem. Soc.* **2015**, *137*, 3502–3505.
- (102) Shih, W.-C.; Gu, W.; MacInnis, M. C.; Timpa, S. D.; Bhuvanesh, N.; Zhou, J.; Ozerov, O. V. *J. Am. Chem. Soc.* **2016**, *138*, 2086–2089.
- (103) Noël-Duchesneau, L.; Lugan, N.; Lavigne, G.; Labande, A.; César, V. *Organometallics* **2014**, *33*, 5085–5088.
- (104) DeMott, J. C.; Gu, W.; McCulloch, B. J.; Herbert, D. E.; Goshert, M. D.; Walensky, J. R.; Zhou, J.; Ozerov, O. V. *Organometallics* **2015**, *34*, 3930–3933.
- (105) Bontemps, S.; Gornitzka, H.; Bouhadir, G.; Miqueu, K.; Bourissou, D. *Angew. Chem. Int. Ed.* **2006**, *45*, 1611–1614.
- (106) Sircoglou, M.; Bontemps, S.; Mercy, M.; Saffon, N.; Takahashi, M.; Bouhadir, G.; Maron, L.; Bourissou, D. *Angew. Chem. Int. Ed.* **2007**, *46*, 8583–8586.
- (107) Miyaura, N.; Suzuki, A. *Chem. Rev.* **1995**, *95*, 2457–2483.
- (108) Cowie, B. E.; Emslie, D. J. H. *Organometallics* **2015**, *34*, 2737–2746.
- (109) Kameo, H.; Nakazawa, H. *Organometallics* **2012**, *31*, 7476–7484.

- (110) Nesbit, M. A.; Suess, D. L. M.; Peters, J. C. *Organometallics* **2015**, *34*, 4741–4752.
- (111) Emslie, D. J. H.; Cowie, B. E.; Kolpin, K. B. *Dalton Trans.* **2012**, *41*, 1101–1117.
- (112) Bontemps, S.; Sircoglou, M.; Bouhadir, G.; Puschmann, H.; Howard, J. A. K.; Dyer, P. W.; Miqueu, K.; Bourissou, D. *Chem. - Eur. J.* **2008**, *14*, 731–740.
- (113) Schindler, T.; Lux, M.; Peters, M.; Scharf, L. T.; Osseili, H.; Maron, L.; Tauchert, M. E. *Organometallics* **2015**, *34*, 1978–1984.
- (114) Harman, W. H.; Peters, J. C. *J. Am. Chem. Soc.* **2012**, *134*, 5080–5082.
- (115) Sircoglou, M.; Bontemps, S.; Mercy, M.; Miqueu, K.; Ladeira, S.; Saffon, N.; Maron, L.; Bouhadir, G.; Bourissou, D. *Inorg. Chem.* **2010**, *49*, 3983–3990.
- (116) Boone, M. P.; Stephan, D. W. *J. Am. Chem. Soc.* **2013**, *135*, 8508–8511.
- (117) Boone, M. P.; Stephan, D. W. *Chem. - Eur. J.* **2014**, *20*, 3333–3341.
- (118) Suess, D. L. M.; Peters, J. C. *J. Am. Chem. Soc.* **2013**, *135*, 4938–4941.
- (119) Suess, D. L. M.; Peters, J. C. *J. Am. Chem. Soc.* **2013**, *135*, 12580–12583.
- (120) Gu, W. Ph.D. Dissertation Chapter VII, Texas A&M University, College Station, TX, 2011.
- (121) Bontemps, S.; Bouhadir, G.; Gu, W.; Mercy, M.; Chen, C.-H.; Foxman, B. M.; Maron, L.; Ozerov, O. V.; Bourissou, D. *Angew. Chem. Int. Ed.* **2008**, *47*, 1481–1484.
- (122) Sircoglou, M.; Bontemps, S.; Bouhadir, G.; Saffon, N.; Miqueu, K.; Gu, W.; Mercy, M.; Chen, C.-H.; Foxman, B. M.; Maron, L.; Ozerov, O. V.; Bourissou, D. *J. Am. Chem. Soc.* **2008**, *130*, 16729–16738.
- (123) Moret, M.-E.; Peters, J. C. *Angew. Chem. Int. Ed.* **2011**, *50*, 2063–2067.

- (124) Suess, D. L. M.; Tsay, C.; Peters, J. C. *J. Am. Chem. Soc.* **2012**, *134*, 14158–14164.
- (125) Anderson, J. S.; Rittle, J.; Peters, J. C. *Nature* **2013**, *501*, 84–87.
- (126) Moret, M.-E.; Zhang, L.; Peters, J. C. *J. Am. Chem. Soc.* **2013**, *135*, 3792–3795.
- (127) Bontemps, S.; Gornitzka, H.; Bouhadir, G.; Miqueu, K.; Bourissou, D. *Angew. Chem. Int. Ed.* **2006**, *45*, 1611–1614.
- (128) Conifer, C. M.; Law, D. J.; Sunley, G. J.; White, A. J. P.; Britovsek, G. J. P. *Organometallics* **2011**, *30*, 4060–4066.
- (129) Harman, W. H.; Peters, J. C. *J. Am. Chem. Soc.* **2012**, *134*, 5080–5082.
- (130) Inagaki, F.; Matsumoto, C.; Okada, Y.; Maruyama, N.; Mukai, C. *Angew. Chem. Int. Ed.* **2015**, *54*, 818–822.
- (131) Barker, G. K.; Green, M.; Stone, F. G. A.; Wolsey, W. C.; Welch, A. J. *J. Chem. Soc., Dalton Trans.* **1983**, 2063–2069.
- (132) Lin, T.-P.; Peters, J. C. *J. Am. Chem. Soc.* **2014**, *136*, 13672–13683.
- (133) Tanoue, K.; Yamashita, M. *Organometallics* **2015**, *34*, 4011–4017.
- (134) Eleazer, B. J.; Smith, M. D.; Popov, A. A.; Peryshkov, D. V. *J. Am. Chem. Soc.* **2016**, *138*, 10531–10538.
- (135) Burford, R. J.; Piers, W. E.; Ess, D. H.; Parvez, M. *J. Am. Chem. Soc.* **2014**, *136*, 3256–3263.
- (136) Davidson, J. J.; DeMott, J. C.; Douvris, C.; Fafard, C. M.; Bhuvanesh, N.; Chen, C.-H.; Herbert, D. E.; Lee, C.-I.; McCulloch, B. J.; Foxman, B. M.; Ozerov, O. V. *Inorg. Chem.* **2015**, *54*, 2916–2935.

- (137) Haibach, M. C.; Wang, D. Y.; Emge, T. J.; Krogh-Jespersen, K.; Goldman, A. S. *Chem. Sci.* **2013**, *4*, 3683.
- (138) Mankad, N. P.; Rivard, E.; Harkins, S. B.; Peters, J. C. *J. Am. Chem. Soc.* **2005**, *127*, 16032–16033.
- (139) Kim, Y.-E.; Oh, S.; Kim, S.; Kim, O.; Kim, J.; Han, S. W.; Lee, Y. *J. Am. Chem. Soc.* **2015**, *137*, 4280–4283.
- (140) Yang, H.; Gabbai, F. P. *J. Am. Chem. Soc.* **2014**, *136*, 10866–10869.
- (141) Korshin, E. E.; Leitus, G.; Shimon, L. J. W.; Konstantinovski, L.; Milstein, D. *Inorg. Chem.* **2008**, *47*, 7177–7189.
- (142) MacInnis, M. C.; MacLean, D. F.; Lundgren, R. J.; McDonald, R.; Turculet, L. *Organometallics* **2007**, *26*, 6522–6525.
- (143) Mitton, S. J.; McDonald, R.; Turculet, L. *Organometallics* **2009**, *28*, 5122–5136.
- (144) Takaya, J.; Iwasawa, N. *J. Am. Chem. Soc.* **2008**, *130*, 15254–15255.
- (145) Whited, M. T.; Deetz, A. M.; Boerma, J. W.; DeRoshia, D. E.; Janzen, D. E. *Organometallics* **2014**, *33*, 5070–5073.
- (146) Westcott, S. A.; Marder, T. B.; Baker, R. T.; Calabrese, J. C. *Can. J. Chem.* **1993**, *71*, 930–936.
- (147) Knorr, J. R.; Merola, J. S. *Organometallics* **1990**, *9*, 3008–3010.
- (148) Peterson, T. H.; Golden, J. T.; Bergman, R. G. *Organometallics* **1999**, *18*, 2005–2020.
- (149) Hartwig, J. F.; Huber, S. *J. Am. Chem. Soc.* **1993**, *115*, 4908–4909.
- (150) Nesbit, M. A.; Suess, D. L. M.; Peters, J. C. *Organometallics* **2015**, *34*, 4741–4752.

- (151) Mkhaliid, I. A. I.; Barnard, J. H.; Marder, T. B.; Murphy, J. M.; Hartwig, J. F. *Chem. Rev.* **2010**, *110*, 890–931.
- (152) Giordano, G.; Crabtree, R. H.; Heintz, R. M.; Forster, D.; Morris, D. E. *Inorg. Synth.* **1979**, *19*, 218–220.
- (153) Chatt, J.; Venanzi, L. M. *J. Chem. Soc.* **1957**, 4735–4741.
- (154) Herde, J. L.; Lambert, J. C.; Senoff, C. V.; Cushing, M. A. *Inorg. Synth.* **1974**, *15*, 18–20.
- (155) APEX2, Version 2 User Manual, M86-E01078, Bruker Analytical X-ray Systems, Madison, WI, June 2006.
- (156) Sheldrick, G.M. “SADABS (version 2008/1): Program for Absorption Correction for Data from Area Detector Frames”, University of Göttingen, 2008.
- (157) Sheldrick, G. M. *Acta Crystallogr. A* **2008**, *64*, 112–122.
- (158) Spek, A. L. *J. Appl. Crystallogr.* **2003**, *36*, 7–13.
- (159) Frisch, M. J., Trucks, G. W., Schlegel, H. B., Scuseria, G. E., Robb, M. A., Cheeseman, J. R., Scalmani, G., Barone, V., Mennucci, B., Petersson, G. A., Nakatsuji, H., Caricato, M., Li, X., Hratchian, H. P., Izmaylov, A. F., Bloino, J., Zheng, G., Sonnenberg, J. L., Hada, M., Ehara, M., Toyota, K., Fukuda, R., Hasegawa, J., Ishida, M., Nakajima, T., Honda, Y., Kitao, O., Nakai, H., Vreven, T., Montgomery, Jr. J. A., Peralta, J. E., Ogliaro, F., Bearpark, M., Heyd, J. J., Brothers, E., Kudin, K. N., Staroverov, V. N., Kobayashi, R., Normand, J., Raghavachari, K., Rendell, A., Burant, J. C., Iyengar, S. S., Tomasi, J., Cossi, M., Rega, N., Millam, N. J., Klene, M., Knox, J. E., Cross, J. B., Bakken, V., Adamo,

C., Jaramillo, J., Gomperts, R., Stratmann, R. E., Yazyev, O., Austin, A. J., Cammi, R., Pomelli, C., Ochterski, J. W., Martin, R. L., Morokuma, K., Zakrzewski, V. G., Voth, G. A., Salvador, P., Dannenberg, J. J., Dapprich, S., Daniels, A. D., Farkas, Ö., Foresman, J. B., Ortiz, J. V., Cioslowski, J. & Fox, D. J. Revision D.01 ed.; Gaussian, Inc.: Wallingford, CT, 2009.

- (160) Zhao, Y.; Truhlar, D. G. *Theor. Chem. Acc.* **2008**, *120*, 215–241.
- (161) CYLview, 1.0b; Legault, C. Y., Université de Sherbrooke, 2009 (<http://www.cylview.org>).
- (162) Gunanathan, C.; Milstein, D. *Chem. Rev.* **2014**, *114*, 12024–12087.
- (163) Gunanathan, C.; Milstein, D. *Acc. Chem. Res.* **2011**, *44*, 588–602.
- (164) van Koten, G.; Timmer, K.; Noltes, J. G.; Spek, A. L. *J. Chem. Soc., Chem. Commun.* **1978**, 250–252.
- (165) Yamashita, M. *Bull. Chem. Soc. Jpn.* **2016**, *89*, 269–281.
- (166) Kwan, E. H.; Kawai, Y. J.; Kamakura, S.; Yamashita, M. *Dalton Trans.* **2016**, *45*, 15931–15941.
- (167) El-Zaria, M. E.; Arii, H.; Nakamura, H. *Inorg. Chem.* **2011**, *50*, 4149–4161.
- (168) Amgoune, A.; Bourissou, D. *Chem. Commun.* **2011**, *47*, 859–871.
- (169) Braunschweig, H.; Dewhurst, R. D. *Dalton Trans.* **2011**, *40*, 549–558.
- (170) Parkin, G. *Organometallics* **2006**, *25*, 4744–4747.
- (171) Owen, G. R. *Chem. Commun.* **2016**, *52*, 10712–10726.
- (172) Himmel, D.; Krossing, I.; Schnepf, A. *Angew. Chem. Int. Ed.* **2014**, *53*, 370–374.
- (173) Davies, H. M. L.; Morton, D. *Chem. Soc. Rev.* **2011**, *40*, 1857.

- (174) Dikarev, E. V.; Shpanchenko, R. V.; Andreini, K. W.; Block, E.; Jin; Petrukhina, M. A. *Inorg. Chem.* **2004**, *43*, 5558–5563.
- (175) Barrow, M. J.; Cradock, S.; Ebsworth, E. A. V.; Rankin, D. W. H. *J. Chem. Soc., Dalton Trans.* **1981**, 1988.
- (176) Pyckhout, W.; Van Alsenoy, C.; Geise, H. J. *J. Mol. Struct.* **1986**, *144*, 265–279.
- (177) Fontaine, X. L. R.; Greenwood, N. N.; Kennedy, J. D.; Thornton-Pett, M.; Peiju, Z. *J. Chem. Soc., Chem. Commun.* **1987**, 1717–1718.
- (178) Ugolotti, J.; Hellstrom, S.; Britovsek, G. J. P.; Jones, T. S.; Hunt, P.; White, A. J. *P. Dalton Trans.* **2007**, 1425–1432.
- (179) Holzhey, N.; Pitter, S. *J. Mol. Catal. A.* **1999**, *146*, 25–36.
- (180) Gupta, M.; Hagen, C.; Kaska, W. C.; Cramer, R. E.; Jensen, C. M. *J. Am. Chem. Soc.* **1997**, *119*, 840–841.
- (181) Xu, W.; Rosini, G. P.; Krogh-Jespersen, K.; Goldman, A. S.; Gupta, M.; Jensen, C. M.; Kaska, W. C. *Chem. Commun.* **1997**, 2273–2274.
- (182) Liu, F.; Goldman, A. S. *Chem. Commun.* **1999**, 655–656.
- (183) Göttker-Schnetmann, I.; Brookhart, M. *J. Am. Chem. Soc.* **2004**, *126*, 9330–9338.
- (184) Nawara-Hultsch, A. J.; Hackenberg, J. D.; Punji, B.; Supplee, C.; Emge, T. J.; Bailey, B. C.; Schrock, R. R.; Brookhart, M.; Goldman, A. S. *ACS Catal.* **2013**, *3*, 2505–2514.
- (185) Arnold, N.; Mozo, S.; Paul, U.; Radius, U.; Braunschweig, H. *Organometallics* **2015**, *34*, 5709–5715.

- (186) Gloaguen, Y.; Bénac-Lestrille, G.; Vendier, L.; Helmstedt, U.; Clot, E.; Alcaraz, G.; Sabo-Etienne, S. *Organometallics* **2013**, *32*, 4868–4877.
- (187) Montiel-Palma, V.; Lumbierres, M.; Donnadiou, B.; Sabo-Etienne, S.; Chaudret, B. *J. Am. Chem. Soc.* **2002**, *124*, 5624–5625.
- (188) Lachaize, S.; Essalah, K.; Montiel-Palma, V.; Vendier, L.; Chaudret, B.; Barthelat, J.-C.; Sabo-Etienne, S. *Organometallics* **2005**, *24*, 2935–2943.
- (189) Miyada, T.; Huang Kwan, E.; Yamashita, M. *Organometallics* **2014**, *33*, 6760–6770.
- (190) Hill, A. F. *Organometallics* **2006**, *25*, 4741–4743.
- (191) Bouhadir, G.; Bourissou, D. *Chem. Soc. Rev.* **2016**, *45*, 1065–1079.
- (192) Addison, A. W.; Rao, T. N.; Reedijk, J.; van Rijn, J.; Verschoor, G. C. *J. Chem. Soc. Dalton Trans.* **1984**, 1349–1356.
- (193) Smith, J. D.; Logan, J. R.; Doyle, L. E.; Burford, R. J.; Sugawara, S.; Ohnita, C.; Yamamoto, Y.; Piers, W. E.; Spasyuk, D. M.; Borau-Garcia, J. *Dalton Trans.* **2016**, *45*, 12669–12679.
- (194) Nakao, Y. *Synthesis* **2011**, *2011*, 3209–3219.
- (195) Fish, R. H.; Tae-Jeong, K.; Stewart, J. L.; Bushweller, J. H.; Rosen, R. K.; Dupon, W. J. *Organometallics* **1986**, *5*, 2193–2198.
- (196) Bruce, M. I.; Humphrey, M. G.; Snow, M. R.; Tiekink, E. R. T.; Wallis, R. C. *J. Organomet. Chem.* **1986**, *314*, 311–322.
- (197) Eisenstadt, A.; Giandomenico, C. M.; Frederick, M. F.; Laine, R. M. *Organometallics* **1985**, *4*, 2033–2039.

- (198) Deeming, A. J.; Peters, R.; Hursthouse, M. B.; Backer-Dirks, J. D. J. *J. Chem. Soc. Dalton Trans.* **1982**, 787–791.
- (199) Moore, E. J.; Pretzer, W. R.; O’Connell, T. J.; Harris, J.; LaBounty, L.; Chou, L.; Grimmer, S. S. *J. Am. Chem. Soc.* **1992**, *114*, 5888–5890.
- (200) Lewis, J. C.; Bergman, R. G.; Ellman, J. A. *J. Am. Chem. Soc.* **2007**, *129*, 5332–5333.
- (201) Berman, A. M.; Lewis, J. C.; Bergman, R. G.; Ellman, J. A. *J. Am. Chem. Soc.* **2008**, *130*, 14926–14927.
- (202) Nakao, Y.; Kanyiva, K. S.; Hiyama, T. *J. Am. Chem. Soc.* **2008**, *130*, 2448–2449.
- (203) Tsai, C.-C.; Shih, W.-C.; Fang, C.-H.; Li, C.-Y.; Ong, T.-G.; Yap, G. P. A. *J. Am. Chem. Soc.* **2010**, *132*, 11887–11889.
- (204) Nakao, Y.; Yamada, Y.; Kashihara, N.; Hiyama, T. *J. Am. Chem. Soc.* **2010**, *132*, 13666–13668.
- (205) Jordan, R. F.; Taylor, D. F. *J. Am. Chem. Soc.* **1989**, *111*, 778–779.
- (206) Guan, B.-T.; Hou, Z. *J. Am. Chem. Soc.* **2011**, *133*, 18086–18089.
- (207) Nagae, H.; Shibata, Y.; Tsurugi, H.; Mashima, K. *J. Am. Chem. Soc.* **2015**, *137*, 640–643.
- (208) Larsen, M. A.; Hartwig, J. F. *J. Am. Chem. Soc.* **2014**, *136*, 4287–4299.
- (209) Sadler, S. A.; Tajuddin, H.; Mkhallid, I. A. I.; Batsanov, A. S.; Albesa-Jove, D.; Cheung, M. S.; Maxwell, A. C.; Shukla, L.; Roberts, B.; Blakemore, D. C.; Lin, Z.; Marder, T. B.; Steel, P. G. *Org. Biomol. Chem.* **2014**, *12*, 7318.

- (210) Obligacion, J. V.; Semproni, S. P.; Chirik, P. J. *J. Am. Chem. Soc.* **2014**, *136*, 4133–4136.
- (211) Obligacion, J. V.; Semproni, S. P.; Pappas, I.; Chirik, P. J. *J. Am. Chem. Soc.* **2016**, *138*, 10645–10653.
- (212) Ackermann, L.; Vicente, R.; Kapdi, A. *Angew. Chem. Int. Ed.* **2009**, *48*, 9792–9826.
- (213) Chen, X.; Engle, K. M.; Wang, D.-H.; Yu, J.-Q. *Angew. Chem. Int. Ed.* **2009**, *48*, 5094–5115.
- (214) Daugulis, O.; Do, H.-Q.; Shabashov, D. *Acc. Chem. Res.* **2009**, *42*, 1074–1086.
- (215) Colby, D. A.; Bergman, R. G.; Ellman, J. A. *Chem. Rev.* **2010**, *110*, 624–655.
- (216) Lyons, T. W.; Sanford, M. S. *Chem. Rev.* **2010**, *110*, 1147–1169.
- (217) Basil, J. D.; Aradi, A. A.; Bhattacharyya, N. K.; Rath, N. P.; Eigenbrot, C.; Fehlner, T. P. *Inorg. Chem.* **1990**, *29*, 1260–1270.
- (218) Kawano, Y.; Yasue, T.; Shimoi, M. *J. Am. Chem. Soc.* **1999**, *121*, 11744–11750.
- (219) Yasue, T.; Kawano, Y.; Shimoi, M. *Angew. Chem. Int. Ed.* **2003**, *42*, 1727–1730.
- (220) Braunschweig, H.; Radacki, K.; Seeler, F.; Whittell, G. R. *Organometallics* **2004**, *23*, 4178–4180.
- (221) Shih, W.-C.; Ozerov, O. V. *Organometallics* **2017**, *36*, 228–233.
- (222) Vilanova, S. P.; Iluc, V. M. *Organometallics* **2016**, *35*, 2110–2123.
- (223) Li, M.; Hua, R. *Tetrahedron Lett.* **2009**, *50*, 1478–1481.
- (224) Seiple, I. B.; Su, S.; Rodriguez, R. A.; Gianatassio, R.; Fujiwara, Y.; Sobel, A. L.; Baran, P. S. *J. Am. Chem. Soc.* **2010**, *132*, 13194–13196.

- (225) Wen, J.; Qin, S.; Ma, L.-F.; Dong, L.; Zhang, J.; Liu, S.-S.; Duan, Y.-S.; Chen, S.-Y.; Hu, C.-W.; Yu, X.-Q. *Org. Lett.* **2010**, *12*, 2694–2697.
- (226) Tobisu, M.; Hyodo, I.; Chatani, N. *J. Am. Chem. Soc.* **2009**, *131*, 12070–12071.
- (227) Hintermann, L.; Dang, T. T.; Labonne, A.; Kribber, T.; Xiao, L.; Naumov, P. *Chem. - Eur. J.* **2009**, *15*, 7167–7179.
- (228) Goldman, A. S. *Science* **2006**, *312*, 257–261.
- (229) Gozin, M.; Weisman, A.; Ben-David, Y.; Milstein, D. *Nature* **1993**, *364*, 699–701.
- (230) Zhang, J.; Leitun, G.; Ben-David, Y.; Milstein, D. *J. Am. Chem. Soc.* **2005**, *127*, 10840–10841.
- (231) Montag, M.; Schwartsburd, L.; Cohen, R.; Leitun, G.; Ben-David, Y.; Martin, J. M. L.; Milstein, D. *Angew. Chem. Int. Ed.* **2007**, *46*, 1901–1904.
- (232) Krogh-Jespersen, K.; Czerw, M.; Zhu, K.; Singh, B.; Kanzelberger, M.; Darji, N.; Achord, P. D.; Renkema, K. B.; Goldman, A. S. *J. Am. Chem. Soc.* **2002**, *124*, 10797–10809.
- (233) Rybtchinski, B.; Cohen, R.; Ben-David, Y.; Martin, J. M. L.; Milstein, D. *J. Am. Chem. Soc.* **2003**, *125*, 11041–11050.
- (234) Hermann, D.; Gandelman, M.; Rozenberg, H.; Shimon, L. J. W.; Milstein, D. *Organometallics* **2002**, *21*, 812–818.
- (235) Gusev, D. G.; Madott, M.; Dolgushin, F. M.; Lyssenko, K. A.; Antipin, M. Y. *Organometallics* **2000**, *19*, 1734–1739.
- (236) Zhu, K.; Achord, P. D.; Zhang, X.; Krogh-Jespersen, K.; Goldman, A. S. *J. Am. Chem. Soc.* **2004**, *126*, 13044–13053.

- (237) Meiners, J.; Friedrich, A.; Herdtweck, E.; Schneider, S. *Organometallics* **2009**, *28*, 6331–6338.
- (238) Vabre, B.; Lindeperg, F.; Zargarian, D. *Green Chem.* **2013**, *15*, 3188–3194.
- (239) Kabachnik, M. M.; Khomutova, Y. A.; Beletskaya, I. P. *Russ. J. Org. Chem.* **1999**, *35*, 26.
- (240) Halophosphonium salts are easily hydrolyzed, trialkylphosphines are easily oxidized by dioxygen, and halodialkylphosphines are sensitive to both H₂O and O₂. Therefore all manipulations involving these materials were carried out under dry argon.
- (241) Hughes, E. D.; Ingold, C. K. *J. Chem. Soc.* **1935**, 244–255.
- (242) Di-tert-butylodophosphine (**605a**) is not commercially available and was prepared from di-tert-butylchlorophosphine (**604a**) and sodium iodide.
- (243) Bricklebank, N.; Godfrey, S. M.; Lane, H. P.; McAuliffe, C. A.; Pritchard, R. G.; Moreno, J.-M. *J. Chem. Soc., Dalton Trans.* **1995**, 2421.
- (244) Godfrey, S. M.; McAuliffe, Robin G.; Pritchard, C. A.; Pritchard, R. G.; Sheffield, J. M.; Thompson, G. M. *J. Chem. Soc., Dalton Trans.* **1997**, 4823–4828.
- (245) Godfrey, S. M.; McAuliffe, C. A.; Mushtaq, I.; Pritchard, R. G.; Sheffield, J. M. *J. Chem. Soc., Dalton Trans.* **1998**, 3815–3818.
- (246) Boro, B. J.; Duesler, E. N.; Goldberg, K. I.; Kemp, R. A. *Inorg. Chem.* **2009**, *48*, 5081–5087.
- (247) Cámpora, J.; Palma, P.; del Río, D.; Álvarez, E. *Organometallics* **2004**, *23*, 1652–1655.

- (248) Castonguay, A.; Beauchamp, A. L.; Zargarian, D. *Organometallics* **2008**, *27*, 5723–5732.
- (249) Martínez-Prieto, L. M.; Melero, C.; del Río, D.; Palma, P.; Cámpora, J.; Álvarez, E. *Organometallics* **2012**, *31*, 1425–1438.
- (250) Bromodiisopropylphosphine (**613b**) needs to be separately prepared from Chlorodiisopropylphosphine (**604b**) and lithium bromide.
- (251) Very finely divided metal powders can be pyrophoric, but we were able to use Mg powder (40–80 mesh) and Ni powder (APS 2.2–3.0 μm), which are not pyrophoric.
- (252) Ionkin, A. S.; Marshall, W. J.; Adelman, D. J.; Fones, B. B.; Fish, B. M.; Schiffhauer, M. F. *Organometallics* **2006**, *25*, 2978–2992.
- (253) Rybtchinski, B.; Ben-David, Y.; Milstein, D. *Organometallics* **1997**, *16*, 3786–3793.
- (254) Arunachalampillai, A.; Loganathan, N.; Wendt, O. F. *Polyhedron* **2012**, *32*, 24–29.
- (255) Jansen, A.; Pitter, S. *Monatshefte Für Chem. Chem. Mon.* **1999**, *130*, 783–794.
- (256) Vogt, M.; Rivada-Wheellaghan, O.; Iron, M. A.; Leitius, G.; Diskin-Posner, Y.; Shimon, L. J. W.; Ben-David, Y.; Milstein, D. *Organometallics* **2013**, *32*, 300–308.
- (257) Jabri, E.; Carr, M.; Hausinger, R.; Karplus, P. *Science* **1995**, *268*, 998–1004.
- (258) De Lacey, A. L.; Fernández, V. M.; Rousset, M.; Cammack, R. *Chem. Rev.* **2007**, *107*, 4304–4330.
- (259) Schilter, D.; Camara, J. M.; Huynh, M. T.; Hammes-Schiffer, S.; Rauchfuss, T. B. *Chem. Rev.* **2016**, *116*, 8693–8749.
- (260) Burgess, B. K.; Lowe, D. J. *Chem. Rev.* **1996**, *96*, 2983–3012.

- (261) Hoffman, B. M.; Lukoyanov, D.; Yang, Z.-Y.; Dean, D. R.; Seefeldt, L. C. *Chem. Rev.* **2014**, *114*, 4041–4062.
- (262) Peters, J. W.; Szilagyi, R. K. *Curr. Opin. Chem. Biol.* **2006**, *10*, 101–108.
- (263) Dos Santos, P. C.; Dean, D. R.; Hu, Y.; Ribbe, M. W. *Chem. Rev.* **2004**, *104*, 1159–1174.
- (264) Steinhagen, H.; Helmchen, G. *Angew. Chem. Int. Ed. Engl.* **1996**, *35*, 2339–2342.
- (265) Lippard, S. *Science* **1995**, *268*, 996–997.
- (266) Stemmler, A. J.; Kampf, J. W.; Kirk, M. L.; Pecoraro, V. L. *J. Am. Chem. Soc.* **1995**, *117*, 6368–6369.
- (267) Suárez, D.; Díaz, N.; Merz, K. M. *J. Am. Chem. Soc.* **2003**, *125*, 15324–15337.
- (268) Estiu, G.; Merz, K. M. *J. Am. Chem. Soc.* **2004**, *126*, 11832–11842.
- (269) Shibasaki, M.; Kanai, M.; Matsunaga, S.; Kumagai, N. *Acc. Chem. Res.* **2009**, *42*, 1117–1127.
- (270) Haak, R. M.; Wezenberg, S. J.; Kleij, A. W. *Chem. Commun.* **2010**, *46*, 2713–2723.
- (271) Delferro, M.; Marks, T. J. *Chem. Rev.* **2011**, *111*, 2450–2485.
- (272) Herbert, D. E.; Ozerov, O. V. *Organometallics* **2011**, *30*, 6641–6654.
- (273) Press, L. P. Ph.D. Dissertation Chapter IV, Texas A&M University, College Station, TX, 2016.
- (274) Horowitz, S.; Trievel, R. C. *J. Biol. Chem.* **2012**, *287*, 41576–41582.
- (275) Fulmer, G. R.; Kaminsky, W.; Kemp, R. A.; Goldberg, K. I. *Organometallics* **2011**, *30*, 1627–1636.

- (276) Borau-Garcia, J.; Gutsulyak, D. V.; Burford, R. J.; Piers, W. E. *Dalton Trans.* **2015**, *44*, 12082–12085.
- (277) Bennett, M. A.; Yoshida, T. *J. Am. Chem. Soc.* **1973**, *95*, 3030–3031.
- (278) Breno, K. L.; Pluth, M. D.; Tyler, D. R. *Organometallics* **2003**, *22*, 1203–1211.
- (279) Crestani, M. G.; García, J. J. *J. Mol. Catal. A.* **2009**, *299*, 26–36.
- (280) Jensen, C. M.; Trogler, W. C. *J. Am. Chem. Soc.* **1986**, *108*, 723–729.
- (281) Ghaffar, T.; Parkins, A. W. *J. Mol. Catal. A.* **2000**, *160*, 249–261.
- (282) Filler, R.; Cantrell, G. L.; Wolanin, D.; Naqvi, S. M. *J. Fluorine Chem.* **1986**, *30*, 399–41.

APPENDIX

SUPPLEMENTARY PUBLICATIONS

- (1) Lee, C.-I.; Shih, W.-C.; Zhou, J.; Reibenspies, J. H.; Ozerov, O. V. "Synthesis of Triborylalkenes by Ir-Catalyzed Tandem C–H Borylation and Diboration", *Angew. Chem. Int. Ed.* **2015**, *54*, 14003–14007.
- (2) Shih, W.-C.; Ozerov, O. V. "One Pot Synthesis of 1,3-Bis(phosphinomethyl)arene PCP/PNP Pincer Ligands and their Nickel Complexes", *Organometallics* **2015**, *34*, 4591–4597.
- (3) Shih, W.-C.; Gu, W.; MacInnis, M. C.; Timpa, S. D.; Bhuvanesh, N.; Zhou, J.; Ozerov, O. V. "Facile Insertion of Rh and Ir into a Boron–Phenyl Bond, Leading to Boryl/Bis(phosphine) PBP Pincer Complexes", *J. Am. Chem. Soc.* **2016**, *138*, 2086–2089.
- (4) Kosanovich, A. J.; Shih, W.-C.; Ramírez-Contreras, R.; Ozerov, O. V. "N–H Cleavage as a Route to New Pincer Complexes of High-Valent Rhenium", *Dalton Trans.* **2016**, *45*, 18532–18540.
- (5) Shih, W.-C.; Ozerov, O. V. "Synthesis and Characterization of PBP Pincer Iridium Complexes and Their Application in Alkane Transfer Dehydrogenation", *Organometallics* **2017**, *36*, 228-233.
- (6) Shih, W.-C.; Gu, W.; MacInnis, M. C.; Herbert, D. E.; Ozerov, O. V. "Boryl/Borane Interconversion and Diversity of Binding Modes of Oxygenous

Ligands in PBP Pincer Complexes of Rhodium”, *Organometallics* **2017**, *36*, 1718–1726.

- (7) Pell, C. J.; Shih, W.-C.; Gatard, S.; Ozerov, O. V. “Formation of (PNP) Rh Complexes Containing Covalent Rhodium–Zinc Bonds in Studies of Potential Rh-Catalysed Negishi Coupling”, *Chem. Commun.* **2017**, *53*, 6456–6459.